DEVELOPMENT OF PILOT SIZE PROCESS FOR ZEOLITE Y AND ZSM-5 PRODUCTION FROM KANKARA KAOLIN

By

SOLOMON GAJERE BAWA

DEPARTMENT OF CHEMICAL ENGINEERING

AHMADU BELLO UNIVERSITY, ZARIA

NIGERIA

NOVEMBER, 2017

DEVELOPMENT OF PILOT SIZE PROCESS FOR ZEOLITE Y AND ZSM-5 PRODUCTION FROM KANKARA KAOLIN

By

Solomon Gajere BAWA, B.Eng (ABU, 2009) MSc. (ABU, 2012)

(Ph.D/ENG/41277/2012-2013)

A THESIS SUBMITTED TO THE

SCHOOL OF POSTGRADUATE STUDIES,

AHMADU BELLO UNIVERSITY, ZARIA

IN PARTIAL FULFILLMENT OF THE REQUIREMNTS FOR THE AWARD OF

DOCTOR OF PHILOSOPHY DEGREE IN CHEMICAL ENGINEERING

DEPARTMENT OF CHEMICAL ENGINEERING

FACULTY OF ENGINEERING

AHMADU BELLO UNIVERSITY, ZARIA

NIGERIA

NOVEMBER, 2017

DECLARATION

I, hereby declare that the work in this thesis titled "DEVELOPMENT OF PILOT SIZE PROCESS FOR ZEOLITE Y AND ZSM-5 PRODUCTION FROM KANKARA KAOLIN" was performed by me in the Department of Chemical Engineering, Ahmadu Bello University, Zaria, under the supervision of Prof. A. S. Ahmed, Dr. P. C. Okonkwo and Dr. S. M. Waziri. The information derived from the literature has been duly acknowledged in the text and a list of references provided. No part of this thesis was previously presented for another degree or diploma at this or any other institution.

Solomon Gajere BAWA _____ _____

Name Signature Date

CERTIFICATION

This thesis titled "DEVELOPMENT OF PILOT SIZE PROCESS FOR ZEOLITE Y AND ZSM-5 PRODUCTION FROM KANKARA KAOLIN" by Solomon Gajere BAWA meets the regulations governing the award of the degree of Doctor of Philosophy (Ph. D) of Ahmadu Bello University, and is approved for its' contribution to knowledge and literary presentation.

Prof. A. S. Ahmed	_____	_____
Chairman, Supervisory Committee	Signature	Date
Dr. P. C. Okonkwo	_____	_____
Member, Supervisory Committee	Signature	Date
Dr. S. M. Waziri	_____	_____
Member, Supervisory Committee	Signature	Date
Prof. B. J. El-Yakubu	_____	_____
Head, Dept. of Chemical Engineering	Signature	Date
Prof. S. Z. Abubakar	_____	_____
Dean, School of Postgraduate Studies	Signature	Date

DEDICATION

This thesis is dedicated to the Almighty God the creator of heaven and earth.

ACKNOWLEDGEMENTS

My unreserved appreciation goes to the God Head (God the Father, the Son and the Holy Spirit) for the wisdom to carry out this project work and for the gift of life. I will ever be grateful to my beloved parents Rev and Mrs. Bawa Gajere for their immeasurable support, love and care. The encouragement of my brothers and sister (David Bawa, Emmanuel Bawa and Ruth Bawa) was highly appreciated.

I will live to remember the great pool of knowledge and contribution of Prof. A.S. Ahmed my abled supervisor, for his close supervision which had aided the success of this work. It is a great privilege to work with a Professor of his type. To Dr. P.C. Okonkwo, and Dr. S.M. Waziri, I remain grateful for their dynamic input and supervision of my work. Their listening ears at all times had been remarkable.

My appreciation will be incomplete if I fail to acknowledge one of my academic mentors, Prof. B.O. Aderemi, his immense contribution to this work from start to finish will ever be remembered. Big thanks goes to Dr. L.C. Edomwonyi-Otu, for his listening ears and contributions, especially the assistance that enabled me to visit iThemba LABS, South Africa.

The warm reception given to me by Prof. M. Maaza, the Chair holder of the UNESCO UNISA African Chair in Nanosciences and Nanotechnology (U2ACN2) at iThemba LABS, Somerset West, Cape Town, South Africa and his kind assistance for my stay toward the concluding part of my Ph.D. bench will never go unnoticed. It had indeed added immense value to the research work. Thanks to all fellows of the U2ACN2 and staff of Materials Research Department, iThemba LABS, South Africa.

My profound appreciation goes to all the members of the PTDF research group ABU, for their constructive criticisms and technical inputs which greatly helped in making the work rich. My appreciation also goes to Engr. Maryam Abubakar for her kind assistance and moral encouragement during this project. And last but not the least I thank my fellow researchers. I am also grateful to all the staff members of the Department of Chemical Engineering, Ahmadu Bello University, Zaria.

ABSTRACT

The successes recorded at the laboratory for the synthesis of zeolite Y and ZSM-5 using Kankara kaolin sourced from Katsina state, Nigeria as starting material necessitated the need for upscale of the production process. This thesis focused on the development of three pilot size production units and characterizing the products obtained from those units. Pilot size reactors for dealumination and production of zeolite Y and ZSM-5 were developed and test run. Manual means of design was adopted; the materials of construction were carefully selected for the fabrication stage. The process of producing zeolite from kaolin involve, kaolin beneficiation, calcination, dealumination, zeolite recipe preparation and crystallization. The capacity of the pilot size dealuminator, zeolite Y and ZSM-5 reactors were 2.5 kg, 2 kg and 4 kg per run respectively. The reaction temperature and time for the production of zeolite Y were 100°C and 7 hours respectively. Low temperature production of ZSM-5 was achieved at 95°C for a period of 5 days. The physicochemical properties of the raw material, intermediate products (beneficiated kaolin, metakaolin and silica), and final products (zeolite Y and ZSM-5) were characterized using Fourier Transformation Infrared (FTIR), X-ray Diffraction (XRD), X-ray Fluorescence (XRF), Thermogravimetry Analysis (TGA), Scanning Electron Microscope (SEM), Transmission Electron Microscope (TEM), Selected Area Electron Diffraction (SAED), Energy Dispertive x-ray Spectrometer (EDS), and Brunauer-Emmett-Teller (BET) methods.

Dealumination reactor efficiency of 88%, 94%, 97% and 98% in terms of solid product quality was obtained from interior surface without coating, silicone caulk coating, ceramic tiles lining and glass lining respectively. The product obtained from the dealumination reaction was majorly alum and silica. The silica-to-alumina ratio of the zeolite Y produced

was 3.08 and the crystals were well formed having a specific surface area, average pore size and pore volume of 321 m^2/g, 34 Å and 0.270668 cm^3/g respectively. The crystals of ZSM-5 produced were good as revealed by SEM, with high specific surface area of 411 m^2/g, average pore size and pore volume of 24 Å and 0.248190 cm^3/g respectively. The silica-to-alumina ratio of the produced ZSM-5 zeolite was 77. The quality of zeolite Y and ZSM-5 produced using the developed pilot size reactors were comparable to those synthesized in the laboratory. From the performance test on hydrocracking reaction carried out in a fixed bed reactor, Pt/H-ZSM-5 performed better than Pt/La-zeolite Y. Maximum conversion of n-hexadecane was 98% at reaction temperature of 265 °C for Pt/H-ZSM-5, while 94 % conversion was obtained for Pt/La-zeolite Y at reaction temperature of 315 °C. The prepared catalysts showed high selectivity for gasoline fraction than diesel and lighter fraction products. Cracking was more favored than isomerization during the hydrocracking reaction. The pilot size production units designed had proven to produce good zeolite Y and ZSM-5 from Kankara kaolin which were active in terms of catalytic performance of the zeolite based formulated catalysts.

TABLE OF CONTENTS

TITLE	PAGE
Title Page	i
Declaration	ii
Certification	iii
Dedication	iv
Acknowledgements	v
Abstract	vi
Table of Contents	viii
List of Figures	xv
List of Tables	xx
List of Plates	xxii
List of Appendices	xxiv
Abbreviations and Symbols	xxv
CHAPTER ONE	
1.0 INTRODUCTION	1
1.1 Background	1
1.2 Research Problem Statement	4
1.3 Research Aim and Objectives	5
1.4 Research Scope	5
1.5 Research Justification	6
CHAPTER TWO	
2.0 LITERATURE REVIEW	7
2.1 Background	7

2.2 Pilot Plant 7

2.2.1 Pilot plant objectives 8

2.2.2 Prerequisite for pilot plant 9

2.3 Reactor Design 10

2.3.1 Batch reactor 12

2.3.2 Continuous-flow, stirred tank reactor (CSTR) 12

2.3.3 Tubular reactor 13

2.4 Materials Selection 13

2.5 Catalyst Formulation 17

2.5.1 Commercial catalyst 18

2.5.2 Fluid catalytic cracking (FCC) catalyst 19

2.6 Zeolite 21

2.6.1 Natural zeolite 22

2.6.2 Synthetic zeolite 23

2.6.3 Global zeolite production and applications 25

2.6.4 Zeolite Y 27

2.6.5 ZSM-5 28

2.7 Kaolin 29

2.7.1 Kaolin purification 30

2.7.2 Thermal treatment of kaolin 31

2.7.3 Acid leaching of metakaolin 32

2.7.4 Application of kaolin 32

2.7.5 Occurrence of kaolin in Nigeria 33

2.8 Material Characterization 34

2.8.1 Energy dispersive x-ray fluorescence 35

2.8.2 X-ray powder diffraction 36

2.8.3 Fourier transform infrared spectroscopy 37
2.8.4 Braunner-Emmett-Teller (BET) surface area measurement 38
2.8.5 Scanning electron microscope 39

CHAPTER THREE

3.0 MATERIALS, EQUIPMENT AND METHODOLOGY 41

3.1 Introduction 41

3.2 Materials and Apparatus 41

3.2.1 Materials 41
3.2.2 Apparatus 43

3.3 Equipment 44

3.4 Design Stage 45

3.4.1 Dealumination unit 45
3.4.2 Sizing of zeolite reactor 48
3.4.3 Engineering drawings 48

3.5 Material Selection for Fabrication 50

3.5.1 Dealumination unit 50
3.5.2 Zeolite Y and ZSM-5 reactor 52

3.6 Pilot Size Process Units Fabrication 53

3.6.1 Dealumination reactor 53
3.6.2 Zeolites reactors 54

3.7 Zeolite Production Process from Kaolin 57

3.7.1 Kaolin beneficiation 57
3.7.2 Calcination of beneficiated kaolin 58
3.7.3 Dealumination of metakaolin 59
3.7.4 Aluminum hydroxide production 60
3.7.5 Sodium silicate production 61
3.7.6 Silica sol preparation 63
3.7.7 Gel preparation for zeolite Y production 64
3.7.8 Crystallization of zeolite Y 64
3.7.9 ZSM-5 production 65
3.7.10 Protonation of zeolites 66
3.7.11 Thermal stabilization of zeolite Y 67

3.8 Physicochemical Characterization 67

3.8.1 Fourier transform infrared spectroscopy (FTIR) 67
3.8.2 X-ray diffraction (XRD) 67
3.8.3 X-ray fluorescence (XRF) 68
3.8.4 Scanning electron microscopy (SEM) 68
3.8.5 Transmission electron microscopy (TEM) 68
3.8.6 Thermo gravimetric analysis (TGA) 69
3.8.7 Brunauer-Emmett-Teller (BET) analysis 69

3.9 Catalyst Performance Test 69

CHAPTER FOUR

4.0 RESULTS AND DISCUSSION 72

4.1 Dealumination Reaction Time 72

4.2 Summary of Design Parameter and Fabricated Equipment 73

4.3 Physicochemical Characterization of Starting Raw Material 75

4.3.1 Fourier transformed infrared radiation analysis of Kankara kaolin 75
4.3.2 X-ray diffraction (XRD) analysis of Kankara kaolin 76
4.3.3 X-ray fluorescence (XRF) analysis of Kankara kaolin 77
4.3.4 SEM and TEM analysis of Kankara kaolin 78

4.4 Characterization of Beneficiated Kaolin and Metakaolin 79

4.4.1 Fourier transformed infrared analysis 79
4.4.2 X-ray diffraction (XRD) analysis 80
4.4.3 X-ray fluorescence (XRF) analysis 81
4.4.4 SEM and TEM analysis of metakaolin 82

4.5 Dealumination Process 84

4.5.1 Fourier transformed infrared radiation analysis of silica 86
4.5.2 X-ray diffraction (XRD) analysis of silica 87
4.5.3 X-ray fluorescence (XRF) analysis of silica 88
4.5.4 SEM and TEM of silica prepared from Kankara kaolin 88

4.6 Dealumination Reactor Efficiency 90

4.6.1 FTIR spectra of the solid reaction product 90
4.6.2 XRD patterns of the solid reaction product 91
4.6.3 Solid product quality 91
4.6.4 Evaluation of reactor efficiency 92

4.7 Physicochemical Characterization of Aluminum Hydroxide 93

4.7.1 FTIT spectrum of aluminum hydroxide produced from Kankara kaolin 93
4.7.2 XRD pattern of aluminum hydroxide produced from Kankara kaolin 94
4.7.3 SEM and TEM Images of aluminum hydroxide produced from Kankara kaolin 95

4.8 Other Intermediate Products Highlight 97

4.9 Zeolite Reactor Development 98

4.9.1 Heating method 98
4.9.2 Products yield 102
4.9.3 Zeolites process development 103
4.9.4 Products quality 107
4.9.5 Laboratory and pilot plant comparison 109
4.9.6 Zeolite transformation and compounding 112

4.10 Physicochemical Characterization of Zeolite Y Produced from Pilot Unit 115

4.10.1 FTIR of zeolite Y 115
4.10.2 XRD analysis of zeolite Y 116
4.10.3 SEM images of zeolite Y 116
4.10.4 TEM image and EDS of zeolite Y 117
4.10.5 TG analysis of zeolite Y 118
4.10.6 BET analysis of Zeolite Y 119

4.11 Physicochemical Characterization of ZSM-5 119

4.11.1 FTIR analysis of ZSM-5 119
4.11.2 XRD pattern of ZSM-5 120
4.11.3 SEM analysis of ZSM-5 121
4.11.4 TEM analysis of ZSM-5 122
4.11.5 BET analysis of ZSM-5 123

4.12 Physicochemical Characterization of Commercial FCCU Catalyst 124

4.13 Performance Test 127

4.14 Preliminary Full Scale Forecast for Reactors Capacity 132

CHAPTER FIVE

5.0 CONCLUSIONS AND RECOMMENDATIONS 133

5.1 Conclusions 133

5.2 Recommendations 134

Contributions to Knowledge 135

Publications 136

REFERENCES 138

APPENDICES 151

ENGINEERING DRAWINGS 194

LIST OF FIGURES

Figure	Title	Page
Figure 2.1	Requirements for industrial catalyst	18
Figure 2.2	A schematic flow diagram of a FCCU unit in petroleum refineries	19
Figure 2.3	A typical composition of FCC catalyst	20
Figure 2.4	The role of different pore size in cracking of residues molecules	21
Figure 2.5	Global zeolite market chat	25
Figure 2.6	Zeolite major consumption by application	26
Figure 2.7	Some common application of zeolite	27
Figure 2.8	Zeolite structure type FAU	28
Figure 2.9	Zeolite structure type MFI ((e.g. ZSM-5) and their porous network	29
Figure 2.10	Relationship between calcinations temperatures and activity of SiO_2 and Al_2O_3	32
Figure 2.11	Different application areas of kaolin	33
Figure 2.12	Nigeria map showing some mineral deposits	34
Figure 2.13	XRF analysis process	35
Figure 2.14	Interaction of incident rays with sample	40
Figure 3.1	Location of Kankara kaolin in Katsina State, Nigeria	42
Figure 3.2	Orthographic views and complete dealumination units	49
Figure 3.3	Zeolites reactor drawing (internal heating)	49
Figure 3.4	Zeolites reactor drawing (external heating)	50
Figure 3.5	Flow diagram of the synthesis of zeolite Y from the reagents prepared	65
Figure 3.6	Process diagram of hydrocracking reaction	70
Figure 4.1	FTIR spectrum of Kankara kaolin	76

Figure 4.2	XRD pattern of Kankara kaolin	77
Figure 4.3	FTIR spectra of beneficiated and metakaolin	80
Figure 4.4	XRD patterns of beneficiated and metakaolin	81
Figure 4.5	FTIR spectrum of silica prepared from Kankara	86
Figure 4.6	XRD pattern of silica prepared from Kankara kaolin	87
Figure 4.7	FTIR spectra of various silica produced from dealumination reaction	90
Figure 4.8	XRD patterns of various silica produced from dealumination reaction	91
Figure 4.9	Product quality of different materials used in the reactor interior	92
Figure 4.10	Reactor efficiency with respect to different materials at the interior part of the reactor	93
Figure 4.11	FTIR spectrum of aluminum hydroxide prepared from Kankara kaolin	93
Figure 4.12	XRD pattern of aluminum hydroxide prepared from Kankara kaolin	95
Figure 4.13	FTIR spectra of zeolite Y produced *via* different heating means	100
Figure 4.14	XRD patterns of zeolite Y produced *via* different heating means	101
Figure 4.15	Yield of zeolite Y produced from developed pilot size reactor	102
Figure 4.16	Yield of ZSM-5 produced from developed pilot size reactor	103
Figure 4.17	Pilot scale production of zeolite Y from Kankara kaolin	104
Figure 4.18	XRD pattern for zeolite Y produced at Run 1	104
Figure 4.19	XRD pattern for zeolite Y produced at Run 2	105
Figure 4.20	XRD pattern for zeolite Y produced at Run 3	105
Figure 4.21	ZSM-5 production process (a) Runs 1 & 2 (b) Run 3	106
Figure 4.22	FTIR of top and bottom layer of zeolite Y produced from pilot unit	107
Figure 4.23	XRD patterns of top and bottom layer of zeolite Y produced from	

pilot unit 108

Figure 4.24 XRD patterns for calcined and uncalcined ZSM-5 (Run 3) 109

Figure 4.25 FTIR of zeolite Y synthesized from pure chemical and kaolin (lab & pilot scale) 110

Figure 4.26 Comparison of XRD patterns of Zeolite Y synthesis in the lab and pilot unit 111

Figure 4.27 Comparison of XRD patterns of ZSM-5 synthesis in the lab and pilot unit 111

Figure 4.28 FTIR of pure and compounded zeolite Y both in the laboratory and pilot unit 112

Figure 4.29 Zeolite Y transformation stages 113

Figure 4.30 FTIR different product of ZSM-5 114

Figure 4.31 ZSM-5 zeolite transformation stages 114

Figure 4.32 FTIR pattern of zeolite Y produced from Kankara kaolin 115

Figure 4.33 XRD pattern of zeolite Y 116

Figure 4.34 TGA result of zeolite Y 119

Figure 4.35 FTIR spectrum of ZSM-5 120

Figure 4.36 XRD pattern of ZSM-5 121

Figure 4.37 FTIR of commercial catalyst 124

Figure 4.38 XRD pattern for commercial catalyst 124

Figure 4.39 XRD pattern of Pt/La Zeolite Y 127

Figure 4.40 XRD pattern of Pt/H-ZSM-5 zeolite catalyst 127

Figure 4.41 n-Hexadecane conversion with variation in reaction temperature 128

Figure 4.42	Product yield of Pt/HZSM-5 with respect to temperature	129
Figure 4.43	Product yield of Pt/HZSM-5 with respect to conversion	130
Figure 4.44	Selectivity of n-hexadecane isomerization on Pt/HZSM-5	131
Figure 4.45	Product yield of Pt/HZSM-5 with respect to petroleum fraction	132
Figure B.1	Graph of water volume expansion with temperature	153
Figure B.2	Sulphuric acid boiling point chat	154
Figure B.3	Quadratic model plot	157
Figure B.4	Polynomial of degree 3 model plot	158
Figure B.5	Polynomial of degree 4 model plot	158
Figure B.6	Polynomial of degree 5 model plot	159
Figure B.7	Polynomial of degree 6 model plot	159
Figure B.8	Exponential model plot	160
Figure B.9	Linear equation model plot	160
Figure C.1	Material balance around the dealuminator	161
Figure D.1	Project view of dealuminator configuration	164
Figure D.2	Aluminum Casing drawing	167
Figure E.1	Mixing configuration	171
Figure E.2	Diagram of the Geldart classification of particles	172

Figure E.3 Power Curve 175

Figure F.1 Diagram of material balance around zeolite Y reactor 179

Figure G.1 Diagram of material balance around ZSM-5 reactor 182

LIST OF TABLES

Table	Title	Page
Table 2.1	Comparison between continuous and batch processes	10
Table 2.2	Mechanical properties of polymers	16
Table 4.1	Values generated from the kinetic model for dealuminator	72
Table 4.2	Estimation of reaction time using graphical method of different equation models	73
Table 4.3	Summary of design parameters for fabrication	73
Table 4.4	Chemical composition of raw Kankara kaolin	78
Table 4.5	Chemical composition of beneficiated and metakaolin	82
Table 4.6	Chemical composition of silica prepared from Kankara kaolin	88
Table 4.7	Summary of dimensions for full scale reactors	132
Table A.1	Density of sulphuric acid at different concentration	152
Table C.1	Material balance in the dealuminator	162
Table C.2	Volume estimation for different reactants	162
Table D.1	Thermal conductivity of selected materials of construction	165
Table E.1	Parameters for metakaolin slurry components	168
Table F.1	Material balance around zeolite Y reactor	179
Table F.2	Volume estimation for different reactants	180

Table G.1 Material balance on ZSM-5 reactor 183

Table G.2 Volume estimation for different reactants 183

Table K.1 Products distribution of n-hexadecane hydrocracking on Pt/ZSM-5 192

LIST OF PLATES

Plate	Title	Page
Plate I	Site of Kankara Kaolin	43
Plate II	Fabrication of dealuminator external part	53
Plate III	Fabrication of dealuminator internal part	54
Plate IV	Complete set-up of zeolite reactor involving internal heating	54
Plate V	Internal configuration of zeolite reactor	55
Plate VI	Reactor cover under fabrication	56
Plate VII	Final stage of zeolite reactor fabrication	56
Plate VIII	Pilot unit for kaolin purification	58
Plate IX	Aluminum hydroxide production unit	61
Plate X	Sodium silicate production unit	62
Plate XI	(A) Hydrocracking reaction set-up (B) GS MS Machine	71
Plate XII	Pilot size dealuminator unit	74
Plate XIII	Zeolite reactor with internal heating	74
Plate XIV	Zeolite reactor with external heating	75
Plate XV	SEM image of raw Kankara kaolin at different magnification	78
Plate XVI	TEM image of raw Kankara kaolin at different magnification	79
Plate XVII	SEM images of Metakaolin at different magnification	83
Plate XVIII	TEM images of Metakaolin at different magnification	84
Plate XIX	Alum obtained after dealumination	85
Plate XX	Silica from Kankara kaolin pilot after dealumination reaction	85
Plate XXI	SEM images of silica prepared from Kankara kaolin	89
Plate XXII	TEM images of silica prepared from Kankara kaolin	89

Plate XXIII	SEM images of aluminum hydroxide at different magnifications	96
Plate XXIV	TEM images of aluminum hydroxide at different magnifications	96
Plate XXV	Concentrated sodium silicate prepared from Kankara kaolin	97
Plate XXVI	Silica sol	97
Plate XXVII	Zeolite reactor (A) internal (B) external heating	99
Plate XXVIII	Internal configuration of zeolite reactor	99
Plate XXIX	SEM images and EDS of zeolite Y	117
Plate XXX	TEM image, EDX and SAED of zeolite Y	118
Plate XXXI	SEM images and EDS of ZSM-5 at different magnification	122
Plate XXXII	TEM images, SAED, and EDS of ZSM-5	123
Plate XXXIII	SEM images and EDX of commercial FCCU catalyst	125
Plate XXXIV	TEM images, SAED and EDX of Commercial FCCU catalyst	126

LIST OF APPENDICES

Appendix	Title	Page
Appendix A	Dealumination reactor calculation	151
Appendix B	Time of dealumination reaction calculation	153
Appendix C	Material balance for dealumination reaction	161
Appendix D	Energy calculation of dealuminator	164
Appendix E	Metakaolin slurry mixing tank and acid holding tank calculation	168
Appendix F	Material balance and sizing of zeolite Y reactor	178
Appendix G	Material balance and sizing of ZSM-5 reactor	182
Appendix H	Calculation on the production of sodium silicate for zeolite Y production	186
Appendix I	Calculation on the production of sodium silicate for ZSM-5 production	187
Appendix J	Preliminary full scale calculation for major equipment	188
Appendix K	n-Hexadecane hydrocracking reaction on Pt/ZSM-5 results	192

SYMBOLS AND ABBREVIATIONS

Symbols

α	Alpha radiation
Θ	Diffraction angle (˚)
λ	Wave length (nm)
ρ_i	density of component I (g/cm^3)
a	Effective cross-sectional area of one adsorbate molecule (m^2)
d	lattice spacing
h	Planck's constant (J.s)
k_a	Thermal conductivity of material a (W/m.K)
m_{total}	Total mass of the reacting system (kg)
n	integer
q'	Energy flow per unit time (J/s)
$-r_A$	Rate of dealumination ($g_{alumina}/g_{metakaolin}.s$)
r	Radius (m)
ps	Saturated vapor pressure (kPa)
w	Number of water molecule per unit cell
x and y	Total number of tetrahedra per unit cell
Cp_{av}	Average specific heat capacity (J/kg.K)

C	Dimensionless constant related to the enthalpy of gas adsorption and condensation
C_{Ac0}	Initial acid concentration (mol/dm^3)
C_{Al}	Concentration of alumina left in the raffinate (mol/dm^3)
C_M	Concentration (mol/dm^3)
D_{msT}	Metakaolin slurry mixing tank diameter (m)
E	energy (J)
H_{msT}	Metakaolin slurry mixing tank height (m)
L	Height of the cylinder (m)
N	Avogadro constant
Ms	mass of sample (g)
P	Partial vapor pressure of adsorbate gas in equilibrium (kPa)
P_0	Saturated pressure of adsorbate gas (kPa)
S	Specific surface area (m^2/g)
T	Reaction temperature (K)
T_f	Final temperature (K)
ΔT	Temperature difference (K)
X_i	Mass fraction of component i
V	Volume of reactants component (m^3)

V_a	Volume of gas adsorbed at equilibrium (ml)
Vmol	volume of mole of gas at STP of Vm (m^3)
V_m	Volume of gas adsorbed in a monolayer (ml)
V_{AcmT}	Actual volume of the slurry mixing tank ((m^3)
V_{mT}	Volume of the slurry mixing tank (m^3)

Abbreviations

BSE	Back-scattered electrons
BET	Brunauer-Emmett-Teller
CSTR	Continuous-flow, stirred tank reactor
ED-XRF	Energy dispersive – X-ray fluorescence
EDS	Energy dispersive x-ray Spectrometer
FCC	Fluid catalytic cracking
FTIR	Fourier transformed infrared radiation
GCMS	Gas chromatography mass spectroscopy
GTL	Gas to liquid
IR	Infrared
IZA	International zeolite association
ND	Not Detected

OO	Other oxides
PTFE	Polytetrafluroethylene
PTDF	Petroleum Technology Development Fund
PVC	Polyvinyl chloride
SAED	Selected area electron diffraction
SEM	Scanning electron microscopy
TGA	Thermogravimetric analysis
TEM	Transmission electron microscopy
XRD	X-ray diffraction.

CHAPTER ONE

INTRODUCTION

1.1 Background

Industrialization remains a major factor in measuring the development of a nation because it reduces the volume of importation and strengthens the economy of the nation. Chemical transformation of raw materials to products is one of the key industrial processes aimed at meeting the ever rising needs of the global teeming population. Catalysts play a central role in most of the chemical transformation process and contributes immensely to the reduction in process thermal energy requirement, process simplification, reduced processing time and most often reduction in materials requirement, thereby increasing output quantity and quality; which translates to higher profitability. Scale up has been usually explained as how to design a pilot or industrial reactor able to replicate through a standard methodology the results obtained in the laboratory. Scaling up of reactors is a fundamental step in the realization and optimization of industrial plants.

Nigeria, with a huge amount of oil reserves estimated to be about 3 7.2 billion barrels and the 13th word producer of petroleum, with four refineries across the nation and a total processing capacity of 450,000 barrels per day consumes approximately 1600 tonnes of zeolite catalyst per day. The catalysts are imported annually over 500,000 tonnes, at a cost of about 5 billion naira (Babalola, 2015). Nigeria has a good potential to develop zeolite for its local use. Nigerian petroleum refining sector has been hit in recent times by high operating costs. This cost is partly attributed to the cost of imported catalysts for the catalytic cracking, reforming as well as the alkylation units. To minimize the refineries' operating cost index, concerted

efforts are currently on-going for the production of an effective, inexpensive and ecologically safe catalyst that can be synthesized from local raw materials. The primary goal in the petroleum refining is efficient conversion of crude oil into high-quality fuel components.

Zeolites are crystalline aluminosilicates materials containing pores and channels of molecular dimensions. They form the most important group of crystalline inorganic microporous solids with many industrial applications such as adsorption, separation and particularly in catalysis. Zeolite catalysts provide vastly superior combinations of strong acid catalytic sites, uniformity of pore structure, and stability, all of which provide improved selectivity, yield, durability and cost over non-zeolite alternative (Ahmed, 2011). The global market for heavier fuels is decreasing while that for middle distillate is increasing at a rapid rate (Ajayi, 2012). Catalytic cracking of gas oil fraction occurs over many types of materials, which include acidified clay, silica, alumina, and zeolites. Relatively high yield of desirable products are obtained with zeolites. Aside being used as catalyst in the catalytic cracking, zeolites are used during filtration of drinking water, gas purification of industrial effluents and emissions, drying of gases and liquids, extraction of metals from complex solutions. ZSM-5 zeolite are the preferred catalysts for gas to liquid (GTL) processes. Production of zeolite catalysts in Nigeria is hampered largely due to lack of proven technical know-how in the zeolite technology (El-Yakub, 2011; Srikanth, 2011; Bose *et al*., 2007). Faujasites class of zeolite (zeolite X and zeolite Y) are known for remarkable stable and rigid structure with the large void space. In hydrocracking, hydrocarbon molecules and hydrogen gas pass over the zeolite catalyst, which converts higher-molecular-weight petroleum fractions to lower-molecular-weight fuels. The Isocracking process of Chevron also uses hydrocracking

catalysts, some containing zeolite to increase the cracking function of these dual-function catalysts (Sherman, 1999).

In general terms, locally sourced raw materials is advantageous in the reduction of operating budget which leads to improvement in firm's competitiveness. Efforts have been geared towards cost effective production of zeolites from local raw materials and waste materials such as local clay, coal fly ash, fly ash from waste papers etc. (Wajima *et al*., 2006; Adamczyk and Bialecka, 2005; Fukui *et al*., 2003; Moreno *et al*., 2002). Geographically, kaolin is found in several parts of Nigeria. Nigeria is one of those countries in Africa that has a wide variety of different natural resources ranging from precious metals, various stones for industrial applications such as barites, gypsum, kaolin and marble. Statistically, the level of exploitation of these minerals is very low in relation to the extent of deposit found in the country. One of the objectives of the new national policy on solid minerals is to ensure the orderly development of the mineral resources of the country (www.nigeria.gov.ng/2012-10-29-11-05-46/). There are tremendous opportunities for investment in the solid mineral sector of the Nigeria economy. An estimated reserve of three billion tonnes of good kaolinitic clay has been identified in many localities in Nigeria, about 800 million tons of proven deposits have been quantified (RMRDC, 2010). Currently, higher quality zeolite Y is produced either by incorporation method from high purity chemicals or patented Engelhard method from kaolin and high purity chemicals (Ahmed, 2014).

Detail kinetic studies had been carried in respect to dealumination of Kankara kaolin (Aderemi, 2000 and 2001). Some useful products had been produced from Kankara kaolin which include alums (Aderemi *et al*., 2006; Edomwonyi-Otu and Aderemi, 2009), alumina (Aderemi and Hameed, 2011; Ahmed and Bawa, 2012) and Faujisite zeolites (Atta *et al*.,

2007), which was a mixture of zeolite X and zeolite Y, as well as having much impurities. Single phase Zeolite Y with large pore was synthesized *via* partial dealumination route (Ajayi, 2012), but the stability of the synthesized zeolite was a challenge, as well as associated impurities which were inherent in the kaolin. Novel dealumination method (Ajayi, *et. at*., 2010) was employed to completely split the metakaolin prepared from Kankara kaolin to obtain silica and alum which were used for laboratory syntheses of zeolite Y (Salahudeen, 2015) and ZSM-5 zeolite (Yunusa, 2015). From that innovative approach of zeolite Y and ZSM-5 synthesis, good quality single phase zeolites were obtained with minimal associated impurities.

The PTDF Chair in Department of Chemical Engineering, Ahmadu Bello University, Zaria in 2014 conceived the ideal of establishing a pilot plant for the production of zeolite Y and ZSM-5 from Kankara kaolin, which requires various units. Development of pilot size units for the production of aluminum hydroxide (Nakakana, 2015) and sodium silicate (Yusuf, 2015) were achieved. But other major pilot size units which include dealuminator, zeolite Y and ZSM-5 reactors, were yet to be develop.

1.2 Research Problem Statement

Nigeria as a major producer of crude oil in the world, the total dependence of Nigeria on imported Zeolite Y catalyst used for refining of petroleum is not a sustainable economic/technological strategy (Salahudeen, 2015). Nigerian kaolin deposit was estimated to be over 3 billion metric tons (Edomwonyi-Otu, *et al*. 2013). The need to harness this abundant mineral for Zeolite Y and ZSM-5 catalysts production which can serve as substitute for the imported ones cannot be over emphasized. Efforts to improve the purity of Zeolite Y catalysts *via* partial dealumination method of metakaolin yielded only little progress due to

the inherent impurities in kaolin (Ajayi, 2012). Novel zeolites synthesis methods which involve a complete split of metakaolin into alum and silica gave an improved zeolite Y and ZSM-5 in terms of purity (Yunusa, 2015; Salahudeen, 2015).

Despite the great successes recorded in the synthesis of good quality zeolite Y and ZSM-5 in the laboratory using Kankara kaolin as raw material, to the best of my knowledge, no pilot plant exists for such novel production process.

1.3 Research Aim and Objectives

The aim of this work is to develop pilot size production units for zeolites production from Kankara kaolin.

The specific objectives of this research work are to:

i. design, fabricate and test run a 2.5 kg per batch dealumination unit;
ii. design, fabricate and test run reactors for zeolites Y (2 kg/batch) and ZSM 5 (4 kg/batch) production;
iii. characterize the raw material, intermediate and final products using FTIR, XRD, XRF, SEM, TEM, TGA, EDS, SAED, and BET;
iv. formulate zeolite based catalysts;
v. conduct performance test for the formulated catalysts on n-hexadecane hydrocracking reaction.

1.4 Research Scope

The scope of the research is to produce zeolites Y and ZSM -5 from the designed pilot plant units, using Kankara kaolin as starting material, as well as to carry out physicochemical

characterization on the as-synthesized products, preparation of zeolite based catalysts and performance test on the prepared zeolite catalyst.

1.5 Research Justification

i. The abundant kaolin deposit in Nigeria would be better utilized economically.

ii. Indigenous knowledge on zeolite production from kaolin would be enhanced

iii. Employment opportunities would be generated

iv. Conservation of foreign exchange earnings thereby enhancing economic growth.

v. Zeolite catalyst from indigenous sources for conversion of petrochemicals into valuable chemicals would be developed.

CHAPTER TWO

LITERATURE REVIEW

2.1 Background

Design is a creative activity, and as such can be one of the most rewarding and satisfying activities undertaken by an engineer, which involves the synthesis and putting together of ideas to achieve a desired purpose. Design principles help in the up scaling of experimental achievement in the laboratory level to pilot scale and as well as commercial scale. Reactors, irrespective of their size are mostly the heart of a manufacturing process which involves chemical transformation (Sinnott, 1999).

2.2 Pilot Plant

A pilot plant allows investigation of a product and process on an intermediate scale before large amounts are committed to full-scale production. It is not possible to design a large complex processing plant from laboratory data alone with any degree of success. Scale-up of a process can also be viewed as a procedure for applying the same process to different output volumes. Pilot plant reduces the risk associated with the construction of large process plants. As such, it serves as a bridge between laboratory process and full scale operations. Some of the challenges associated with full scale operations that are hidden at the laboratory level are exposed at the pilot plant stage. In addition, pilot plants are used to train personnel for a full-scale plant, as technical know-how is being gained during the process of running the pilot plant which will be very helpful during full scale-up operations. The design of a commercial plant can be unsuitable if the available experience is not extensive enough to scale up the information from laboratory tests. The pilot plant must be understood not as a scale-up of

laboratory equipment but as a small scale simulation of the future industrial operations. Results of the laboratory studies will be used to choose the most suitable process and will lead to the selection of the equipment for each stage of the flow sheet

2.2.1 Pilot plant objectives

As a result of experience with a pilot plant, the decision to proceed with the full scale plant project will be based on a proven process, and on a more reliable economic estimate. This, however, is not the only purpose of a pilot plant. Studies of a process can be carried out in the pilot plant while the industrial plant is working. In this way, it is possible to determine the most suitable economic operating conditions. In a case such as this where both plants work simultaneously, the objective of the pilot plant is to find the best conditions of operation. On the other hand, when the pilot plant is built as an intermediate stage between the laboratory studies and the industrial plant, its main objective is to confirm the design characteristics of the full scale plant. Another important objective of a pilot plant is personnel training. In this case, personnel will be trained not only for operation of the different types of equipment, but also for control of the process (Sinnott, 1999). The training will help get the full scale plant in operation, reducing the time needed to reach its design capacity, and avoiding damage to some of the equipment as a result of improper operation. The objectives of a pilot plant, therefore, can differ depending on the specific circumstances of each project, and the decision for its construction can include one or several of the following objectives:

1. To optimize the operating parameters of the process,
2. To study the effects of recirculating process streams and of accumulation of impurities over long periods,
3. To obtain process information necessary to specify and design the full scale plant,

4. To test process control systems and procedures,
5. To test materials of construction,
6. To optimize the design of the equipment,
7. To obtain sufficient information to prepare detailed and reliable estimates of capital and operating costs and to prepare a reliable economic evaluation of the project,
8. To gain operating experience and train the personnel that will operate the full scale plant,

2.2.2 Prerequisite for pilot plant

A pilot plant requires a substantial investment and often long term operation is needed to achieve the desired objectives. Thus a thorough analysis must be carried out before a decision is made to build a pilot plant. issues such as expenses and length of the project must be weighed against the expected advantages to be gained in fulfilling the objectives of a pilot plant. A pilot plant is usually not considered until the project is sufficiently advanced and well defined to the extent that there is reasonable assurance that the overall project is feasible. Developed processes from pilot plant to full scale industry can either be operated as batch or continuous processes. Continuous processes are designed to operate 24 hours a day, 7 days a week, throughout the year. However, some down time will be allowed for maintenance and, for some processes such as, catalyst regeneration. The plant attainment; that is, the percentage of the available hours in a year that the plant operates, will usually be 90 to 95% (Sinnott, 1999). It is calculated using Equation 2.1:

$$Attainment\ \% = \frac{hours\ operated}{8760} \times 100 \qquad (2.1)$$

Batch processes are designed to operate intermittently. Some or all of the process units being frequently shut down and started up. Characteristics of both batch and continuous processes are presented in Table 2.1.

Table 2.1: Comparison between continuous and batch processes (Sinnott, 1999)

Continuous Process	Batch process
Production rate greater than 5×10^6 kg/h	Production rate less than 5×10^6 kg/h
Single product	A range of products or product specifications
No severe fouling	Severe fouling
Proven processes design	Uncertain design
Established market	New product

2.3 Reactor Design

In the design of an industrial scale reactor for a new process, or an old one that employs a new catalyst, it is common practice to carry out both bench and pilot plant studies before finalizing the design of the commercial scale reactor. The bench scale studies yield the best information about the intrinsic chemical kinetic and the associated rate expression. The pilot scale studies can provide a test of the applicability of the correlations and an indication of potential limitations that physical processes may place on conversion rates. Chemical engineers have traditionally approached kinetics studies with the goal of describing the behavior of reacting systems in terms of macroscopically observable quantities such as temperature, pressure, composition, and Reynolds number (Hill, 1977). A general direct

method of measuring the rate of a reaction does not exist. One can only determine the amount of one or more product or reactant species present at a certain time in the system under observation.

There are several potential sources of the experimental data that are essential for proper reactor design.

1. **Bench scale experiments**: The reactors used in these experiments are usually designed to operate at constant temperature, under conditions that minimize heat and mass transfer limitations on reaction rates. This facilitates an accurate evaluation of the intrinsic chemical effects.

2. Pilot plant studies: The reactors used in these studies are significantly larger than those in bench scale laboratory experiments. One uses essentially the reverse of the design procedures developed to come up with the reaction rate from the pilot plant data. It may be difficult to separate the intrinsic chemical effects from any heat and mass transfer effects in the analysis of data of this type.

3. Operating data from commercial scale reactors: If one's company has access to actual operating data on another commercial installation of the same type as that contemplated, it provides the closest approximation to the conditions likely to be encountered in industrial practice. Such access may result from licensing arrangements or from previous experience within the company. In such systems physical limitations on rates of heat and mass transfer may disguise the true kinetics to a significant degree.

2.3.1 Batch reactor

The batch reactor, as its name implies, processes reactants in discrete batch. All reactants are loaded into the reactor and allowed to react; the resulting products are then removed. Composition of material within the reactor changes over time. Batch reactors are widely used in the chemical industry for producing materials that are needed in limited quantity, particularly in those cases where the processing cost represents only a small fraction of the total value of the product. The starting point for the development of the basic design equation for a well-stirred batch reactor is a material balance involving one of the species participating in the chemical reaction (Levenspiel, 1999; Missen *et al*., 1999).

2.3.2 Continuous-flow, stirred tank reactors (CSTR)

The design of the continuous flow, stirred tank reactor (CSTR) incorporates both constant flow of material through the reactor and complete mixing within it. These reactors are used primarily for carrying out liquid phase reactions in the organic chemicals industry, particularly for systems that are characterized by relatively slow reaction rates (Hill, 1977). The most important feature of the CSTR is its mixing characteristics. At steady state, the composition of material is both uniform throughout the reactor and invariant over time. The idealized model of reactor performance presumes that the reactor contents are perfectly mixed so that the system properties are uniform throughout. The effluent composition and temperature are thus identical with those of the reactor contents (Levenspiel, 1999; Missen *et al*., 1999).

2.3.3 Tubular reactors

Tubular reactors are normally used in the chemical industry for extremely large-scale processes, the simplest model of the behavior of tubular reactors is the plug flow model. The essential features of this idealized model require that there be no longitudinal mixing of fluid elements as they move through the reactor and that all fluid elements take the same length of time to move from the reactor inlet to the outlet. Each plug of fluid is assumed to be uniform in temperature, composition, and pressure, which is equivalent to assuming that radial mixing is infinitely rapid. However, there may well be variations in composition, temperature, pressure, and fluid velocity as one moves in the longitudinal direction. With respect to these variations, however, the model requires that mass transport *via* diffusion or turbulent mixing processes be negligible and that the plugs of materials do not interact with one another except for transmission of the hydrodynamic forces giving rise to the fluid motion (Nauman, 2002; Hill, 1977).

2.4 Material Selection

Many factors have to be considered when selecting engineering materials. The most economical material that satisfies both process and mechanical requirements should be selected; this will be the material that gives the lowest cost over the working life of the plant, allowing for maintenance and replacement. Other factors, such as product contamination and process safety, must also be considered. The important characteristics to be considered when selecting a material of construction for process equipment are mechanical properties (strength-tensile strength, Stiffness, toughness, hardness-wear resistance, fatigue resistance, creep resistance); effect of high and low temperatures on the mechanical properties; corrosion resistance, special properties (thermal conductivity, electrical resistance, magnetic

properties); welding, casting; availability in standard sizes-plates, sections, tubes and cost (Sinnott, 1999). The corrosion rate depends on the temperature and concentration of the corrosive fluid. An increase in temperature usually results in an increased rate of corrosion; though not always. The rate will depend on other factors that are affected by temperature, such as oxygen solubility.

Carbon and low alloy steels will oxidize rapidly at high temperatures and their use is limited to temperatures below 500°C, Chromium is the most effective alloying element to give resistance to oxidation, forming a tenacious oxide film. Chromium alloys should be specified for equipment subject to temperatures above 500°C in oxidizing atmospheres. Pilot plant tests, and laboratory corrosion tests under simulated plant conditions, will help in the selection of suitable materials if actual plant experience is not available. The relative cost of equipment made from different materials will depend on the cost of fabrication, as well as the basic cost of the material. In a given situation, it may prove more economical to install a cheaper material with a high corrosion rate and replace it frequently; rather than select a more resistant but too expensive material. This strategy would only be considered for relatively simple equipment with low fabrication costs, and where premature failure would not cause a serious hazard. With some processes, the prevention of the contamination of a process stream, or a product, by certain metals, or the products of corrosion, overrides any other considerations when selecting suitable materials (Walas, 1990).

The stainless steels are the most frequently used corrosion resistant materials in the chemical industry. To impart corrosion resistance, the chromium content must be above 12 %, and the higher the chromium content, the more resistant is the alloy to corrosion in oxidizing conditions. Nickel is added to improve the corrosion resistance in non-oxidizing

environments. A wide range of stainless steels is available, with compositions tailored to give the properties required for specific applications. They can be divided into three broad classes according to their microstructure (Sinnott, 1999; Perry and Green, 1997):

1. Ferritic: 13-20 % Cr, < 0.1 % C, with no nickel

2. Austenitic: 18-20 % Cr, > 7 % Ni

3. Martensitic: 12-10 % Cr, 0.2 to 0.4 % C, up to 2 % Ni

The uniform structure of austenite makes it desirable for corrosion resistance, and it is these grades that are widely used in the chemical industry. Type 304 (the so-called 18/8 stainless steels), the most generally used stainless steel, contains the minimum Cr and Ni that give a stable austenitic structure. The carbon content is low enough for heat treatment not to be normally needed with thin sections to prevent weld decay. Type 316, in this alloy, molybdenum is added to improve the corrosion resistance in reducing conditions, such as in dilute sulphuric acid, and, in particular, to solutions containing chlorides. The austenitic stainless steels have greater strength than the plain carbon steels, particularly at elevated temperatures (Sinnott, 1999).

Plastics are being increasingly used as corrosion-resistant materials for chemical plant construction. They can be divided into two broad classes: Thermoplastic materials (which soften with increasing temperature, e.g. polyvinyl chloride (PVC) and polyethylene.); and Thermosetting materials (which have a rigid, cross-linked structure, e.g. the polyester and epoxy resins). The biggest use of plastics is for piping. The mechanical strength and operating temperature of plastics are low compared with that of metals. The mechanical strength, and other properties, can be modified by the addition of fillers and plasticizers. Plastics can be

considered to complement metals as corrosion-resistant materials of construction (Kuye and Ayo, 2007, Sinnott, 1999). Table 2.2 shows some common polymers and some of their associated properties such as tensile strength, elastic modulus and density.

Table 2.2: Mechanical properties of polymers (Sinnott, 1999)

Materials	Tensile strength (N/mm^2)	Elastic modulus (kN/mm^2)	Density (kg/m^3)
PVC	55	3.5	1400
Polyethylene (low density)	12	0.2	900
Polypropylene	35	1.5	900
PTFE	21	1.0	2100
GRP polyester	100	7.0	1500
GRP epoxy	250	14.0	1800

GRP: Glass fiber-reinforced plastics

Polytetrafluroethylene (PTFE), known under the trade names Teflon and Fluon, is resistant to all chemicals, except molten alkalies and fluorine, and can be used at temperatures up to 250°C. It is a relatively weak material, but its mechanical strength can be improved by the addition of fillers (glass and carbon fibers). It is expensive and difficult to fabricate. PTFE is used extensively for gaskets and gland packing. As a coating, it is used to confer non-stick properties to surfaces, such as filter plates. It can also be used as a liner for vessels.

Ceramics are compounds of non-metallic elements and include the following materials used for chemical plant: Glass, the borosilicate glasses (hard glass), stoneware, acid-resistant bricks and tiles, refractory materials, cements and concrete, glass linings, also known as glass

enamel, have been used on steel and iron vessels for many years. High-quality bricks and tiles are used for lining vessels, ditches and to cover floors. The linings are usually backed with a corrosion-resistant membrane of rubber or plastic, placed behind the titles, and special acid-resistant cements are used for the joints.

2.5 Catalyst Formulation

Most often a catalyst formulation consists of a multitude of components, each of which performs an essential task in the creation of a commercially viable catalyst. The task of developing a suitable catalyst for commercial applications involves many considerations, ranging from obvious factors like catalyst activity and selectivity to variables like the catalyst shape and the composition of the binder used in a pelletizing process. Figure 2.1 illustrates some important requirements to consider when developing a catalyst for industrial applications. The art of catalyst formulation involves reconciling conflicting demands that may be imposed by such requirements. The keystone of the arch is a material that has high intrinsic activity and selectivity for promoting the reaction of interest. This material may be used in bulk form or, more commonly, it will be supported on a carrier material that may or may not have catalytic activity of its own. The activity per unit volume is of practical significance because process economics are often strongly dependent on the cost of packed reactor space. Consequently, the catalyst should have a high specific surface area, and it should have a pore structure such that reactants can gain easy access to the inner surfaces of the catalyst pellet.

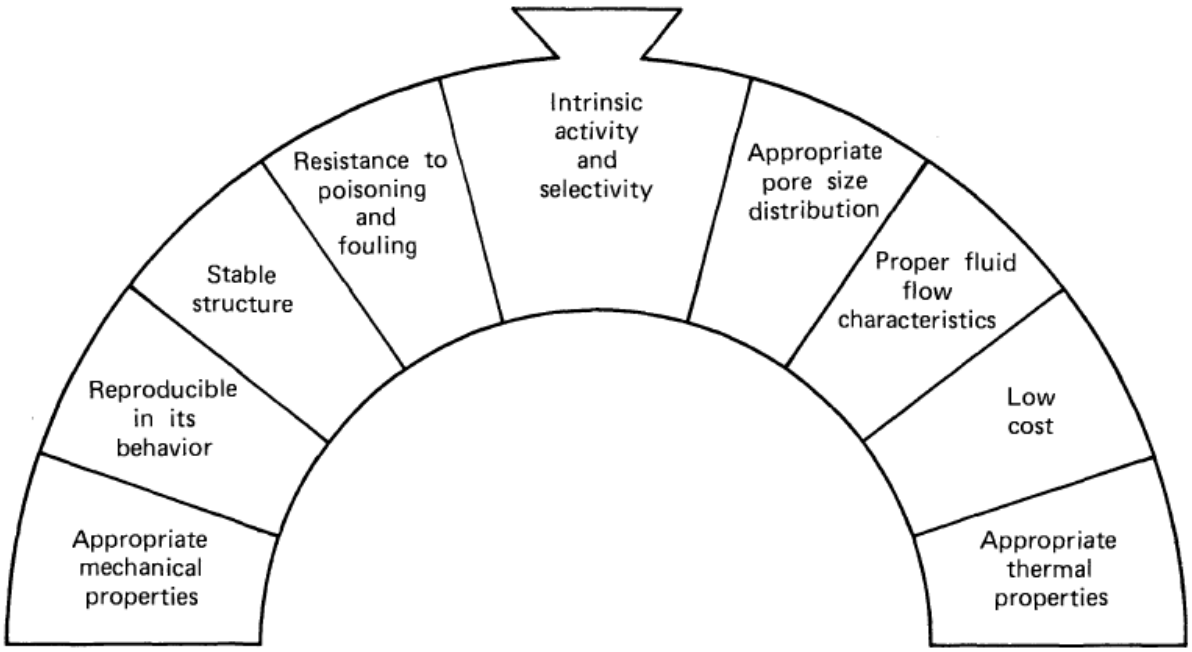


Figure 2.1: Requirements for industrial catalyst (Hill, 1977)

2.5.1 Commercial catalyst

The lifetime of a catalyst is another factor that plays a key role in determining process economics. This lifetime is the period during which the catalyst produces the desired product in yields in excess of or equal to a designated value. The life of a catalyst may terminate due to several reasons such as unacceptable changes in activity and/or selectivity, physical attrition, or because of unacceptable changes in mechanical properties arising from thermal cycling or other factors in the process environment. Resistance to poisoning and fouling as well as to other catalyst deactivation processes is an attribute to be preferred in commercial catalysts. Mechanical and geometric properties also play a strong role in determining if a given formulation will give rise to a commercially viable catalyst. The finished catalyst must also be mechanically robust to avoid attrition during handling and loading and to avoid crushing during operation.

2.5.2 Fluid catalytic cracking (FCC) catalysts

The need to upgrade less valuable petroleum products into gasoline has been recognized since around 1910. Catalysts are the heart of FCC units are the catalysts themselves. The development of active and stable FCC catalysts went parallel with the FCC design development. It was known, that for cracking of C-C bonds, the acid catalysts are needed (Hudec, 2011). Modern FCC catalysts are fine powders with a bulk density of 0.80 to 0.96 g/cm^3 and having a particle size distribution ranging from 10 to 150 µm and an average particle size of 60 to 100 µm (Hudec, 2011). A schematic diagram of a modern FCCU is shown in Figure 2.2.

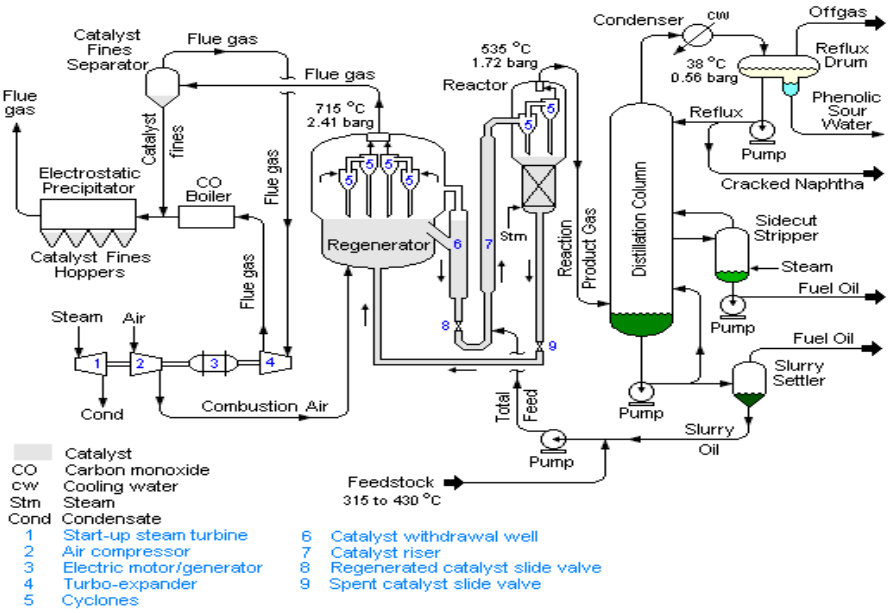


Figure 2.2: A schematic flow diagram of a FCCU in petroleum refineries (https://en.wikipedia.org/wiki/Fluid_catalytic_cracking)

The design and operation of an FCC unit is largely dependent upon the chemical and physical properties of the catalyst. The desirable properties of an FCC catalyst are:

i. Good stability to high temperature and to steam

ii. High activity

iii. Large pore sizes

iv. Good resistance to attrition

v. Low coke production

The major components of the compounded catalyst used in the FCC unit is shown in Figure 2.3. As of 2006, FCC unit were in operation at 400 petroleum refineries worldwide and about one-third of the crude oil refined in those refineries is processed in an FCC unit to produce high-octane gasoline and fuel oils (James, 2006; David, 2006).

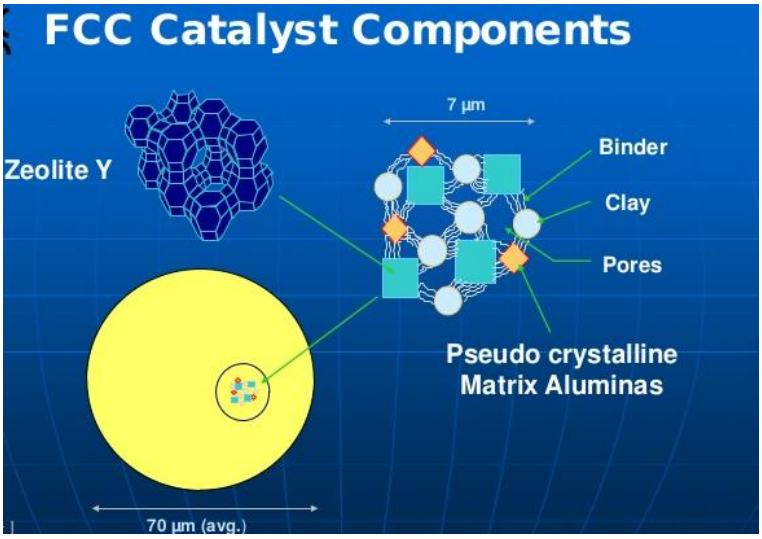


Figure 2.3: A typical composition of FCC catalyst (Hudec, 2011)

Generally, the philosophy of the FCC-catalyst preparation is: to have weak acid centers in macroporous part of catalyst particles to ensure pre-cracking of the great molecules of residue to smaller molecules which could enter to the mesopores with stronger acidity. Product of cracking in mesopores could finally enter the zeolite micropores to crack over strongest

zeolite acid centers into the smaller molecules, mainly gasoline fraction, as illustrated in Figure 2.4.

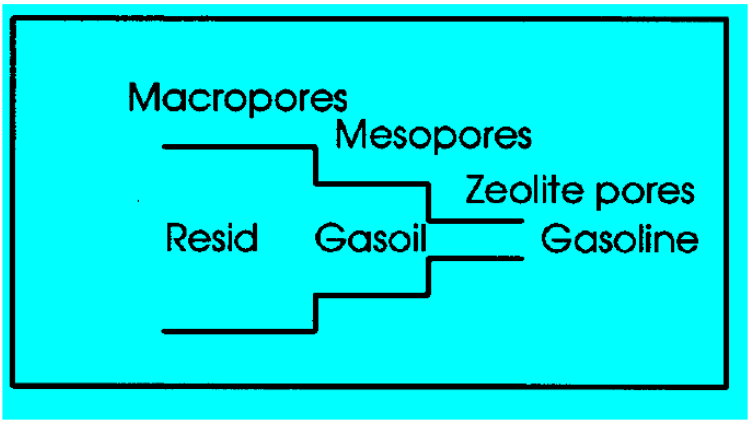


Figure 2.4: The role of different pore sizes in cracking of residues molecules to gasoline (Ajayi, 2012)

2.6 Zeolite

Zeolites are aluminosilicates compounds which are crystalline and possess uniform pores, channels and cavity. The basic elements in the structure of zeolite are aluminium, silicon and oxygen, in its frameworks it has cations and water within the pores. The structure formula for zeolite is based on the crystallographic unit cell, the smallest unit of structure, represented as: $M_{x/n}\left[(AlO_2)_X(SiO_2)_y\right].wH_2O$

where M is an alkali or alkaline earth cation, w is the number of water molecules per unit cell, x and y are the total number of tetrahedra per unit cell, and the ratio y/x usually has values of 1 to 5. In case of high silica zeolite, y/x can be ranging from 10 to 100 (Bekkum *et al*., 1991). The International Zeolite Association (IZA) database shows that the number of structural types of unique microporous frameworks has been growing rapidly, from 27 in 1970, to 38 in 1978, to 64 in 1988, to 98 in 1996, and to 133 in 2001. In 2007, this number has reached 174 (Cejka *et al*., 2010; Xu *et al*., 2007; Flanigen 2001; Dyer, 1988) and as at

2015, the number of IZA structures has increased to 225 (Li *et al*., 2015). It has been reported that over 20 elements may be introduced into zeolite frameworks, and taking into account the diversity of zeolite compositions, the number of unique zeolites might be enormous. These porous materials have also been extensively used in the detergent industry and in a variety of adsorption and separation processes such as the drying, the removal of CO_2 from, and the desulfurization for natural gas, and the separation of xylene isomers, of alkenes, and of O_2/N_2 from air. In the past half century, molecular sieves have played increasingly important roles as catalysts in the petroleum refining, petrochemical, and other chemical industries (Cejka *et al*., 2010).

Mesoporous materials have the advantages of ordered mesoporous channels with size of 2-50 nm, as well as very large specific surfaces and pore volumes. However, since the channels in these materials are surrounded by amorphous walls, mesoporous materials have less thermal and hydrothermal stability than do microporous molecular sieves.

2.6.1 Natural zeolite

Natural zeolites were first discovered in cavities and vugs of basalts in 1756. During the 19th century, the microporous properties of natural zeolites and their usefulness in adsorption and ion exchange were gradually recognized (Xu *et al*., 2007; Oliver, 2000). The first natural microporous aluminosilicates, i.e., natural zeolite, was discovered more than 200 years ago, and after long-term practical applications, the intrinsic properties of natural zeolites such as reversible water-adsorption capacity were fully recognized. By the end of the 19th century, during exploitation of ion-exchange capacity of some soils, it was found that natural zeolites exhibited similar properties: some cations in natural zeolites could be ion-exchanged by other metal cations. Meanwhile, natural chabazite could adsorb water, methanol, ethanol, and

formic acid vapor, but could hardly adsorb acetone, diethyl ether, or benzene. Soon afterwards, scientists began to realize the importance of such features, and use these materials as adsorbents and desiccants. Later, natural zeolites were also used widely in the field of separation and purification of air (Xu *et al.*, 2007; Cheetham *et al*.,1999).

Over 40 types of natural zeolites have been found, but fewer than 30 of them have had their structures solved (www.chemistryexplained.com/Va-Z/Zeolite.html,march2216). Natural zeolites are widely used in the fields of drying and separation of gases and liquids, softening of hard water, treatment of sewage, and melioration of soils. Some well selected or modified natural zeolites are also used as catalysts or supports of catalysts in industry.

2.6.2 Synthetic zeolite

However, it was not until the 1940s that a series of zeolites with low Si/Al ratios were hydrothermally synthesized through mimicking of the geothermal formation of natural zeolites. The successful synthesis of zeolites laid the foundation for rapid development of zeolite industry in the 20th and 21st centuries (Xu *et al*, 2007; Guisnet *et al*., 2002).

Natural zeolites could not meet the huge demands in industry, it becomes an urgent necessity to use synthetic zeolites besides the natural ones. Synthetic zeolite came on board in 1940s (Xu *el. al*., 2007) when a series of zeolites with low Si/Al ratios were hydrothermally synthesized through mimicking of the geothermal formation of natural zeolites. The successful synthesis of zeolites laid the foundation for rapid development of zeolite industry in the 20th and 21st centuries.

The application of low-temperature hydrothermal techniques facilitated the extensive industrial production of zeolites. By the end of 1954, zeolites A and X began to be produced

industrially. Following this, a number of companies in the United States, such as Linde, Mobil, and Exxon, imitated the formation of natural zeolites and produced a series of synthesized zeolites with an intermediate Si/Al ratio (Si/Al = 2–5), including NaY, mordenite, zeolite L, erionite, chabazite, clinoptilolite, and so on. These zeolites were widely applied in the fields of gas purification and separation, catalytic processes of petroleum refining and petrochemistry, and ion exchange.

Since the 1960s, zeolites have been widely used as catalysts and catalyst supports in petroleum refining. At present, zeolites have become the most important adsorbents and catalysts in the petroleum industry. The period from 1954 to the early 1980s is the golden age for the development of zeolites. Zeolites with low, medium, and high Si/Al ratios were extensively explored, and this greatly facilitated the applications of zeolites and stimulated industrial progress (Monnier *et al*., 1993). In order to increase the thermal stability and acidity of zeolites, Breck et al., (2007) synthesized zeolite Y (Si/Al=1.5~3.0), which played an extremely important role in the catalysis of hydrocarbon conversion (Xu *et al*., 2007).

In the past 25 years, the emergence of zeolites with low (Si/Al=1.0~1.5), medium (Si/Al=2.0~5.0), and high Si/Al ratios (Si/Al=10~100), as well as pure-silica zeolites, facilitated the study of both the structure and property of molecular sieves and porous compounds, and promoted their applications. Because of their excellent ion-exchange capacities, zeolites A and X can be used as auxiliary agents in the detergent industry, in radioactive waste treatment and storage, and in the treatment of industrial liquid wastes.

2.6.3 Global zeolite production and applications

Research has shown the trend of zeolite demand and the review generated from zeolite market in a global scale, which is represented in a bar chat in Figure 2.5. Zeolite continues to experience a favorable market even into the near future. The three major key areas where zeolite is needed in terms of the application are in detergent builder, adsorbent and catalysis as shown in Figure 2.6. Figure 2.7 enumerates other sectors where zeolite is of great importance.

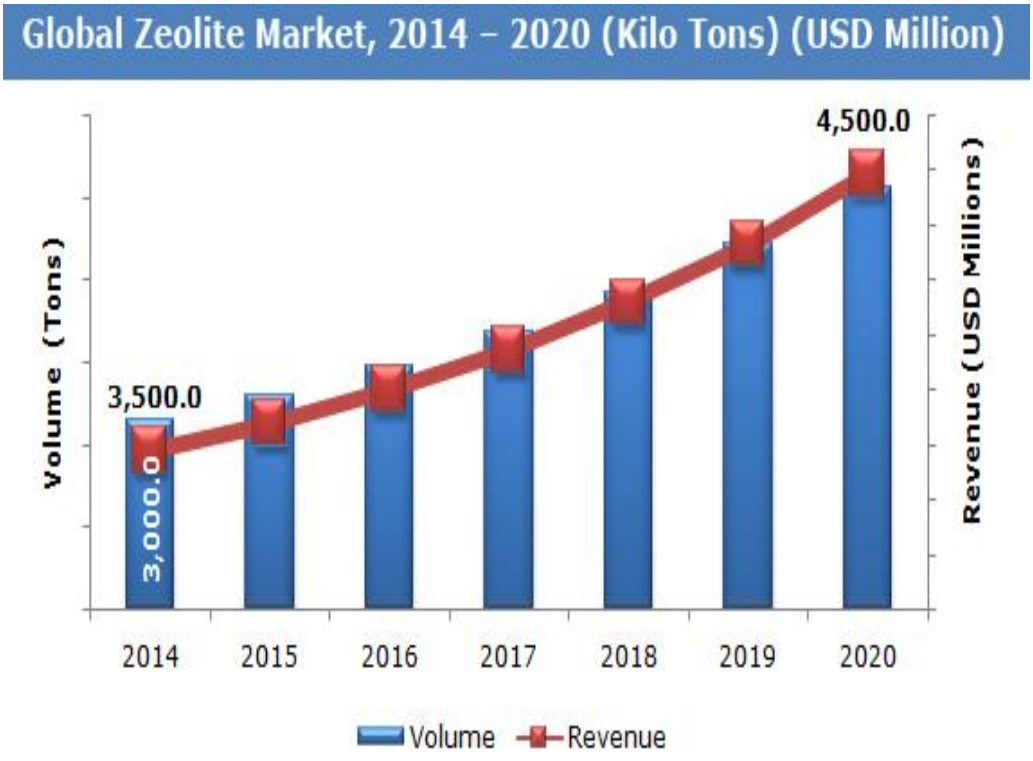


Figure 2.5: Global zeolite market chat (Zion research analysis, 2015)

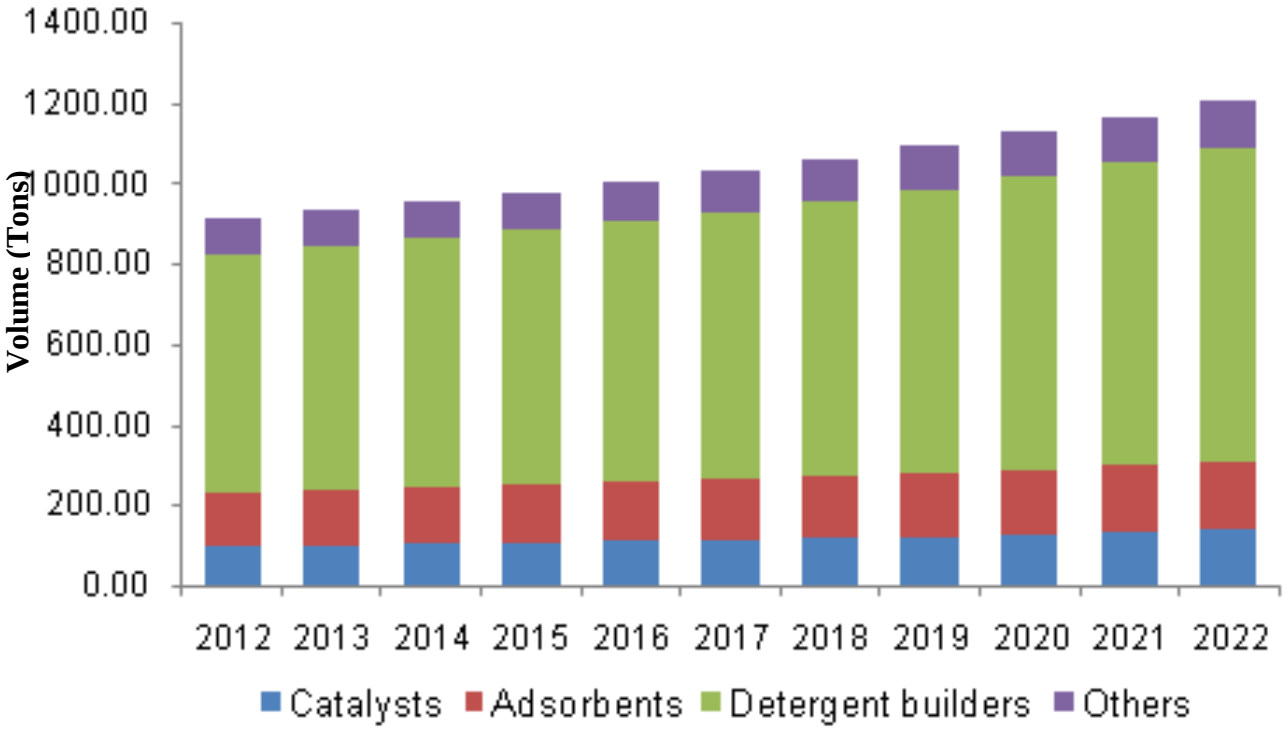


Figure 2.6: Zeolite major consumption by application (Zion research analysis, 2015)

Zeolites are used in wide range of commercial and domestic applications. Major applications include; usage as adsorbents, catalysts for petroleum refining and petrochemical processes, and ion exchangers in water purification (Cejka *et al*., 2010). They are majorly used as detergent builder and auxiliary agents in the soap and detergent industry. Figure 2.6, gives an estimate of major areas where zeolite is used. Some key sectors that employ the use of zeolite are shown in Figure 2.7.

Zeolite Y and ZSM-5 are two of the most important zeolites used as FCCU catalyst. In fact, ZSM-5 is regarded as good octane booster. The application of zeolites has its largest economic impact in the FCC processes (Weitkamp, 1999).

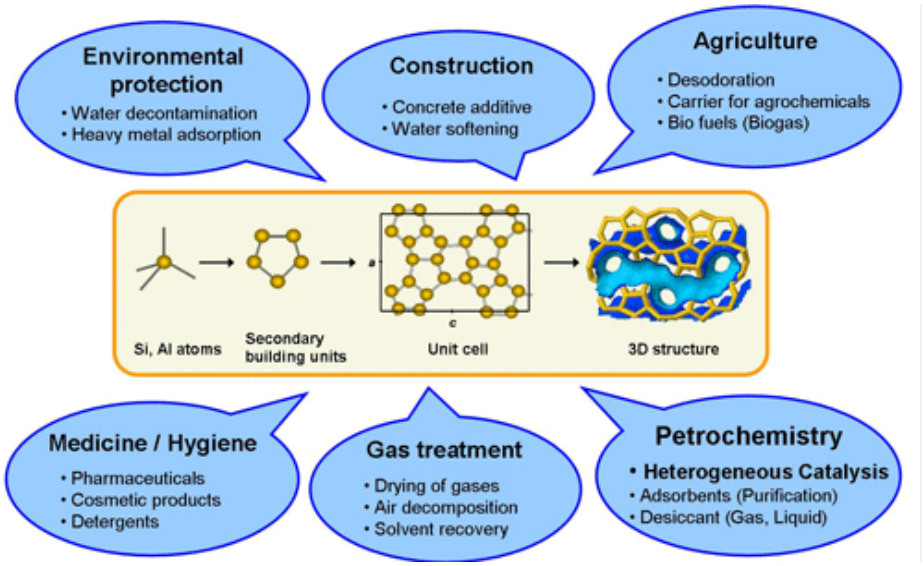


Figure 2.7: Some common applications of zeolite (Weitkamp, 1999)

2.6.4 Zeolite Y

Zeolites Y based catalysts is valuable in many important catalytic applications involving hydrocarbon conversion since their initial commercial introduction in 1959 (Baerlocher *et al*., 2007). The most important use of zeolite Y is as a cracking catalyst, the chemical formula for NaY is $Na_7(AlO_2)_7(SiO_2)_{17}$:$32H_2O$. Zeolite Y exhibits the FAU (faujasite) structure. Zeolite Y has a void volume fraction of 0.48, with a Si/Al ratio > 1.5. It thermally decomposes at 793ºC. Zeolite Y has superseded zeolite X in this use because it is both more active and more stable at high temperatures due to the higher Si/Al ratio. It is also used in the hydrocracking units as a platinum/palladium support to increase aromatic content of reformulated refinery products (Bhatia, 1990). The faujasite structure is similar to the LTA structure however, the sodalite cage is linked with double 6-ring resulting in a super cage with 12 ring pore opening as shown in Figure 2.8. It has 3-dimensional channel system and can be imagined as stacking layers of sodalite cages similar to the arrangement of carbon atoms in diamond (Dyer, 1988).

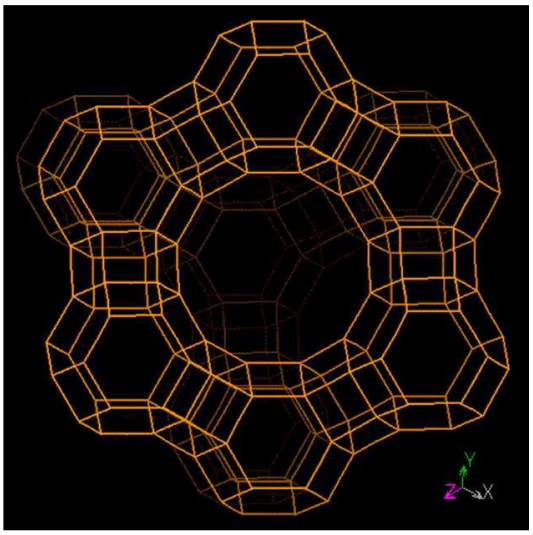


Figure 2.8: Zeolite structure type FAU (Chandrasekhar, 1999)

2.6.5 ZSM-5

ZSM-5, which means Zeolite Sieve of Molecular porosity (or Zeolite Socony Mobil – 5), structure type MFI – mordenite framework inverted is an aluminosilicate zeolite mineral belonging to the pentasil family of zeolites. Its chemical formula is H_m $[(AlO_2)_m$ $(SiO_2)_{96-m}]$ $.16H_2O$. $(0 < m < 27)$. At the beginning of the 1960s, scientists at Mobil Corporation started to use organic amines and quaternary alkylammonium cations as templates in the hydrothermal synthesis of high-silica zeolites, and this is considered a milestone in the progress of zeolite synthesis. In 1972, Argauer and Landelt synthesized the first important member of the pentasil family, ZSM-5, using Pr_4NCl or Pr_4NOH as the template at 120 °C (Kordatos, *et. al*., 2008), whereas in 1973, Chu synthesized ZSM-11 using Bu4Nþ as the template. In 1974, Rosinski and Rubin prepared ZSM-12 using Et_4Nþ as the template, followed by the syntheses of ZSM-21 and ZSM-34 in 1977 and 1978; later on, Wadlinger and Kerr synthesized high-silica zeolite beta (BEA) (Xu et al., 2007). The 10-ring channel system gives ZSM-5 a unique shape selectivity property, as shown in Figure 2.9, which allow

it to be widely used in catalysis and sorption, it is an important source of catalyst in petroleum refining and petrochemical industry and they are even better utilized than zeolite Y (Jiri *et al*., 2007).

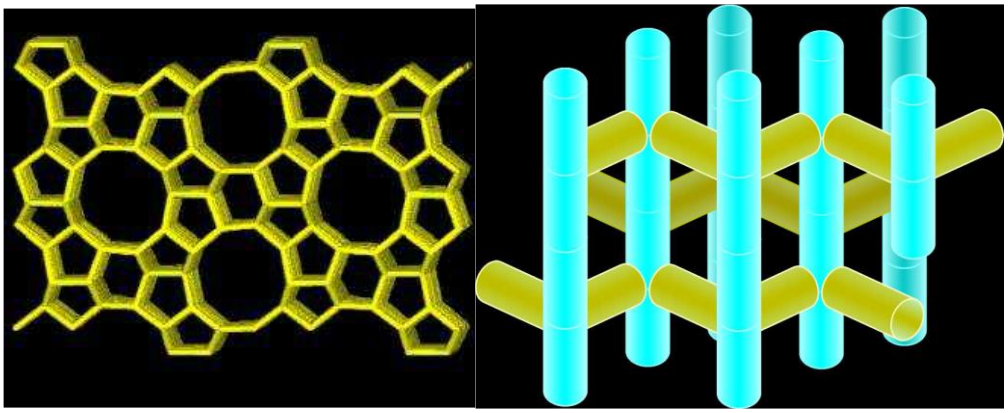


Figure 2.9: Zeolite structure type MFI ((e.g. ZSM-5) and their porous network
(http://chemeducator.org/sbibs/s0004003/spapers/430114wv.htm)

ZSM-5 pore size is of a dimension 0.54-0.56 nm. The nature of its pore structure is unique and is excellent in shape selectivity, while the ability to develop internal acidity makes it an interesting material for catalytic reactions. The possibility of synthesizing ZSM-5 at temperatures between 90 to 100 °C and atmospheric pressure has also been reported. Among the several templates used for the synthesis of ZSM-5, the most common is tetrapropyl ammonium bromide (TPABr) (Kordatos, *et. al*., 2008). ZSM-5 is a zeolite with a high silica and low aluminium content. The reaction and catalysis chemistry of the ZSM-5 is due to this acidity. The ZSM-5 zeolite catalyst is used in the petroleum industry for hydrocarbon inter-conversion.

2.7 Kaolin

Kaolin commonly called china clay consists mainly of kaolinite mineral and has the empirical formula of $Al_2Si_2O_5(OH)_4$. The major components are silica and alumina, with associated

impurities such as quartz, mica, feldspar, illite, kyanite, montmorrillonite and haematite (Aroke *et al*., 2013; Mgbemena *et al*., 2013; Vaculikova *et al*., 2011). Kaolin is also a dioctahedral 1:1 layered clay mineral, whose structure is a tetrahedral silica sheet alternating with an octahedral alumina sheet. The sheets are arranged so that the tips of the silica tetrahedrons and the adjacent layers of the octahedral sheet form a common layer. (Aroke *et al*., 2013). The kaolinite group include kaolinite, nacrite and dickite, It is made up of pseudohexagonal flexible sheets of triclinic crystals with a diameter of 0.2-12 μm, with density of 2.1-2.6 g/cm^3 (Christopher *et al*., 2002).

2.7.1 Kaolin purification

Kaolin is usually mined in it impure form. Accordingly, the accompanying minerals here termed inherent impurities impair the primary characteristics of kaolin and affect its utility for various end applications (Saikia, *et al*., 2003). Deposits of kaolin are usually associated with various impurities like quartz, anatase, rutile, pyrite, siderite, feldspar, etc, depending on the origin and depositional environment (Grimshaw, 1971). Improvement on the properties of kaolin by chemical methods is difficult, because of the high passivity of this material (Belver *et al.,* 2002). The processes of kaolin upgrading include sieving, magnetic separation (Asmatulu, 2002; Shoumkov, *et al*., 1987), selective flocculation (Farhount, 1989), application of ultrasound (Komskaja, *et al*., 1971), leaching with various chemicals like oxalic acid and other organic acids (Veglio *et al*., 1996; Ambikadevi and Lalithambika, 2000). Combination of various methods of beneficiation are applied for kaolin treatment, namely; wet method (i.e. soaking and sieving), deflocculating, thermal and acid treatment. Additionally, most by-products resulting from use of chemical method of purification, as highlighted before, might possess challenges during separation procedure.

2.7.2 Thermal treatment of kaolin

Upon heating, kaolin starts to lose water at approximately 450°C, and the dehydration approaches completeness at about 525°C (Christopher *et al*., 2002). The water vapor in Equation (2.2) carries away about 13.96% of the mass of the stoichiometric kaolinite during dehydroxylation, which occurs primarily on the phase boundary. A mechanism of dehydroxylation includes a transport of OH- groups to the phase boundary, then the reaction of the groups on the boundary and, finally, transport of the products to the edge of the crystal.

$$Al_2Si_2O_5(OH)_{4(s)} \xrightarrow{450 - 600°C} Al_2Si_2O_{7(s)} + 2H_2O_{(g)} \quad (2.2)$$

The rate of dehydroxylation is determined by the slowest process. It was revealed that this process is diffusion of the water molecules between layers of the kaolinite structure (Kozik *et al*., 1992; Horvăth, 1976; Toussaint *et al*., 1963). In kaolinite, the hydroxyl ions are strongly bonded to the aluminosilicate framework structure and can only be eliminated at temperatures above 450 °C. During the dehydroxylation process, considerable atomic rearrangement occurs (Granizo *et al*., 2000; Madani *et al*.,1990 and Alkan *et al*.,2005). The conditions of kaolin calcinations strongly influence the reactivity of the solids obtained; the best conditions for obtaining very reactive metakaolin have been discussed by different authors who reported values between 600 and 800°C (Belver *et al*., 2002). Since the transformation temperature ranges from 600 to 900°C, various authors have declared that the temperature of calcinations affects the rate of dealumination and phase of zeolite formed (Chandrasekhar, 1996; Chandrasekhar and Pramada, 1999; Feng *et al*., 2009). The relationship between calcinations temperatures and solubilities of active SiO_2 and Al_2O_3 is presented in Figure 2.10.

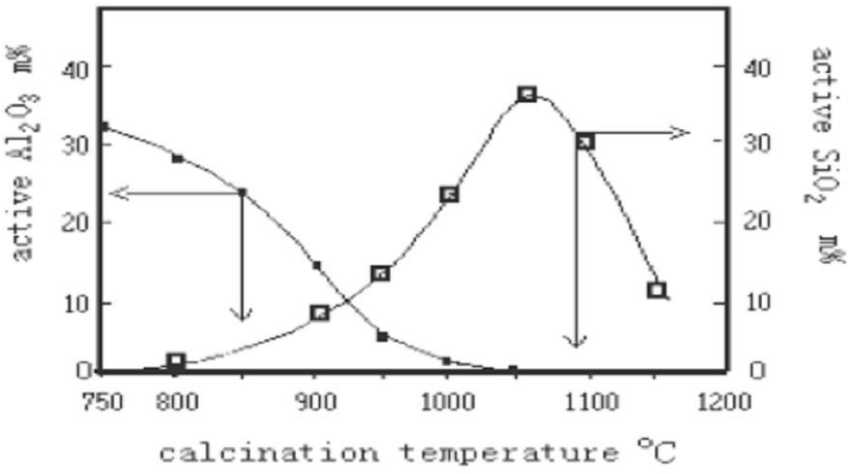


Figure 2.10: Relationship between calcinations temperatures and activity of SiO_2 and Al_2O_3 (Ajayi, 2012)

2.7.3 Acid leaching of metakaolin

The acid activation of metakaolin has been reported in various articles (Caballero *et al.*, 2007; Colina *et al*., 2002, Aderemi, 2000; Hanzliček *et al*., 2002; Hulbert and Huff, 1970). These reports showed that metakaolin is more reactive and is easily attacked by acid and alkaline, causing partial destruction of the metakaolin structure which dependent on the concentration of the acid or alkaline and the reaction time. The unlocking of the alumina component in the metakaolin *via* acid means is referred to as dealumination. Silica which is inert to most acid is one of the products of the dealumination process. The reaction of dealumination is represented in Equation (2.3).

$$Al_2Si_2O_7 + 3H_2SO_4 \longrightarrow Al_2(SO_4)_3 + 2SiO_2 + 3H_2O \qquad (2.3)$$

2.7.4 Application of kaolin

Kaolin is widely used in the paper industry for its high whiteness and low abrasion. It is also used in the other industries like construction, ceramics, rubber and porcelain manufacturing

(Vaculikova *et al*., 2011). As food additive, in toothpaste, as a light diffusing material in white incandescent light bulbs and cosmetics (Mgbemena *et al*., 2013). Kaolin is used in paint production to extend titanium dioxide and modify gloss levels, for semi-reinforcement properties in rubber (Krishnan *et al*., 2012; Songfang et al., 2011; Ma and Bruckard, 2010). Summary of the estimated usage of kaolin is shown in Figure 2.11.

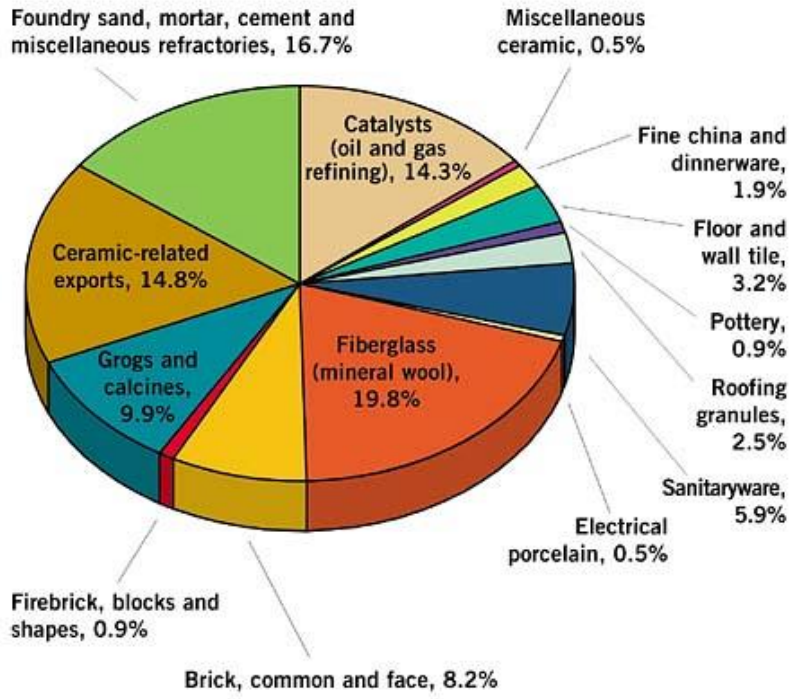


Figure 2.11: Different application areas of kaolin (http://eicl.in/about/wiki/kaolin/)

2.7.5 Occurrence of kaolin in Nigeria

According to Sheik (1999), the Nigerian clay deposits are basically of two types - the basement derived or residual clay and the sedimentary or detrital clay. Most Nigerian detrital clay deposits were probably laid down as sedimentary mud in the ancient marine and blackish water environment. This is most likely the reason for the high content of inherent impurities, found in some Nigerian kaolinite clays. Figure 2.12 shows kaolin and other mineral deposits found across the Nation.



Figure 2.12: Nigeria map showing some mineral deposit (Ahmed, 2012)

2.8 Material Characterization

Materials are often identified through various techniques namely, chemical composition analysis using Energy Dispersive X-ray Flourescence (EDXRF), mineral structure identification using X-ray Diffraction (XRD), surface bond type identification using Fourier Transform Infrared Spectroscopy (FTIR), shape structure, particle size and morphology using Scanning Electron Microscopy (SEM) and Braunner-Emmett-Teller (BET) surface area measurement.

2.8.1 Energy dispersive x-ray fluorescence

XRF spectroscopy is an analytical technique that exposes a solid sample to an x-ray source. The X-rays from the source have the appropriate excitation energy that causes elements in the sample to emit characteristic X-rays. A qualitative elemental analysis is possible from the characteristic energy, or wavelength, of the fluorescent x-rays emitted. A quantitative elemental analysis is possible by counting the number (intensity) of x-rays at a given wavelength (Verma, 2007). Three electron shells are generally involved in emissions of x-rays during XRF analysis of samples as represented in Figure 2.13: The K, L, and M shells. Multiple-intensity peaks are generated from the K, L, or M shell electrons in a typical emission pattern, also called an emission spectrum, for a given element. The focus of XRF analysis is directed on the x-ray emissions from the K and L shells because they are the most energetic lines. K lines are typically used for elements with atomic numbers from 11 to 46 (sodium to palladium), and L lines are used for elements above atomic number 47 (silver). M-shell emissions are measurable only for metals with an atomic number greater than 57 (lanthanum) (Ajayi, 2012).

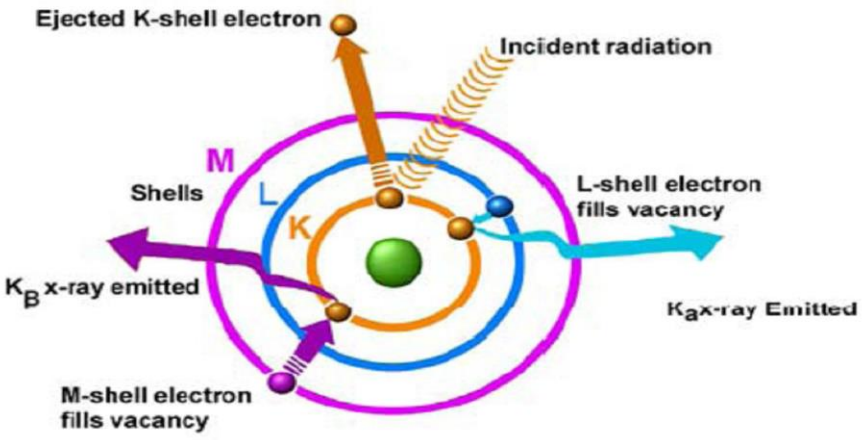


Figure 2.13: XRF analysis process (Kovo, 2011)

2.8.2 X-ray powder diffraction

X-ray powder diffraction (XRD) is a rapid analytical technique primarily used for phase identification of a crystalline material. X-ray diffraction is now a common technique for the study of crystal structures and atomic spacing. X-ray diffraction is based on constructive interference of monochromatic X-rays and a crystalline sample. These X-rays are generated by a cathode ray tube, filtered to produce monochromatic radiation, collimated to concentrate, and directed toward the sample. The interaction of the incident rays with the sample produces constructive interference (and a diffracted ray) when conditions satisfy Bragg's Law ($n\lambda=2d \sin \theta$). This law relates the wavelength of electromagnetic radiation to the diffraction angle and the lattice spacing in a crystalline sample. These diffracted X-rays are then detected, processed and counted. By scanning the sample through a range of 2θ angles, all possible diffraction directions of the lattice should be attained due to the random orientation of the powdered material. Conversion of the diffraction peaks to d-spacings allows identification of the mineral because each mineral has a set of unique d-spacings. Typically, this is achieved by comparison of d-spacings with standard reference patterns (Weller, 1994).

X-ray diffractometers consist of three basic elements: An X-ray tube, sample holder, and an X-ray detector. X-rays are generated in a cathode ray tube by heating a filament to produce electrons, accelerating the electrons toward a target by applying a voltage, and bombarding the target material with electrons. When electrons have sufficient energy to dislodge inner shell electrons of the target material, characteristic X-ray spectra are produced. These spectra consist of several components, the most common being Kα and Kβ. Kα consists, in part, of Kα1 and Kα2. Kα1 has a slightly shorter wavelength and twice the intensity as Kα2. The

specific wavelengths are characteristic of the target material (Cu, Fe, Mo, Cr). Filtering, by foils or crystal monochrometers, is required to produce monochromatic X-rays needed for diffraction. Kα1and Kα2 are sufficiently close in wavelength such that a weighted average of the two is used. Copper is the most common target material for single-crystal diffraction, with Cu Kα radiation = 1.5418Å. These X-rays are collimated and directed onto the sample. As the sample and detector are rotated, the intensity of the reflected X-rays is recorded. When the geometry of the incident X-rays impinging the sample satisfies the Bragg Equation, constructive interference occurs and a peak in intensity occurs. A detector records and processes this X-ray signal and converts the signal to a count rate which is then output to a device such as a printer or computer monitor. The geometry of an X-ray diffractometer is such that the sample rotates in the path of the collimated X-ray beam at an angle θ while the X-ray detector is mounted on an arm to collect the diffracted X-rays and rotates at an angle of 2θ. The instrument used to maintain the angle and rotate the sample is termed a goniometer (Ajayi, 2012; Clearfield *et al*., 2008; Duane and Robert, 1997).

2.8.3 Fourier transform infrared spectroscopy

Fourier transform infrared spectroscopy is most useful for identifying chemicals that are either organic or inorganic. It can be utilized to quantitate some components of an unknown mixture. It can be applied to the analysis of solids, liquids, and gases. The term Fourier Transform Infrared Spectroscopy (FTIR) refers to a fairly recent development in the manner in which the data is collected and converted from an interference pattern to a spectrum. Today's FTIR instruments are computerized which makes them faster and more sensitive than the older dispersive instruments. FTIR is perhaps the most powerful tool for identifying types of chemical bonds (functional groups). The wavelength of light absorbed is

characteristic of the chemical bond as can be seen in this annotated spectrum. By interpreting the infrared absorption spectrum, the chemical bonds in a molecule can be determined. FTIR spectra of pure compounds are generally so unique that they are like a molecular "fingerprint". Because the strength of the absorption is proportional to the concentration, FTIR can be used for some quantitative analyses (Ajayi, 2012).

2.8.4 Braunner-Emmett-Teller (BET) surface area measurement

The gas adsorption method is used for measuring the amount of gas adsorbed on the surface of a powder sample as a function of the pressure of the adsorbate gas, and is used to determine the specific surface area of a powder sample. When the gas is physically adsorbed by the powder sample, Equation (2.4) holds when P/P_0 is in the range of 0.05 to 0.30 for pressure P of the adsorbate gas in equilibrium for the volume of gas adsorbed, V_a.

$$\frac{1}{V_a\left(\frac{P_0}{P}-1\right)} = \frac{(C-1)}{V_m C} \times \frac{P}{P_0} + \frac{1}{V_m C} \tag{2.4}$$

where, P = Partial vapor pressure of adsorbate gas in equilibrium, (kPa); P_0 = Saturated pressure of adsorbate gas; V_a = Volume of gas adsorbed at equilibrium, ml; V_m = Volume of gas adsorbed in a monolayer, ml; C= Dimensionless constant related to the enthalpy of adsorption and condensation of the adsorbate gas (Rouquerol *et al*., 1999).

The specific surface area, S, is determined from V_m the volume of gas adsorbed in a monolayer on the sample as shown in Equation (2.5).

$$S = \frac{V_m \times N \times a}{m \times 22400} \tag{2.5}$$

S = Specific surface area, m^2/g; N = Avogadro constant; a = Effective cross-sectional area of one adsorbate molecule, m^2; m = mass of the test powder, g (Everelt, 2006).

2.8.5 Scanning electron microscope

The scanning electron microscope (SEM) is a type of electron microscope that images the sample surface by scanning it with a high-energy beam of electrons in a raster scan pattern. The electrons interact with the atoms that make up the sample producing signals that contain information about the sample's surface topography, composition and other properties such as electrical conductivity. There are basically two types of interaction between the electron beam and the samples. These are called elastic and inelastic interaction as shown in Figure 2.14. The type of signals produced by a SEM include secondary electrons, back-scattered electrons (BSE), characteristic X-rays, light (cathode luminescence), specimen current and transmitted electrons. Secondary electron detectors are common in all SEMs, but it is rare that a single machine would have detectors for all possible signals. The signals result from interactions of the electron beam with atoms at or near the surface of the sample. In the most common or standard detection mode, secondary electron imaging or SEI, the SEM can produce very high-resolution images of a sample surface, revealing details about less than 1 to 5 nm in size. Due to the very narrow electron beam, SEM micrographs have a large depth of field yielding a characteristic three-dimensional appearance, useful for understanding the surface structure of a sample (Goldstein *et al*., 1981).

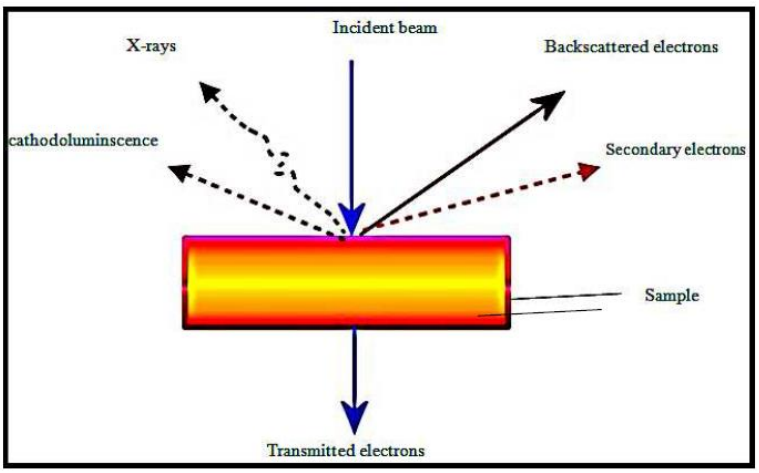


Figure 2.14: Interaction of incident rays with sample (Goldstein, 1981)

When the primary electron beam interacts with the sample, the electrons lose energy by repeated random scattering and absorption within a teardrop-shaped volume of the specimen known as the interaction volume, which extends from less than 100 nm to around 5 μm into the surface. The size of the interaction volume depends on the electron's landing energy, the atomic number of the specimen and the specimen's density. The energy exchange between the electron beam and the sample results in the reflection of high-energy electrons by elastic scattering, emission of secondary electrons by inelastic scattering and the emission of electromagnetic radiation, each of which can be detected by specialized detectors. Electronic amplifiers of various types are used to amplify the signals which are displayed as variations in brightness on a cathode ray tube. The raster scanning of the CRT display is synchronized with that of the beam on the specimen in the microscope, and the resulting image is therefore a distribution map of the intensity of the signal being emitted from the scanned area of the specimen. The image is captured and displayed on a computer monitor and saved to a computer's hard disc. Magnification in a SEM can be controlled over a range of up to 6 orders of magnitude from about 10 to 500,000 times.

CHAPTER THREE

MATERIALS, EQUIPMENT AND METHODOLOGY

3.1 Introduction

The materials used during the research are stated in this chapter. All the equipment used during the production process and characterization as well as the methods employed are also documented in this chapter.

3.2 Materials and Apparatus

3.2.1 Materials

The materials used during this research include:

1. Kankara kaolin (Katsina, Nigeria) : The location is shown in Figure 3.1 and the deposit site is shown in Plate I.

2. Distilled and deionized water

3. Concentrated sulfuric acid (Lobal Chemie, 98%)

4. Sodium hydroxide pellets (Lobal Chemie, ≥98%)

5. Amorphous silica (Prepared from Kankara kaolin)

6. Sodium silicate solution (Prepared from Kankara kaolin)

7. Aluminum hydroxide (Prepared from Kankara kaolin)

8. Activated alumina (Sigma-Aldrich)

9. Barium chloride (Chemlight)

10. Silica sol (prepared from Kankara kaolin)

11. Lanthanum chloride (Fisher Chemicals)

12. Ammonium chloride (Fisher Chemicals)

13. Tetrapropylammonium bromide (TPABr) (Sigma-Aldrich)

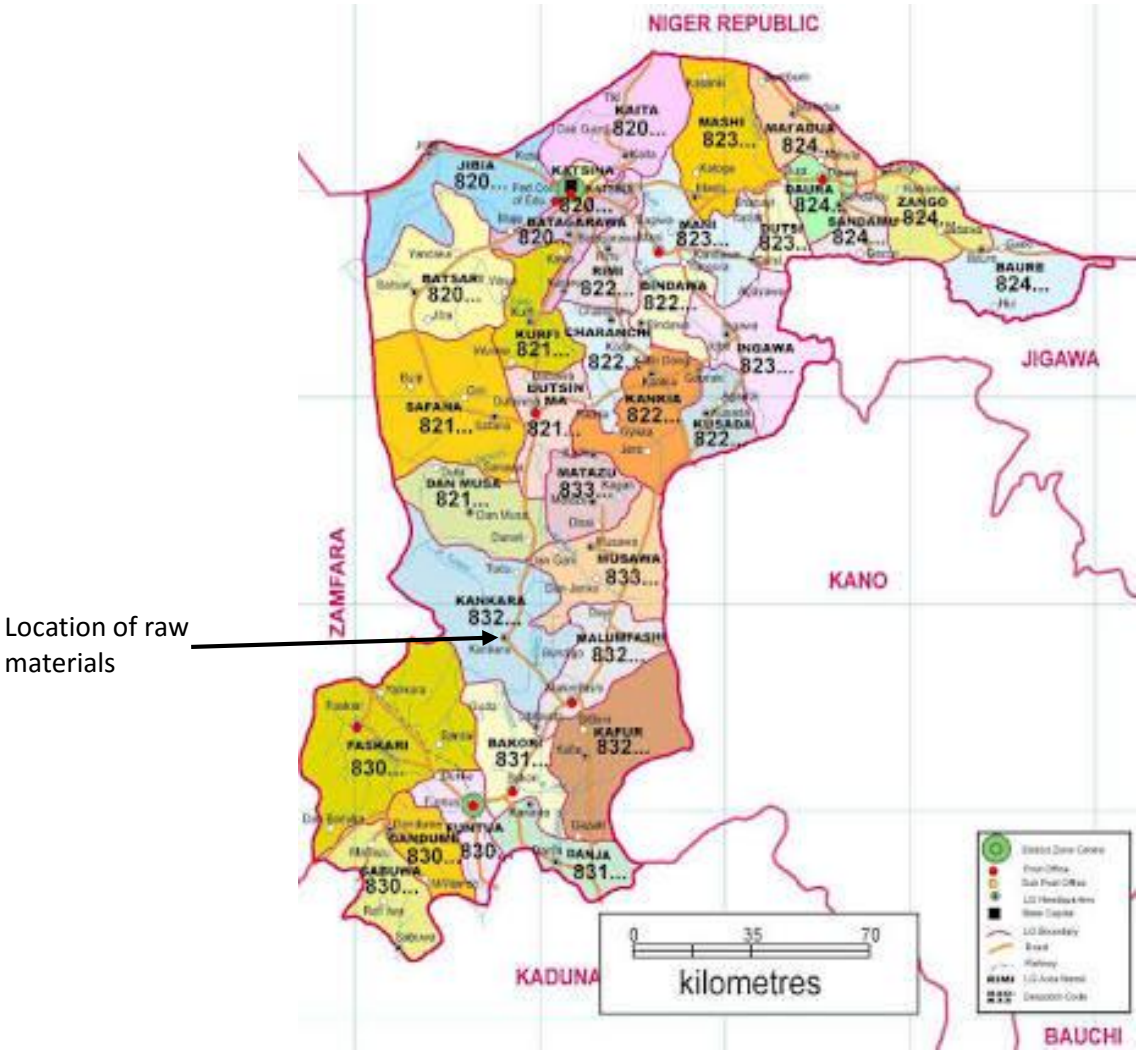


Figure 3.1: Location of Kankara kaolin in Katsina State, Nigeria (www.maps-steetview.com)

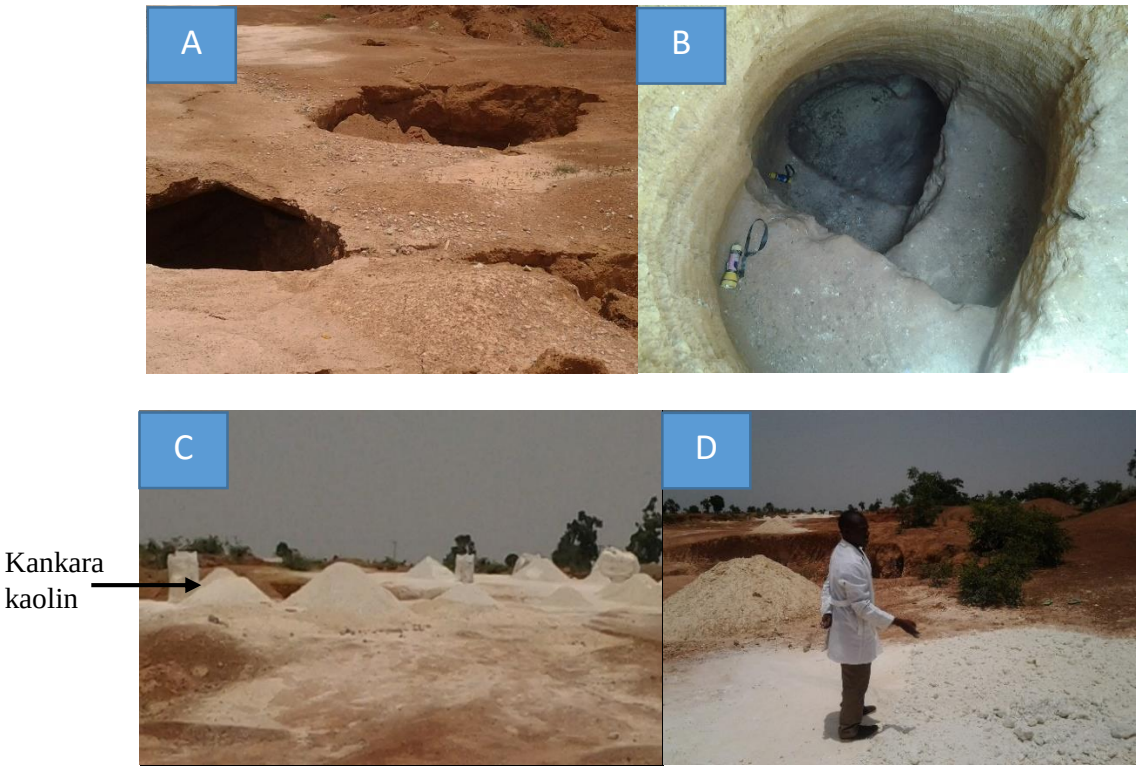


Plate I: Site of Kankara kaolin (a) Collapse pit (b) active pit (c) heaps of mined Kankara kaolin (d) atmospheric drying of Kankara kaolin

3.2.2 Apparatus

1. Measuring cylinders, 1000 ml (Superior, W-Germany)

2. Polypropylene bottles, 25000 ml (China)

3. Spatula

4. Tong

5. Wash bottles and brushes (plastic types)

6. Petri dishes

7. Tyler mesh sieve (Mesh size 200)

8. Ceramic Buckner funnel, (Graopiex, England)

9. Ceramic crucibles (500 ml and 1000 ml)

10. Air tight desiccator (Technico, England)

11. Ceramic mortar and pestle

12. Filter papers (Whatman, 1-541)

13. Full range pH paper (BDH, 1-14)

14. Plastic funnels (Techmel, USA)

3.3 Equipment

1. Electric furnace. (Nabertherm; 30 - 1400°C)

3. Electric ovens (NYC – 101; 30 - 400°C, and Nabertherm; 30 - 650°C)

4. Weighing balances (Weda, T18; 0 – 100kg, Metler Toledo; AB204; 0 - 210g)

5. High vacuum pump (Edwards, E2M5)

8. High torque stirrer (Trieb, 73 – 660 rpm)

9. Heavy duty laboratory high shear mixer (Silverson, L2R)

10. Hot plate with magnetic stirrer (AMTAST, MS300)

11. Water Deionizer (LAB-IoN, 5R2)

12. Water distiller (Lasany, LPH-4)

13. Ball milling machine (Overveld, 12254)

14. Ultrasonicator (Heating – ultrasonic, 350)

3.4 Design Stage

Manual design method was largely employed in this work, alongside Microsoft Excel was used for computation and plotting of graphs. AutoCAD was use for the engineering drawings. A The dealumination and zeolite reaction units were the units designed in this work.

3.4.1. Dealumination unit

The dealumination unit comprises of:

i. Dealumination reactor (dealuminator)
ii. Metakaolin slurry mixing tank, and
iii. Acid holding tank

3.4.1.1 Dealuminator

Batch reactor model was chosen for the design of the dealuminator due to the following reasons:

• Easy and simple instrumentation is possible with the batch reactor, since the proposed pilot-size reactor is expected to handle 2.5 kg of metakaolin per batch.

• Desired conversion and kinetic data can be easily generated as reaction progresses in a batch reactor. Hence aiding optimization of operating conditions.

• Because the initial slurry is a pseudo plastic heterogeneous mixture with clogging abilities (by Geldart classification, a type C or cohesive particles), efficient agitation, a condition required for effective mass and energy transfer during the dealumination reaction can be easily achieved via batch reaction.

• Cost of fabrication due to lesser requirement for instrumentation and automation is reduced with a batch reactor.

The capacity of the dealumination unit is to handle the dealumination of **2.5 kg metakaolin per batch (basis):** Average alumina content from X-ray fluorescence (XRF) analysis = 40%. Equation (3.1) shows the reaction during dealumination, as acid reacts with alumina content of the metakaolin.

$$Al_2Si_2O_{7\,(s)} + 3H_2SO_{4\,(l)} \longrightarrow Al_2(SO_4)_{3(l)}.3H_2O + 2SiO_{2\,(s)} \qquad (3.1)$$

Metakaolin Sulphuric acid Alum Silica

Detail calculation for the dealuminator design and the dealumination reaction time were done from the basics and presented in Appendices A and B respectively. Equation (3.2) which was adopted from the work of Aderemi *et al*, (2001) was used as the kinetic model.

$$-r_{Al} = 131.6e^{\frac{-3837.8}{T}}C_{Ac0}C_{Al} \qquad (3.2)$$

Where $-r_{Al}$ = rate of dealumination; T = reaction temperature; C_{Ac0} = acid initial concentration; C_{Al} = concentration of alumina

The material balance for the components involved in the dealumination reaction were accounted for and presented in Appendix C. since the dealumination reaction was an endothermic reaction, the dealuminator was properly lagged to avoid much heat loss to the surrounding from the internally generated heat of hydration. The insulation thickness was calculated by using Equations (3.3 to 3.5), detail calculation is shown in Appendix D.

$$q' = \frac{2\pi L\Delta T_{overall}}{\frac{\ln(\frac{r_2}{r_1})}{k_a} + \frac{\ln(\frac{r_3}{r_2})}{k_b} + \frac{\ln(\frac{r_4}{r_3})}{k_c}} \qquad (3.3)$$

Where q' = energy flow per unit time; L = height of the cylinder; r_1= internal radius of reactor; r_2: outer radius of reactor; r_3: internal radius of reactor casing; r_4: outer radius of reactor casing; k_a= thermal conductivity of material use for the reactor; k_b= thermal conductivity of material use as insulator; k_c= thermal conductivity of material used as reactor casing; ΔT : Temparature difference.

During dealumination process, due to associated heat of hydration, the average temperature of reacting system was assumed to be 120°C (393 K)

$$q' = \frac{m_{total} Cp_{av} \Delta T}{t} \tag{3.4}$$

Where: m_{total} = Total mass of the reacting system; $Cp_{av} = Avearage\ specific\ heat\ capacity$; t = time.

$\Delta T : Temparature\ difference$; T_i is the initial temperature of the reacting system during dealumination.; T_f is the final temperature of the reacting system just before quenching; t is the time for the dealumination reaction.

$$q' = \frac{2\pi L \Delta T_{overall}}{\frac{\ln\left(\frac{r_2}{r_1}\right)}{k_s} + \frac{\ln\left(\frac{r_3}{r_2}\right)}{k_w} + \frac{\ln\left(\frac{r_4}{r_3}\right)}{k_a}} \tag{3.5}$$

3.4.1.2 Metakaolin slurry tank

The metakaolin slurry tank comprised of the vessel and an electrical motor in which the stirrer was attached. The design calculation and specification of the mixing tank as well as the power rating of the motor are presented in Appendix E. Some of the basis Equations used are given in Equations (3.6) and (3.7). For power requirement the relationship between Power number, Reynolds number and Froude number was established as (Sinnott, 1999):

$$N_P = f(Re, Fr) \tag{3.6}$$

Where: $N_P = Power\ number$ $Re = Reynolds\ number$ $Re = Froude\ number$

Equation (3.6) then becomes

$$\frac{P}{\rho N^3 {D_T}^5} = f\left(\frac{\rho N {D_T}^2}{\mu}, \frac{N^2 D_T}{g}\right) \tag{3.7}$$

3.3.1.3 Acid Holding Tank

Based on the amount of the acid needed for the dealumination, the specification of the acid holding tank was made and shown in Appendix E.

3.4.2 Sizing of zeolite reactor

The detailed calculations of material balances, energy consideration and sizing of the zeolite reactors for the production of zeolite Y and ZSM-5 are presented in Appendices F and G respectively. The basis of design for the dealumination reactor was 2.5 kg of metakaolin/batch, while for zeolite Y and ZSM-5 reactors were 2 and 4kg of products per batch respectively. From the basis of each reactor the volume and subsequently other dimensions were evaluated.

3.4.3 Engineering drawings

AutoCAD 2016, was used for the drawings of all the three pilot size units involve in the zeolite production from Kankara kaolin. The pilot size dealumination unit comprises of three components namely, the reactor referred to as dealuminator, metakaolin slurry mixing tank and acid holding tank. The orthographic view and the complete set-up of the unit is shown in Figure 3.2.

Heat distribution was one of the major factors to be considered during zeolite production. Figures 3.3 and 3.5 shows the orthographic and complete views of zeolites reactors which employs internal and external heating method respectively.

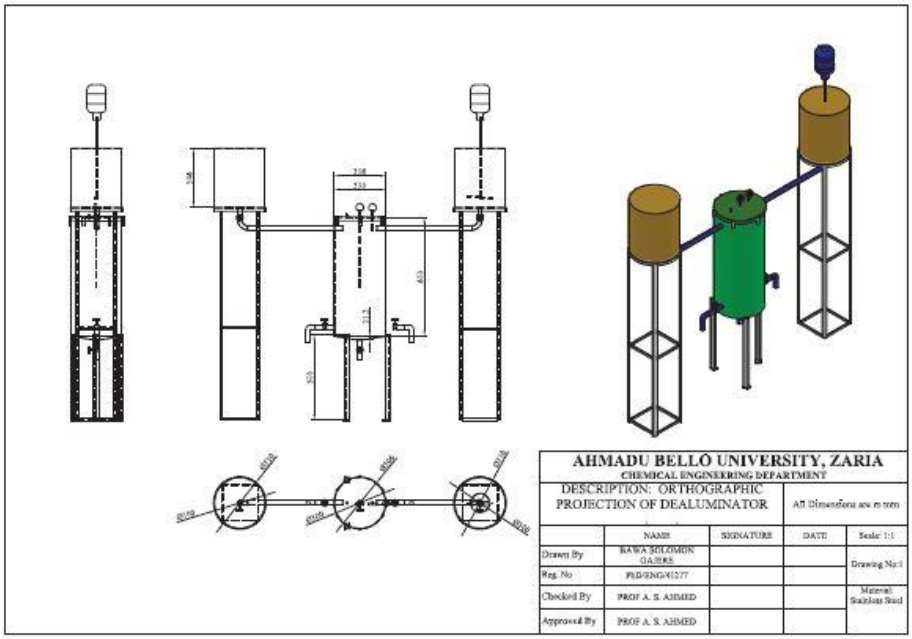


Figure 3.2: Orthographic view and complete dealumination unit

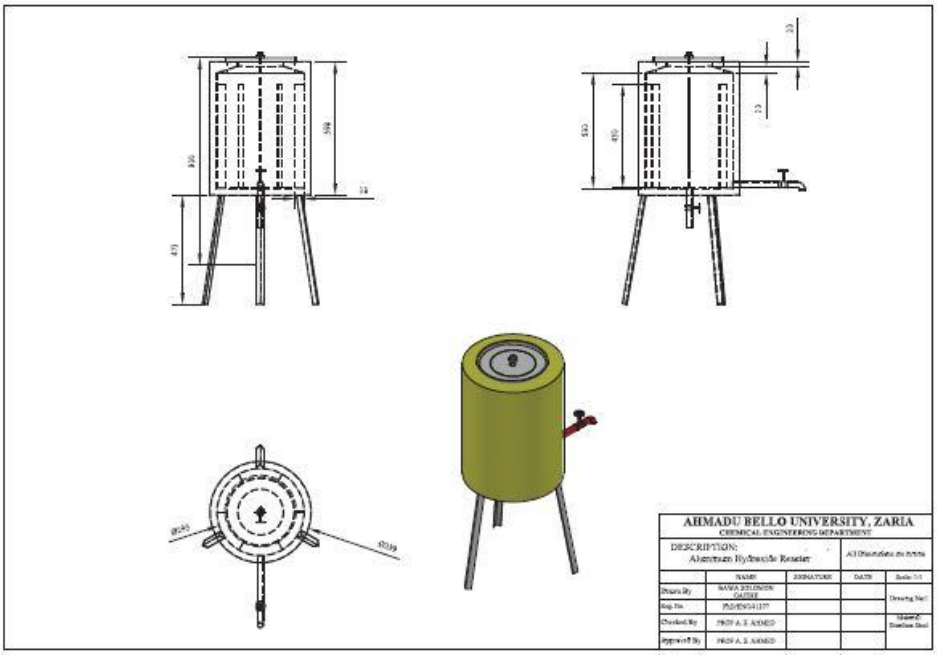


Figure 3.3: Zeolite reactor drawings (internal heating)

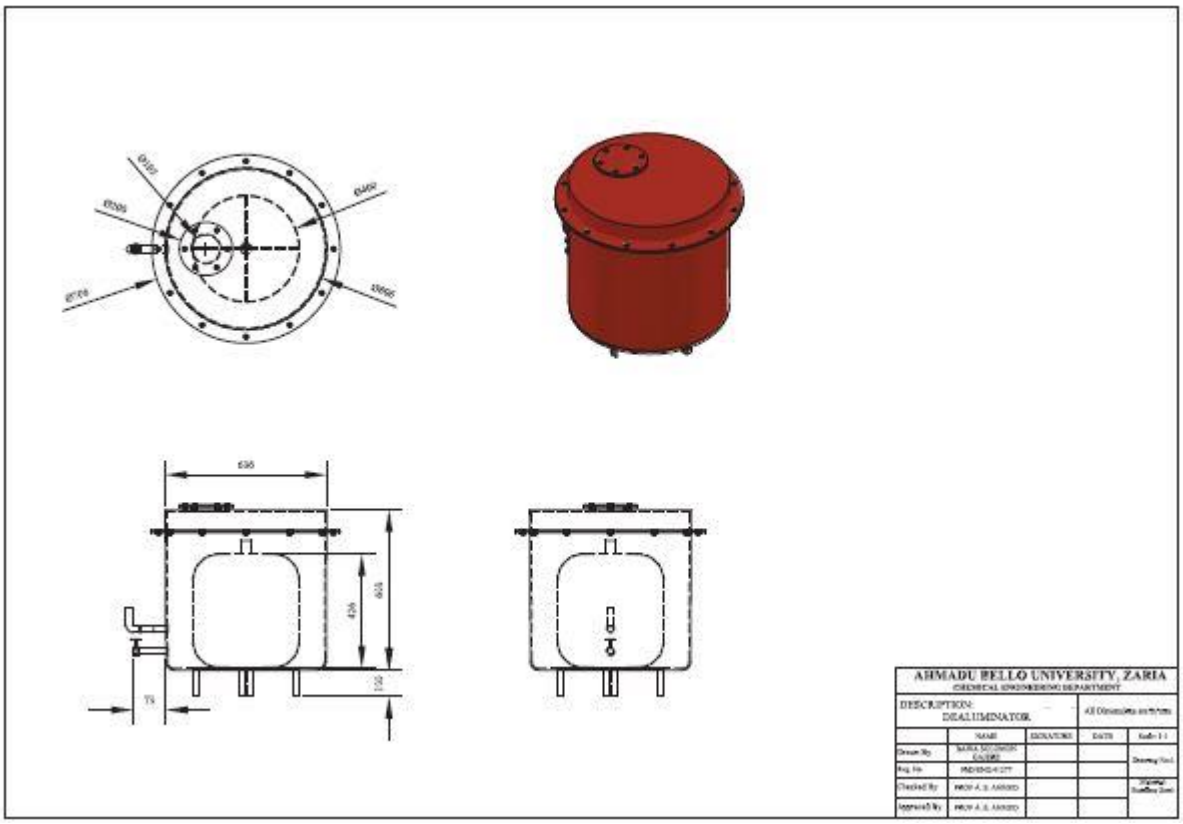


Figure 3.4: Zeolite reactor drawing (external heating)

3.5 Material Selection for Fabrication

After the completion of the design, the next critical step was to carefully select the materials for construction, considering the facts that the reactions were either highly acidic in the case of dealumination process and highly basic in the case of zeolite production.

3.5.1 Dealumination unit

Glass is an ideal material for storing many types of chemicals, including most acids and bases. Reason being that glass is a material that is inert to many chemicals and is nonporous, which means it will not absorb absorb chemicals nor contaminate the chemicals. The major drawback for the usage of glass is the fact that it breaks easily and make sharp, dangerous shards when broken. Polyethylene is also good material also for acid storage. The material

selected for the pilot size acid holding tank was polyethylene which would be housed externally with stainless steel (Type 304). The casing would withstand corrosion of acid at ambient temperature in case of splashing of acid during operation. The stainless steel casing of 2mm thickness would serve, since much pressure build-up was not expected in the acid holding tank. The casing would also prevent accidental puncturing of the polyethylene, being a plastic material by a sharp object within the pilot plant.

The metakaolin slurry tank do not contain corrosive materials. The best material to be use was stainless steel considering durability and avoiding rust. During fabrication plastic container made of polypropylene was used for the metakaolin pilot size component of the dealumination unit. The stand of the electric motor for the stirrer was made of stainless steel (type 304).

The best material for the fabrication of the dealumination reactor (dealuminator) was stainless steel type 316, which could withstand the corrosive nature of the concentrated sulfuric acid to be used during the dealumination reaction at temperature between 120 - 140˚C. considering cost, the material selected was stainless steel material, type 304 being a close alternative. Stainless steel has high resistance ability to acidic corrosive medium, at mild temperature. But the internal part of the dealuminator was coated with suitable materials such as silicon caulk, ceramic tales and glass lining, that was inert to the acidic environment within the reactor. Glass wool fiber, a very good heat insulator was selected as lagging material to minimize heat loss from the dealuminator to the surrounding environment. The external part of the temperature and pressure gauges were made of stainless steel materials, which was mounted at the cover of the reactor to provide readings for the reaction temperature and pressure of the system respectively. The thickness of the steel sheets used

for the dealuminator was 3mm for easy working and minimize cost, since the system and process would not involve much pressure build-up. Considering safety of the system, pressure relief valve provision was made at the top part of the dealuminator.

The piping system, valves and connection accessories were basically made of Polyvinyl chloride (PVC) and stainless steel materials.

3.5.2 Zeolite Y and ZSM-5 reactors

Similar configurations were used for the production of zeolite Y and ZSM-5. The fundamental difference was in the output and ratio of the silica to alumina recipes also varies. The same reactor was not used for the production of the two products, so as to avoid contamination, hence the internal part was made in such a way that it gave room for flexibility of replacing the internal part based on the type of zeolites to be produced. The contents for zeolite Y production was highly alkaline as such polypropylene material was chosen as the fabrication material for the reactor which could withstand a temperature above 100°C being the reaction temperature. Considering internal heating, the heating element was lined with Teflon material to avoid direct contact of the heating element with the contents. Teflon could withstand the temperature employed as well as the basic corrosive environment. For the external heating the heating element was made of stainless steel material which would not have direct contact with the reaction mixture, hence lining was not required. The reaction being endothermic, glass wool was used as the insulating material to minimize heat loss to the environment. Stainless steel, type 304 was chosen as the material for the fabrication of the zeolites reactors external part. The temperature prop wire was also lined with Teflon tape, especially the part that made contact with the reaction contents.

The piping system, valves and connection accessories were basically made of Polyvinyl chloride (PVC) and stainless steel materials.

3.6 Pilot Size Process Units Fabrication

3.6.1 Dealumination reactor

The external part of the dealumination reactor (dealuminator) during fabrication shown in Plate II, the rough surface during the wielding process was polished and the reactor lagged properly. Gauges were placed at the cover of the reactor for monitoring of the process. The internal part of the reactor (dealuminator) was shown before and after coating with ceramic tiles in Plate III.



Plate II: Fabrication process of dealuminator external part (A) initiation stage (B) polished surface (C) with lagging

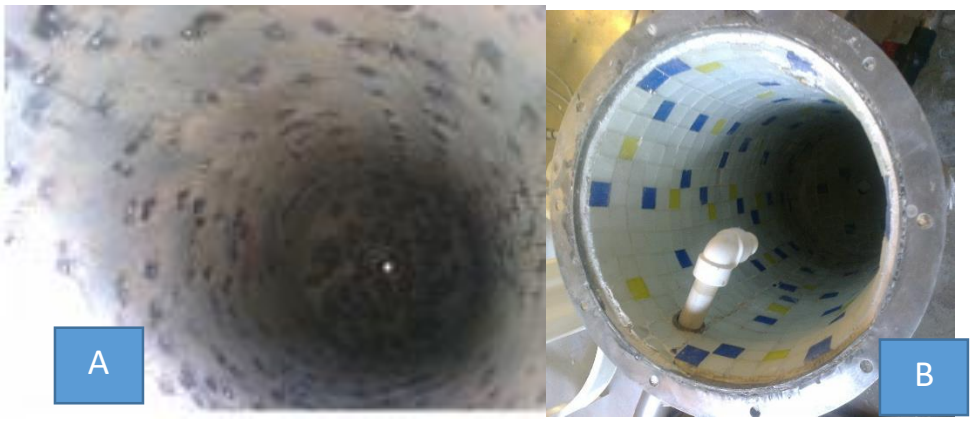


Plate III: Fabrication process of dealuminator internal part (A) before lining (B) after lining with ceramic tiles

3.6.2 Zeolites reactors

The distinguish factor of the two zeolites reactors configuration is basically on the heating means and the position of the heating element.

3.6.2.1 Internal means of heating configuration

The heating element was made in such a way that it was inserted inside the reacting medium. The step-wise process of it fabrication was not captured but the complete set-up is shown in Plate IV.



Plate IV: Complete set-up of zeolite reactor involving internal heating

3.6.2.2 External means of heating configuration

The materials of fabrication were basically stainless steel, type 304 with thickness of 3mm. Plate VA shows the internal part of the hollow stainless steel vessel and the position of the heating element was neatly bore as shown in Plate VB. The heating element made of stainless steel material was placed at the base on the reactor and the container holder was made slightly above the heating element as shown in Plate VC and VD respectively. The heating element was positioned at the base to ensure good heat distribution within the reactor.



Plate V: Internal configuration of the zeolites reactor (A) hollow vessel (B) showing position of the heating element (C) heating element inserted (D) container holder positioned

The cover of the reactor was accurately produced from a stainless steel sheet and the hole bored on, as shown in Plate VI A and B respectively. The bored hole would serve as a means through which the temperature prop wire will pass through, it would also serve as an access

for adjusting the polypropylene container in the internal part of the reactor. Several components were wielded together using stainless steel electrodes as shown in Plate VI D.

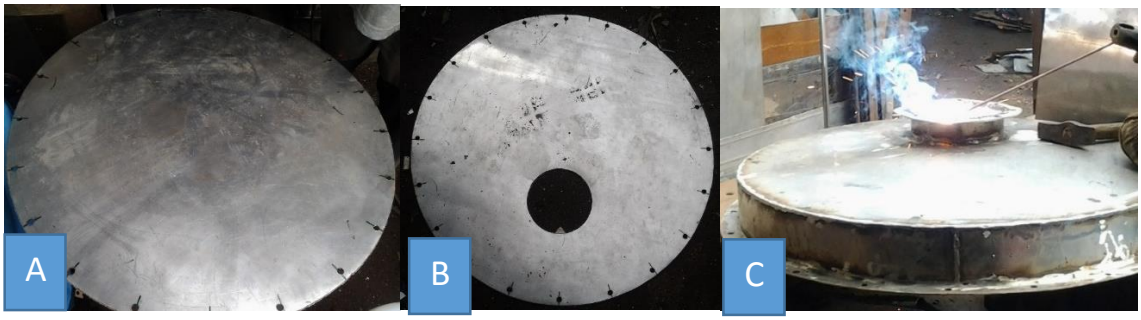


Plate VI: Reactor cover under fabrication (A) the cut circular sheet (B) reactor cover sheet with a hole bore on it (D) assembled reactor cover

Some of the final process of the fabricating the zeolite reactor involved filing of rough edges and insulating the reactor as shown in Plate VII A and B respectively. The stainless steel reactoe was fixed after the insulation process and the final outlook of the reactor is as shown in Plate VII C, and Plate VII D showed the interior zeolites reactor outlook.

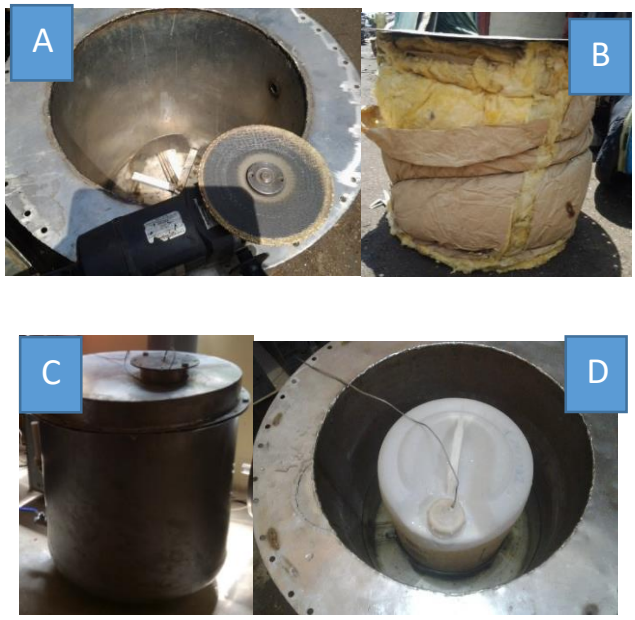


Plate VII: Final stage of zeolite reactor fabrication (A) filing process (B) insulated external reactor part (C) external part (D) interior part

3.7 Zeolite Production Process from Kaolin

3.7.1 Kaolin beneficiation

The starting material was kaolin clay sourced from the deposit at Kankara town of Katsina state, Nigeria, which is located at latitude 11˚55'52.10"N and longitude 7˚24'40.14"E. Kaolin purification plant set-up by the Petroleum Technological Development Fund (PTDF) Chair, Department of Chemical Engineering, ABU, Zaria was used for the beneficiation process. The purification plant employed the wet beneficiation method. The aim of the wet beneficiation method was to purify the kaolin clay from soluble impurities such as soluble salts of group 1 and 2 elements, of the periodic table. Impurities which were denser than kaolin such as quartz were separated at different points during the purification process. The purification process involved the crushing of the kaolin clay and transferring it to the blunging tank. Water was added and the slurry was blunged by vigorous stirrer until homogeneity was achieved. Heavier quartz settled at the bottom of the blunging tank while kaolin and fine quartz slurry passed through a sieve by opening the outlet beside the blunging tank into sedimentation tank 1, some fine quartz were trapped by the sieve while the kaolin slurry passed through the sieve. Some of the fine quartz settled at the base of sedimentation tank 1 (T_1), while the kaolin slurry flowed to kaolin clay slurry collection tank as overflow. The slurry was transported to a hydro cyclone with the help of a pump for further separation. The underflow of the hydro cyclone flowed to the recycling tank while the overflow flowed to the sedimentation tank 2 (T_2), where the purified kaolin settled at the base of the tank while the overflow of the tank is a clear layer of water which goes to the sink. Finally, the purified kaolin clay was collected at the bottom outlet of sedimentation tank 2. The purified kaolin clay was thickened using a casted slab, after which it was dried atmospherically followed by

oven drying at 100°C for 12 h. The dried purified kaolin clay was ball milled. The picture for the purification unit is shown in and Plate VIII.



Plate VIII: Pilot unit for kaolin purification

3.7.2 Calcination of beneficiated kaolin

The fine ball milled beneficiated kaolin was thermally activated *via* calcination. The condition of calcination was 750°C for 2 hours in the exposed element electric furnace. Ceramic saggars were used to hold the beneficiated kaolin for the calcination process, inside the furnace. The control panel attached to the furnace was used to program the heating operation. The chemical equation which represents the calcination process is shown in Equation (3.8).

$$Al_2O_3 \cdot 2SiO_2 \cdot 2H_2O \longrightarrow Al_2O_3 \cdot 2SiO_2 + 2H_2O \quad (3.8)$$

The thermal process converts kaolin to metakaolin, a reactive and amorphous phase of kaolin.

3.7.3 Dealumination of metakaolin

The metakaolin was separated into silica and alum (which contains alumina) by using concentrated (98 wt%) sulphuric acid in the developed dealumination unit. The acidic condition for the reaction was 60 wt%. The sulphuric acid was the excess reactant. The equation of the reaction is shown in Equation (3.9).

$$Al_2O_3 \cdot 2SiO_2 + 3H_2SO_4 \longrightarrow Al_2(SO_4)_3 + 2SiO_2 + 3H_2O \quad (3.9)$$

For a typical batch, 2.5 kg metakaolin was mixed with 4656 cm^3 of water in the metakaolin slurry mixing tank using the stirrer. The slurry was emptied into the dealumination reactor by opening the valve. 4027cm^3 of sulphuric acid 98 wt% was also channeled into the dealumination reactor. The unlocking of the alumina from metakaolin began immediately the two reactants came in contact with each other. The heat of hydration generated was sufficient to drive the endothermic dealumination reaction. The temperature and pressure gauges were mounted on the reactor cover to monitor the temperature and pressure as the reaction progressed. More so, a pressure relief valve was mounted as a safety measure. At the end of the reaction, 16814 cm^3 of water was added via the metakaolin slurry tank to quench the reaction and reduce the acidic content of the products obtained. The products obtained were alum and silica. The silica was thoroughly washed, because of the excess acid used. The washed silica was sent to the sodium silicate unit of the pilot plant, where it served as the major starting material for the production of sodium silicate, a recipe for zeolite synthesis. While the alum was sent to the aluminum hydroxide production unit.

The internal part of the dealuminator was lined with silica curl, ceramic tiles, and glass. With these different configurations several dealumination runs were conducted. The silica product

obtained from the dealumination runs were analyzed and the efficiency of the different configurations were evaluated. More so, the quality of the silica products was determined *via* the chemical composition analysis (XRF).

3.7.4 Aluminum hydroxide production

The two reactants for this unit are liquid single alum and sodium hydroxide. 30 liters of alum from the alum tank was simultaneously fed into the CSTR reactor (developed by Nakakana (2015)), with 10 liters of 50 wt% sodium hydroxide solution to produce aluminium hydroxide and sodium sulphate as by-product. The production process was a semi-batch process. The reaction was carried out at room temperature with continuous stirring and the pH of the solution in the reactor was closely monitored. The reaction was terminated when the pH was between 7 and 8. Equation (3.10) expresses the chemical reaction of the formation of aluminium hydroxide.

$$Al_2(SO_4)_3 + 6NaOH \longrightarrow 2Al(OH)_3 + 3Na_2SO_4 \qquad (3.10)$$

The precipitated aluminum hydroxide formed was washed thoroughly until the clear liquid part was free of sulphate. Filter bags were used for the filtration and the cake was dried at 110°C for 12 hours. The dried aluminum hydroxide was ball milled to obtained fine particles of the aluminum hydroxide, which was then calcined in the furnace at 400°C for 2 hours. Aluminum hydroxide unit picture is shown in Plate IX.



Plate IX: Aluminum hydroxide production unit

3.7.5 Sodium silicate production

The sodium silicate production unit (developed by Yusuf (2015)) was used to produce the sodium silicate needed for zeolite production. The unit was operated in two different concentration level depending on the targeted zeolite, either zeolite Y or ZSM-5 zeolite. But the principle of reaction was the same. The equation for the reaction is as shown in Equation (3.11). Plate III shows the picture of the sodium silicate unit used.

$$2NaOH + xSiO_2 + H_2O \longrightarrow Na_2O(SiO_2)_x + 2H_2O \qquad (3.11)$$

3.7.5.1 Sodium silicate for zeolite Y production

Silica produced from the dealumination unit served as the bed in the fixed bed reactor. The amount of silica required was 5.13 kg. Amount of sodium hydroxide needed was 4.50 kg, which was dissolved in 15 liters of water in the sodium hydroxide chamber of the unit.

Detailed calculation of the amount of reactants used is presented in Appendix C. Pump was used to transport the sodium hydroxide solution from the holding chamber into the fixed bed reactor where the two reactants were in contact for the reaction to take place. The pilot size unit for sodium silicate production is shown in Plate X. The leaching process lasted for 3 hours at 100°C with continuous circulation of the reacting mixture. After the reaction the solution was filtered with the help of filter bags. The residue was washed while the filtrate was concentrated to the required amount needed for Zeolite Y production.



Plate X: Sodium silicate production unit

3.7.5.2. Sodium silicate production for ZSM-5 synthesis

2.86 kg of silica obtained from the dealumination unit was used as the bed in the fixed bed reactor part of the sodium silicate unit. 1.20 kg of sodium hydroxide was dissolved in 10

liters of water in the sodium hydroxide chamber of the unit. Detail calculation of the amount of reactants used is presented in Appendix D. A pump was used to transport the sodium hydroxide solution from the holding chamber into the fixed bed reactor where the two reactants were in contact for the reaction to take place. The leaching process lasted for 1 hour at 90°C with continuous circulation of the reacting mixture. After the reaction the solution was filtered with the help of filter bags. The residue was washed while the filtrate was diluted with 28.57 liters of deionized water.

3.7.6 Silica sol preparation

To prepare 2 liters of concentrated silica sol for ZSM-5 zeolite production, 6 liters of 1 M H_2SO_4 was titrated with 20 liters dilute sodium silicate as prepared in 3.4.5.1. The reaction temperature was 50°C, with stirring as the reaction progressed the equation for the reaction is represented in Equation (3.12). At the end point, a cloudy viscous gel was formed with pH value greater than 7, which was cool to room temperature.

$$Na_2O.3SiO_2 + H_2SO_4 \longrightarrow 3SiO_2 + Na_2SO_4 + H_2O \qquad (3.12)$$

The gel was washed repeatedly with hot de-ionized water to free the Si-O-Si framework from Na_2SO_4 being the by-product of the hydrolysis. $BaCl_2$ solution was added to the filtrate after washing to confirm the total removal of SO_4^{2-} from the silica sol solution. The test was repeated until no white precipitate was formed on addition of the $BaCl_2$. The essence of washing the gel was to remove the trapped Na_2SO_4 in the pores of the gel network. The obtained gel was concentrated to 2 liters *via* evaporation technique.

3.7.7 Gel preparation for zeolite Y production

3.7.7.1 Seed gel

0.050 kg sodium hydroxide was dissolved in 0.245 kg deionized water, 0.025 g aluminum hydroxide was added and stirred until dissolved. 0.280 kg of the prepared sodium silicate solution was added to the resulting solution and stirred for 20 minutes. The resultant gel was stored in air tight container and allowed to age at room temperature for 24 hours.

3.7.7.2 Feed gel

5 g sodium hydroxide was dissolved in 4.585 kg deionized water, 0.441 kg aluminum hydroxide was added and stirred until dissolved. 4.988 kg of the prepared sodium silicate solution was added to the resulting solution and stirred with a high-shear turbine mixer until the gel appears somewhat smooth.

3.7.7.3 Overall gel

579 g of the aged seed gel was added to the feed gel and mixed vigorously, the resulting overall gel was transferred into the zeolite Y rector and capped very well, which was allowed to age at room temperature for 24 hours.

3.7.8 Crystallization of zeolite Y

After the ageing period of 1 hour the reaction temperature of the reactor was set at 100°C, and the reaction time was 7 hours, thereafter, a settled solid crystal was observed at the base of the reactor with thick liquid layer above it. After the crystallization, the resulting zeolite Y crystal was filtered and washed with deionized water until the pH was less than 9. The resulting NaY (sodium base zeolite Y) was dried at 110°C for 12 hours. block diagram of the

zeolite Y production process is shown in Figure 3.5. The process was repeated several runs to ascertain the product yield.

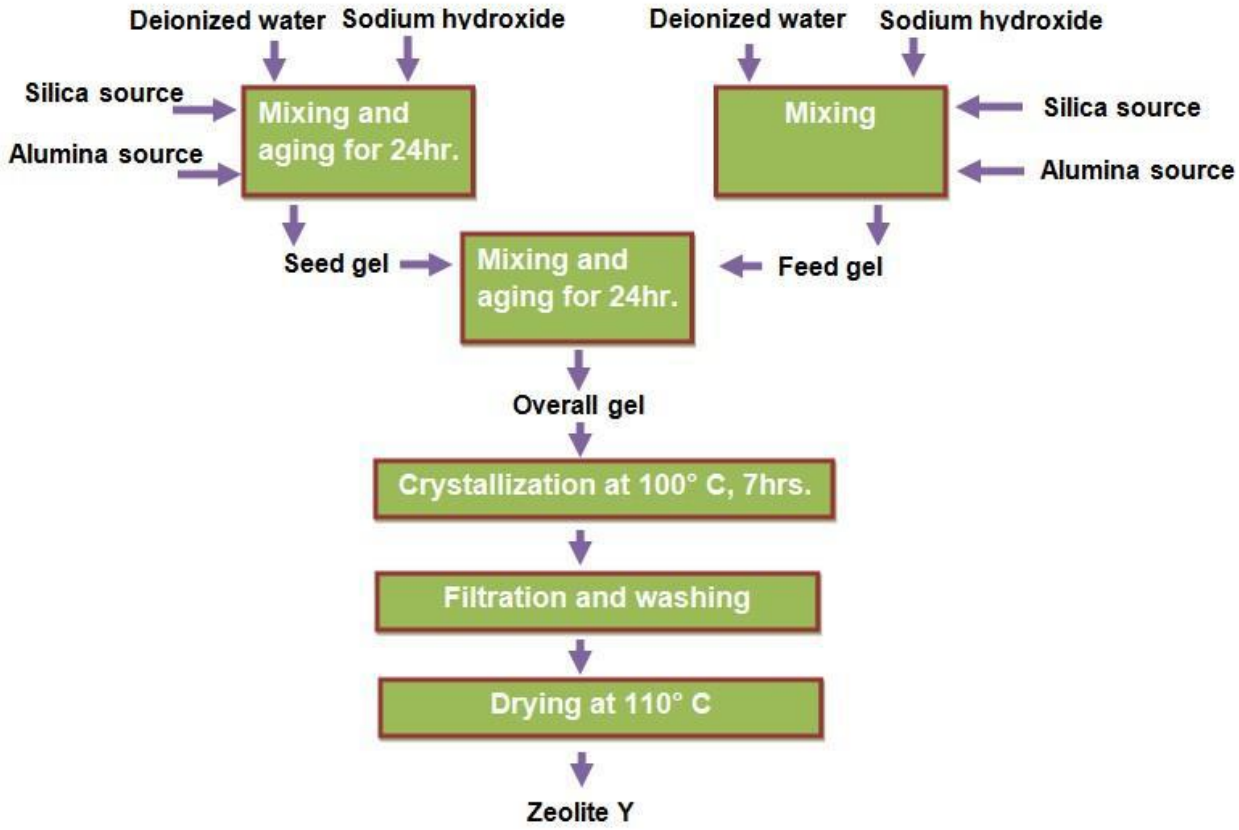


Figure 3.5: Flow diagram for the synthesis of zeolite Y from the reagents prepared

3.7.9 ZSM-5 production

0.280 kg of sodium hydroxide was dissolved in 1 liter of de-ionized water, 0.012 kg of alumina was added and the mixture was stirred until dissolved. It was labelled solution 1 (S_1). 0.068 liters of 96 wt% of H_2SO_4 and 0.160 kg of Tetrapropylammonium bromide (TPABr), and stirred until dissolved, the solution was labelled solution 2 (S_2). Solutions 1 and 2 were mixed simultaneously and added to 1 liter of silica sol and the mixture shaken vigorously. The resultant mixture was transferred into the zeolite reactor. The reaction temperature and

time were 95°C and 5 days, respectively. After the reaction, the liquid part was carefully decanted and the white solid crystals was washed several times until the pH was about 8. The solid product was dried in an oven at 100°C for 12 hours. the dried sample was calcined at 500°C for 2 hours to decompose the organic amine template to form sodium form of ZSM-5. The production process was repeated to evaluates the yield of the product.

3.7.10 Protonation of zeolites

3.7.10.1 Protonation of sodium form of zeolite Y

The protonation was done at the laboratory scale. 1.0 M solution of NH_4Cl was prepared and exchanged with sodium form of zeolite Y (Na-Zeolite Y) at 80°C using 10 ml solution to 1 g solid ratio and stirring the solution for 20 minutes (Gao *et al*., 2012; Du *et al*., 2013). After the exchange reaction the slurry was suction filtered using vacuum pump and washed thoroughly with distilled water and dried at 100°C for 6 hours. The resulting product was the NH_4-zeolite Y. The NH_4-zeolite Y was calcined at 650°C in air for 2 hours to form H-zeolite Y.

3.7.10.2 Protonation of sodium form of ZSM-5

1 g to 10 ml of sodium form of ZSM-5 and 1.0 ml was used NH_4SO_4 were used for the ion exchange respectively. The mixture was stirred for 20 minutes at room temperature. The resultant mixture was filtered using a vacuum pump. The residue was thoroughly washed with deionized water to remove of sodium sulphate that might had form on the surface of the zeolite. The residue was then dried in the oven at 100°C for 12 hours, the dried NH_4-ZSM-5 was then calcined at 500°C for 2 hours to obtain H-ZSM-5.

3.7.11 Thermal stabilization of zeolite Y

The produced H-zeolite Y was thermally stabilized by impregnation of rare earth metal (La). The reaction was carried out using wet impregnation reaction to make zeolite RE Y. 0.01 M solution of $LaCl_3.7H_2O$ was prepared and mixed with the protonated zeolite (H-zeolite Y) at 80°C using 12.5 ml solution to 1 g solid ratio and stirring the solution for 1 hour (Gao *et al*., 2012; Du *et al*., 2013). After the reaction the product was filtered using a vacuum pump, washed thoroughly with distilled water. The wet cake of the zeolite was hydrothermally calcined at 650°C in air for 2 h.

3.8 Physicochemical Characterization

Kankara kaolin, beneficiated kaolin, metakaolin, silica, zeolites Y, ZSM-5and zeolite based catalyst were characterized using FTIR, XRD, XRF, SEM, TEM, EDS and SAED.

3.8.1 Fourier transform infrared spectroscopy (FTIR)

Perkin Elmer FTIR Spectrometer was used for the FTIR analysis. In a typical analysis 0.07g wafer of the sample consisting of 1% of the sample and 99% KBr window was used. The mixture was pressed under pressure to produce a thin film wafer. The wafer was inserted in the sample holder of the FTIR equipment, then, FTIR spectra of the sample was recorded from 400 to 4000 cm^{-1}. Prior to the sample analysis background spectrum of air at ambient condition was ran.

3.8.2. X-ray diffraction (XRD)

The amount of sample used was 2g of each sample for the XRD analysis. XRD patterns were recorded from Bragg's angle of 5° to 75° using Bruker Adavanced D_8 diffractometer,

operated at continuous scanning, scanning speed of 5°/min, generator settings of 10 mA and 40 kV, and CuKα node material.

3.8.3 X-ray fluorescence (XRF)

The chemical compositions of the materials used were determined using XRF machine; Minipal 4, Pananalytical X-ray fluorescence analyzer.

3.8.4 Scanning electron microscope (SEM)

SEM analysis was carried out using Zciss Emission Scanning Electron Microscope. In a typical run a very small amount of the sample was picked with a tweezer and placed on the sample stab. The sample was treated with acetone to wash off impurity and ensure particles dispersion. The stab containing the treated sample was placed in the sputter coater for surface polishing with gold film. After the sample preparation and sputtering the sample stab was placed in the analysis chamber of the SEM equipment, the vacuum was on. The magnification and voltage were set and the focus of the microscope was manipulated until a sharp clear image was obtained and picture captured.

3.8.5 Transmission electron microscope (TEM)

Samples were prepared by drop-coating one drop of specimen solution onto a holey carbon coated nickel grid. This was then dried under a Xenon lamp for about 10 minutes, where after the sample coated grids were analyzed under the microscope. Transmission electron micrographs were collected using an FEI Tecnai G2 20 field-emission gun (FEG) TEM, operated in bright field mode at an accelerating voltage of 200 kV. Energy dispersive x-ray spectra were collected using an EDAX liquid nitrogen cooled Lithium doped Silicon detector.

3.8.6 Thermo gravimetric analysis (TGA)

Thermo gravimetric analyses were carried out using PerkinElmer thermo gravimetric analyzer TGA 4000. The method used was thermal scanning from 30 to 900˚C at heating rate of 10˚C/min and cooling at 20˚C/ from 900 to 30˚C. Nitrogen was used as the purge gas at flow rate of 20 ml/min. In a typical run 10 – 30 mg sample was placed in the platinum crucible, then placed in the TGA furnace. The equipment was conditioned for about 30 minutes before the thermal scan was commenced.

3.8.7 Brunauer-Emmett-Teller (BET)

BET Nitrogen adsorption, surface area analysis was carried out using Microtristar II. Outgassing was carried out at 300°C for 4 hours and N_2 absorption/desorption at 77.350K.

3.9 Catalyst Performance Test

Protonated Zeolite Y and ZSM- 5 produced from the Kankara kaolin were used for n-hexadecane hydrocracking reaction after platinum was anchored in the zeolites. Incipient wetness impregnation method was used to anchor the platinum to the produced zeolite. The impregnated catalysts were subsequently dried at room temperature. Prior to reaction the catalysts received an oxidative pretreatment at 350°C followed by a reduction at 225°C. Calcination was conducted under flowing air (121 ml/min) while applying a heating rate of 0.3°C/min. Catalysts were calcined at 350°C for 3 hours under air before cooling to 225°C under nitrogen prior to the start of the reduction at 225°C overnight under flowing hydrogen (120 ml/min). Thereafter, the reactor was pressurized and H_2 and n-C16 flow commenced. A fixed bed reactor was used for the reaction, was directly connected to an online gas chromatograph (GC) for products analyses, products distribution is shown in Appendix K.

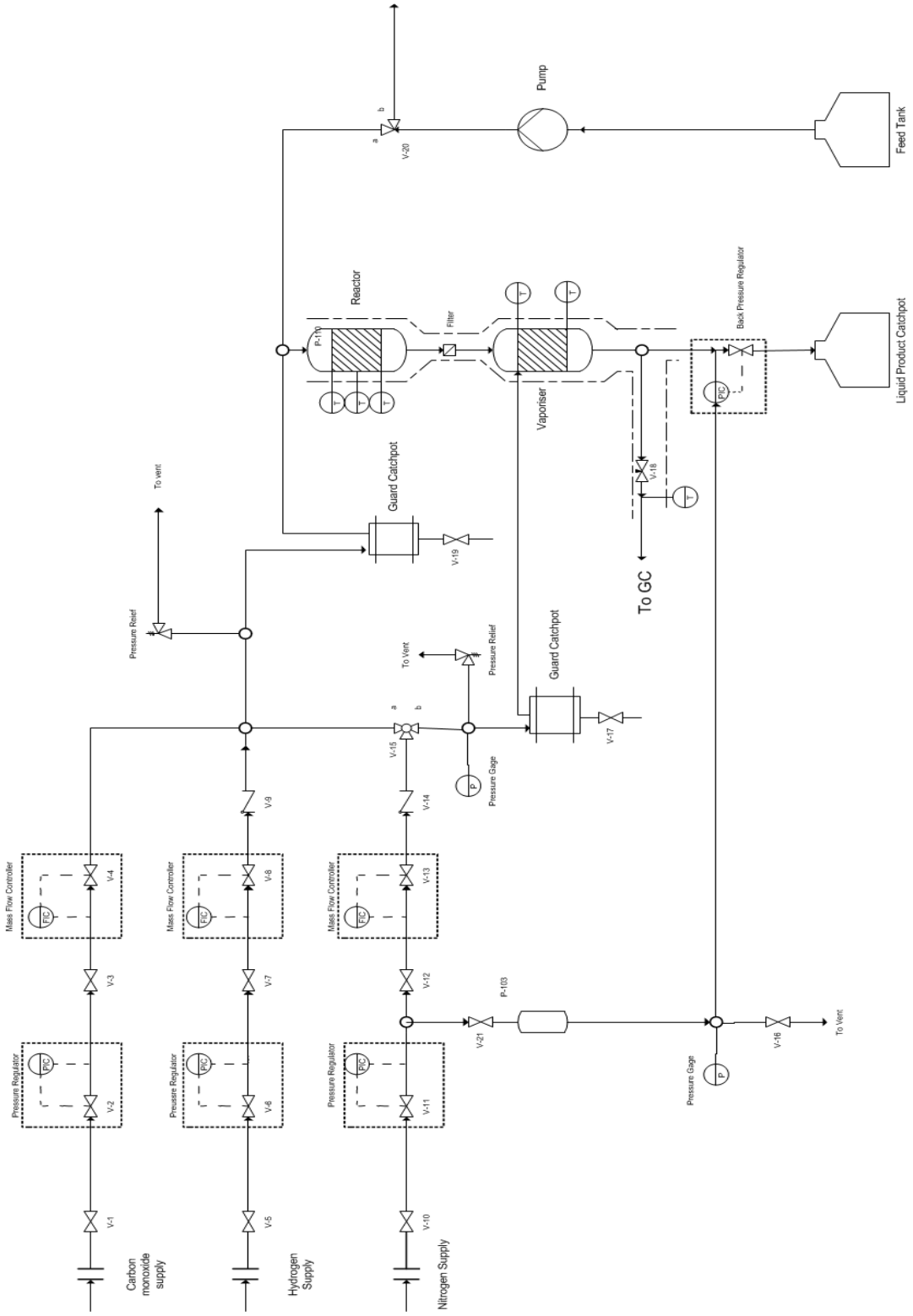


Figure 3.6: Process diagram of hydrocracking reaction

The set-up of the hydrocracking reaction used is presented in Plate XI A. The hydrocracking reaction products were channeled into the GC MS as shown in Plate XI B.

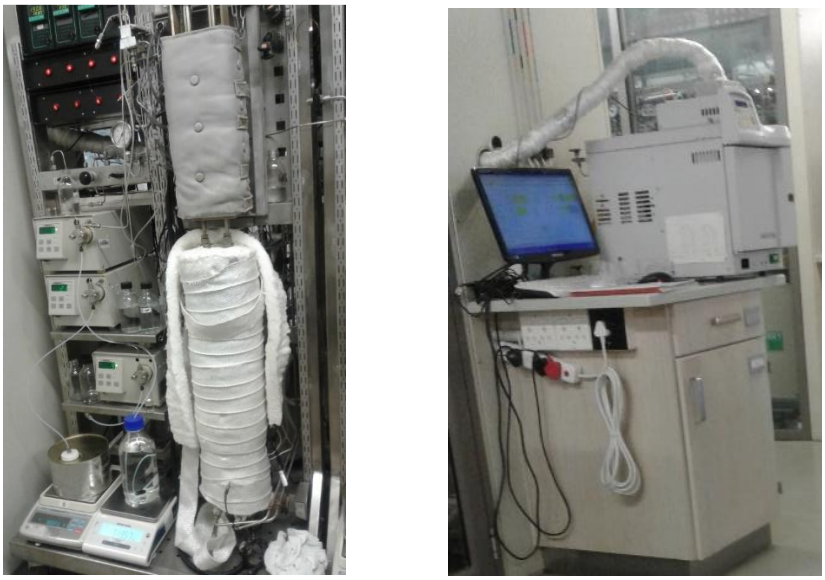


Plate XI: (A) Hydrocracking reaction set-up (B) GC MS machine

CHAPTER FOUR

RESULTS AND DISCUSSION

4.1 Dealumination Reaction Time

From the kinetic model used, values were generated based on the desired conversion and presented in Table 4.1, and the data were used to fit into different equation models in Microsoft Excel. The reaction time was evaluated based on the area under the graph and presented in Table 4.2. The polynomial model of order 6 had the best fit as seen from the highest R^2 value of 0.9962 which had reaction time of about 42 mins. It was observed that, the lower the R^2 value the higher the reaction times, which showed the less suitable the model.

Table 4.1: Values generated from the kinetic model for dealuminator

X_{Al}	$1/-r_{Al}$	$-r_{Al}$
0	36.06832	0.027725
0.1	40.07591	0.024953
0.2	45.0854	0.02218
0.3	51.52617	0.019408
0.4	60.11386	0.016635
0.5	72.13663	0.013863
0.6	90.17079	0.01109
0.7	120.2277	0.008318
0.8	180.3416	0.005545
0.9	360.6832	0.002773
0.95	721.3663	0.001386

Table 4.2: Estimation of reaction time using graphical method of different equation models

Model	R^2	Model equation	Area	t (mins)
Polynomial	0.8123	$y = 1258.3x^2 - 748.17x + 103.04$	119.1621	46.4732
model	0.9224	$y = 3270.4x^3 - 3434.3x^2 + 956.26x + 2.4297$	117.553	45.8457
	0.9678	$y = 8764.1x^4 - 13348x^3 + 6395.5x^2 - 896.62x + 51.066$	109.4487	42.6850
	0.9876	$y = 24649x^5 - 49602x^4 + 34930x^3 - 9825.1x^2 + 960.37x + 30.104$	110.3788	43.0477
	0.9962	$y = 70184x^6 - 176077x^5 + 165775x^4 - 71565x^3 + 13850x^2 - 883.07x + 37.995$	107.1274	41.7797
	Average			43.97
Exponential Model	0.8655	$y = 24.811e^{2.7583x}$	123.6009	48.2043
Linear model	0.5471	$y = 475.38x - 73.91$	144.3007	56.2773

4.2 Summary of Design Parameters and Fabricated Equipment

The summary of the design parameters for the dealumination unit and zeolite reactor are presented in Table 4.3. Dealumination unit diagram, 3-D view and picture are shown in Figures 4.1, 4.2 and Plate IV respectively.

Table 4.3: Summary of design parameters for fabrication

Unit	Equipment	Volume (cm^3)	Height (cm)	Diameter (cm)	Power rating (W)
Dealumination	Acid holding tank	5,000	29.42	14.71	-
	Metakaolin slurry tank	20,000	38.55	25.70	-
	Dealumination reactor	30,000	53.46	26.73	-
	Motor for stirrer	-	-	-	66 W
Zeolite	Zeolite reactor	20,000	47.70	23.35	-
	Heating element	-	-	-	2 kW

The developed pilot size dealumination unit is shown in Plate XII.



Plate XII: Pilot size dealumination unit

Plate XIII and XIV Show the zeolite reactor involving internal and external heating respectively.

Inserted heating element



Plate XIII: Zeolite reactor with internal heating

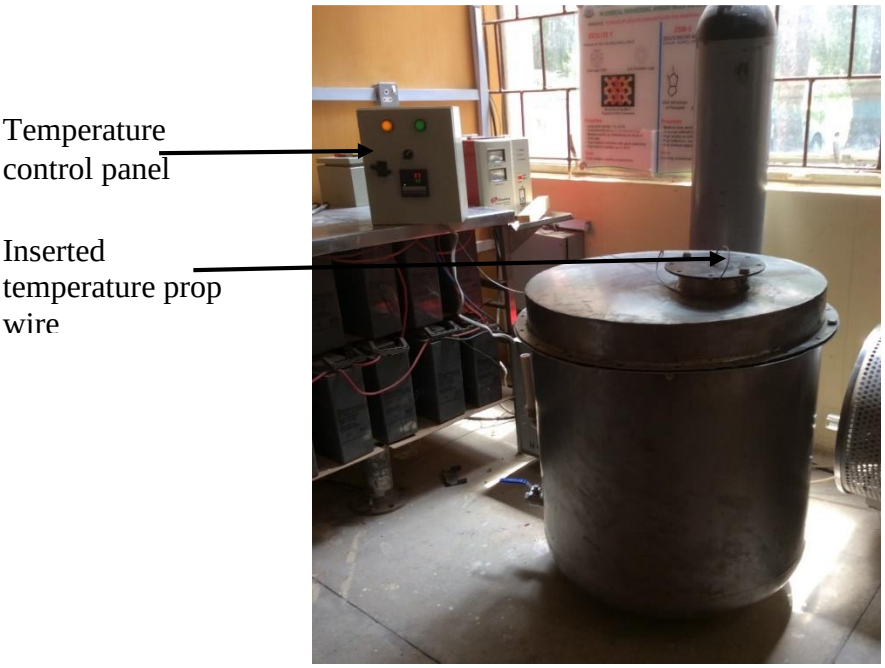


Plate XIV: Zeolite reactor with external heating

4.3 Physicochemical Characterization of Starting Material

Kaolin clay was the starting material which was sourced from Kankara town, Katsina State, Nigeria. The characterization done to ascertain the nature of the raw materials are discussed in the following sub-sections

4.3.1 Fourier transformed infrared (FTIR) analysis of Kankara kaolin

The FTIR spectrum of the raw Kankara kaolin, depicted in Figure 4.1, showed peaks at 3690, 3449, 1032, 923 and 786 cm^{-1}, which agree with the characteristics peaks of kaolinite (Saikia *et al*., 2003; Ekosse, 2010). The bands at 3690 and 3449 cm^{-1} were attributed to OH- vibration and the bands of the stretching OH groups coordinated to the octahedral cations. Well-crystalline kaolin exhibits two peaks at 3669 and 3652 cm^{-1}, which were noticeable in the raw kaolin used in this work (Russell and Fraser, 1994). The Si-O stretching bands were observed at 1042 and 1008 cm^{-1}, while bands at 786cm^{-1} was assigned to both Si-O-Si and

free silica or quartz material. On the other hand, the bands 546 and 691 cm^{-1} were attributed to both Si-O-Al bending or Al octahedral and Si-O out-of-plane bending respectively. The band noticeable at 468 cm^{-1} was assigned to Si-O-Si in plane bending (Belver *et al.*, 2002).

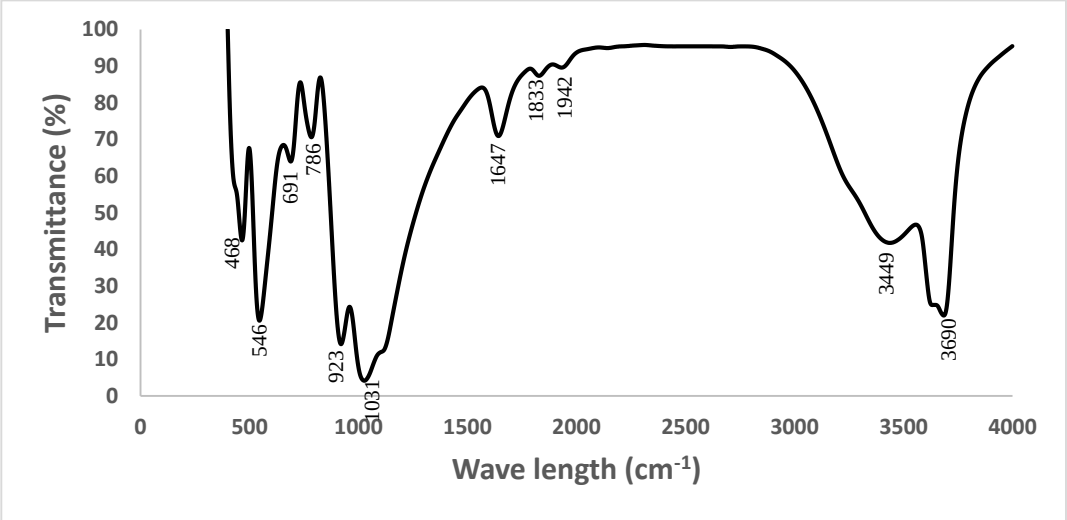


Figure 4.1: FTIR spectrum of Kankara kaolin

4.3.2 X-ray diffraction (XRD) analysis of Kankara kaolin

From the XRD pattern shown in Figure 4.2, the sharp peaks of the pattern were an indication that the Kankara kaolin was crystalline as also evident by the high intensity counts. The crystalline nature observed was because the mineral was formed by nature and also confirmed the deposit being a primary source of kaolin. The observable characteristic peaks of kaolinite at Bragg's angle of 12.4, 19.9, 20.4, 24.9, 34.9, 36.0, 36.1, 38.4, 45.2, 54.9 and 62.3° confirmed that the raw material was kaolinite with other associated impurities such as quartz, the crystalline form of silica (26.7°), mica (17.4°) (Chen, 1977; Ajayi *et al*., 2010; Panda *et al*., 2010).

Kaolinite $Al_2Si_2O_5(OH)_4$, muscovite $KAl_2(Si_3Al)O_{10}(OH,F)_2$, and Quartz SiO_2 were the minerals present in the kaolin, the identification of this minerals agree with literature

(Mohiuddin *et al*., 2016; El-Sherbiny *et al*., 2015; Panda *et al*., 2010; Lenarda *et al*., 2007; Pinheiro *et al*., 2005). The high crystalline peak at Bragg's angle of 27.5 indicated the presence of potash rich feldspar.

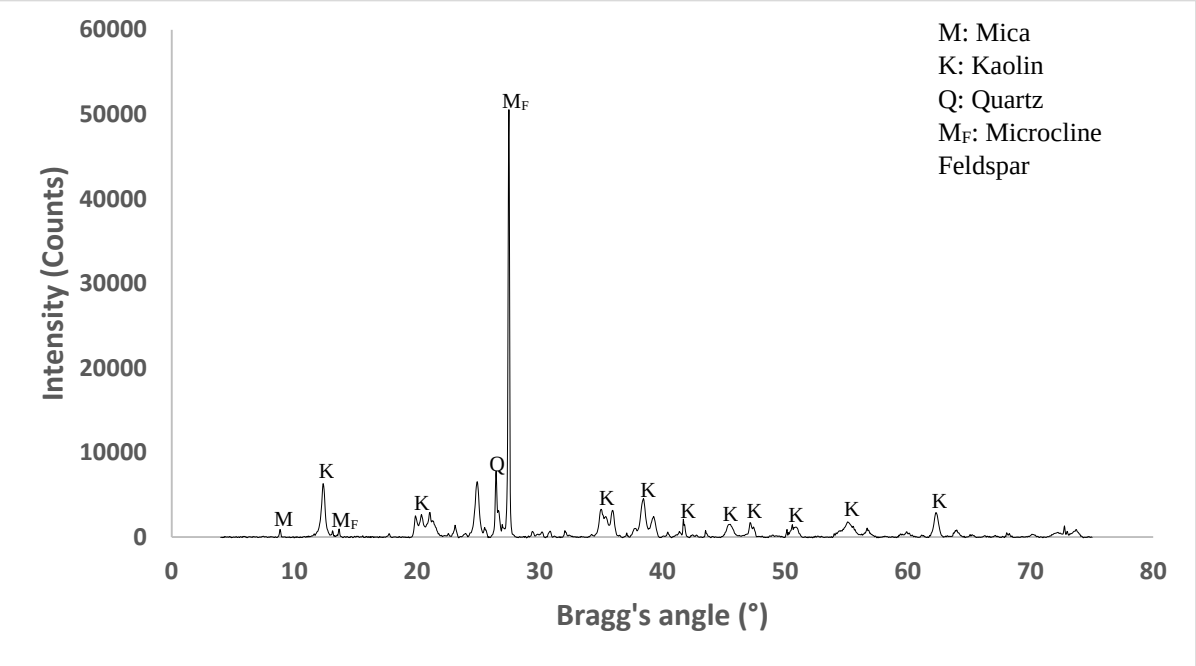


Figure 4.2: XRD pattern of raw Kankara kaolin

4.3.3 X-ray fluorescence (XRF) analysis of Kankara kaolin

The chemical composition of the raw kaolin in mass fraction expressed in per cent is presented in Table 4.4. The molar silica to alumina ratio when calculated was greater than 2, the expected molar silica to alumina ratio of pure kaolin. The high value of 2.5 as the silica to alumina ratio could be attributed to large amount of quartz associated with the raw kaolin. The observation also confirmed the inherent impure nature of kaolin being a natural mineral deposit.

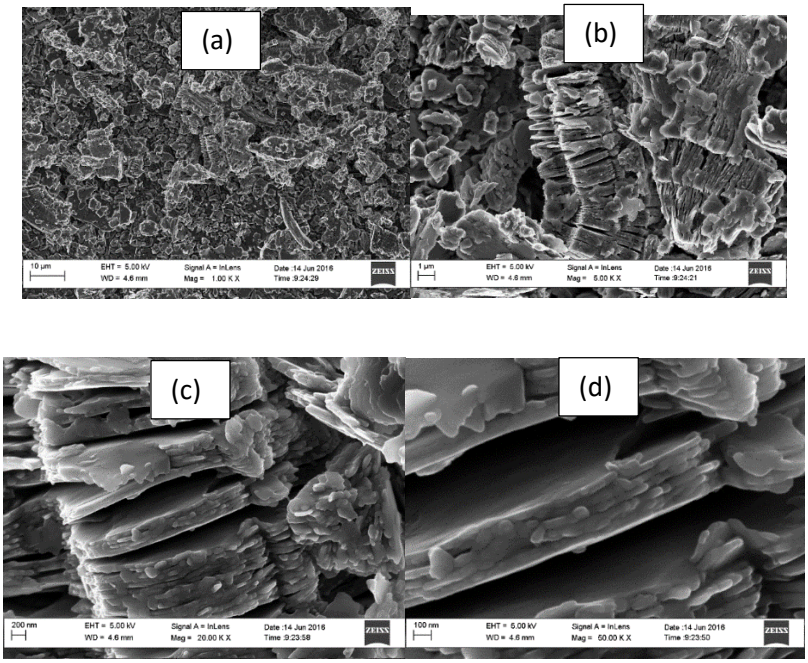
Table 4.4: Chemical composition of raw Kankara kaolin

SiO_2	Al_2O_3	Na_2O/K_2O	Fe_2O_3	CaO	MgO	TiO_2	OO
55.94	36.76	3.48	1.10	0.86	0.44	0.13	1.29

OO: Other oxides

4.3.4 SEM and TEM analysis of Kankara kaolin

The SEM analysis showed clearly the platelet structure of kaolinite clay reported in the literature which portrays booklets morphology (Abo-El-Enein, *et al*., 2013; Bergaya, 2013; Haq *et al*., 2009). The booklet morphology became clearer as the magnification increased. The closely packed flaky particles were stacked together in agglomerates, as depicted in Plate XV, as the magnification increased from 1,000 to 50,000 i.e. (a) to (d) the plate-like nature of the kaolin was vividly observed. Noticeable small aggregate particles found in between the silica-alumina plates, under higher magnification, were indicative of inherent impurities.



.**Plate XV: SEM image of raw Kankara kaolin at different magnifications**

Plate XVI shows the TEM images of the raw Kankara kaolin at different magnifications. The images showed overlapping of the clay particles, but the definite shape of a unit clay particle could be barely seen as the magnification increased as observed in Plate XVI (a) to (c). It has been reported that natural kaolins are often associated with high- defect structures. (Ma and Eggleton, 1999). Tetrahedral and hexagonal morphology could be obvious despite overlapping of some of the particles.

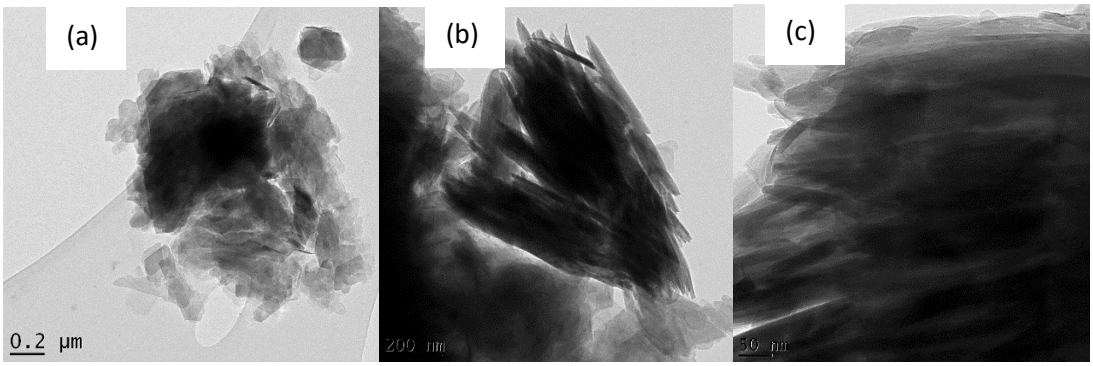


Plate XVI: TEM image of raw Kankara kaolin at different magnifications

4.4 Characterization Beneficiated Kaolin and Metakaolin

4.4.1 Fourier transformed infrared (FTIR) analysis

The FTIR spectrum of the raw Kankara kaolin, depicted in Figure 4.3, showed peaks at 3697, 3667, 1073, 921 and 793 cm^{-1}, which agree with the characteristics peaks of kaolinite as also observed in the beneficiated kaolin. The bands at 3697 and 3448 cm^{-1} were attributed to OH- vibration and the bands of the stretching OH groups coordinated to the octahedral cations, which was largely observed in the beneficiated kaolin than the metakaolin sample, owing to the fact that during the calcination of beneficiated kaolin the OH group was given off, as shown in Figure 4.3. The Si-O stretching bands were observed at 1078 and 1038 cm^{-1}, while bands at 793cm^{-1} was assigned to both Si-O-Si and free silica or quartz material. On the other

hand, the bands 545 and 699 cm^{-1} were attributed to both Si-O-Al bending or Al octahedral and Si-O out-of-plane bending respectively. Those band noticeable at 472 cm^{-1} was assigned to Si-O-Si in plane bending.

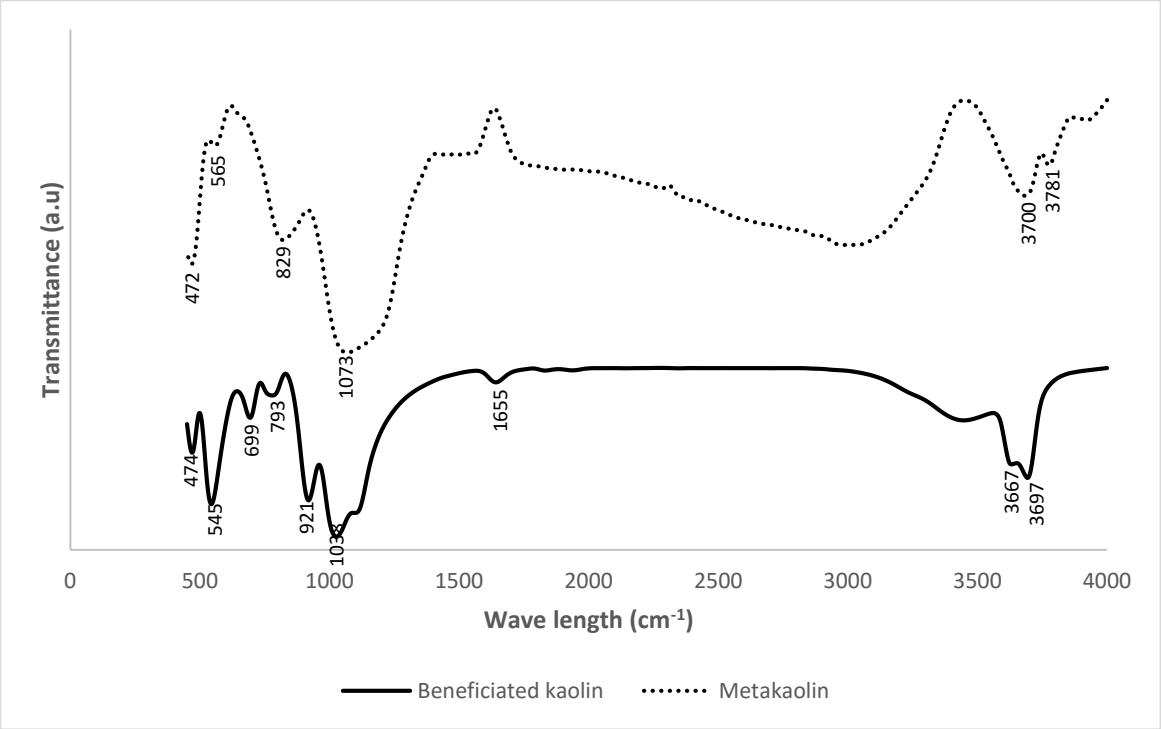


Figure 4.3: FTIR spectra of beneficiated and metakaolin

4.4.2 X-ray diffraction (XRD) analysis

Figure 4.4 presents the XRD patterns of the beneficiated kaolin and metakaolin. It could be seen from the XRD pattern that the peaks at Bragg's angles of 12.35, 19.89, 20.38, 24.88, 34.94, 35.95, 36.06, 38.35, 45.24, 54.88 and 62.37° responsible for the kaolinite mineral were more prominent after beneficiation. It was also observed that the peak at 26.6° responsible for quartz was still observed even after beneficiation. But the peak at 27.5 connotes the presence of feldspar rich in potash, drastically reduced to a very low intensity counts. This observation affirmed the solubility of the potash compound in water. The result was in

agreement with the XRF analysis, which shows decrease in the amount of K_2O after the beneficiation process. Reduction in mica peak after beneficiation was also evident. Most of the kaolin peaks in the beneficiated sample were found to collapse when it was converted to metakaolin as expected, these observations were similar to those reported for metakaolins by other researchers (Elimbi *et al*., 2011; Belver *et al*., 2002; Akolekar *et al*., 1997). The crystalline peak that persist in the metakaolin sample was that of quartz. Past works have shown that crystalline silica is inert to calcination treatment even at 1050°C (Edomwonyi-Otu, *et al*., 2013).

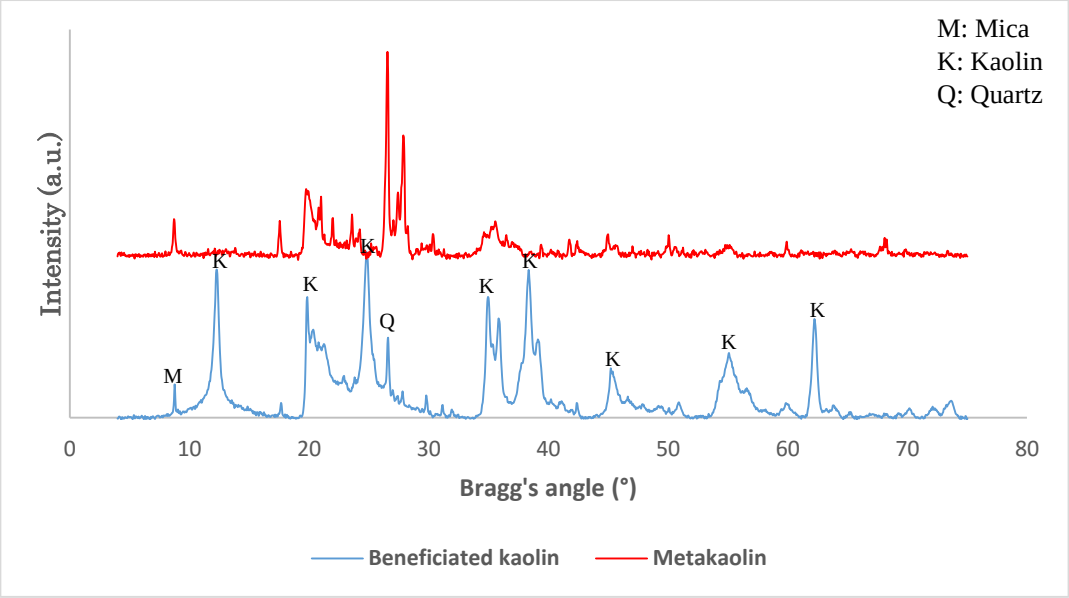


Figure 4.4: XRD patterns of beneficiated and metakaolin

4.4.3 X-ray fluorescence (XRF) analysis

The chemical composition of beneficiated kaolin and metakaolin is presented in Table 4.5. The silica to alumina ratio of beneficiated kaolin and metakaolin were 2.3 and 2.2 respectively, as calculated from the chemical composition of the samples. The value obtained were lower than that obtained for the raw kaolin, the closer the value to 2, the pure the kaolin.

The decrease in the ratio shows that the pilot plant wet beneficiation means of kaolin purification was effective. It was observed that the alumina content increases steadily with beneficiation, which suggests that, the goal of the beneficiation process which is aimed at decreasing the ratio of silica to alumina was achieved. This also implies that the materials removed during the beneficiation process are high in silica content, basically, montmorillonite, mica and quartz as reported (Ahmed, 1986), and free silica which is known to be present in clays.

Table 4.5: Chemical composition of raw kaolin, beneficiated and metakaolin

Oxides	Raw kaolin	Beneficiated kaolin	Metakaolin
SiO_2	55.94	54.96	55.20
Al_2O_3	36.76	40.27	42.05
Na_2O/K_2O	3.48	1.02	0.98
Fe_2O_3	1.10	0.85	0.78
CaO	0.86	0.53	0.41
MgO	0.44	0.28	0.19
TiO_2	0.13	0.14	0.13
OO	1.29	1.95	0.26

OO: Other oxides

The CaO, MgO, K_2O, Fe_2O_3, TiO_2 contents are observed to reduce significantly from the raw kaolin to the beneficiated kaolin suggesting the elimination of some of their soluble salts and insoluble coarse mineral particulates.

4.4.4 SEM and TEM of metakaolin

Metakaolin is essentially a highly reactive disordered structure of anhydrous alumina-silicate obtained from the calcination of kaolinite clay. It was observed from Plate XV, that the booklet morphology that was earlier obvious in the SEM image of the raw and kaolin had been lost. The nature of collapse of the metakaolin was seen clearly as the magnification increased from Plate XVII (a) to (d), the observed disorderly arrangement makes metakaolin

to be an amorphous material. Even though the metakaolin SEM image still possessed some relatively low platelet morphology, the morphology of the metakaolin was lump-like. The lump-like morphology could be attributed to the highly amorphous nature of the material as a result of the crumbling of the kaolinite structure as was already identified by the analysis of the XRD results. The relatively low platelet morphology observed in the material could be as a result of the crystalline silica contained in the clay even after the metakaolinization as the XRD results have earlier shown. The particle structure portrayed a hollow anhedral morphology showing irregular particle shapes. The irregularity of the particles could be as a result of the structural crumbling of the initial kaolinite structure experienced during the metakaolinization process as was already confirmed by the XRD and the SEM analyses of the same material (metakaolin). The TEM image of metakaolin did not show any definite shape as shown in Figure 4.8. No clear observable shape of the material as the magnification increased from (a) to (c) of Plate XVIII, this support the norms that metakaolin is an amorphous material.

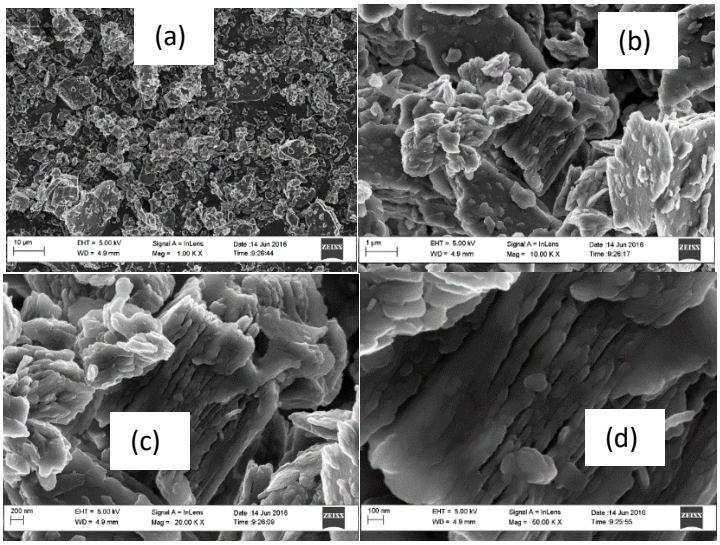


Plate XVII: SEM images of metakaolin at different magnifications

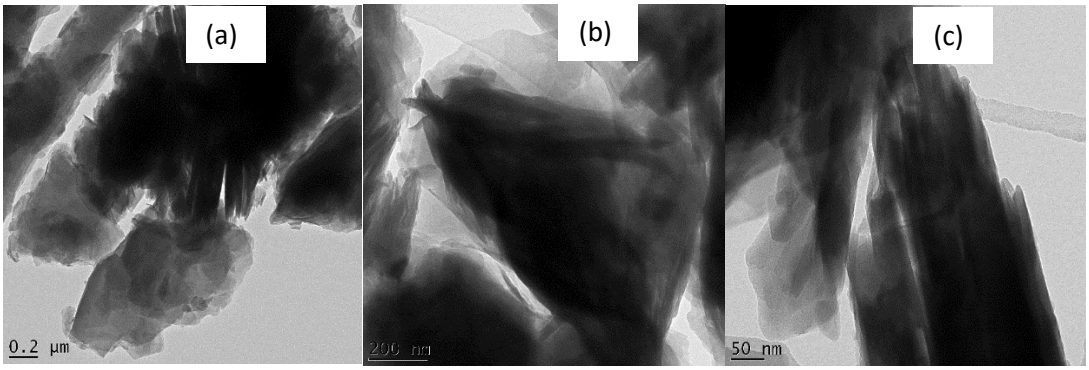


Plate XVIII: TEM images of metakaolin

4.5 Dealumination Process

The two dealumination products obtained were silica, being the solid product and alum, the liquid product. Plate XIX, shows the alum obtained after the reaction between metakaolin and acid in the dealumination reactor. The part A of the figure showed coloration in the alum produced from dealuminator, this was as result of the leaching of the iron content of the stainless steel used at high temperature of the reaction. After lining of the interior part of the reactor with material that is inert to concentrated acid at high temperature the alum obtained was void of such coloration as can be seen in part B of Plate XIX.

The silica obtained from the dealumination after thorough washing was dried, the white floppy powder obtained is as shown in Plate XX. The silica was further characterized for its physicochemical properties. The leaching effect of the interior part of the reactor had no observable effect on the silica as observed with the alum.

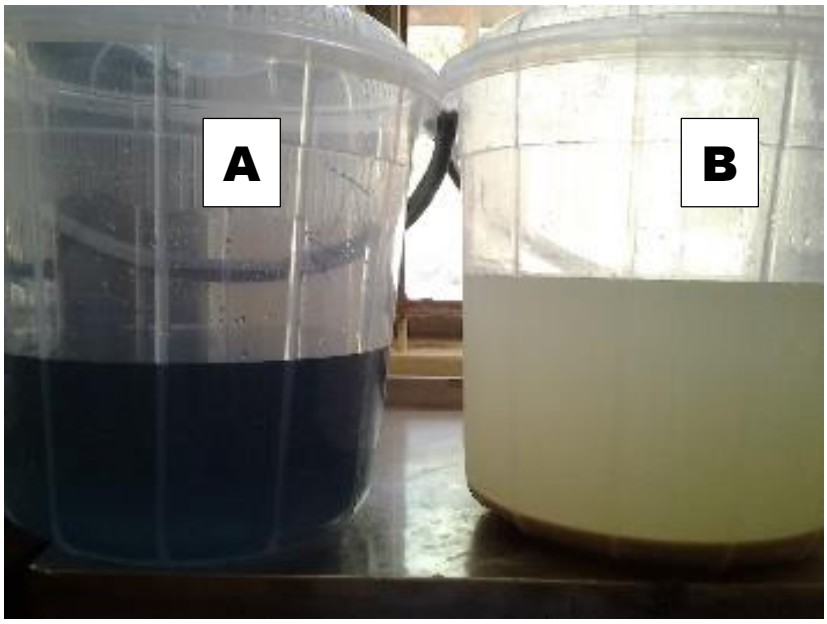


Plate XIX: Alum obtained after dealumination (A) with leaching (B) without leaching of reactor internal surface



Plate XX: Silica produced from Kankara kaolin after dealumination reaction

4. 5.1 Fourier transformed infrared (FTIR) analysis of silica

The FTIR spectrum of the silica produced from the pilot plant of the dealumination unit is presented in Figure 4.5. The spectrum possessed bands at wavelengths of 474, 806, 1102, 1649 and 3452 cm^{-1}. The band noticeable at 474 cm^{-1} was assigned to Si-O-Si in plane bending (Belver *et al.,* 2002). The band at 806 cm^{-1}, was due to the symmetric bending of O–Si–O (El-Naggar, 2013). The band at 1102 cm-^{1} was attributed to cluster of Si^{4+} and O^{2-} ions on the surface of Si–O vibration. The band at 1649 cm^{-1} was attributed to bending of H–O–H bonds. The band at around 3452 cm^{-1} was attributed to the –OH stretching (Lee *et al*., 2013). The curve in the spectrum appeared smooth which indicated that the sample is void of associated impurities. The purity of the silica is of importance especially when it comes to zeolite synthesis which is sensitive to the presence of impurities. Since the silica is one of the major ingredient for the preparation of the recipe for zeolite production.

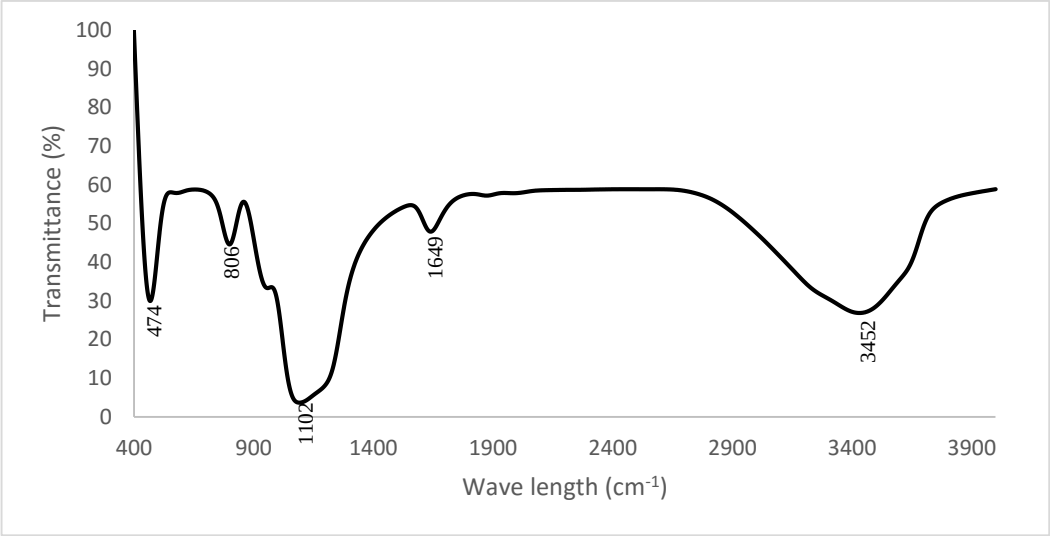


Figure 4.5: FTIR spectrum of silica prepared from Kankara kaolin

4.5.2 X-ray diffraction (XRD) analysis of silica

It could be observed that the XRD pattern of the silica shown in Figure 4.6 appeared amorphous but it consisted of few crystalline peaks. The prominent of this crystalline peak occurs at Bragg's angle of 26.6˚ which indicated the presence of crystalline silica known as quartz. As it could be observed the silica peak was the most prominent of all the peaks, implying that the material was predominantly silica. Some of the impurities observed were compounds of iron and calcium known as hematite and aragonite respectively. Hence it could be deduced that the silica obtained via dealumination of kaolin contains some impurities though in minimal concentration.

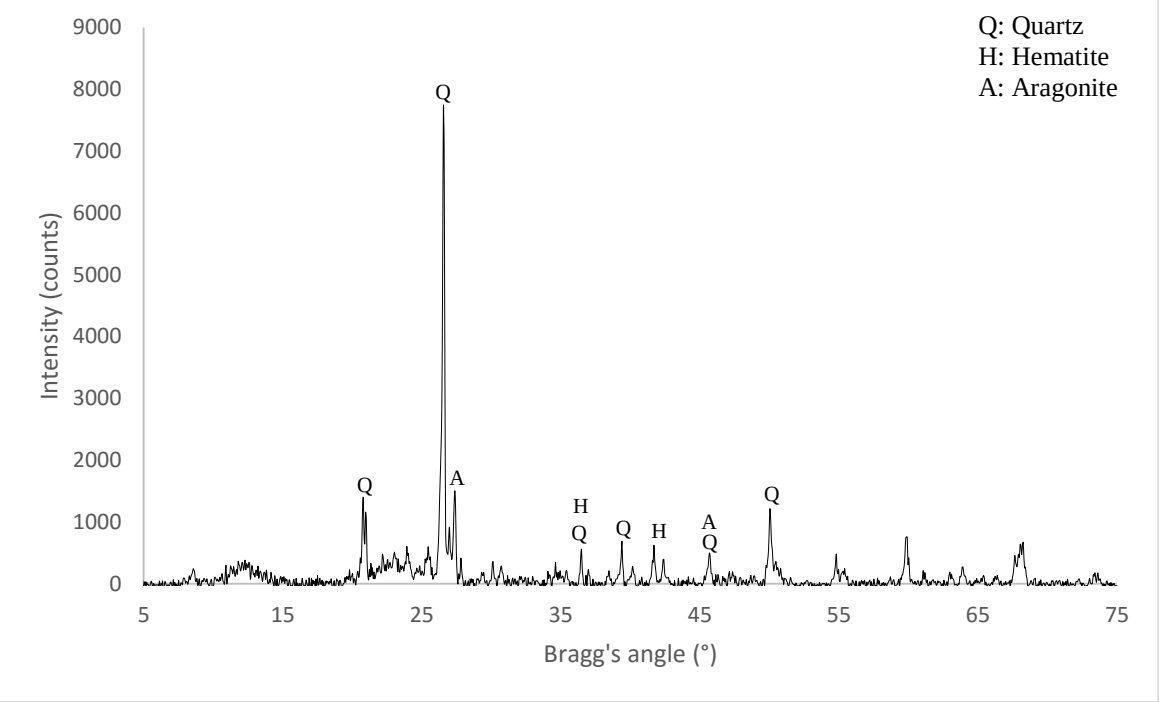


Figure 4.6: XRD pattern of silica prepared from Kankara kaolin

4.5.3 X-ray fluorescence (XRF) analysis of silica

From the chemical composition reveal by the XRF analysis of the silica obtained, presented in Table 4.6, it could be seen that the purity level of the silica was about 97 % w/w. And the alumina content was below detection, this observation shows the extent of the efficiency of the pilot scale metakaolin dealumination unit. The complete splitting of the two major constituents of kaolin was greatly achieved. The combined composition of Na_2O and K_2O was 1.2 % which was lower than the partially dealumination engage by previous researchers which lead to a low quality of zeolite produced, and the major challenge was the presence of potassium ion in higher quantity to the value obtained in this work. Only single dealumination was employed rather than the double dealumination reported (Salahudeen, 2015), to obtain high quality silica.

Table 4.6: Chemical composition of silica prepared from Kankara kaolin

SiO_2	Al_2O_3	Na_2O/K_2O	Fe_2O_3	CaO	MgO	TiO_2	OO
96.50	ND	1.20	0.23	0.18	ND	ND	1.89

ND: Not Detected OO: Other Oxides

4.5.4 SEM and TEM of silica prepared from Kankara kaolin

Plate XXI showed the SEM images of the prepared silica scanned at different magnifications. It could be observed from the highest magnification that the material possessed booklet structure containing sheets of silica. The lower magnifications revealed the tetrahedral shape of the particles. Therefore, the morphology of the silica was tetrahedral euhedral morphology. The distorted shape of the silica was evident of its amorphous nature, as also revealed by the TEM images shown in Plate XXII.

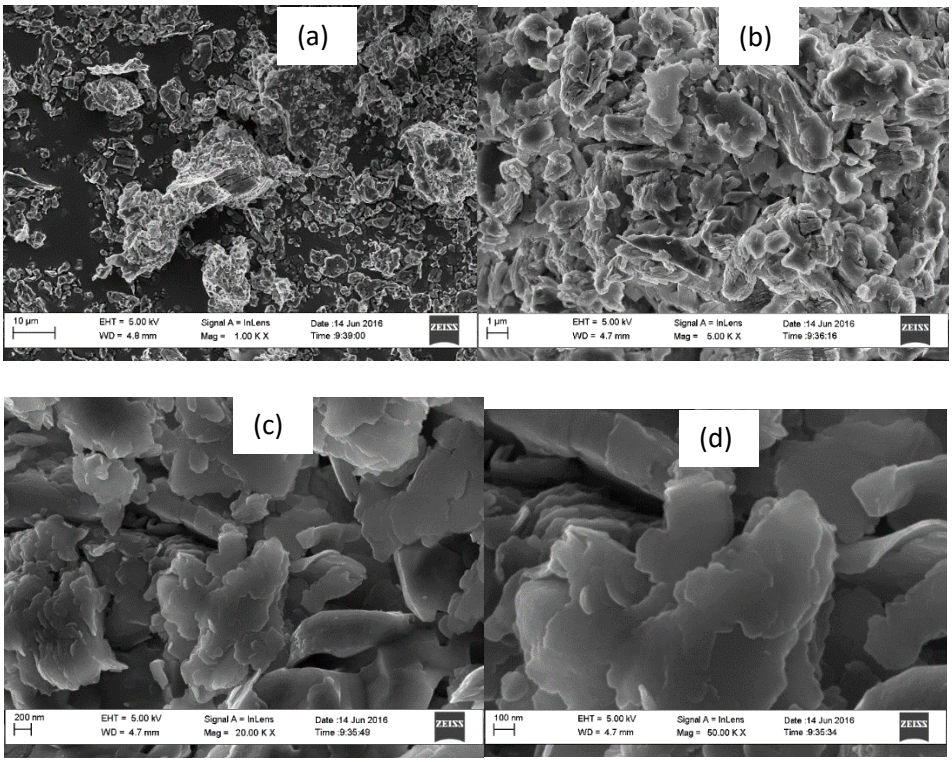


Plate XXI: SEM images of silica prepared from Kankara kaolin

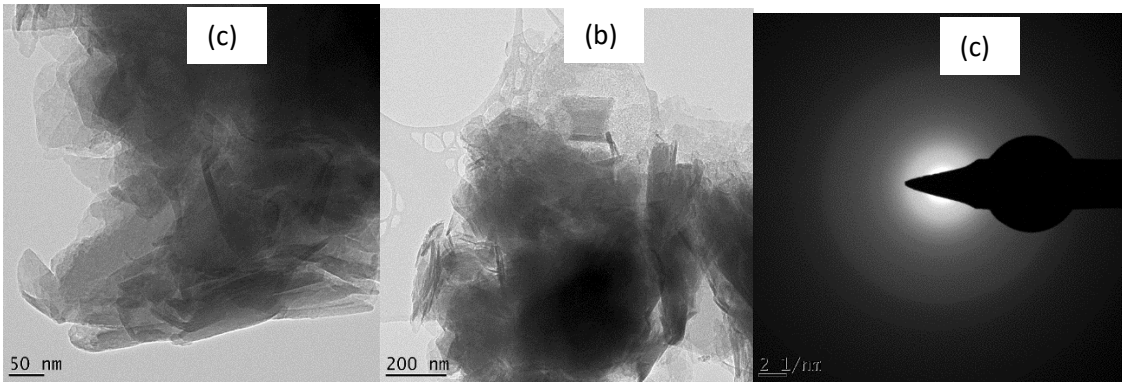


Plate XXII: TEM images of silica prepared from Kankara kaolin

4.6 Dealumination Reactor Efficiency

4.6.1 FTIR spectra of the solid reaction product

The vibrational spectra in Figure 4.7, show no much significant changes in the functional groups present in all the solid dealumination product obtained, known as silica. The vibrations at 473 cm^{-1} are related to the deformation mode of Si-O. The bands at 803 cm^{-1}, were due to the symmetric bending of O-Si-O (El-Naggar, 2013). At 1124 cm^{-1} bands were observed which could be attributed to cluster of Si^{4+} and O^{2-} ions on the surface of Si-O vibration. The bands at 1652 cm^{-1} were as a result of bending of H-O-H bonds. Finally, the bands around 3508 cm^{-1} were attributed to the –OH stretching (Lee *et al*., 2013).

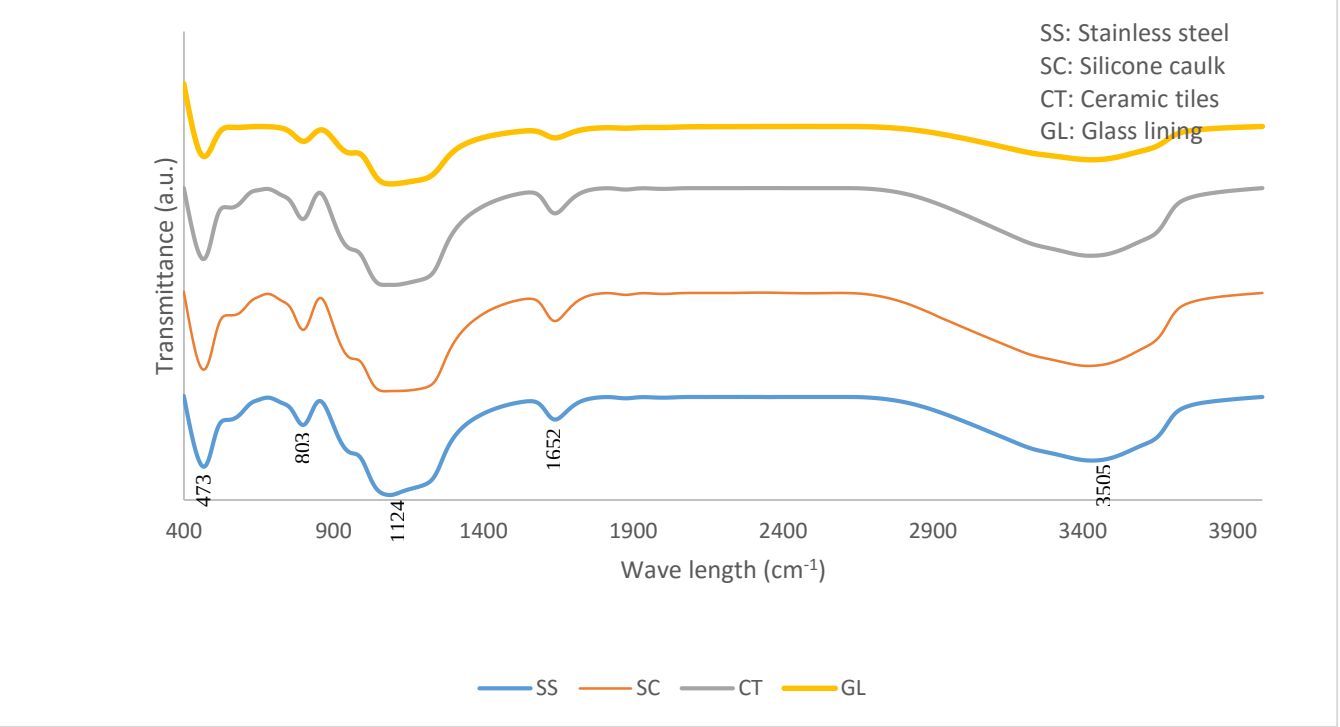


Figure 4.7: FTIR spectra of various silica produced from dealumination reaction

4.6.2 XRD patterns of the solid reaction product

The silica products obtained were void of residual kaolinite as prominent peaks for the mineral at 12.4, 20.4, 24.8 and 34.9° were absent, as seen from Figure 4.8. The peaks of quartz which is silica mineral was identified. The high peak at 26.2° was due to the presence of crystalline silica, while the other lower peaks shows that the silica was largely amorphous. More so, the presence of broad peaks in all the XRD patterns connotes the amorphous nature of the silica. The impurity phase observes from the XRD pattern was aragonite, a calcium based mineral. Despite the different configuration of the interior part of the dealumination reactor, similar XRD patterns were obtained.

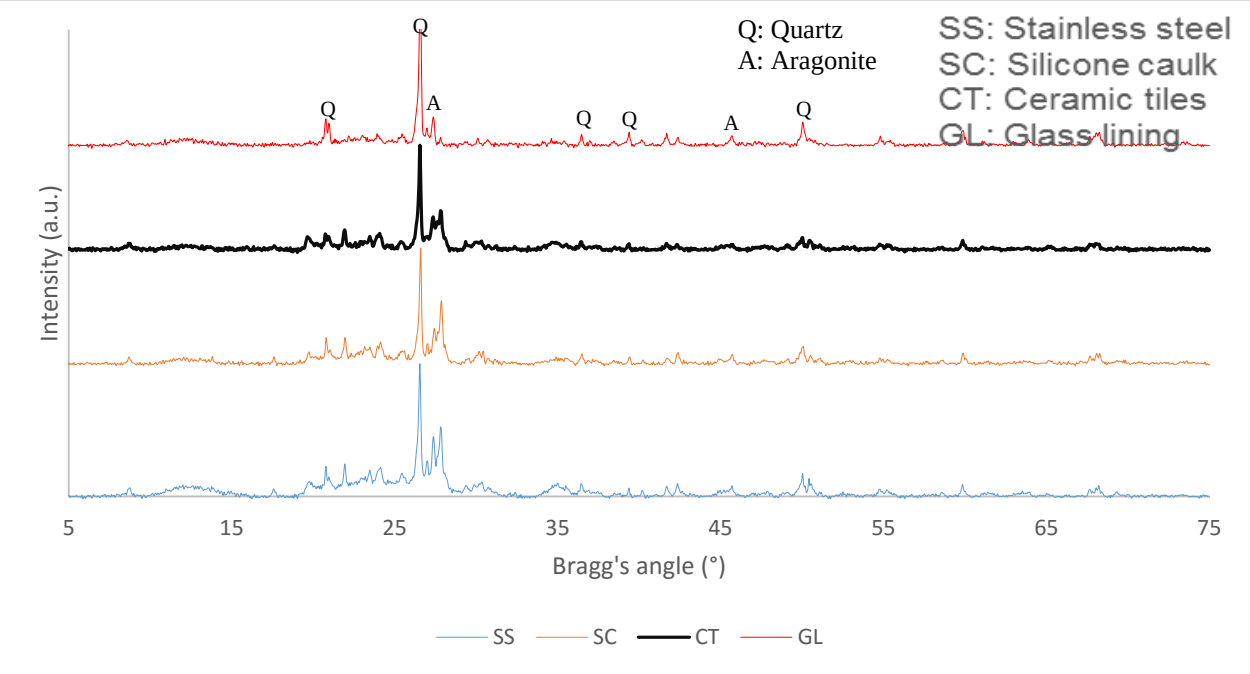


Figure 4.8: XRD patterns of various silica products from dealumination reaction

4.6.3 Solid product quality

The dealumination process at the laboratory level of 94% was better than the pilot scale of 86% when the dealumination reactor was made up of stainless steel, Type 304 and coated

with silicone caulk, based on the quality of the product obtained. The reason being that not all the energy of hydration generated during the reaction was used to drive the dealumination process, because part of the energy carried out leaching of iron content of the stainless steel via the corrosive nature of the reaction medium. This was visible, as the liquid product was greenish instead of being milky, the color observed suggested the presence of Fe_2SO_4. But when the lining of the interior surface was properly done to prevent the corrosive mixture to have contact with the stainless steel surface of the reactor better results were obtained. Lining with ceramic tiles and glass gave higher results than the laboratory experiment, as shown in Figure 4.9.

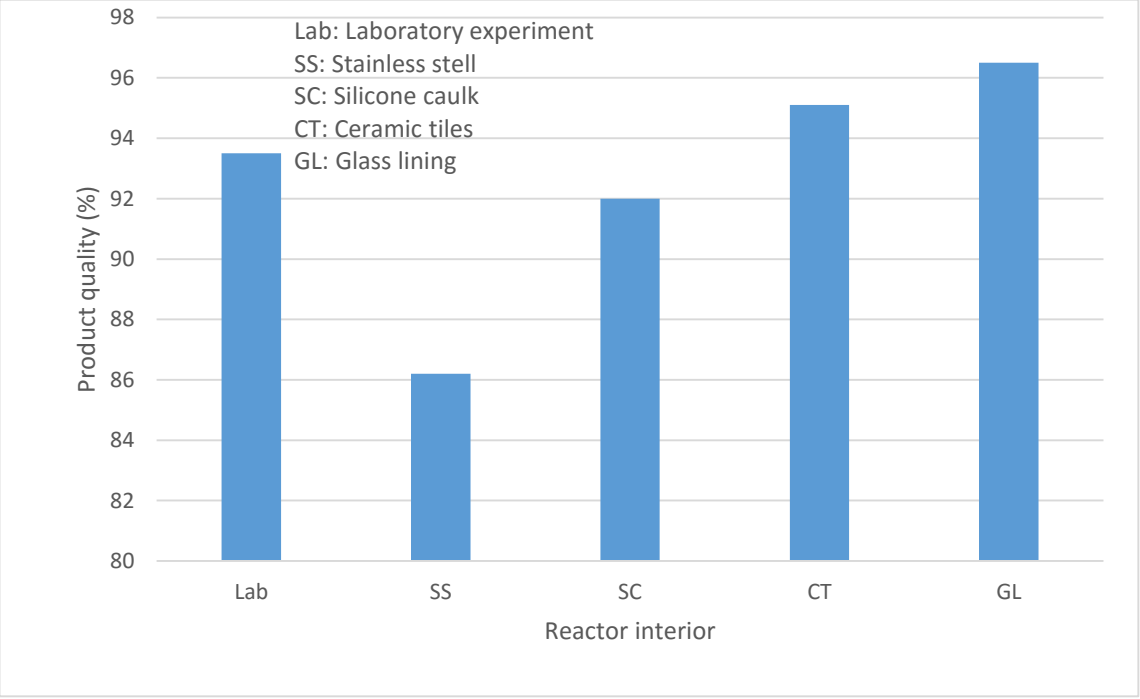


Figure 4.9: Product quality of different materials used in the reactor interior

4.6.4 Evaluation of reactor efficiency

The trend of the reactor efficiency is much similar to the product quality of the dealumination reaction as shown previously in Figure 4.9. And the same explanation holds, but the increase

in the efficiency of both ceramic tiles and glass lining of 96 and 98% respectively as shown in Figure 4.10, was due to the effective utilization of the heat generated to drive the reaction, being an endothermic in nature. Despite their efficiency were high and satisfactory but the glass lining was more durable as the tiles usually fall-off with time.

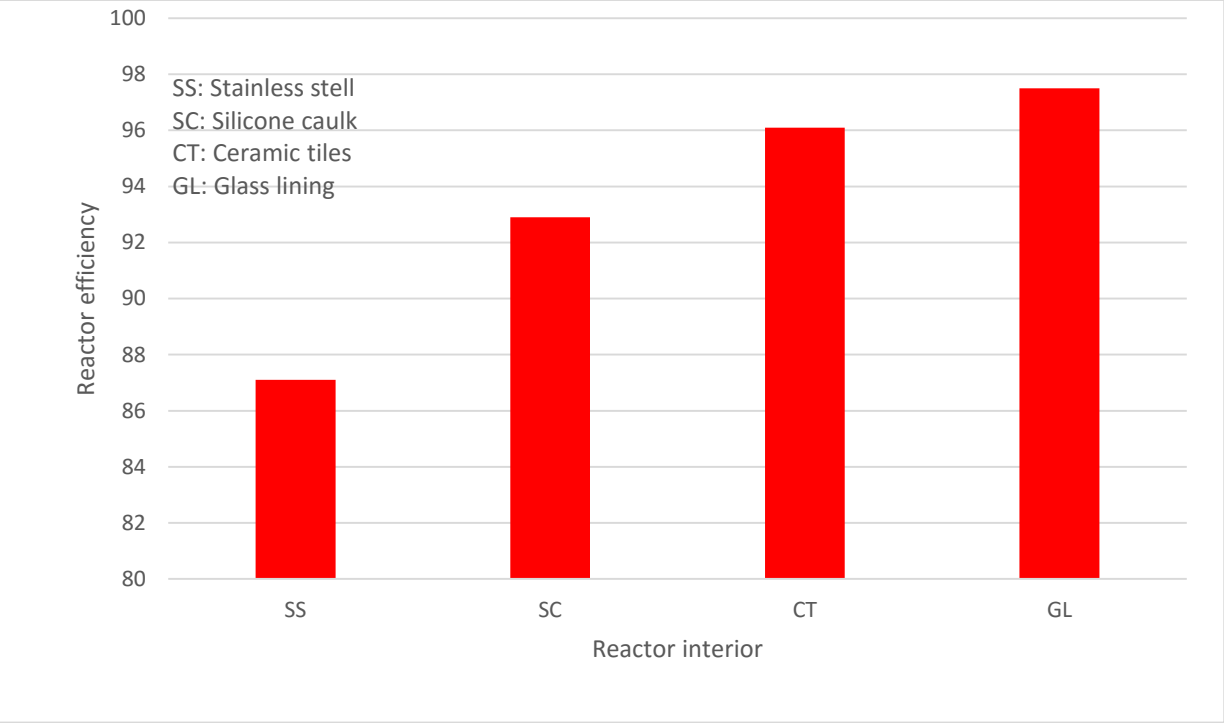


Figure 4.10: Reactor efficiency with respect to different materials at the interior part of the reactor

4.7 Physicochemical Characterization of Aluminum Hydroxide

4.7.1 FTIT spectrum of aluminum hydroxide produced from Kankara kaolin

The FTIR spectrum of the aluminum hydroxide produced at the pilot scale is shown in Figure 4.11. The bands between 570 and 800 cm^{-1} were due to the symmetric bending of O–Al –O

(El-Naggar, 2013), as well as the band at 1649 cm^{-1}. The band 3448 cm^{-1} was attributed to OH- vibration and the bands of the stretching OH group.

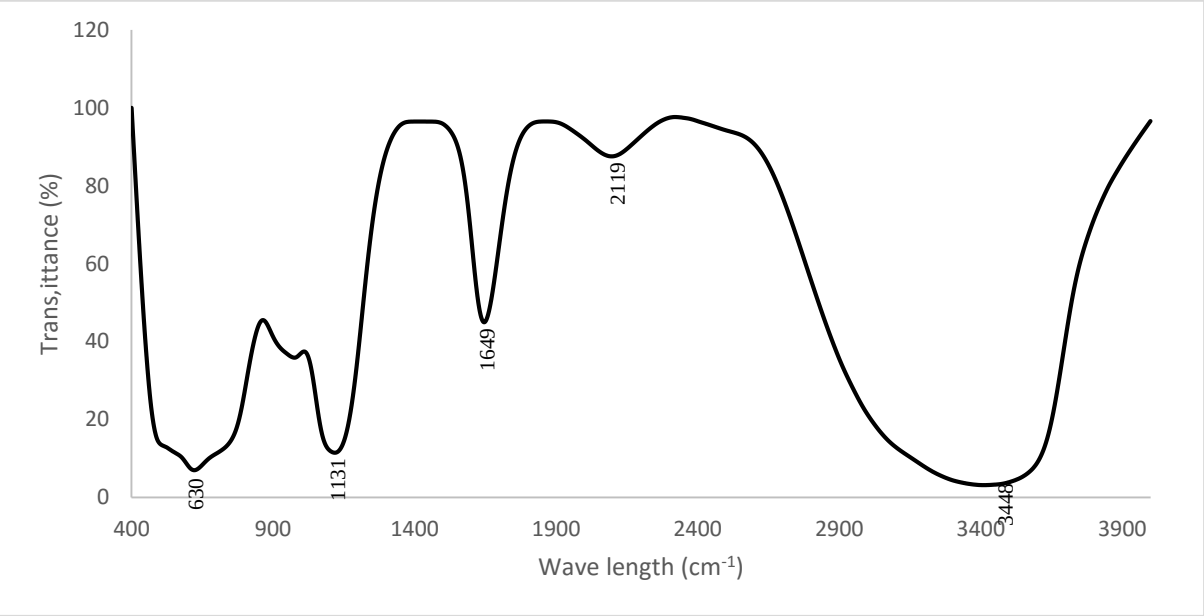


Figure 4.11: FTIR spectrum of aluminum hydroxide prepared from Kankara kaolin

4.7.2 XRD pattern of aluminum hydroxide produced from Kankara kaolin

The XRD pattern obtained from the XRD analysis of the aluminum hydroxide produced at the pilot unit, shows it was amorphous as evident by the broad peaks and low intensity counts observed in Figure 4.12. The peaks at 28, 38, 49 and 65° were the characteristic peaks for the boehmite phase of aluminium hydroxide (Du *et al*., 2009; Lee *et al*., 2009). The amorphous nature of the aluminum hydroxide produced was highly desired, because it would be reactive when used subsequently for zeolite recipe preparation.

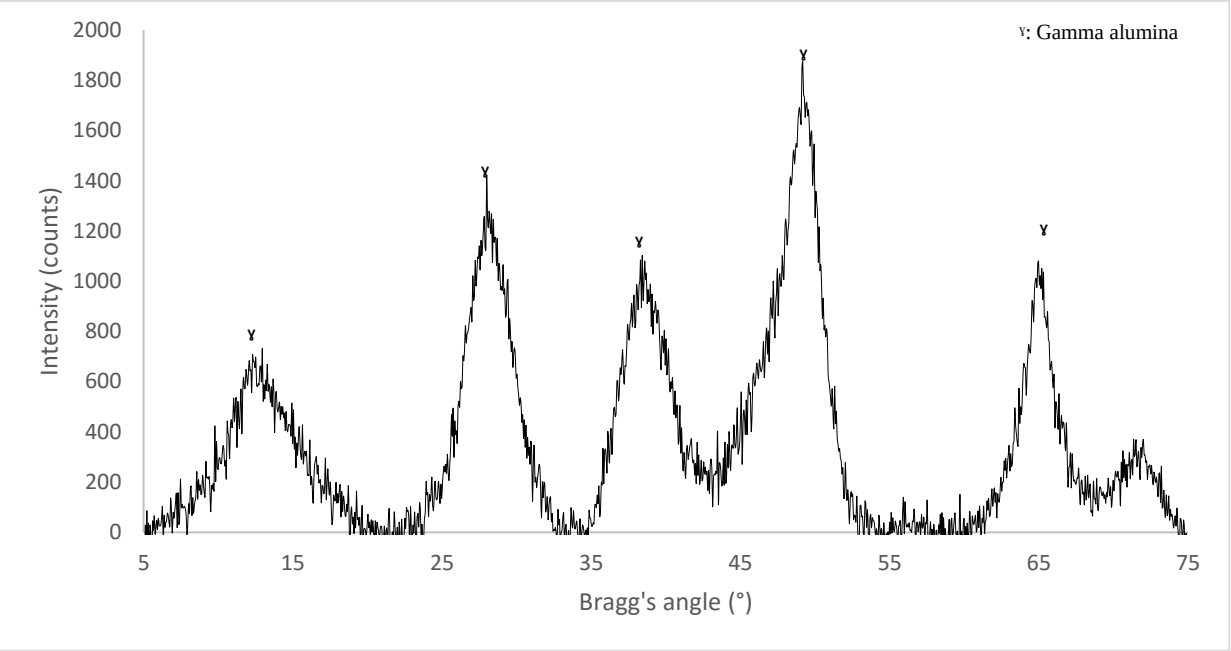


Figure 4.12: XRD pattern of aluminum hydroxide prepared from Kankara kaolin

4.7.3 SEM and TEM images of aluminum hydroxide produced from Kankara kaolin

It could be observed from Plate XXIII the micrograph of the aluminum hydroxide at lower magnifications showed aggregated lumps. Each lump represented a macrostructure which consisted of agglomerated particles with irregular particle shapes. Therefore, it could be deduced from the images that the aluminum hydroxide possessed a lumpy anhedral morphology, this further showed the amorphous nature of the aluminum hydroxide produced as already shown by the XRD result at higher magnification the particles seem to possess a definite shape, although the shape was not clearly defined. The structural morphology was a flake-like euhedral morphology. It could be observed that the structural images revealed by the TEM were blurred as shown in Plate XXIV, this showed the amorphous nature of the material as already identified by the XRD and SEM results of the same sample. The actual crystal shape of the material could not be revealed even at the highest magnification.

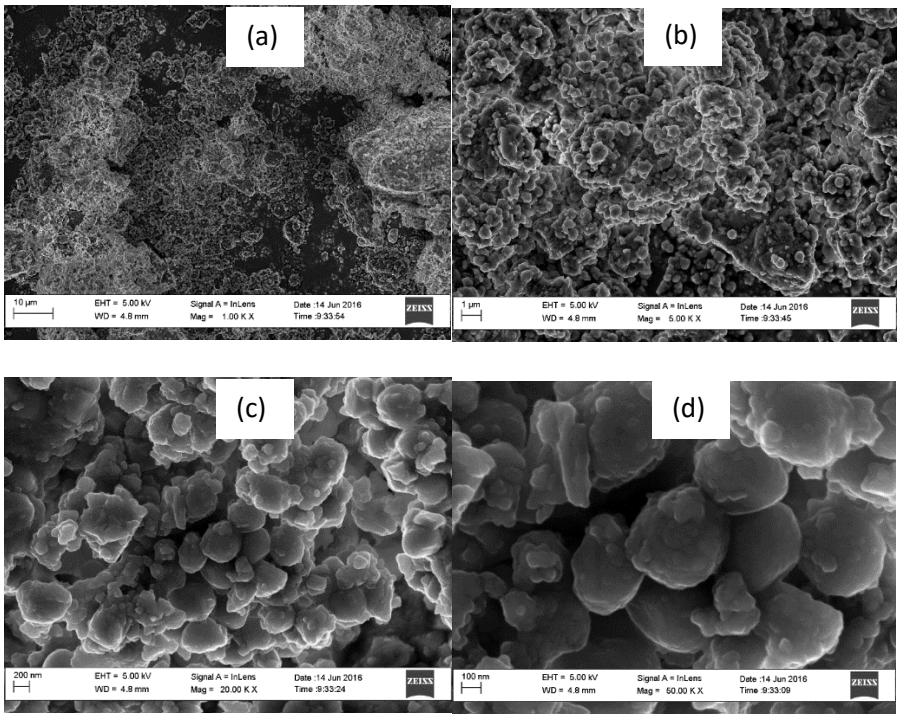


Plate XXIII: SEM images of aluminum hydroxide at different magnifications

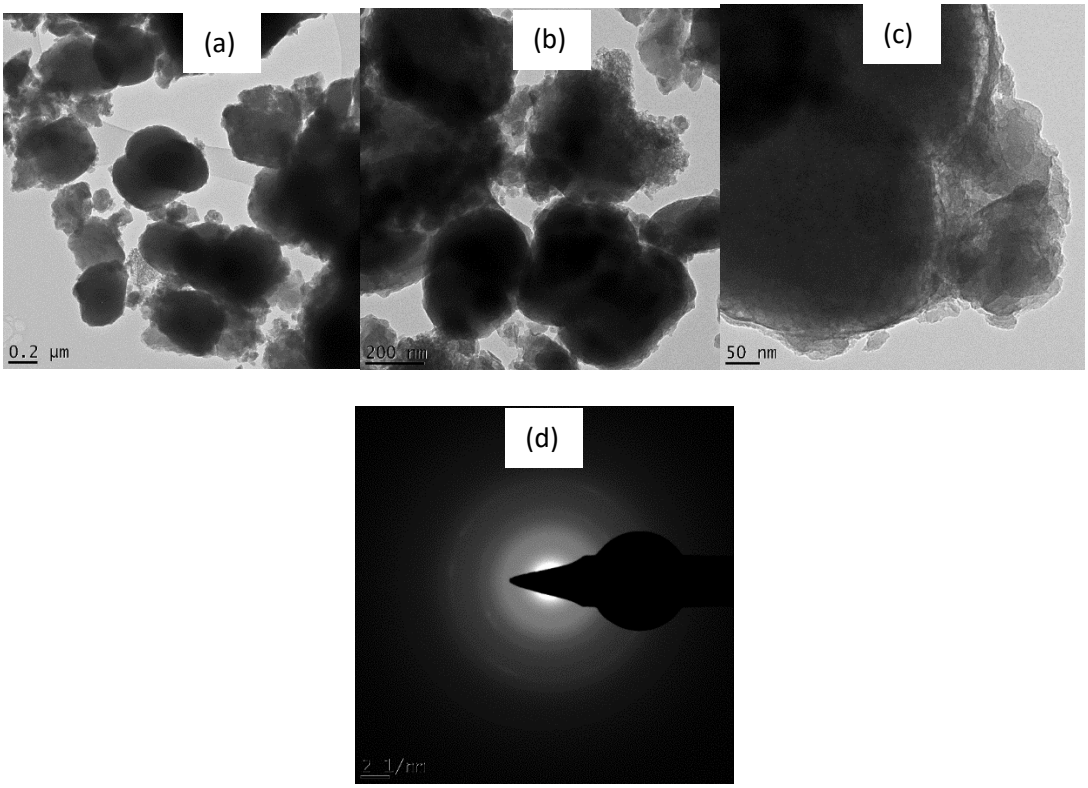


Plate XXIV: TEM images of aluminum hydroxide at different magnifications

4.8 Other Intermediate Products

Some of the intermediates include dilute and concentrated sodium silicate as well as silica sol. For zeolite Y production, the sodium silicate pilot unit was used to produce dilute sodium silicate which was concentrated and presented in Plate XXV. Silica sol was prepared from dilute solution of sodium silicate via acidification technique. Plate XXVI, shows the freshly prepared silica sol which was concentrated and dispersed with ultra-sonicator for ZSM-5 zeolite production.



Plate XXV: Concentrated sodium silicate prepared from Kankara kaolin

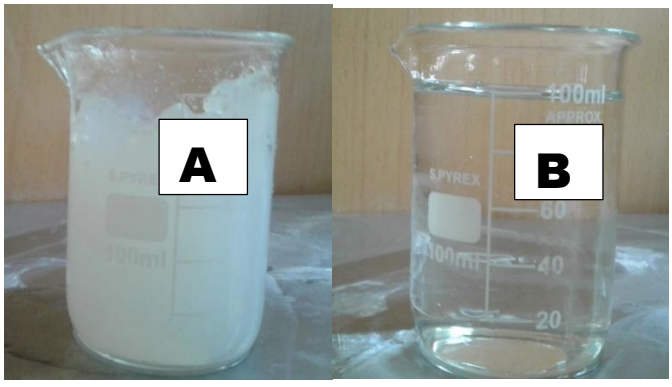


Plate XXVI: Silica sol (A) Freshly prepared (B) Dispersed concentrated silica sol

4.9 Zeolite Reactor Development

4.9.1 Heating method

The initial zeolite reactors for both the production of zeolite Y and ZSM-5 zeolites involved internal heating source, based on that the heating element was lined with Teflon and the volume of recipe needed was much for a test run. Since the material preparation was tasking, it was wise to begin the production process step wise not at full capacity of the pilot plant. The internal means of heating could not afford such kind of flexibly as the heating element height was almost the height of the reactant contents to ensure good heat distribution during the zeolite crystallization phase which was the most vital step in the zeolite production process. Despite good zeolite was produced with the reactor with internal heating, shown in Plate XXVII (A), the challenges enumerated informed the choice of considering an alternative reactor configuration which could handle a step wise progression of production to full capacity of the reactor and the cost of Teflon lined heating element. To cope with the earlier challenge another zeolite configuration was set-up, in which the heating element was not in direct contact with the reaction content. A water-bath kind of heating means was fabricated (Plate XXVII B), and the heating element was made of stainless steel, which was position below the holder of the vessel where the reaction takes place. The entire reactor was a closed vessel to maximize the steam produced for effective heating. With such content the volume of reactants could be varied.



Plate XXVII: Zeolite reactor (A) internal (B) external heating

More so, the heating element was not exposed to corrosive environment and the need for coating the surface with Teflon was overcome. The only components that was in direct contact with reaction mixture was the temperature prop as shown in Plate XXVIII which was connected to the control system to maintain the reaction temperature. This configuration was flexible in terms of the type of zeolite to be produced. The only component to be change is the vessel holding the reaction mixture. Good quality zeolite was produced with this configuration.

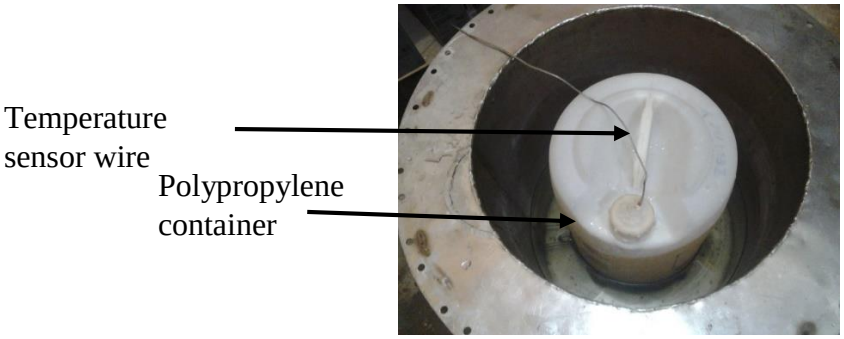


Plate XXVIII: Internal configuration of zeolite reactor (external heating)

4.9.1.1 FTIR spectra of produced zeolite

It could be observed from Figure 4.13, that the FTIR spectra of samples were similar to each other, i.e. the laboratory synthesized zeolite Y and those produced from the pilot plant *via*

internal and external means of heating. The zeolites possessed IR transmittance bands at wavelength around 468, 571, 600, 769, 1000, 1658 and 3466 cm^{-1}. Prior studies reported that the characteristic FTIR bands for zeolitic lattice are in the wavelength range of 460–1200 cm^{-1} (Modi *et al*., 2012). Particularly the characteristic FTIR bands for zeolite Y are located around 1000, 769 and 715 cm^{-1} (Zhang *et al*., 2008). The band at 468 cm^{-1} was attributed to Si–O tetrahedral deformation. The band at 571 cm^{-1} was attributed to Si–O–Al octahedral stretching. The band at 571 cm^{-1} was attributed to Si–O–Al in-plane bending. The band at 776 cm^{-1} was attributed to Si–O–Al out-of-plane bending. The broad band stretching between 950 and 1020 cm^{-1} was attributed to Al–OH vibration and Si–O tetrahedral stretching vibration (in plane). The band at 1662 cm^{-1} was attributed to vibration of water molecule. The band at 3466 cm^{-1} was attributed to O–H bond stretching vibration (Percival *et al*., 1974; Kloprogge *et al*., 1999; Steudel *et al*.,2009; Benincasa *et al*., 2001; 2009; Pal *et al*., 2013).

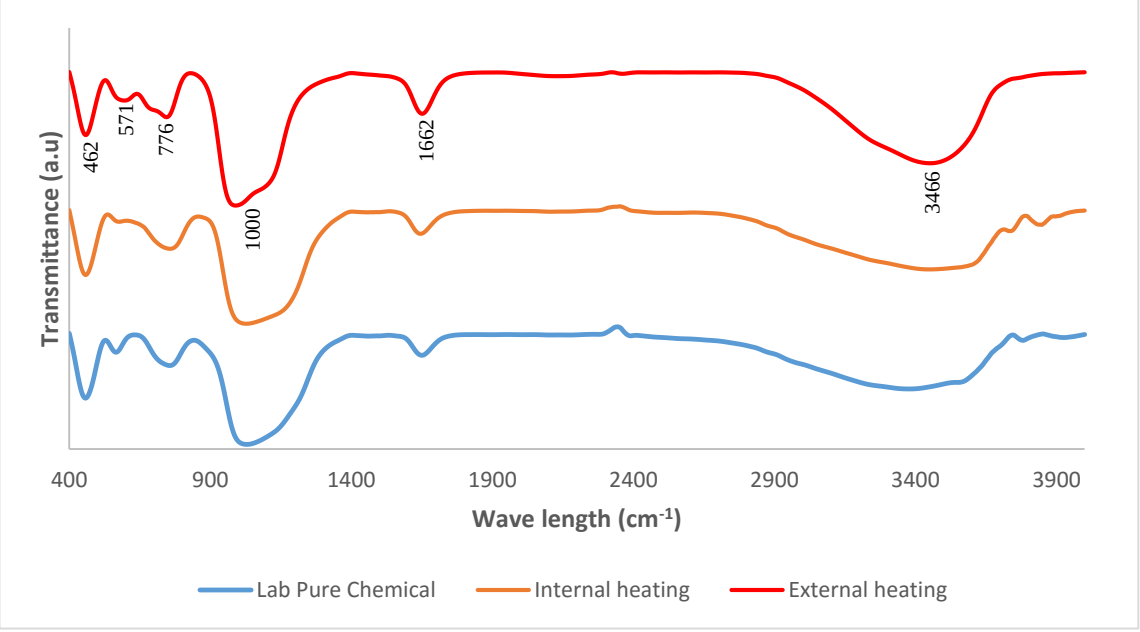


Figure 4.13: FTIR spectra of zeolite Y produced *via* different heating means compared with reference

4.9.1.2 XRD pattern of produced zeolite

The zeolite Y peaks found at Bragg's angle of about 6, 10, 12, 16, 19, 20, 24, 27, 31 and 32˚ (Ginter *et al*., 1992; Robson, 2001; Treacy and Higgins, 2001) could be observed in the three XRD patterns presented in Figure 4.14. However, the intensity of the characteristic peak of zeolite Y at Bragg"s angle of 6.15 was prominent in all the samples, but the sharpness of the peak varied among the samples. The nature of the peak gives information about the crystallinity of the zeolite. The height of the prominent peak at about 6 ° Bragg's were almost similar with the pilot plant zeolite Y with external heating, having the highest. The pilot plant production was comparable to the laboratory synthesis, which was a step in the right direction. The XRD intensity of the characteristic peak of a mineral indicates the extent of crystallinity and the concentration of the crystalline content of the material (Bebon *et al*., 2002; Pal *et al*., 2013).

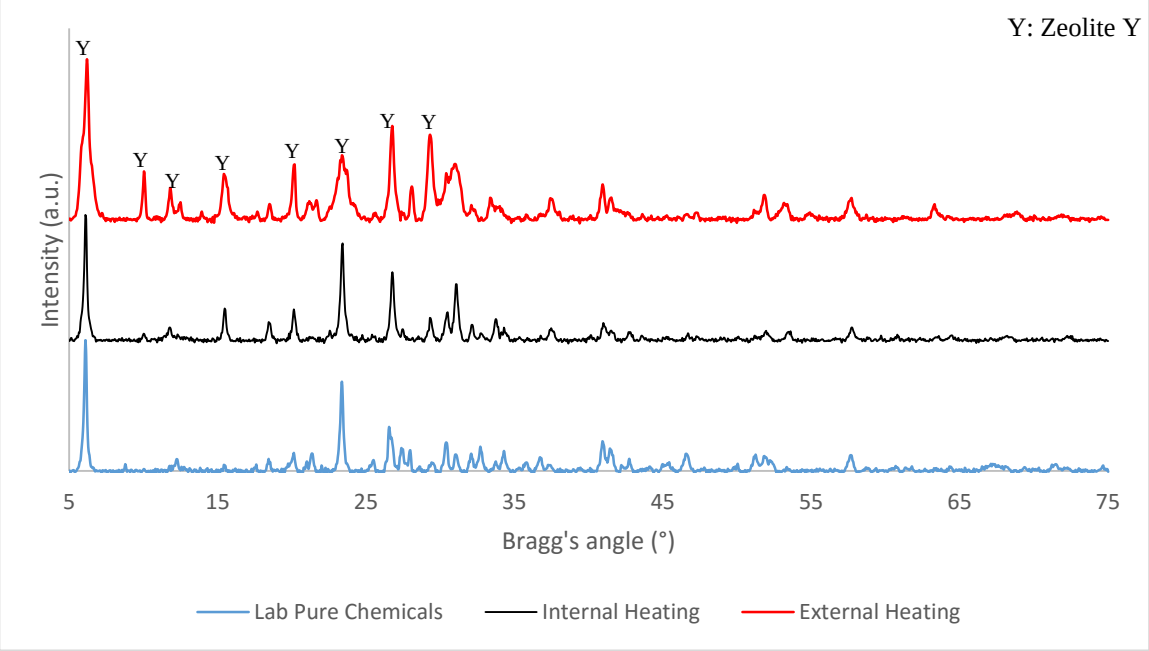


Figure 4.14: XRD patterns of zeolite Y produced *via* different heating means compared with reference

4.9.2 Products yield

The amount of zeolite was quantified gravimetrically to ascertain the efficiency of the developed zeolite production process. The yield for both zeolite Y and ZSM-5 were analyzed. The yield of zeolite Y production was evaluated based on the amount of product obtained against expected amount of product in gravimetric terms. Increase in yield was observed, as shown in Figure 4.15, as the production process was repeated. The observed increase was attributed to mastering of the process as well as minimizing loss of materials, since the process from start to finish was enormous.

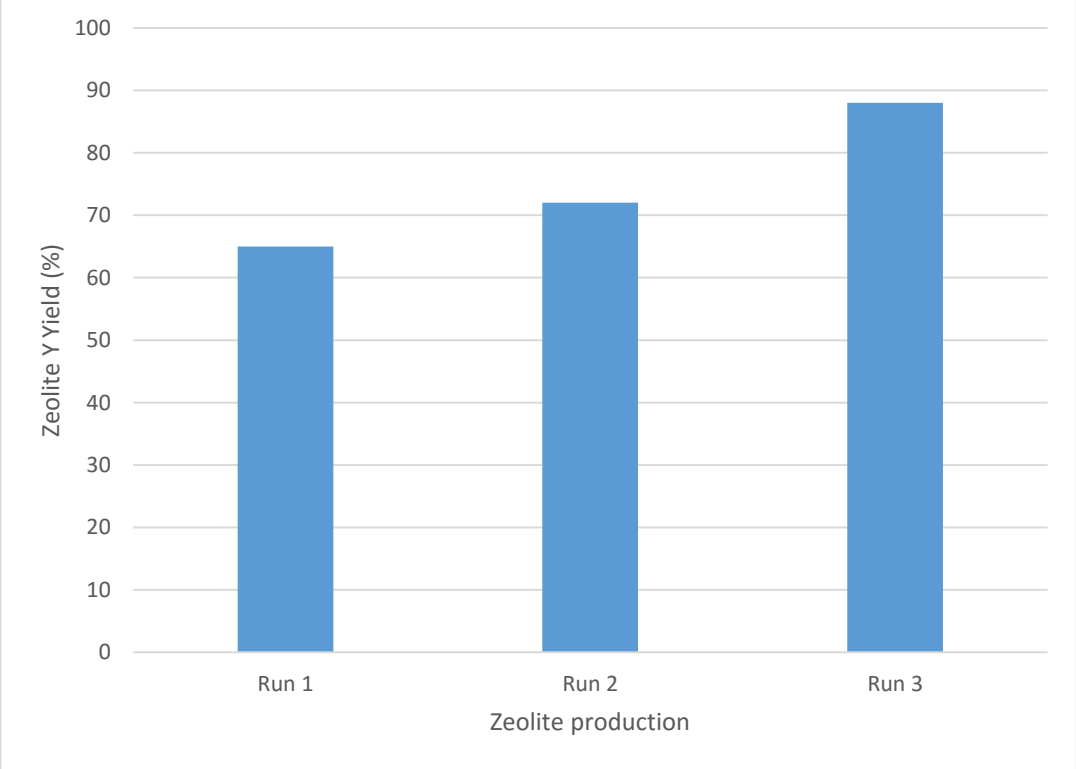


Figure 4.15: Yield of zeolite Y produced from developed pilot size reactor

The first production of ZSM-5 yield was small compared to that of zeolite Y, this was attributed to the lower concentration of silica sol used. But when the silica sol concentration was perfected higher ZSM-5 yield was obtained as presented in Figure 4.16.

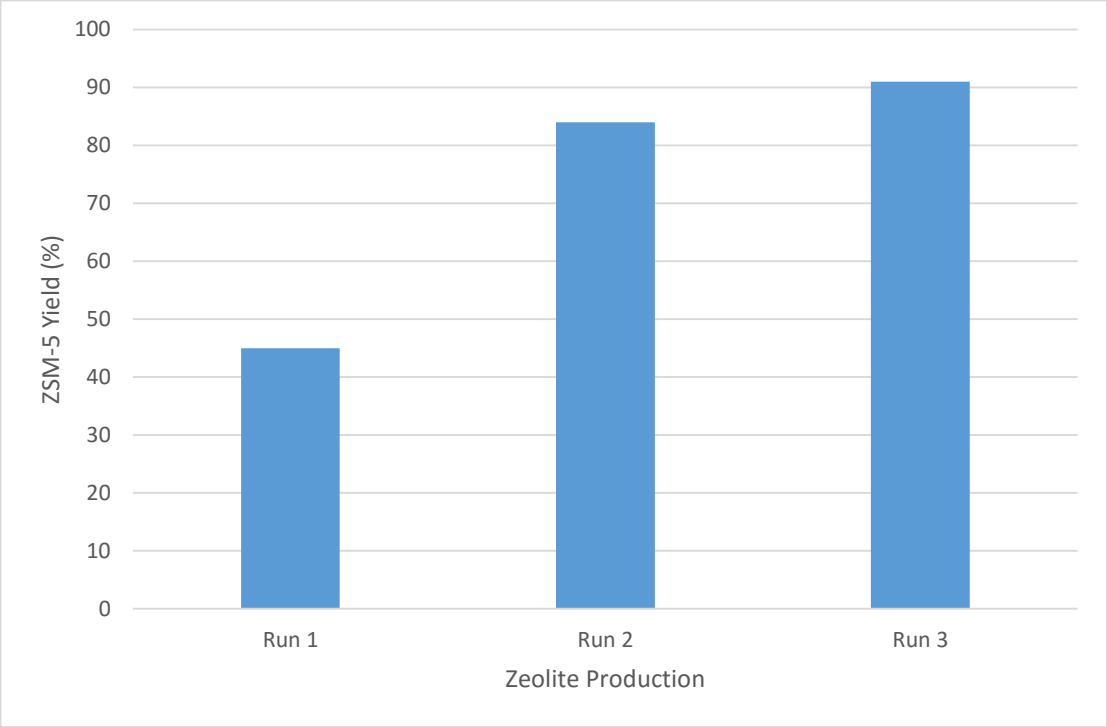


Figure 4.16: Yield of ZSM-5 zeolite produced from developed pilot size reactor

4.9.3 Zeolites process development

The major peaks for zeolite dominate the XRD pattern shown in Figure 4.17, but the intensity of run 3, was so high that the peaks for Runs 1 and 2 were suppress and could not be clearly seen, as such individual XRD patterns for all the three separate production runs were presented in Figures 4.18, 4.19 and 4.20 for the first, second and third production respectively.

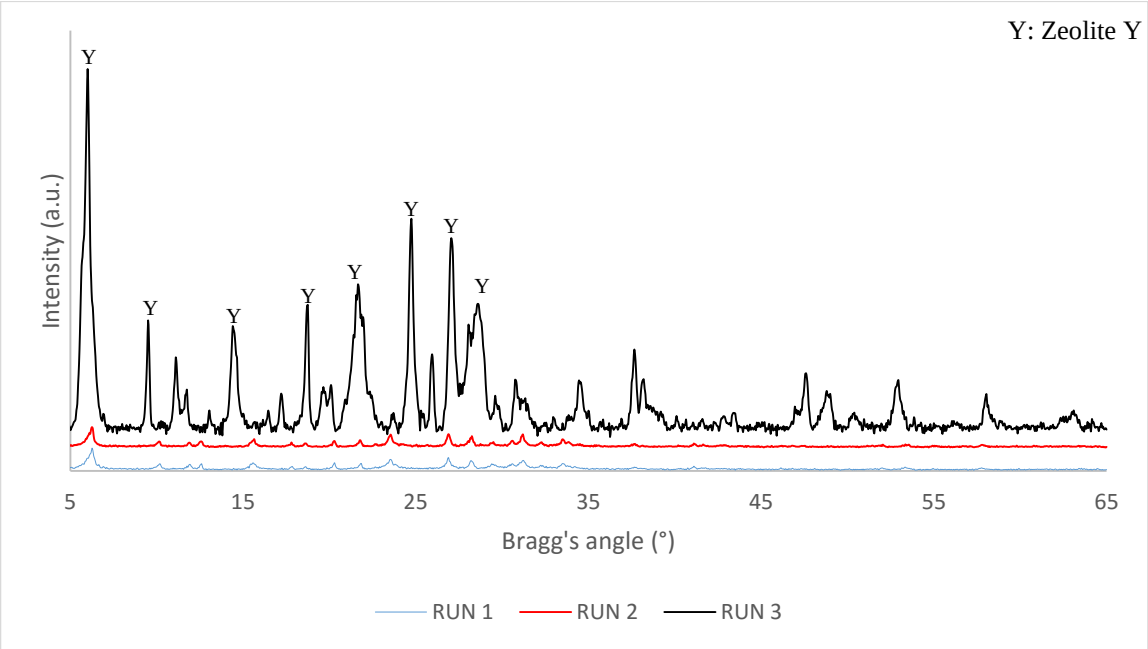


Figure 4.17: Pilot scale production of zeolites Y from Kankara kaolin

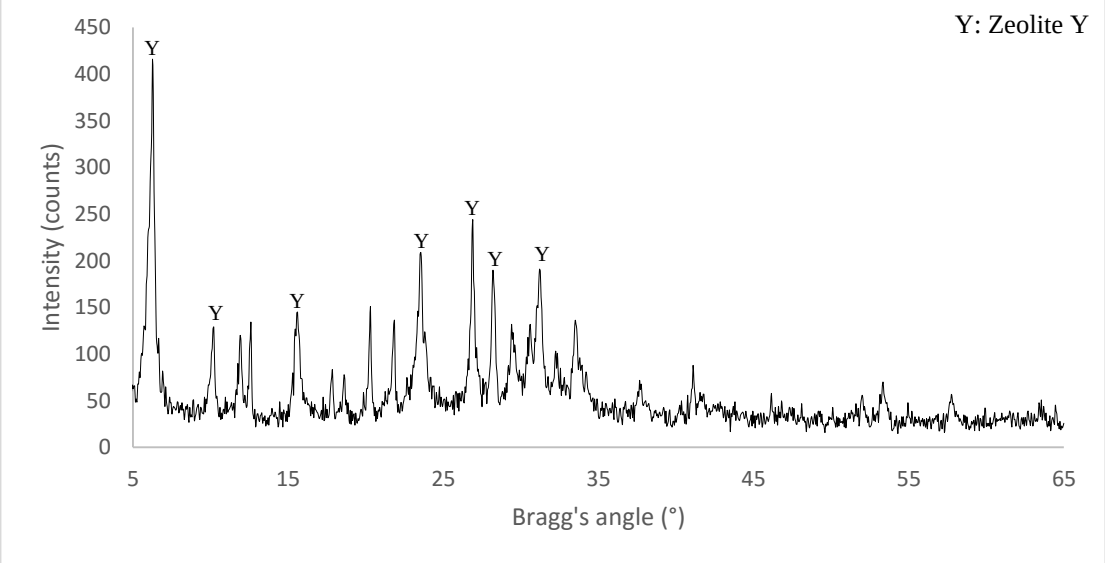


Figure 4.18: XRD pattern for zeolite Y produced at Run 1

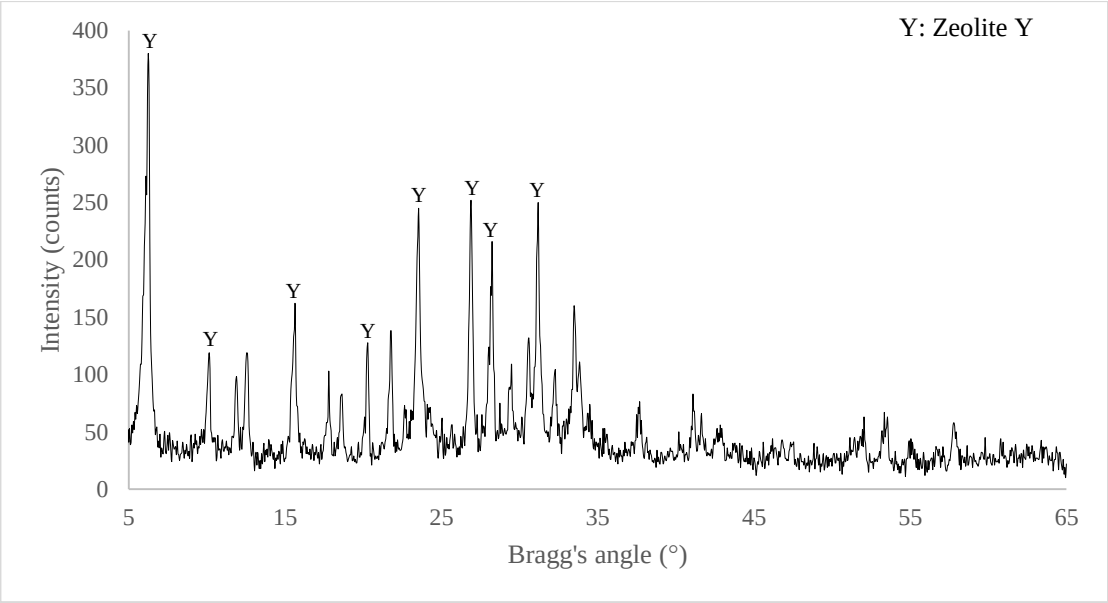


Figure 4.19: XRD pattern for zeolite Y produced at Run 2

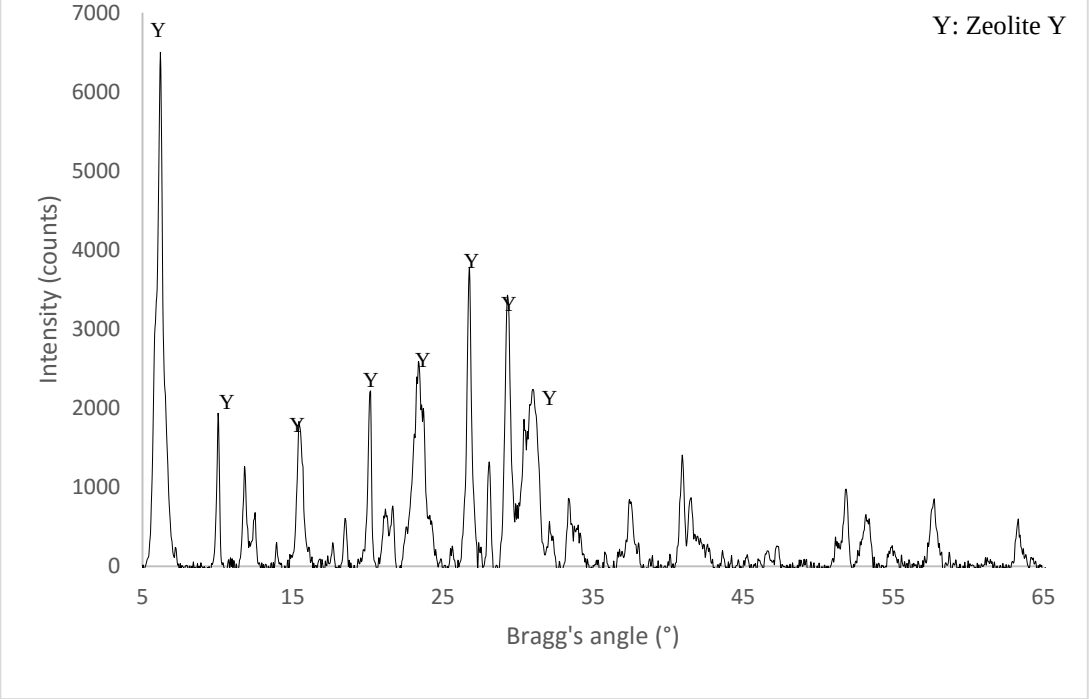


Figure 4.20: XRD pattern for zeolite Y produced at Run 3

The three different zeolite Y XRD pattern affirm the reproducibility of zeolite Y from established pilot plant process. All the important peaks of zeolite Y were present and the dominance of the peak at 6.15 Bragg's angle was evident in all the three zeolite Y samples.

Production development process for ZSM-5 was investigated. The first run did not crystallize well because of the concentration of silica sol stated earlier. But the second and third runs were good, the characteristic peak of ZSM-5 at Bragg's angle of 7.9, 8.9, 23.1, 23.9 and 24.4 ° (Treacy and Higgins, 2001) were present as observed in Figure 4.21. As in the case of zeolite Y, the reproducibility of ZSM-5 was dually ascertained.

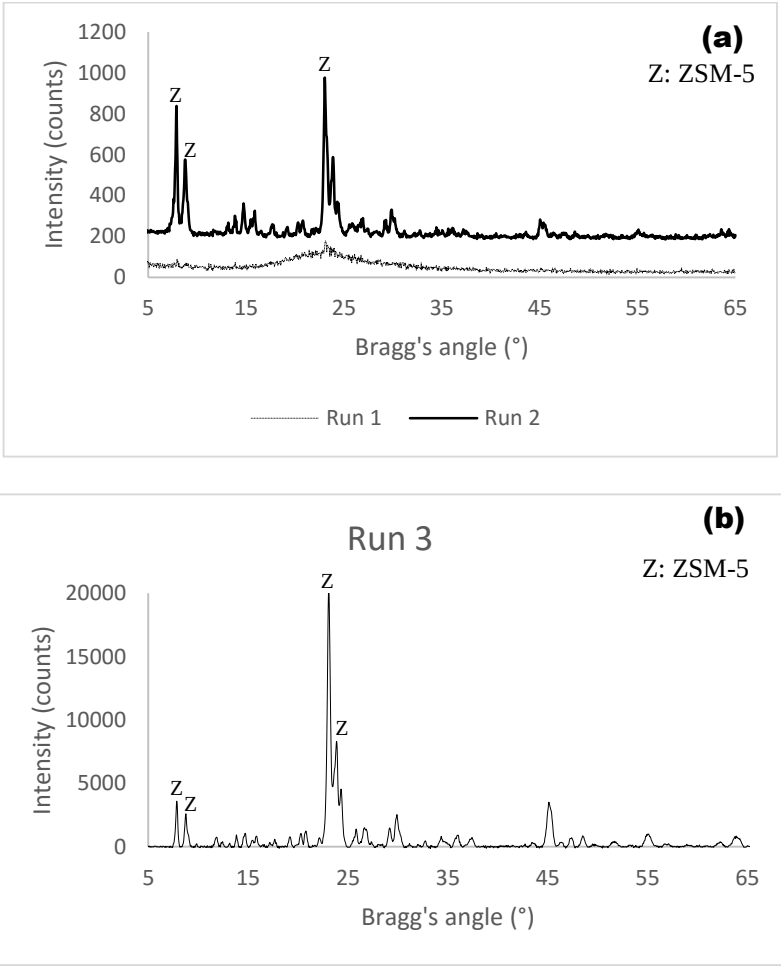


Figure 4.21: ZSM-5 reproducibility (a) Runs 1 & 2 (b) Run 3

4.9.4 Products Quality

For zeolite Y the crystallized zeolite was observed to be in two layers, the top and bottom. The two separates layer were washed, dried and analyzed separately. The FTIR spectra and the XRD patterns are shown in Figures 4.22 and 4.23 respectively. The FTIR spectra were similar, while in the XRD pattern for the bottom layer of the zeolite Y, a prominent peak at Bragg's angle of 28.04 was observed. The observed peak connotes the presence of hypersthene $(Mg, Fe)_2 Si_2O_6$ (Chan, 1977). Off white coloration was observed with the bottom layer product, in contrast to the whitish crystal of the top layer, the presence of Fe^{2+} might be responsibility for the observed color. The top layer was used for further analysis and application.

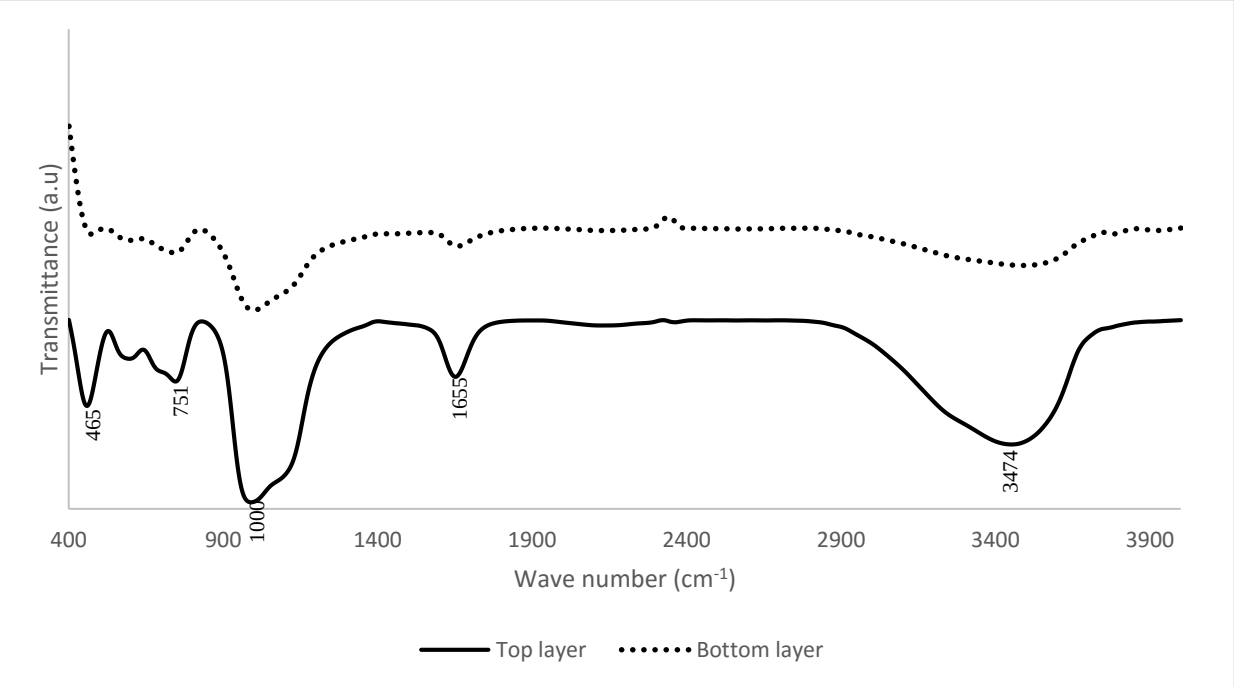


Figure 4.22: FTIR of top and bottom layer of zeolite Y produced from pilot unit

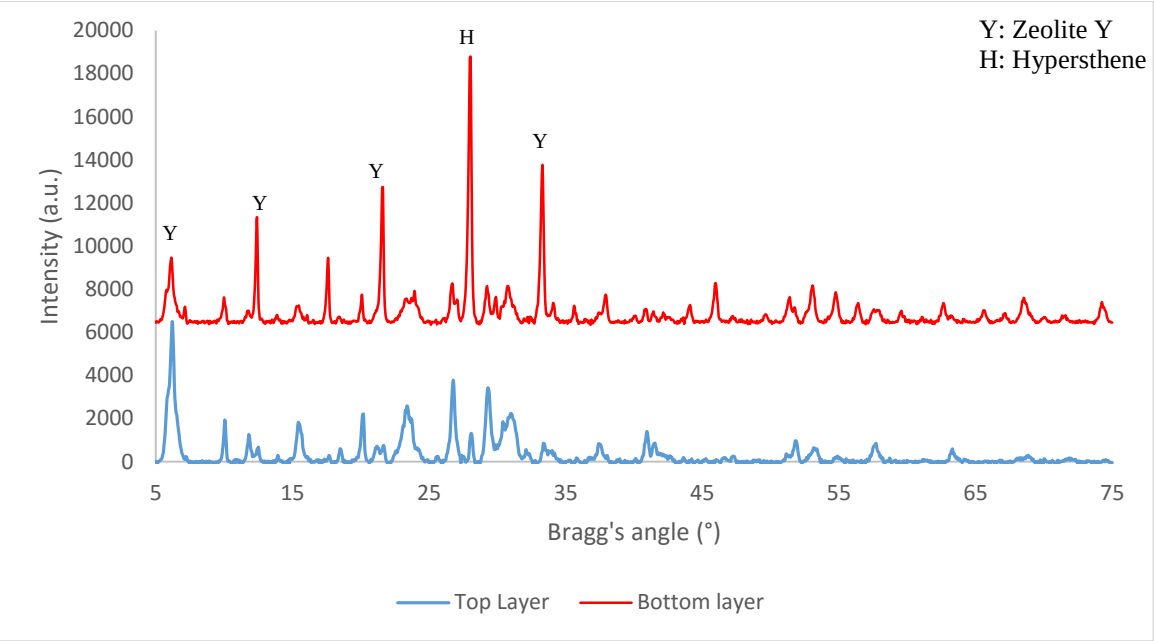


Figure 4.23: XRD patterns of top and bottom layer of zeolite Y produced from pilot unit

It was observed from Figure 4.24, that template reduced the well-formed ZSM-5 crystal peak, especially the peaks at 7.9 and 8.9° which are among the major peaks for the identification of ZSM-5 sample. The template being the frame work in which the zeolite is formed was the only component giving off during the calcination of the dried ZSM-5 zeolite. The calcination temperature was 500°C, which does not have any negative effect on the crystallinity of ZSM-5 zeolite produced.

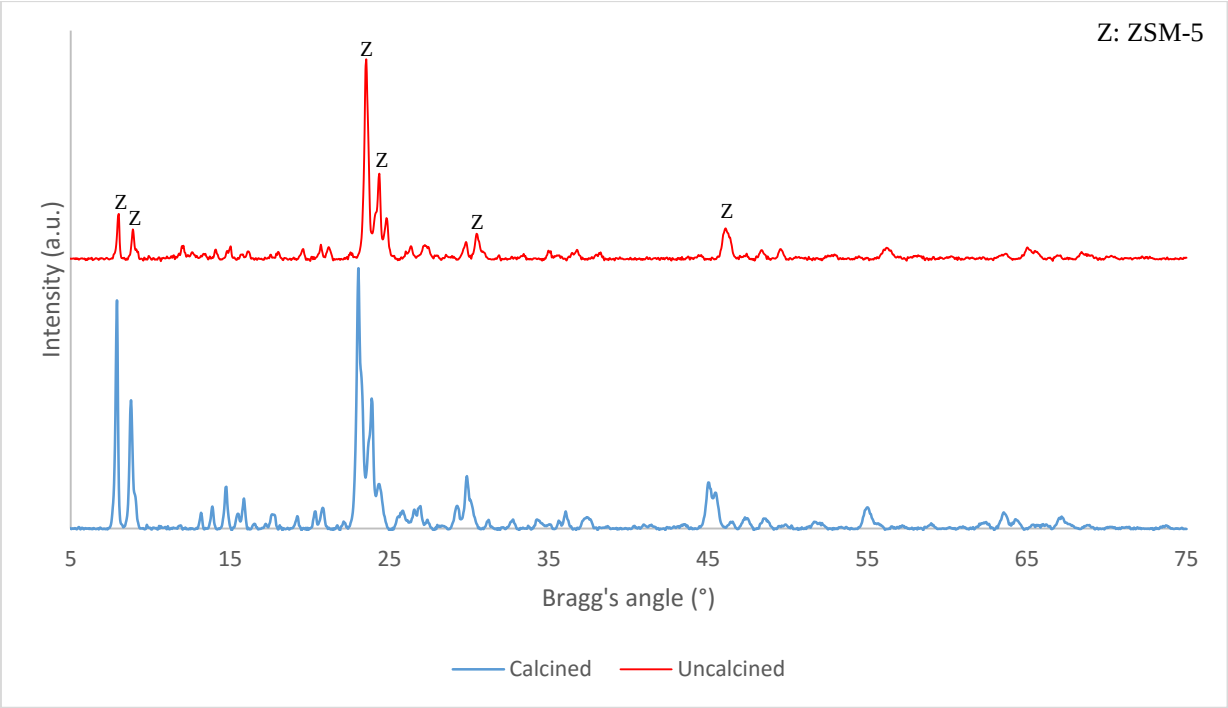


Figure 4.24: XRD patterns for calcined and uncalcined ZSM-5 (Run 3)

4.9.5 Laboratory and pilot plant comparison

The laboratory synthesis of zeolite Y and ZSM-5 were compared with the same products obtained at the pilot plant, to ascertain the areas that needed improvement. The FTIR spectra and the XRD patterns were carefully studied.

It was observed that the FTIR spectra of samples were similar to each other. The FTIR spectra of the sodium based zeolite possessed IR transmittance bands at wavelength of around 468, 571, 600, 769, 1000, 1658 and 3466 cm^{-1}. Prior studies reported that the characteristic FTIR bands for zeolitic lattice are in the wavelength range of 460–1200 cm^{-1} (Modi *et al.*, 2012) and the bands in these range of wavelength indicate the crystallinity of the material (Shen *et al.*, 2014). Particularly the characteristic FTIR bands for zeolite Y are located around 1000, 769 and 715 cm^{-1} (Zhang *et al.*, 2008). The band at 461 cm^{-1} was attributed to Si–O

tetrahedral deformation. The band at 573 cm^{-1} was attributed to Si–O–Al octahedral stretching. The band at 748 cm^{-1} was attributed to Si–O–Al in-plane bending. The broad band stretching between 950 and 1020 cm^{-1} was attributed to Al–OH vibration and Si–O tetrahedral stretching vibration (in plane). The band at 1655 cm^{-1} was attributed to vibration of water molecule. The band at 3468 cm^{-1} was attributed to O–H bond stretching vibration (Percival *et al*., 1974; Kloprogge *et al*., 1999; Steudel *et al*.,2009; Benincasa *et al*., 2001; 2009; Pal *et al*., 2013). Good similarity was observed from Figure 4.25, between the pilot plant production and the zeolite produced with pure chemicals.

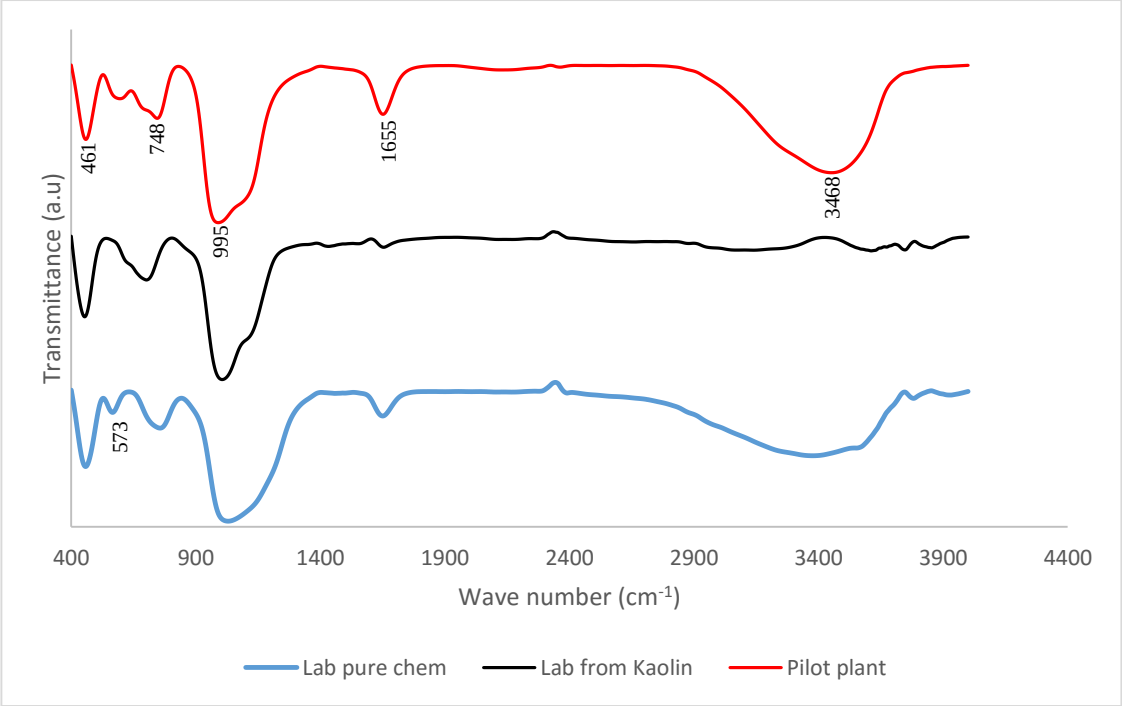


Figure 4.25: FTIR of zeolite Y synthesized from pure chemical, kaolin both in the laboratory and pilot plant.

From Figure 4.26, satisfactory correlation was noticed between laboratory synthesis from pure chemicals and the zeolite at pilot scale using kaolin. All the prominent peaks for zeolite Y were present and the sharp peaks as well as the high intensity was an evident to the crystalline nature of the zeolite. As such the pilot plant production process has proven to be

reliable. The production of ZSM-5 zeolite from the pilot plant as well as the laboratory synthesized ZSM-5 showed good agreement in terms of the XRD patterns as shown in Figure 4.27, all the prominent peaks were present and alike.

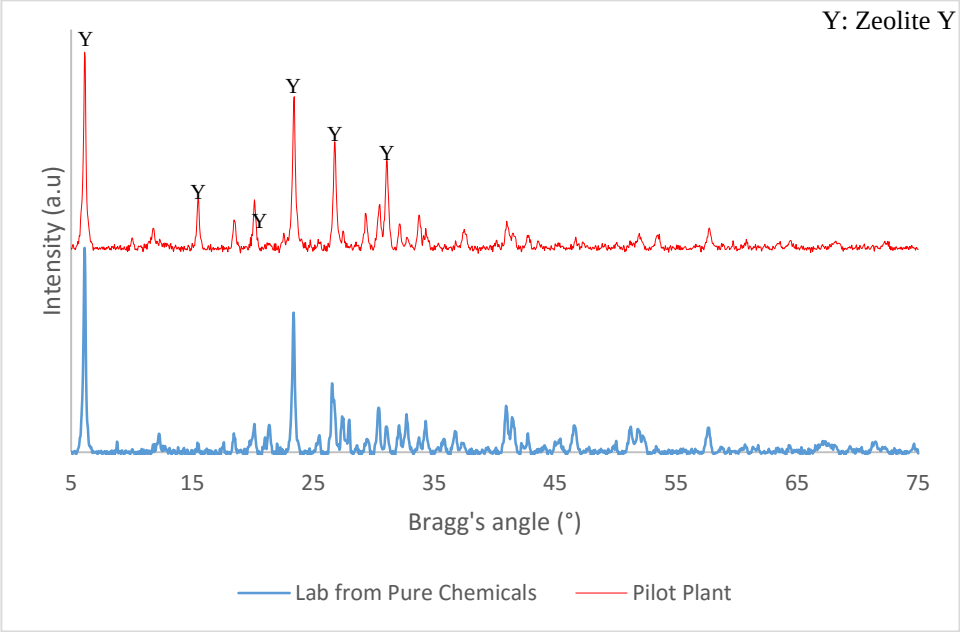


Figure 4.26: Comparison of XRD patterns of Zeolite Y synthesis in the lab and pilot unit

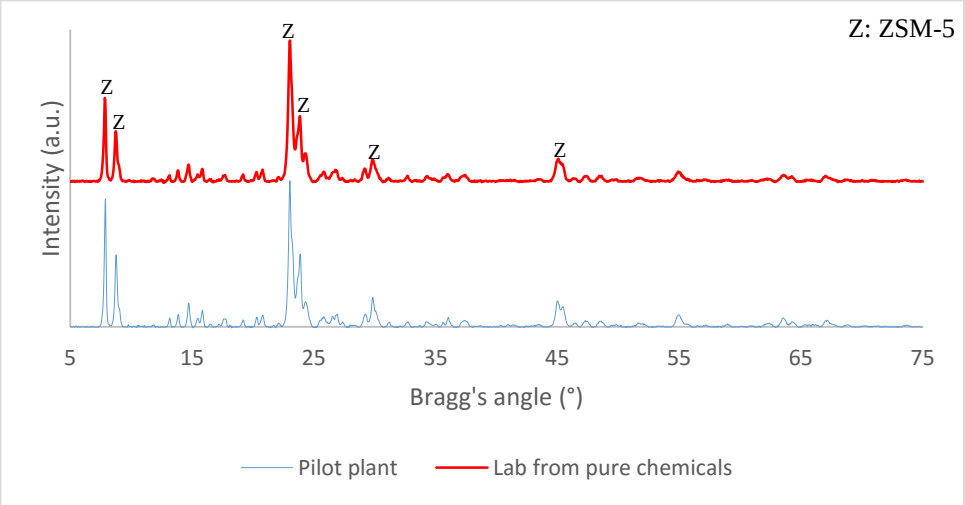


Figure 4.27: Comparison of XRD patterns of ZSM-5 synthesis in the lab and pilot unit

4.9.6 Zeolite transformation and compounding

The transformation of the sodium based zeolite Y to the hydrogen form, then followed by the stabilization of the pronated zeolite with lanthanum chloride and finally producing the compounded catalyst all showed similar trend in the IR band position. The functional groups in the other materials used for the compounding of the catalyst are similar to the base material, which could be the reason for lack of extra band in the compounded catalyst with regard to the protonated and stabilized zeolite Y, as presented in Figure 4.28, but the intensity of the band at about 3500 cm_{-1} decreased with compared to the protonated and stabilized zeolite Y. The band at around 3500 cm^{-1} was attributed to the –OH stretching (Lee *et al*., 2013).

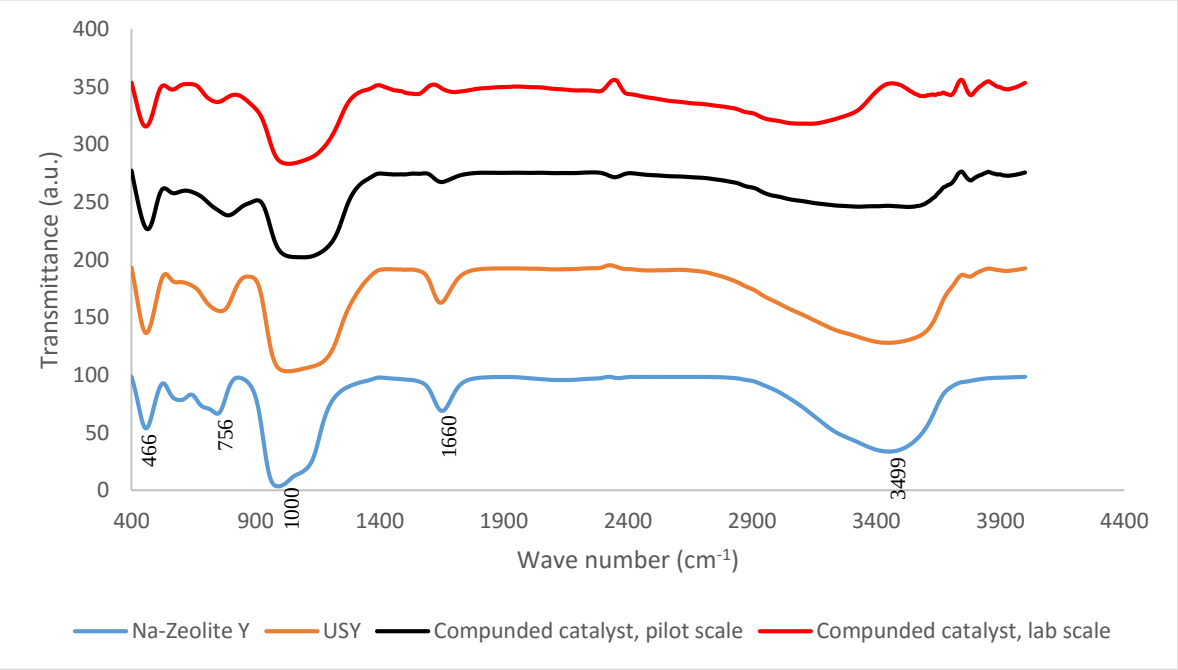


Figure 4.28: FTIR of pure and compounded zeolite Y both in the laboratory and pilot plant

From Figure 4.29, the crystallinity of zeolite Y was maintained after the stabilization process, which decreased after compounding. The observation was expected as some of the material

used for the catalyst compounding were amorphous. The major peak of zeolite found at Bragg's angle of about 6 ° reduced, because just a fraction of the zeolite Y was used for compounding the overall zeolite catalyst.

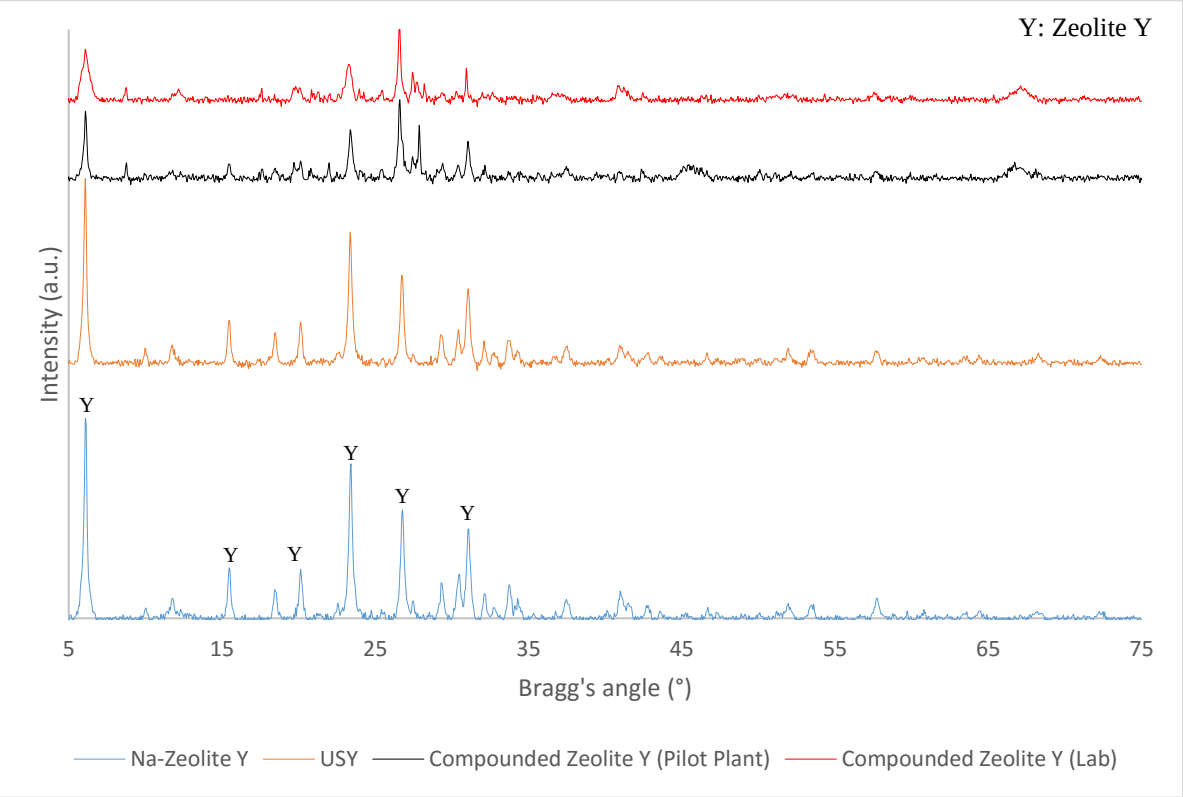


Figure 4.29: Zeolite Y transformation stages

The IR spectra of ZSM-5 zeolite showed general spectra features at 550, 850, 1100, 1125, 1400, 1650 and 3340 cm^{-1} presented in Figure 4.30. The vibration modes near 1107, 802 and 457 cm^{-1} were assigned to internal vibrations of SiO_4, AlO_4 tetrahedra. While the vibrational nodes near 558 cm^{-1} was due to the double-ring tetrahedral vibration and to the asymmetric stretching of SiO_4 and AlO_4 tetrahedra in the zeolite framework respectively. Formation of ZSM-5 zeolite was evident following the presence of infrared band.

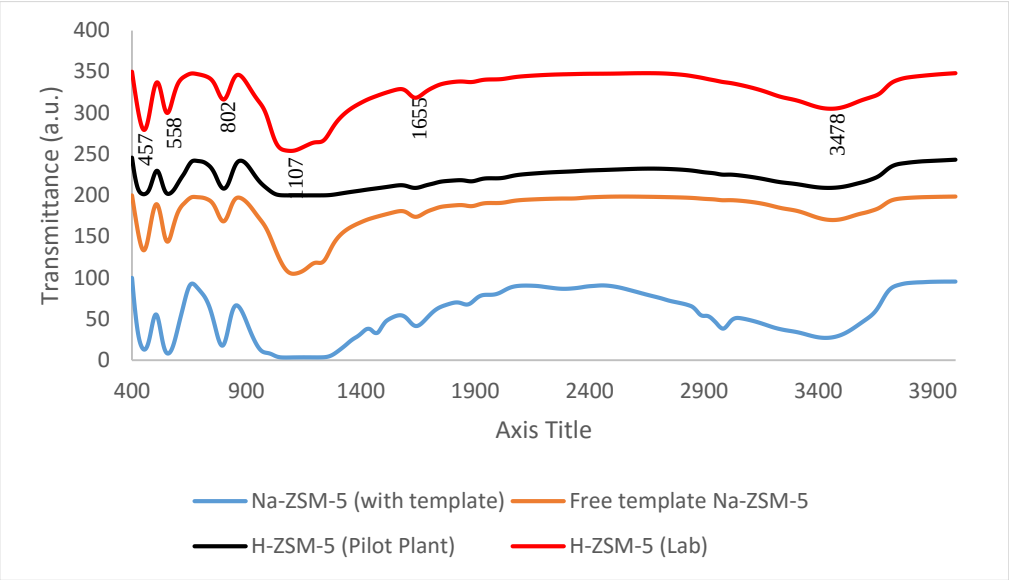


Figure 4.30: FTIR different product of ZSM-5 zeolite

Formation of zeolite at the pilot scale level was also ascertained form the observed XRD patterns presented in Figure 4.31. Similarity was also observed between the pilot plant production and the laboratory synthesis. Post crystallization treatment did not destroy the crystallinity of the zeolite, more so, calcination which was aimed at removing the template had no side effect to the crystallinity of the zeolite.

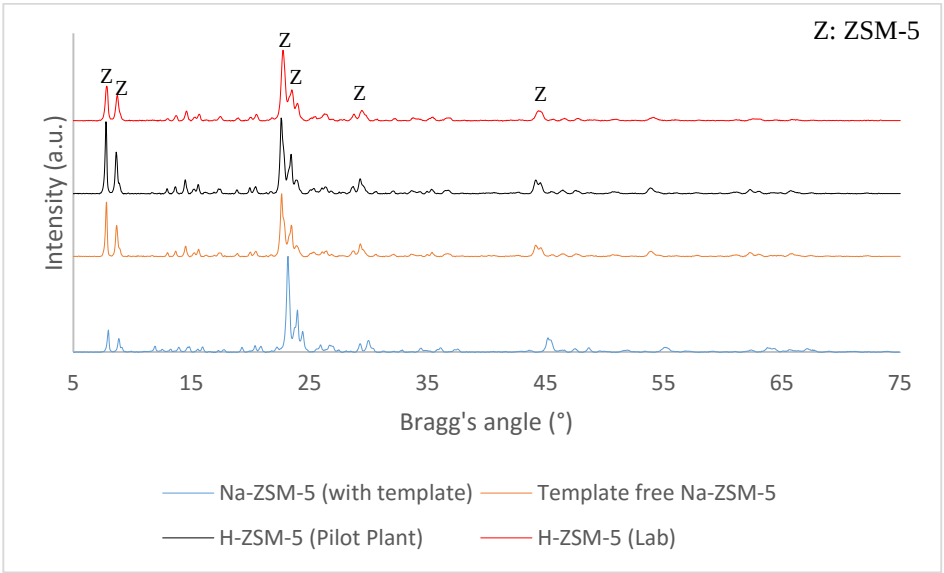


Figure 4.31: ZSM-5 zeolite transformation stages

4.10 Physicochemical Characterization of Zeolite Y Produced from pilot unit

4.10.1 FTIR of zeolite Y

Figures 4.32 shows the FTIR spectra of zeolite NaY, It could be observed that the FTIR spectra of the sample possessed IR transmittance bands at wavelength of around 480, 550, 800, 1100, 1650 and 3500 cm-1. Prior studies reported that the characteristic FTIR bands for zeolitic lattice are in the wavelength range of 460–1200 cm^{-1} (Modi *et al*., 2012) and the bands in these range of wavelength indicate the crystallinity of the material (Shen *et al*., 2014). Particularly the characteristic FTIR bands for zeolite Y are located around 1100, 790 and 715 cm^{-1} (Zhang *et al*., 2008). The band at 458 cm^{-1} was attributed to Si–O tetrahedral deformation. The band at 558 cm^{-1} was attributed to Si–O–Al octahedral stretching. The band at 802 cm^{-1} was attributed to Si–O–Al out-of-plane bending. The broad band stretching between 950 and 1020 cm^{-1} was attributed to Al–OH vibration and Si–O tetrahedral stretching vibration (in plane).

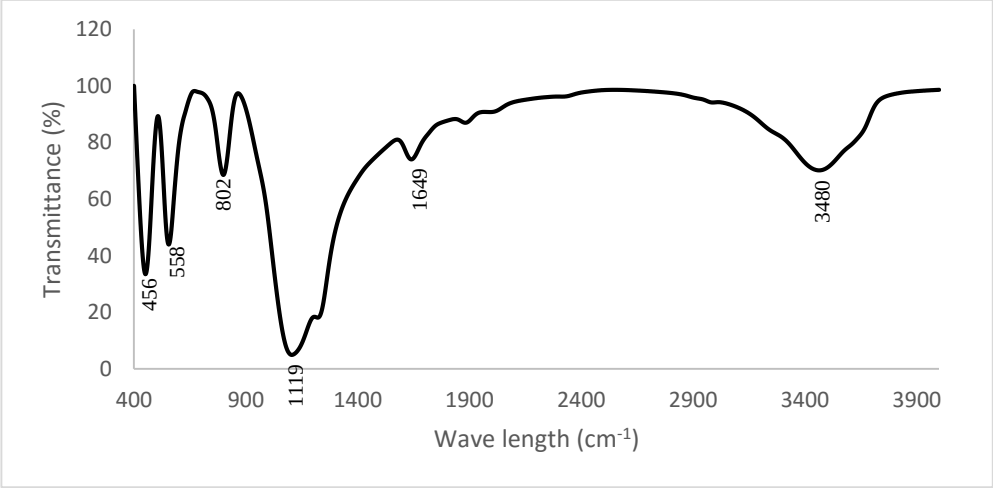


Figure 4.32: FTIR Pattern of zeolite Y produced from Kankara kaolin

The band at 1649 cm^{-1} was attributed to vibration of water molecule. The band at 3480 cm^{-1} was attributed to O–H bond stretching vibration (Percival *et al.*, 1974; Kloprogge et al., 1999; Steudel *et al*.,2009; Benincasa *et al*., 2001; 2009; Pal *et al*., 2013).

4.10.2 XRD analysis of zeolite Y

Figure 4.33 shows the XRD pattern of zeolite Y produced from the pilot plant. The zeolite Y peaks found at Bragg's angle of about 6, 10, 12, 16, 19, 20, 24, 27, 31 and 32˚ (Ginter *et al*., 1992; Robson, 2001; Treacy and Higgins, 2001) could be observed in the XRD pattern. The high intensity counts associated with the pattern showed that the zeolite was crystalline.

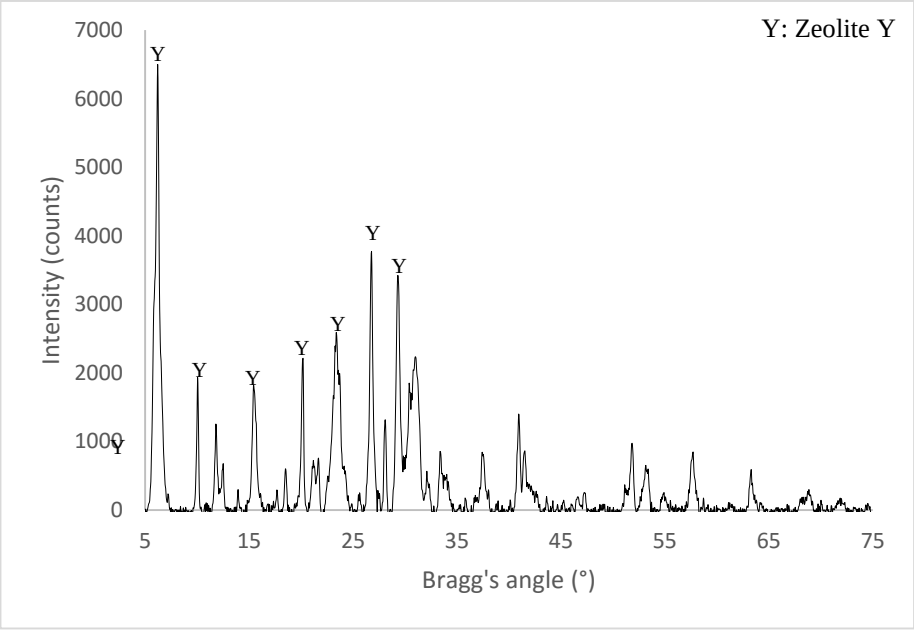


Figure 4.33: XRD pattern of zeolite Y

4.10.3 SEM images of zeolite Y Produced from Kankara kaolin

SEM micrograph scanned at magnifications of 1000, 10000, 20000 and 50000 as well as the EDS of the zeolite Y produced is shown in Plate XXI (a) to (d) respectively. At 10000 magnification, the zeolite Y particles appeared densely agglomerated which become clearer

at higher magnification, however, at the 50000 magnification clear pictures of evenly distributed individual particles having regular tetrahedral shapes could be observed. It could be deduced from the images that the zeolite Y possessed an agglomerated tetrahedral morphology, having an average particle size of about 200 nm. From the SEM analysis, the EDS (Plate XXIX d) quantified the components of zeolite Y had the following composition: O = 48.63 %; Na = 14.40 %; Al = 14.54 % and Si = 22.43%. The carbon seen from the EDS was as a result of the organic solvent used for the digestion. From the composition obtained, the ratio of Si to Al was found to be 1.54, while the silica to alumina ratio was evaluated as 3.08. With this ratio, it was confirmed that the Faujasite zeolite produced was type Y and not type X.

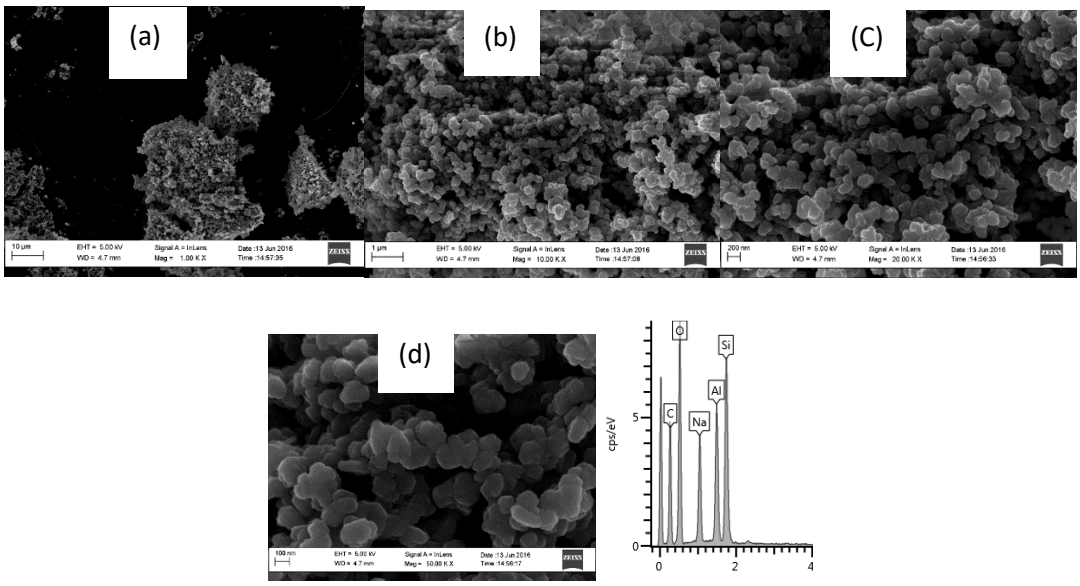


Plate XXIX: SEM images and EDS of zeolite Y

4.10.4 TEM image and EDS of zeolite Y

The clear boundary shapes of the crystals could be seen from the TEM images presented in Plate XXX (a) to (c) in order of increased magnifications. The channel was more visible at

the highest magnification (c). The crystal shape appeared to be hexagonal although the crystals images overlapped each other, as a result, the crystal shapes were not clearly revealed. The EDS (d) of the sample from the TEM analysis was in conformity with the result gotten from SEM-EDS analysis, with the silica higher than alumina in the produced zeolite. The SAED (e) also showed that the zeolite was a well crystalline material.

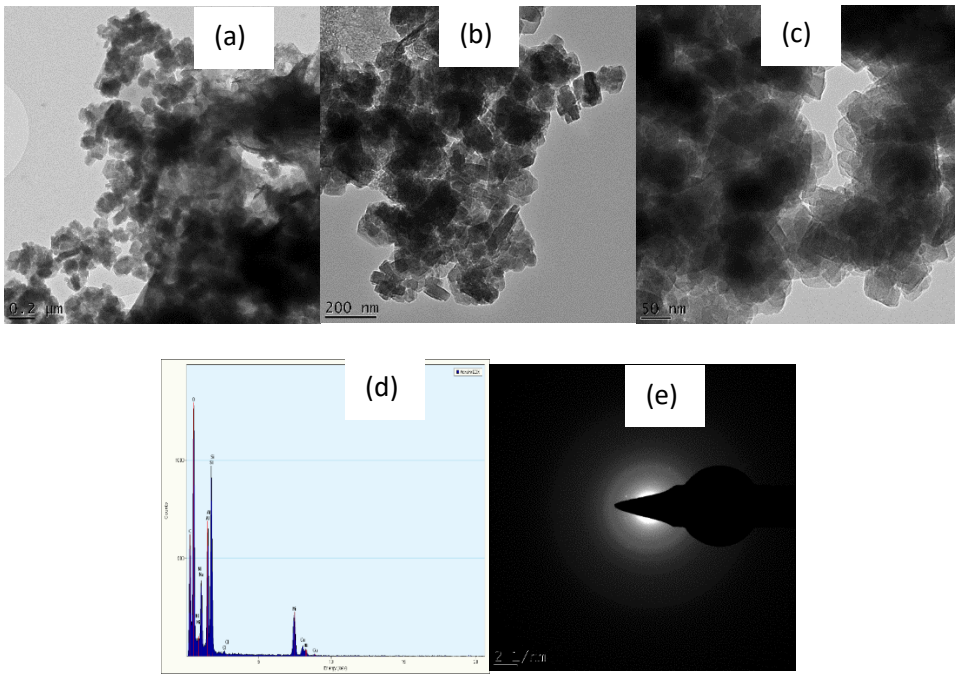


Plate XXX: TEM image, EDS and SAED of zeolite Y

4.10.5 TG analysis of zeolite Y

The bulk of the mass loss was between 100 and 200 °C, as could be observed in Figure 4.34. This loss could be attributed to the evaporation of the trapped water molecules in the internal framework of the zeolite as the temperature increased. Beyond the temperature of 200 °C, the zeolite was relatively stable till a temperature of 750 °C. This observation, ascertained the stability of zeolite over the range of analysis temperature employed.

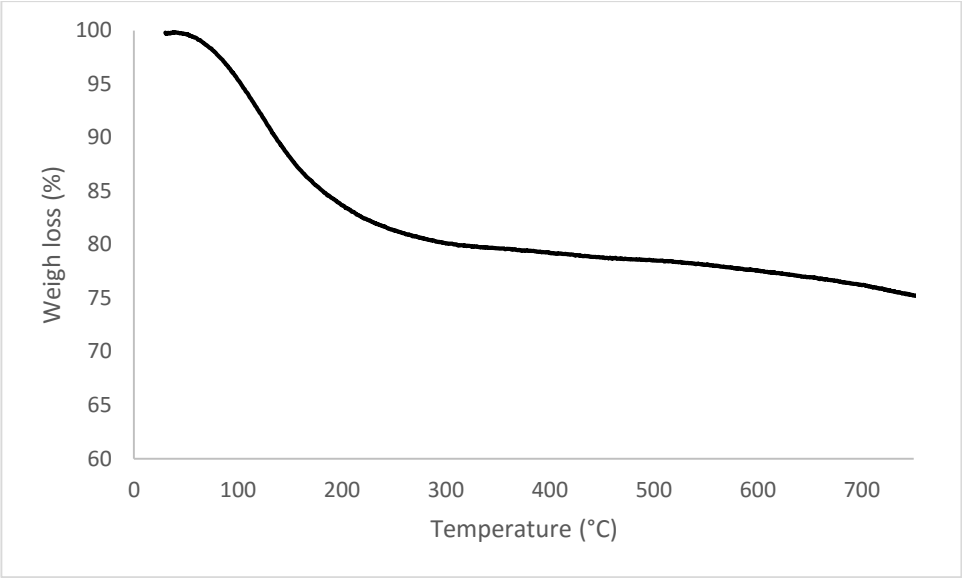


Figure 4.34: TGA result of zeolite Y

4.10.6 BET analysis of zeolite Y

Zeolite Y had specific surface area of 321 m^2/g as revealed from the BET analysis, and having pore size and pore volume of 34 Å and 0.271 cm^3/g. The thermally stabilized zeolites produced had good BET properties, generally having surface areas within higher than the products reported by many other researchers (Alaba, *et al*., 2015; Ding et al., 2007; Liu *et al*., 2003). The pore size is large enough to accommodate molecules of larger diameter mostly found in the heavy gas oil feed stock. This implies that diffusion resistance will not be a much challenge.

4.11 Physicochemical Characterization of ZSM-5 Produced from developed Zeolite Reactor

4.11.1 FTIR analysis of ZSM-5 Produced

The FTIR spectrum recorded in the 400 – 4000 cm^{-1} range for the kaolin based ZSM-5, the IR spectrum shows characteristic bands at 452 cm^{-1} (T–O bending vibration), 556 cm^{-1}

(double 5 ring vibration), 804 cm^{-1} (external symmetric stretch), 1119 cm^{-1} (external asymmetric stretching vibration of Si–O–T linkage) and 1232 cm^{-1} (asymmetric stretch vibration) indicating a pure ZSM-5 was obtained as shown in Figure 4.35. The presence of this band is linked to the external linkages between TO_4 tetrahedra and is a structure sensitive IR band (Triantafyllidis *et al*., 2004). Formation of ZSM-5 was evident following the presence of infrared band.

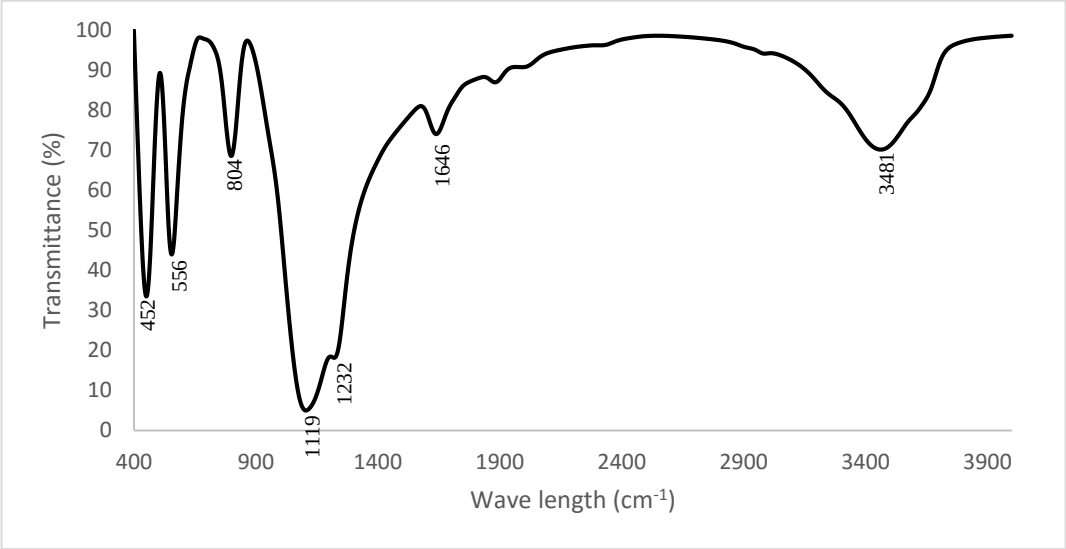


Figure 4.35: FTIR spectrum of ZSM-5

4.11.2 XRD pattern of ZSM-5 produced

Figures 4.36 shows the X-ray diffraction (XRD) patterns of the zeolites at sodium and hydrogen form respectively. The samples had peaks at 2θ value of 7.9°, 8.9°, 23.1°, 23.8° and 24.5° positions which are related to the diffractions of [101], [200], [501], [151] and [133] MIF planes, respectively (Frantz *et al*., 2016). These results confirm the formation of a crystalline ZSM-5. More so, exhibiting characteristic X-ray diffraction peaks at 2θ value of 7–9°, and 22–25°, which is a confirmation of a typical structure of ZSM-5.

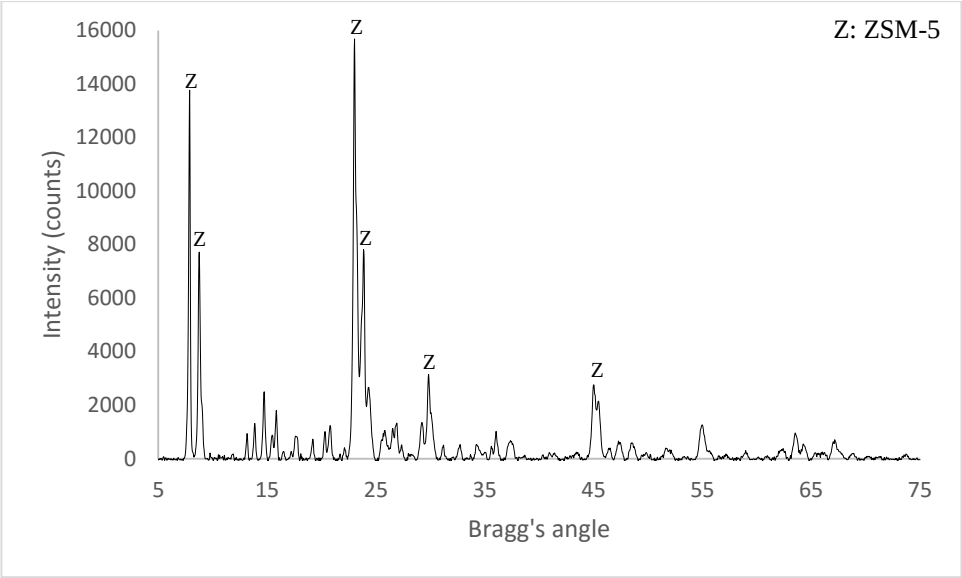


Figure 4.36: XRD pattern of ZSM-5

4.11.3 SEM analysis of ZSM-5 produced

The SEM image of the ZSM-5 produced was ellipsoidal in shape as shown in Plate XXXI (a) and (b), the Image in (b) which was of higher magnification showed that the zeolite crystals were evenly distributed. The sizes of the zeolite were uniformly distributed and did not contain amorphous substance or other crystalline impurities. The uniformity in the zeolite morphology suggested that good crystals of the product was obtained as also shown form the XRD pattern. From the composition obtained, the ratio of Si to Al was found to be 38.64, while the silica to alumina ratio was evaluated as 77.28. The Si to Al ratio is an important parameter that could be used to measure the catalytic activity of the zeolite. Generally, Si to Al ratio of zeolite determine its chemical and thermal stability, the literature value of Si to Al ratio of ZSM-5 zeolite is from 10 to 500 (Al-Bagomi, 2013). The Si to Al ratio was within the range of reported value. The higher the Si to Al ratio the thermally and chemically stable

the zeolite become (Esmaelli *et al*., 2011) and reduces cracking rate of olefins (Li *et al*., 2007).

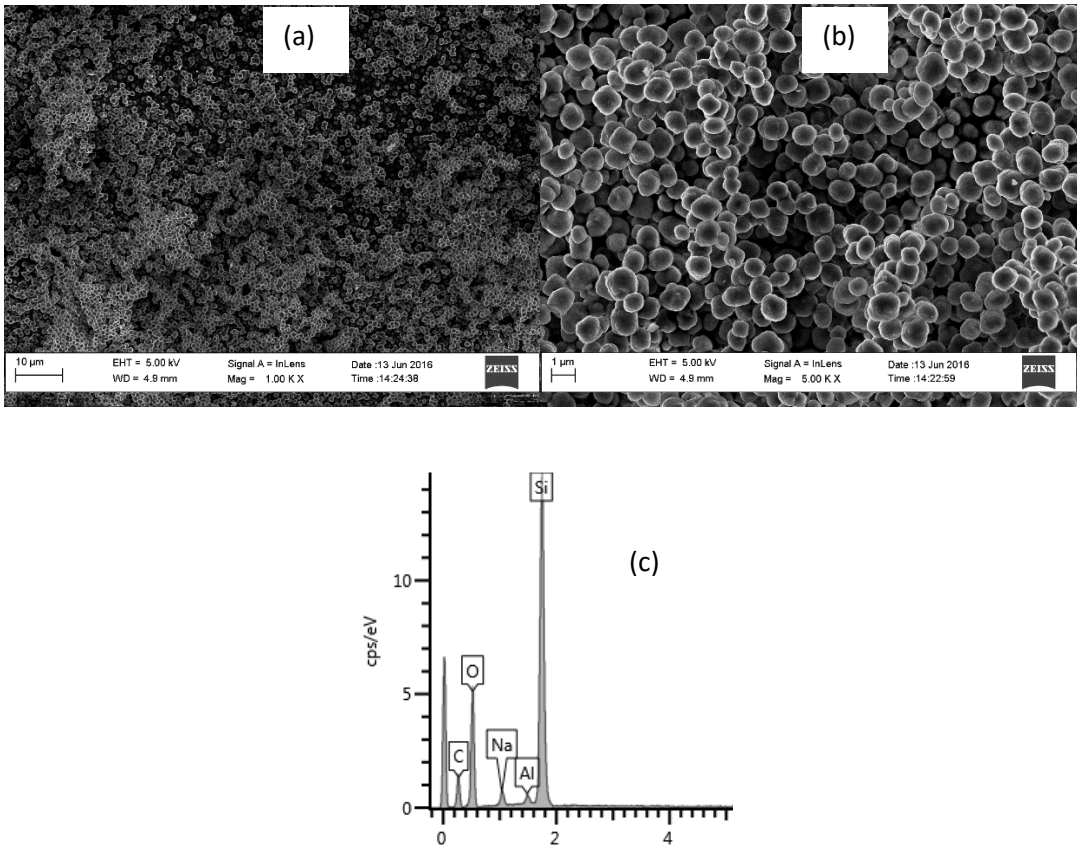


Plate XXXI: SEM images and EDS of ZSM-5 at different magnification

4.11.4 TEM analysis of ZSM-5 produced

The TEM images of ZSM-5 was found to be crystalline as seen in Plate XXXII (a) and (b). The ZSM-5 crystals were distributed. The EDS (c) also was in conformity with the SEM-EDS, proving that the zeolite was highly siliceous as expected, owing to the high value of silicon in comparison to the aluminum. It was observed that the ZSM-5 was highly crystalline as revealed by the SAED (Plate XXXII d).

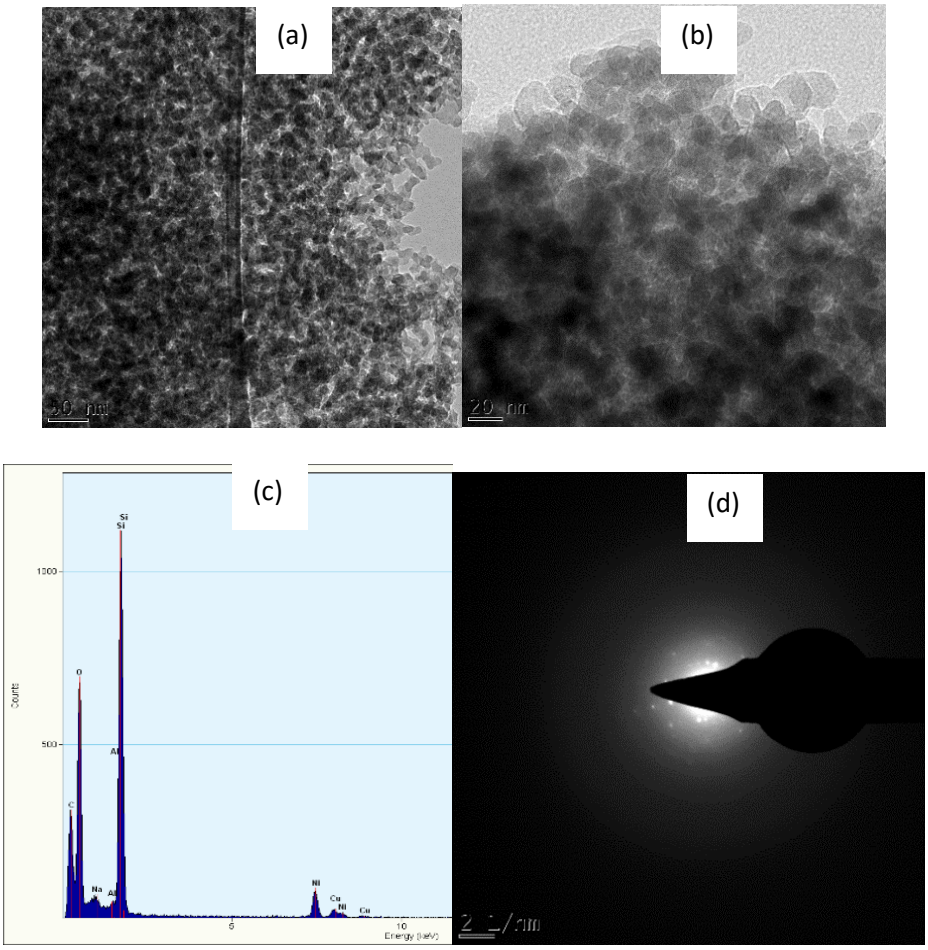


Plate XXXII: TEM images, SAED, and EDS of ZSM-5

4.11.5 BET analysis of ZSM-5 produced

A high specific surface area of 411 m^2/g is achieved for the HZSM-5 which is higher than previously reported value (Frantz *et al*., 2016; Mohiuddin et al., 2016; Yunusa, 2015; Pan *et al*., 2014). Wang *et al*., obtained BET surface area of 313,4 m2/g for ZSM-5 prepared at 160 °C for 5 days. Also in Silve *et al*., work where the the synthesis of zsm-5 was done at 170 °C for 2 days had a BET surface area of 355 m^2/g and pore volume value of 0.22 cm^3/g. The pore size and pore volume from the BET analysis were 24 Å and 0.24819 cm^3/g.

4.12 Physicochemical Characterization of Commercial Catalyst

The FTIR spectrum and the XRD pattern presented in Figures 4.37 and 4.38 respectively possessed the characteristics of zeolite Y. it is the commercial catalyst used for FCCU operation.

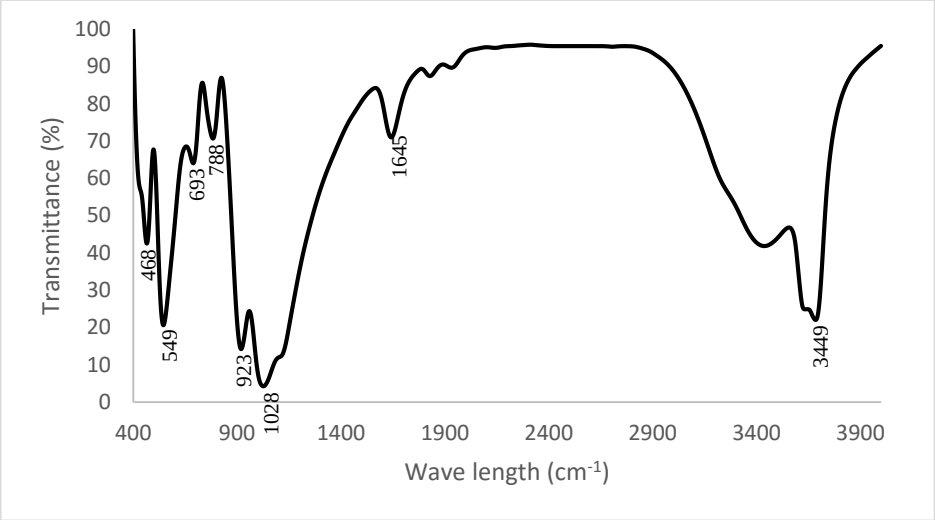


Figure 4.37: FTIR of commercial catalyst

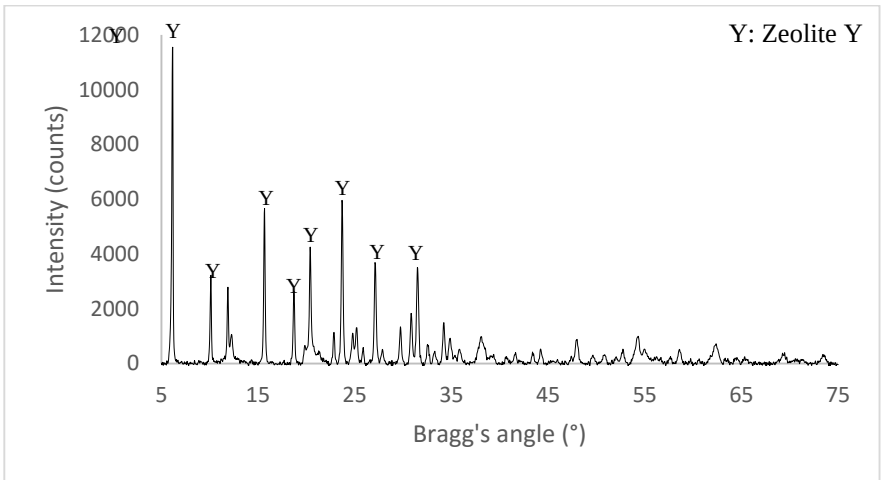


Figure 4.38: XRD pattern for commercial catalyst

From the SEM analysis and EDS analysis shown in Plate XXXIII, the components of commercial FCCU catalyst were: O = 52.17 %; Al = 22.77 %; Si = 23.42; Cl = 0.79; and Ti = 0.85. The EDS showed in Plate XXV, the carbon observed from the graph was as a result of the organic solvent used for the digestion. From the composition obtained, the ratio of Si to Al was found to be 1.03, while the silica to alumina ratio was evaluated as 2.06. The low value was influenced by other additive used for the overall formulation of the catalyst. As could also be observed from the SEM image, having distinct particles in different sizes and shapes.

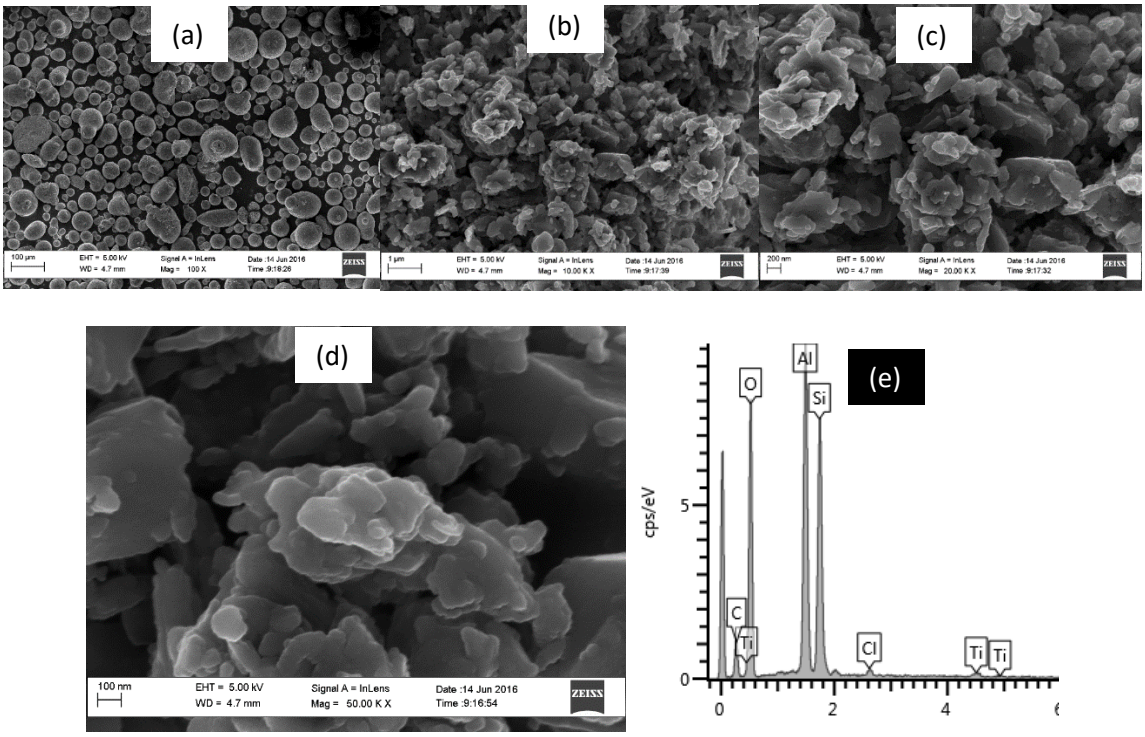


Plate XXXIII: SEM images and EDS of commercial FCCU catalyst

The TEM images further confirmed that the commercial FCCU catalyst was highly crystalline as seen in Plate XXXIV as well as the SAED.

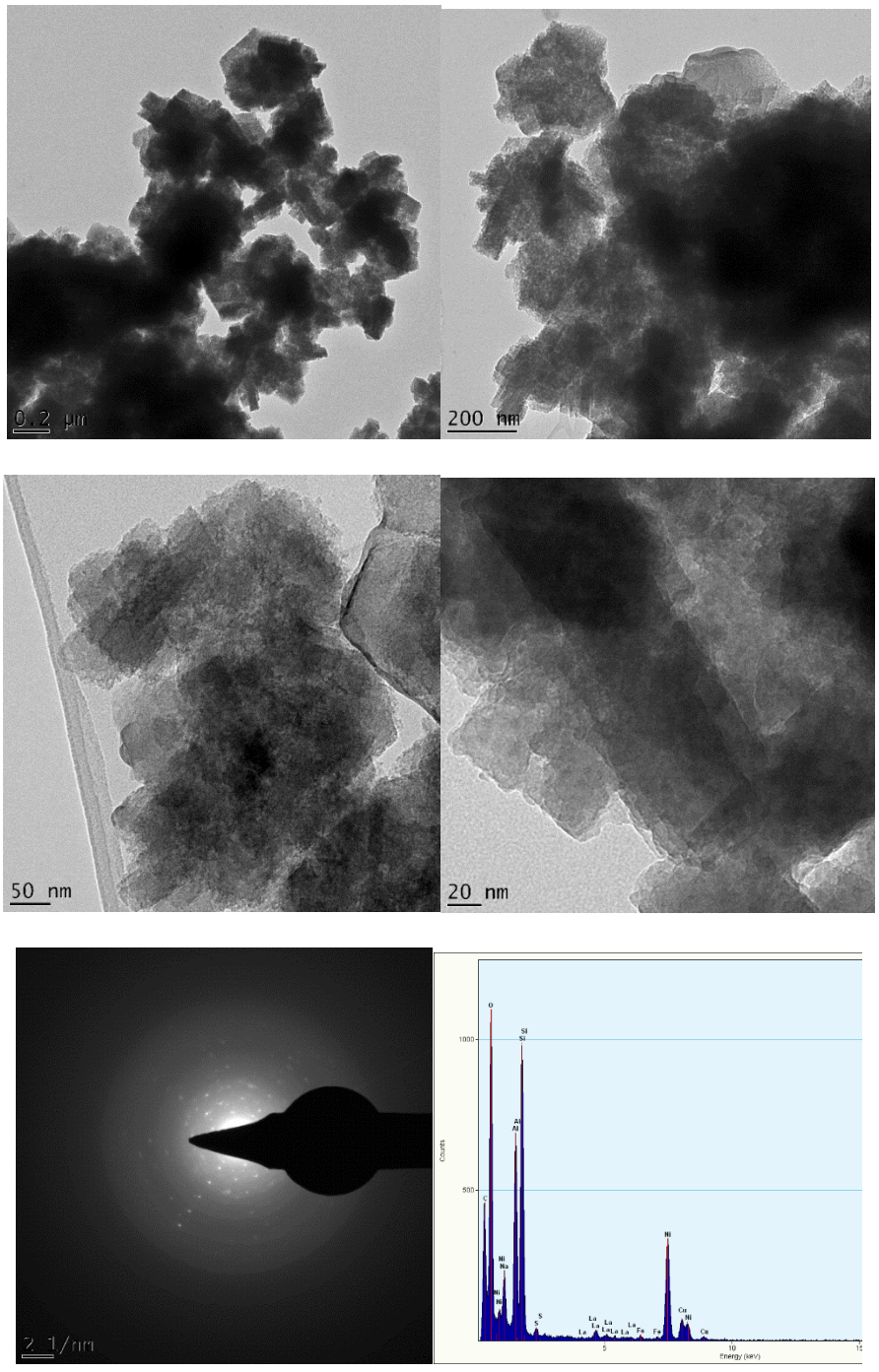


Plate XXXIV: TEM images, SAED and EDS of Commercial FCCU catalyst

The BET surface area was high having value of 303.61 m^2/g, pore volume of 0.16 cm^3/g and pore size of 20.68 Å.

4.13 Performance Test

The XRD pattern of the Pt/La-Zeolite Y and Pt/H-ZSM-5 shown in Figures 4.39 and 4.40 showed characteristic peak for both Zeolite Y and ZSM-5 zeolite respectively. The samples were both highly crystalline owing to the high intensity counts as well as sharp peaks of the diffractogram. Intensity decrease was observed after the anchoring of Platinum to the H-ZSM-5 frame work as expected, which imply the entrance of platinum species into the channel (Niaei, *et al*, 2012).

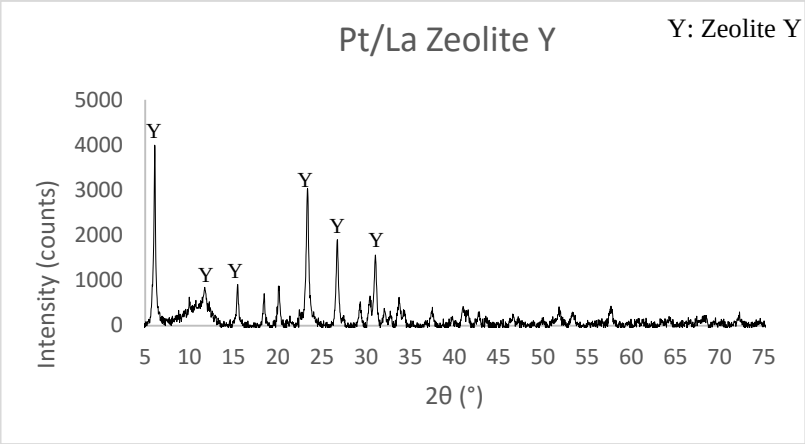


Figure 4.39: XRD pattern of Pt/La Zeolite Y

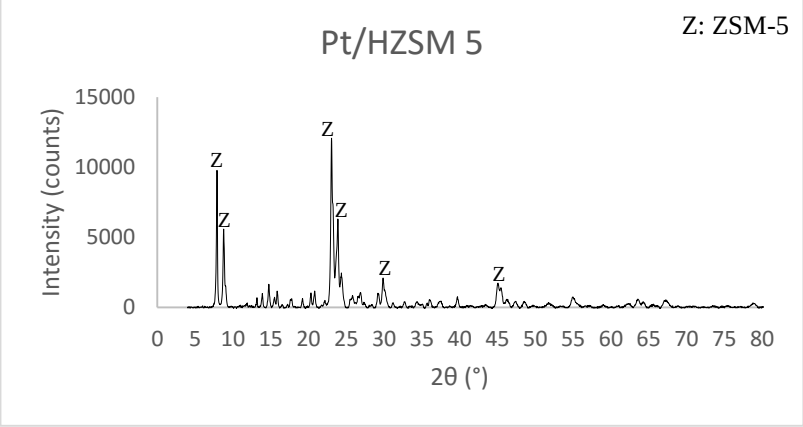


Figure 4.40: XRD pattern of Pt/H-ZSM-5 zeolite catalyst

It was observed that the conversion of n-hexadecane was depended on the reaction temperature as shown in Figure 4.41. The extent of conversion increased as the reaction temperature increased from 205 °C to 265 °C, where the minimum and maximum conversions of 9.44% and 98.16% were observed respectively for ZSM-5, while zeolite Y catalyst range of temperature was from 205°C to 315°C. The maximum conversion for zeolite Y catalyst was observed at 315 °C with a value of 93.95 % against 98.16 % at 265 °C for ZSM-5 catalyst. This could be attributed to the high activity of the ZSM-5 owing to its high silica to alumina ratio. Further analysis was focused on the ZSM-5 catalyst.

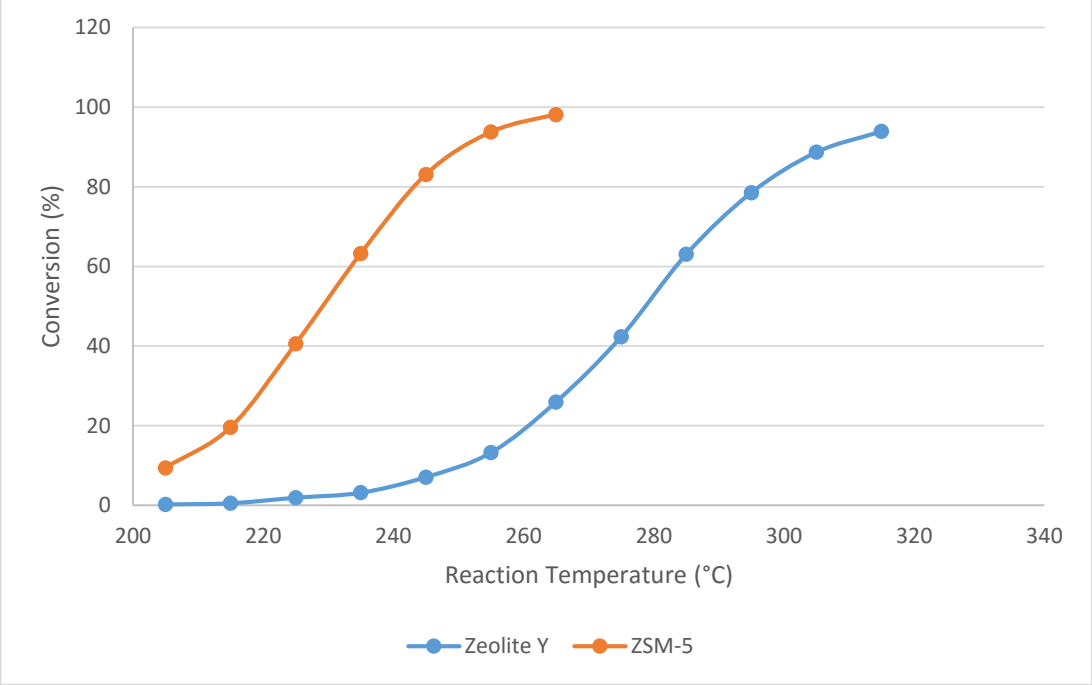


Figure 4.41: n-Hexadecane conversion with variation in reaction temperature

Two types of reaction occur during hydro conversion of n-alkanes on Pt/HZSM-5, isomerization and hydrocracking. As reaction temperature increases, increase in both cracking and isomerization products, until a temperature of about 240°C was reached where the maximum isomerization products were obtained. Beyond 240°C the isomers formed were

cracked as could be seen with the continuous increase of the yield in percent of the cracked products as shown in Figure 4.42. This observation was also a good indication on the activity of the catalyst used for the reaction.

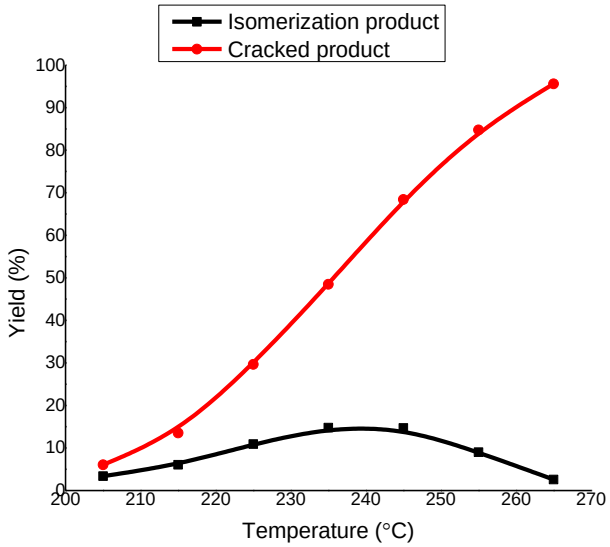


Figure 4.42: Product yield of Pt/HZSM-5 with respect to conversion

A larger percentage of the converted reactant was by cracking rather isomerization. Figure 4.43, shows the yield of cracked products to be more that the isomers formed.

The difference between the two type of products formed was increasing as evident by the widening of the gap between the two products curve. Linear increase was observed at low conversion but at high conversion cracking dominated the reaction process, as the isomers were more energies by the high temperature to diffuse into the active side mostly, within the pore of the HZSM-5. This phenomenon favored the cracking reaction over isomerization at high conversion which translate to higher temperature of the reaction.

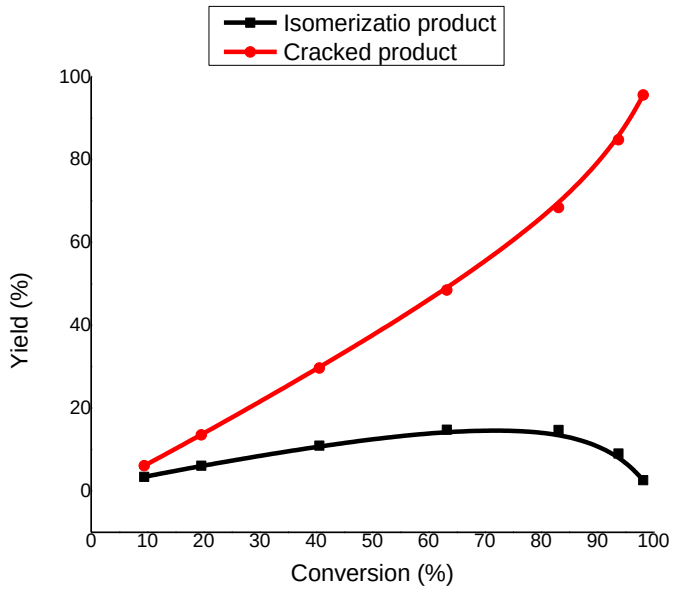


Figure 4.43: Product yield of Pt/HZSM-5 with respect to conversion

The most important products of isomerization on Pt/H-ZSM-5 are those with a single methyl branching. This is seen from Figure 6, in which the selectivity of isomerization was plotted against conversion. Both the sluggish formation of dimethyl isomers and the absence of i-alkanes with an ethyl or bulkier side chain are in contrast to isomerization on large-pore zeolites, whereby the large pore diameter could accommodate hydrocarbon molecules of larger hydrodynamic diameter. At high conversion the single (mono) methyl group began to undergo secondary cracking producing cracked product with lower carbon number which was in conformity with the observation in Figure 4.44.

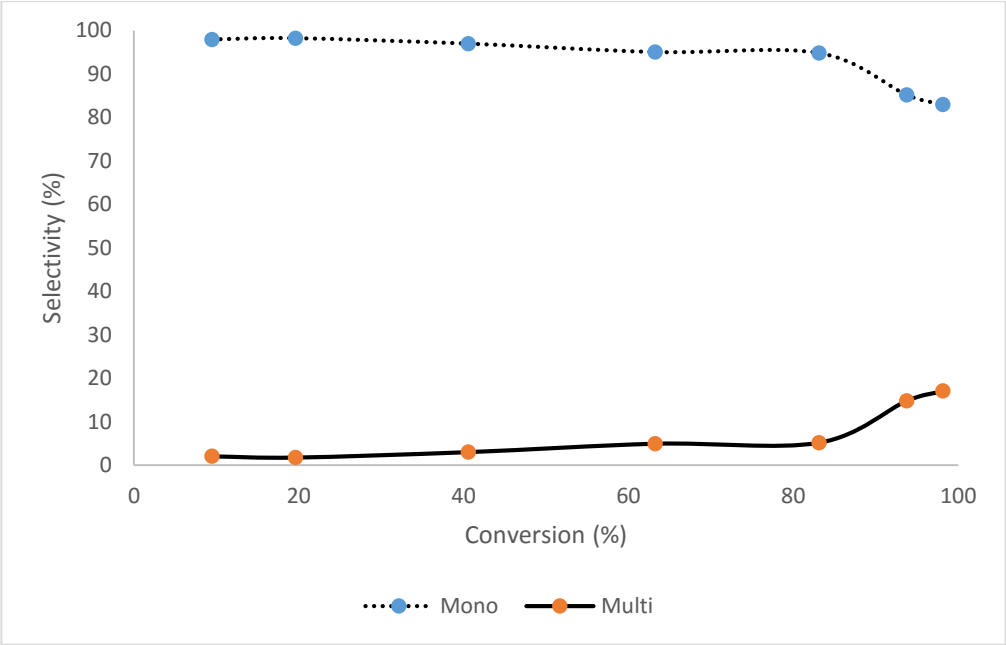


Figure 4.44: Selectivity of n-hexadecane isomerization on Pt/HZSM-5

Figure 4.45, presents the products distribution of the hydrocracking reactions over the Pt/HZSM-5. The yield of naphtha for gasoline fraction was the highest all through the reaction process. From start to 255°C, the diesel fraction was next in the yield of products. Beyond 255°C, more of the LPG were formed as compared to lower temperature, this might be attributed to over cracking occurring had begun. The dominance nature of the cracking reaction was as a result of the presence of much active sites in the framework of the zeolite used, again is a sign of an active catalyst.

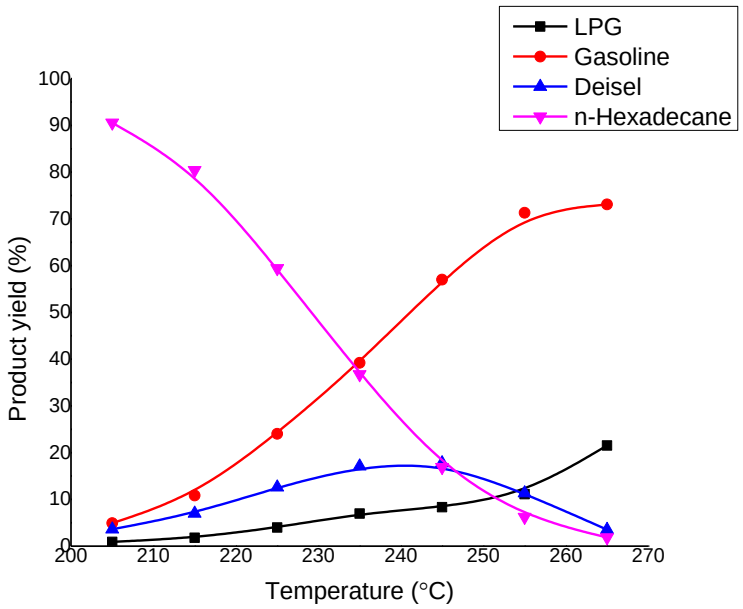


Figure 4.45: Product yield of Pt/HZSM-5 with respect to petroleum fraction

4.14 Preliminary Full Scale Forecast for Reactor Capacity

Based on geometrical similarity, the pilot scale equipment was scale-up to full scale design, the summary of the three major reactors are presented in Table 4.7 while the details are in Appendix J.

Table 4.7: Summary of dimensions for full scale reactors

Equipment	Capacity (tons/batch)	Volume (m^3)	Height (m)	Diameter (m)
Dealuminator	0.032	61.2	6.8	3.4
Zeolite Y reactor	0.051	325.8	11.8	5.9
ZSM-5 reactor	0.151	538.0	14.0	7.0

CHAPTER FIVE

CONCLUSIONS AND RECOMMENDATIONS

5.1 CONCLUSIONS

From the results of the investigation carried out, the following conclusions were drawn:

I. Pilot plant units for dealumination, zeolite Y and ZSM-5 production of capacity 2.5kg metakaolin, 2 kg and 4 kg respectively were designed, fabricated and tested.

II. The purity level for the silica obtained from the dealumination reaction was 98 % and the efficiency of the final configuration of dealumination reactor was 97 %.

III. Material selection for the internal part of dealumination reactor plays a pivotal role to the performance of the dealuminator.

IV. Good quality zeolite Y was produced from both external and internal means of heating during zeolite reaction. But, the external means of heating was more preferable because of the flexibility it offers.

V. Zeolite Y and ZSM-5 were comparable to the laboratory synthesized zeolites in terms of their physicochemical properties.

VI. The physicochemical properties of the zeolite Y produced from Kankara kaolin was comparable with that of a commercial zeolite Y sample obtained from KRPC.

VII. Zeolite Y and ZSM-5 zeolite were both active when tested for their catalytic performance. The conversion for ZSM-5 was higher with 98 % at 265 °C while zeolite Y gave the highest conversion of 94 % at 315 °C.

VIII. Cracking reaction outweigh the isomerization process. Branched hydrocarbon products with single methyl group was much higher than double methyl group.

IX. Selectivity for gasoline fraction was higher than the diesel and LPG fractions.

5.2 RECOMMENDATIONS

Based on this research the following recommendations are made:

I. Detailed kinetics studies for the novel method for dealumination should be carried out in the dealumination pilot unit.

II. Reactor for high pressure zeolite production should be developed, which may lead to the reduction in crystallization time especially for the ZSM-5 production.

III. Developing of the kinetics for the zeolite reactions should be looked into.

IV. The Nigerian government and relevant stake holders should invest in the further development of the findings of this research work towards the commercialization of the process.

V. The efficiency of the integrated zeolite pilot plant should be investigated in details.

VI. Reproducibility should be further investigated.

VII. Quantitative XRD analysis should be looked into.

CONTRIBUTION TO KNOWLEDGE

1. Development of a durable dealumination reactor (dealuminator) under strong acidic environment with an efficiency of about 90%.
2. Production of silica from the developed pilot unit with purity level of 97%.
3. Development of pilot size zeolite reactors for both internal and external means of heating.
4. Production of zeolite Y and ZSM-5 at pilot scale level using Kankara kaolin as starting material *via* the novel method approach.
5. Catalytic activity of the zeolite Y and ZSM-5 developed from the developed pilot size reactor unit was good, having conversion value of 94% and 98% respectively.

PUBLICATIONS

JOURNAL

1. S.G. Bawa, A.S. Ahmed, P.C. Okonkwo and S.M. Waziri (2017). Development of Pilot Scale Dealumination Unit of 2.5 Kg Metakaolin Per Batch Capacity. Nigerian Journal of Technology (NIJOTECH). 36(3): 829 – 834.

2. **S.G. Bawa**, A.S. Ahmed and P.C. Okonkwo (2016). The Study of Thermal Effect on the Surface Properties of Gamma-alumina Synthesized from Kankara Kaolin. Nigerian Journal of Technology (NIJOTECH). 35(1): 66-70.

3. **BAWA, S.G**., AHMED, A.S., OKONKWO, P.C., WAZIRI, S.M., EDOMWONYI-OTU, L.C. and MAZA, M. (2017). Characterization of Zeolite Y Produced from Kaolin at Pilot Scale. Nigerian Journal of Scientific Research (NJSR). 16(1): 87 -92.

4. **BAWA, S.G**., BROSIUS, R., AHMED, A.S., OKONKWO, P.C., WAZIRI, S.M., FLETCHER, J.C.Q. (2017). Hydrocracking Reaction on Formulated Pt/ZSM-5 Catalyst Prepared from Kankara Kaolin. Nigerian Journal of Scientific Research (NJSR). 16(1): 100 - 105.

CONFERENCE

1. **S.G. Bawa**, A.S. Ahmed, P.C. Okonkwo, S.M. Waziri, N. Salahudeen, S. Yunusa, M. Yusuf, S. Nakakana and A. Alabi (2015). Production of Zeolite Y at Pilot Scale from Kankara Kaolin. Proceedings of the Nigerian Materials Congress (NIMACON). November, 23-26: 306 -311.

2. **S.G. Bawa**, A.S. Ahmed, P.C. Okonkwo and S.M. Waziri (2015). Development of 2.5kg/Batch Dealuminator for Kankara Kaolin. Proceedings of the Nigerian Materials Congress (NIMACON). November, 22-26: 150 - 157.

3. **S.G. Bawa**, R. Brosius, A.S. Ahmed, P.C. Okonkwo, S.M. Waziri and J.C.Q. Fletcher (2016). Catalytic Activity of Pt/H-ZSM-5 Produced from Kaolin Zeolite Pilot Plant. Book of Proceedings of the 15th Annual International Conference/Nigerian Materials Congress. November, 21-25: 589 - 592.

4. **S.G. Bawa**, A.S. Ahmed, P.C. Okonkwo and S.M. Waziri (2016). Efficiency of Pilot Scale Dealumination Reactor. Book of Proceedings of the 15th Annual International Conference/Nigerian Materials Congress. November, 21-25: 566- 569.

5. **S.G. Bawa**, A.S. Ahmed, P.C. Okonkwo S.M. Waziri, S. Yunusa and M. Yusuf (2016). Pilot Scale Production of ZSM-5 from Kankara Kaolin. Book of Proceedings of the 15th Annual International Conference/Nigerian Materials Congress. November, 21-25: 560- 564.

6. **S.G. Bawa**, A.S. Ahmed, P.C. Okonkwo, S.M. Waziri and M. Maza (2016). Characterization of Zeolite Y produced from Pilot Plant using Kaolin as Starting Material. Book of Proceedings of the 15th Annual International Conference/Nigerian Materials Congress. November, 21-25: 555- 559.

REFERENCES

Abo-El-Enein, S. A., Heikal, M., Amin, M. S. and Negm, H. H. (2013), Reactivity of dealuminated kaolin and burnt kaolin using cement kiln dust or hydrated lime as activators. Construction and Building Materials, 47: 1451–1460.

Adamczyk, Z. and Bialecka, B. (2005), Hydrothermal Synthesis of Zeolites from Polish Fly Ash, *Polish Journal of Environmental Studies*, 14(6): 713-719

Aderemi, B.O. and Oludipe, J.O.: (2000). Dealumination of Kankara Kaolin Clay – Development of Governing Rate Equation. *Nigerian Journal of Engineering*, 8(2), 22-30.

Aderemi, B.O, Oloro, E.F, Joseph, D, Oludipe, J. (2001) Kinetics of the Dealumination of Kankara Kaolin Clay, *Nigerian Journal of Engineering*, 9 (1), 40-44.

Aderemi, B.O; Ahmed, A.S; Abdul B.D (2006). Production of alum from Kankara clay. In *Journal of Nigeria Society Chemical Engineering*. 21(1,2), 120-124.

Aderemi B.O. and Hameed, B.H. (2011), Alumina from kaolin – Extraction and Characterization. Nigerian Metallurgical Society Conference, November: 75-80.

Adewuyi, Y., Klocke, D., Buchanan, J., 1995. Effects of high-level additions of ZSM-5 to a fluid catalytic cracking (FCC) RE-USY catalyst. Applied Catalysis A 131, 121–133.

Ahmed, K.S. (1986), Development of phosphate bonded fireclay refractory castables. An M.Sc thesis. Department of Chemical Engineering, Ahmadu Bello University, Zaria, Nigeria.

Ahmed, A. S. (2011), Potentials and Development of Zeolite Catalysts for Nigerian Oil and Gas Industry, Annul Lecture of the PTDF Professorial Chair in Chemical Engineering, ABU., Zaria, booklet, November.

Ahmed, A. S. and Bawa, S. G. (2012), Development of Large Surface Area Alumina from Kankara Kaolin for Zeolite Support, International Symposium in Zeolite and MicroPorous Crystals (ZMPC), Hiroshima, July.

Ahmed, A. S. (2014), Indigenous Process Technology Development for the Production of Zeolite Catalyst from Kaolin, Annul Lecture of the PTDF Professorial Chair in Chemical Engineering, ABU., Zaria, August.

Ahmed, A. S. (2014), Materials Development: Frontier of Technological Advancement, Inaugural Lecture. Ahmadu Bello University, Zaria.

Ajayi, A. O., Atta, A. Y., Aderemi, B. O. and Adefila, S.S. (2010), Novel Method of Metakaolin Dealumination Preliminary Investigation, *Journal of Applied Sciences Research*, 6(10), 1539-1546.

Ajayi, O. A. (2012), Development of Large Pore Zeolite from Kaolinite Clays, Unpublished PhD Thesis, Ahmadu Bello University, Zaria-Nigeria.

Alaba, P. A., ahaya Muhammad Sani, Y. M., and Daud, W. M. (2015), Synthesis and Characterization of Hierarchical Nanoporous HY Zeolite From Acid Activated Kaolin. *American Journal of Materials Science*, 5(3B): 11-15

Al-Bogami, S. A. (2013). Catalytic Conversion of Benzothiophene over a H-ZSM-5 Catalyst Reactivity and a Kinetic Model; Unpublished Ph D Thesis, University of Western Ontario London, Canada.

Alkan, M., Hopa, C., Yilmaz, Z., Guler, H (2005). The effect of alkali concentration and solid/liquid ratio on the hydrothermal synthesis of zeolite NaA from natural kaolinite. *Microporous Mesoporous Materials*, 86, 176–184.

Al-Khattaf, S., (2003), The Influence of Alumina on the Performance of FCC Catalysts during Hydrotreated VGO Catalytic Cracking, *Journal of Energy & Fuels*, 17, 62-68.

Ambikadevi, V. R. and Lalithambika, M. (2000). Effect of organic acids on ferric iron removal from iron-stained kaolinite. *Applied Clay Sciences*, 16, 133–145.

Aroke, U. O., El-Nafaty, U. A. and Osha, O. A. (2013), Properties and Characterization of Kaolin Clay from Alkaleri, North-Eastern Nigeria. *International Journal of Emerging Technology and Advanced Engineering*, 3(11): 387-392.

Asmatulu, R., (2002). Removal of discoloring contaminants of east Georgia kaolin clay and its dewatering. *Turkey Journal of Engineering Environmental Sciences*. 26, 447–453.

Atta, A. Y., Ajayi, O. A. and Adefila, S. S. (2007), Synthesis of Faujasite Zeolites from Kankara Kaolin Clay. *Journal of Applied Sciences Research*, 3(10): 1017-1021.

Babalola, R., Omoleye, J.A., Adefila, S.S., Hymore, F.K. and Ajayi, O.A. (2015), Comparative Analysis of Zeolite Y from Nigerian Clay and Standard Grade. International Conference on African Development Issues (CU-ICADI) 2015: Materials Teclmology Track, 179 – 182.

Baccouche, A., Srasra, E. and Maaoui, M.E. (1998), Preparation of Na-P1 and Sodalite Octahydrate Zeolites from Interstratified Illite-Smectite. *Applied Clay Sciences*, 13, 255-273.

Baerlocher, C., Meier, W. H. and Olson, D. H. (2007), "Atlas of Zeolite Framework Types", 6th edition, Amsterdam, Netherlands, Elsevier.

Bebon, C., Colson, D., Marrot, B., Klein, J. P., Renzo, F. D. (2002), Synthesis of Zeolites: Study and Applications of a New Process of Homogeneous Shaking out of the Medium to Minimize the Shear Rate during the Crystallization. *Microporous and Mesoporous Materials*, 53 13-20.

Belver, C., M.A.B. Munoz and M.A. Vicente (2002). Chemical Activation of a Kaolinite under Acid and Alkaline Conditions. *Chemical Material*. 14: 2033-2043.

Benincasa, E., Brigatti, M. F., Medici, L. and Poppi, L. (2001), K-rich Rectorite from Kaolinized Micaschist of the Sesia-Lanzo Zone. *Italy Clay Mineral*, 36: 421–433.

Bekkum, V. H., Cjansen, J. and Mflanigen, E. (1991), Zeolite and molecular sieves. Introduction to zeolite science and practice. 58: 13-23.

Berendsen, W.R., P. Radmer, and M. Reuss, (2006), Pervaporative separation of ethanol from an alcohol--ester quaternary mixture, *Journal of membrane science*, 280(1-2): 684-692.

Bergaya, F, and Lagaly, G., (eds.), (2013), Handbook of Clay Science, vol. 5 for Description of Kaolinite Structure, 2nd ed. Elsevier Ltd., Amsterdam.

Bergaya, F., and Lagaly, G., (2006), Handbook of Clay science ed. F. Bergaya, B.K.G. Theng, and G. Lagaly.

Bhatia, S. (1990), "Zeolite Catalysis: Principles and Applications". Boca Raton, Florida, CRC Press Inc.

Bogdanov, B., Georgiev, D., Angelova, K. and Hristov, Y. (2009) Synthetic Zeolites and Their Industrial and Environmental Applications (Review). International Science Conference, Stara Zagora, 4-5 June, 5.

Bosch, P., L. Ortiz, and I. Schifter, (1983), Synthesis of Faujasite Type Zeolites from Calcined Kaolins. *Industrial & Engineering Chemistry, Product Research and Development*, 22(3): 401-406.

Bose, S. D., Saha, R. K. and Gupta, P. S. (2007), FCC Riser Hydrodynamics: Effect of some Operative Variables, *Indian Journal of Chemical Technology*, 14: 473-480.

Boukadir, D., Bettahar, N. and Derriche. Z. (2002), Synthesis of Zeolites 4A and HS from Natural Materials, *Annales de Chimie - Science des Matériaux*, 27: 1-13.

Breck, D. W. (1974), Zeolite Molecular Sieves, Structure, Chemistry and Use. John Wiley & Sons, New York, London, Sydney, Toronto.

Breck, D.W. (1964) Crystalline Molecular Sieves. *Journal of Chemical Education*, 41, 678-689.

Burhan, D. and Emin, C. (2009), Investigation of Central Anatolian Clays by FTIR Spectroscopy. *International Journal of Natural and Engineering Sciences*, 3 (3): 154-161.

Caballero, I., Colina, F.G., Costa, J. (2007). Synthesis of X-type zeolite from dealuminated kaolin by reaction with sulfuric acid at high temperature. *Industrial and Engineering Chemistry Research* 46, 1029–1038.

Cañizares, P., Duran, A., Dorado, F. and Carmona, M. (2000) The Role of Sodium Montmorillonite on Bounded Zeolite-Type Catalysts. *Applied Clay Science*, 16, 273-287.

Cejka, J. Corma, A. and Zone, S. (2010), Zeolites and Catalysis, Synthesis, Reactions and Applications. WILEY-VCH Verlag GmbH & Co. KGaA, Weinheim.

Chandrasekhar, S., and Ramaswamy, S., (2002), ‘‘Influence of Mineral Impurities on the Properties of Kaolin and Its Thermally Treated Products.’’ *Applied Clay Science*, 21 (3–4) 133–142.

Chandrasekhar, S., (1996), Influence of Metakaolinization Temperature on the Formation of Zeolite 4A from kaolin clay Minerals, *Applied Clay Science*, 31: 253-261.

Chandrasekhar, S. and Pramada, P. N. (1999), Investigation on the Synthesis of Zeolite NaX from Kerala Kaolin. *Journal of porous materials*, 6(4): 283-297.

Chareonpanich, M., Namto, T., Kongkachuichay, P., Limtrakul, J., (2004). Synthesis of ZSM-5 zeolite from lignite fly ash and rice husk ash. *Fuel Process Technology*. 85, 1623–1634.

Chen, P. (1977), “Tables of Key Lines in X-ray Powder Diffraction Patterns of Minerals in Clays and Associate Rocks”, Indiana, Bloomington.

Cheetham, A. K., Ferey G. and Loiseau, T (1999). Open-Framework Inorganic Materials, Angewerson Chemical International Ed. 38, 3268-3292.

Chica, A., Corma, A., Miguel, P.J., (2001), Isomerization of C5–C7 n-alkanes on unidirectional large pore zeolites: activity, selectivity and adsorption features, *Catalysis Today*, (65) 101.

Christopher, B., Nigel, D. and Jack, Y. (2002), The Thermal Stability of Mixed Phenylphosphonic Acid/water Intercalates of Kaolin and Halloysite: A TG-EGA and VT-DRIFTS study, *Journal of Material Chemistry*, 12: 273-278.

Clearfield, A., Reibenspies, J., and Bhuvanesh, N. (2008), Principle and application of powder diffraction, Chichester Wiley 397.

Colina, F.G., Esplugas, S. and J. Costa (2002). High-temperature Reaction of Kaolin with Sulfuric Acid. *Industrial and Engineering Chemistry Research*, 41(17): 4168-4173.

David S.J. Jones and Peter P. Pujado (Editors) (2006), Handbook of Petroleum Processing (First ed.), Springer. ISBN 1-4020-2819-9.

Ding, F., Ng, S. H., Xu, C. and Yui, S. (2007), Reduction of Light Cycle Oil in Catalytic Cracking of Bitumen-Derived Crude HGOs though Catalyst Selection. *Fuel Processing Technology*, 88: 833–845.

Dohnalova, Z., Svoboda, L., and Sulcova, P. (2008), Characterization of Kaolin Dispersion using Acoustic and Electroacoustic Spectroscopy. *Journal of Mining and Metallurgy*, 44B: 63-72.

Du, X., Wang, Y., Su, X. and Li, J. (2009), Influences of pH Value on the Microstructure and Phase Transformation of Aluminium Hydroxide. *Powder Technology*, 192: 40–46.

Du, X., Zhang, H., Li, X., Tan, Z., Liu, H. and Gao, X. (2013), Cation Location and Migration in Lanthanum-Exchanged NaY zeolite. Chinese Journal of Catalysis 34: 1599–1607.

Duane, M.M. and Robert, C.R. (1997), X-ray Diffraction and the identification and analysis of Clay Minerals second edition ed., Oxford University Press 378.

Dyer, A (1988). An Introduction to Zeolite Molecular Sieves John Wiley & Sons, Inc.

Edomwonyi-Otu, L. C. and Aderemi, B. O. (2009), Alums from Kankara Kaolin. *Journal of Research in Engineering*, 6(1): 105-111.

Edomwonyi-Otu, L. C., Aderemi, B. O., Ahmed, A. S., Coville, N. J. and Maaza, M. (2013), Influence of Thermal Treatment on Kankara Kaolinite. *Opticon1826*, 15(5): 1-5.

Ekosse, Georges-Ivo E (2010). Kaolin deposits and occurrences in Africa: Geology, mineralogy and utilization. *Applied Clay Science*, Volume 50, Issue 2, 212-236.

Elimbi, A., H.K. Tchakoute, D. Njopwouo (2011). Effects of calcination temperature of kaolinite clays on the properties of geopolymer cements. *Construction and Building Materials*, Volume 25, Issue 6, 2805-2812.

El-Naggar, A. Y. (2013), Characterization of Modified and Polymer Coated Alumina Surfaces by Infrared Spectroscopy. *Journal of Spectroscopy*, 1: 1-5.

El-Sherbiny, S., Morsy, F. A., Hassan, M. S. and Mohamed H. F. (2015), Enhancing Egyptian Kaolinite via Calcination and Dealumination for Application in Paper Coating. *Journal of Coating Technology Research*, 12(4): 739-749.

El-Yakub B. (2011), Petroleum Industry Nigerian Content Initiative: Catalysis as a Key Requirement for Sustainable Petrochemicals Industry, Symposium Paper Prersentation.

Esmaeili, N., Kazemian, H. and Bastani, D. (2011). Controlled Crystallization of LTA Zeolitic Nanoparticles from Clear Solution Using Organic Template. *Iran Journal of Chemical Engineering*. 30: 2.

Everett, D.H. (2006), Basic Principles of colloid science. 2006, London: *Royal Society of Chemistry*. 243.

Farhount, N., 1989. Beneficiation of kaolins of islands of Milos. Unpublished PhD thesis, National Technical University, Athens.

Feng, H., Li, C., Shan, H., (2009). Effect of calcination temperature of kaolin microspheres on the in situ synthesis of ZSM-5. *Catalysis Letter*, 129, 71–78.

Flanigen, E. M. (2001). Zeolites and molecular sieves: An historical perspective. Studies in Surface Science Cataysis, 137 (Introduction to Zeolite Science and Practice (2nd Edition)), 11-35.

Frantz, T. S., Ruiz, W. A., Rosa, C. A. and Mortola, V. B. (2016). Synthesis of ZSM-5 with high sodium content for CO_2 adsorption. *Microporous and Mesoporous Materials*, 222: 209 – 217.

Fukui, K., Nishimoto, T., Takiguchi, M. and Yoshida, H. (2003), Effects of NaOH Concentration on Zeolite Synthesis from Fly Ash with a Hydrothermal Treatment Method, *Journal of the Society of Powder Technology*, 40: 497-504.

Gao, X., Qin, Z., Wang, B., Zhao, X., Li, J., Zhao, H., Liu, H. and Shen, B. (2012), High silica REHY Zeolite with Low Rare Earth Loading as High Performance Catalyst for Oil Conversion. Applied Catalysis A: General, 413: 254–260.

Ginter, D. M., Bell, A. T. and Radke, C. J. (1992), "Synthesis of Microporous Materials, Molecular Sieves". New York, Van Nostrand Reinhold.

Goldstein, J.I., Newbury, D.E., Echlin, P., Joy, D.C., Fiori, C. and Lifshin, E. (1981), Scanning Electron Microscope and X-ray Microanalysis, New York Plenum Press, 673.

Granizo, M. L., Blanco-Varela, M. T. and Palomo, A. (2000). "Influence of the starting kaolin on alkali-activated materials based on metakaolin. Study of the reaction parameters by isothermal conduction calorimetry." *Journal of Materials Science*, 35(24): 6309-6315.

Grimshaw, R.W. (1971). Physics and Chemistry of Clay, 4th ed. Ernest Benn, London, ISBN: 0510-47701-7.

Guisnet, M. and Ribeiro, F. R. (2002), Deactivation and Regeneration of Zeolite Catalyst. *Catalyst Science Series*, 9: 12-17.

Haq, A., Iqbal,Y., Riaz Khan, M. (2009). Phase and Microstructural Characterization of Kaolin Clays from North Western Pakistan. *Journal of Pakistani Materials Society*, 3 (2).

Hill, G. Charles Jr (1977), "Chemical Engineering Kinetics and Reactor Design". New York, John Wiley & Sons pp. 265-275.

Horváth, I., Sedlec (1976). kaolinite dehydroxylation kinetics. In Book of Proceeding for the 7th Conference on Clay Mineral and Petrol. Karlovy Vary, 121–127.

Houssin, C. J. (2003) Nanoparticles in Zeolite Synthesis, Unpublished PhD Thesis, Schuit Institute of Catalysis, Eindhoven University of Technology, The Netherlands, pp. 6.

Htun, M.M.H., Htay, M.M. and Lwin, M.Z. (2012) Preparation of Zeolite (NaX, Faujasite) from Pure Silica and Alumina Sources. International Conference on Chemical Processes and Environmental Issues (ICCEEI), Singapore, 15-16 July 2012, 212-216.

Hudec, P. (2011), FCC Catalyst - Key Element in Refinery Technology, 45th International Petroleum Conference, June 13, 2011, Bratislava, Slovak Republic.

Hulbert, S. F., Huff, D. H. (1970), Kinetics of alumina removal from a calcined kaolin with nitric, sulphuric and hydrochloric acids, *Clay Minerals*, 8 (337), pp. 340–345.

James. G. Speight (2006). The Chemistry and Technology of Petroleum (4th ed.). CRC Press. ISBN 0-8493-9067-2.

Jiang, J., Duanmu, C., Yang, Y., Gu, X., Chen, J., 2014. Synthesis and characterization of high siliceous ZSM-5 zeolite from acid-treated palygorskite. *Powder Technology*, 251, 9–14.

Jiri, C., Herman, V.B., Avelino, C., and Ferdi, S., (2007), Introduction to zeolite science and Practice, 3rd revised edition ed., Amsterdam Elsevier 1058.

Khatamian, M., Irani,M., (2009). Preparation and characterization of nanosized ZSM-5 zeolite using kaolin and investigation of kaolin content, crystallization time and temperature changes on the size and crystallinity of products. *Journal of Iran Chemical Society*, 6, 187–194.

Kim, S.D., Noh, S.H., Park, J.W., Kim,W.J., (2006). Organic-free synthesis of ZSM-5 with narrowcrystal size distribution using two-step temperature process. *Micropores and Mesopores Material*, 92, 181–188.

Kloprogge, J. T., Frost, R. L. and Hickey, L. (1999), "Infrared Absorption and Emission Study of Synthetic Mica–Montmorillonite in Comparison to Rectorite, Beidellite and Paragonite". *Journal of Materials Science Letters*, 18: 1921-1923.

Komskaja, M., Dolin, A., Yatsunova, S., (1971). Enrichment of kaolin. Otkryt. Izobret. Prom. Obraztsy Tovar. Znaki 48 (5), 42–56.

Kordatos, K., Gavela, S., Ntziouni, A., Pistiolas, K. N., Kyritsi, A. and Kasselouri-Rigopoulou, V. (2008), Synthesis of High Siliceous ZSM-5 Zeolite Using Silica from Rice Husk Ash. *Microporous and Mesoporous Materials*, 115: 189-196.

Kovo, A.S. (2011), Development of Zeolites and Zeolite Membranes from Ahoko Nigerian Kaolin. Unpublished PhD Thesis, School of Chemical Engineering and Analytical Science, University of Manchester, UK.

Kovo, A.S., Hernandez, O., Holmes, S.M., (2009). Synthesis and characterization of zeolite Y and ZSM-5 from Nigerian Ahoko Kaolin using a novel, lower temperature, metakaolinization technique. *Journal of Materials Chemistry*, 19, 6207–6212.

Kovo, A. S. and Edoga, M. O. (2007), Production and Characterization of Zeolite from Ahako Clay in Kogi State – Nigeria, http://lejpt.academicdirect/A07/31/40.htm.

Kozík, T. et al. (1992). The temperature dependence of the electric conductivity of unfired porcelain mixture. Ceramics-Silikáty, 36, N_2, 69–72.

Krishnan, A.K., George, T.S., Anjana, R., Joseph, N. and George, K.E. (2012), Effect of Modified Kaolin Clays on the Mechanical Properties of Polypropylene/Polystyrene Blends. *Journal of Applied Polymer Science*, 127 (2): 1409–1415.

Kuye, A. and Ayo, D. (2007), Basic Concepts in Process Equipment and Plant Design. Publication of Raw Materials Research and Development Council, Nigeria.

Lee, S. O., Jung, K. H., Oh, C. J., Lee, Y. H., Tran, T. and Kim, M. J. (2009), Precipitation of Fine Aluminium Hydroxide from Bayer Liquors. *Hydrometallurgy*, 98: 156–161.

Lee, J. S., Kim, H. S., Park, N., Lee, T. J. and Kang, M. (2013), Low Temperature Synthesis of α-Alumina from Aluminium Hydroxide Hydrothermally Synthesized using [Al(C2O4)x (OH)y] Complexes. *Chemical Engineering Journal*, 230: 351–360.

Lenarda, M., L.Storaro, Talon, A., E.Moretti and Riello, P (2007). Solid acid catalysts from clays: Preparation of mesoporous catalysts by chemical activation of metakaolin under acid conditions. *Journal of Colloid and Interface Science*, 311, 537-543.

Levenspiel, O. (1999), Chemical Reaction Engineering, 3rd Edition, John Wiley & Sons New York.

Li, J., Corma A. and Yu, J. (2015), Synthesis of New Zeolite Structures: Reviewed article. *Royal Society of Chemistry*, 44, 7112-7127.

Li, X., Li, C., Zhang, J., Yang, C. and Shan, H. (2007), Effects of Temperature and Catalyst to Oil Weight Ratio on the Catalytic Conversion of Heavy Oil to Propylene Using ZSM5 and USY Catalysts. *Journal of Natural Gas Chemistry*, 16: 92–99.

Liu, X., Yan, Z., Wang, H. and Luo, Y. (2003), In-situ Synthesis of NaY Zeolite with Coal-Based Kaolin, *Journal of Natural Gas Chemistry*, 12: 63-70.

Luz, A. B., and Middea, A., (2004), Purification of Kaolin by Selective Flocculation. Center for Mineral Technology-CETEM, Rio de Janeiro.

Ma, C. and Eggleton, R. A. (1999), Surface Layer Types of Kaolinite; a High Resolution Transmission Electron Microscope Study. *Clays and Clay Minerals*, 47: 181–191.

Ma, X. and Bruckard, W.J. (2010). The Effect of pH and Ionic Strength on Starch–Kaolinite Interactions. *International Journal of Mineral Processing*, 94: 111–114.

Madani, A., Aznar A, Sanza J, Serratosa J.M. (1990). Si and Al NMR study of zeolite formation from alkali-leached kaolinites. Influence of thermal activation. Journal of Physical Chemistry 94:760-765.

McCabe & Smith (2005). Unit Operations of Chemical Engineering' McGraw-Hill, New York

Mezni, M., Hamzaoui, A., Hamdi, N. and Srasra, E. (2011) Synthesis of Zeolites from Low-Grade Tunisian Natural Illite by Two Different Methods. Applied Clay Science, 52, 209-218.

Missen, R.W., Charles A. Mims, C.A. and Saville, B.A. (1999), Introduction to Chemical Reaction Engineering and Kinetics, John Wiley & Sons, Inc., New York.

Modi, C. K. and Trivedi, P. M. (2012), Zeolite-Y Based Nanohybrid Materials: Synthesis, Characterization and Catalytic Aspects. Microporous and Mesoporous Materials, 155: 227–232.

Mohiuddin, E., Isa, Y. M., Mdleleni, M.M., Sincadu, N., Key, D. and Tshabalala, T. (2016), Synthesis of ZSM-5 from Impure and Beneficiated Grahamstown Kaolin: Effect of Kaolinite Content, Crystallization Temperatures and Time, *Applied Clay Sciences*, 119: 213-221.

Moreno, N., Querol, X., Plana, F., Andres, J. M., Janssen, M. and Nugteren, H. (2002), Pure Zeolite Synthesis from Silica Extracted from Coal Ashes, *Journal of Chemical Technology and Biotechnology*, 77: 274-279.

Mgbemena, C. O., Ibekwe, N. O., Sukumar, R. and Menon, A. R. (2013), Characterization of Kaolin Intercalates of Oleochemicals derived from rubber seed (*Hevea brasiliensis*) and tea seed (*Camelia sinensis*) oils. *Journal of King Saud University – Science*, 25: 149-155.

Mohiuddin, E., Isa, Y. M., Mdleleni, M.M., Sincadu, N., Key, D. and Tshabalala, T. (2016), Synthesis of ZSM-5 from Impure and Beneficiated Grahamstown Kaolin: Effect of Kaolinite Content, Crystallization Temperatures and Time, *Applied Clay Sciences*, 119: 213-221.

Monnier, A., Schuth, F., Huo, Q., Kumar, D., Margolese, D., Maxwell, R. S., Stucky, G. D., Krishnamurty, M., Petroff, P., Firouzi, A., Janicke, M. and Chmelka, B. F. (1993), Cooperative Formation of Inorganic-Organic Interfaces in the Synthesis of Silicate Mesostructures. *Science*, 261: 1299–1303.

Nakakana, S. (2015), development of Pilot-Scale Reactor for the Production of Aluminum Hydroxide from Alum Derived from Kankara Kaolin for Zeolite Y Synthesis. Unpublished MSc Thesis, Ahmadu Bello University, Zaria, Nigeria.

Nauman, E. B. (2002), Chemical Reactor Design, Optimization and Scale-up. MCGraw-Hill, New York.

Niaei, A., Salari, D. P., Nakhostin, P. P. and Mousavi, S. M. (2012), Selectivity Catalytic Reduction of NO with Ammonia over Nanostructure H-ZSM-5 Supported Transition Metal Oxide Catalysts, International Conference on Applied Life Sciences (ICALS2012), Turkey.

Oliver, R. W. (2000), The Coming Biotech Age: The Business of Bio-Materials. New York, McGraw Hill.

Pal, P., Das, J. K., Das, N. and Bandyopadhyay, S. (2013), Synthesis of NaP Zeolite at Room Temperature and Short Crystallization Time by Sonochemical Method. *Ultrasonics Sonochemistry*, 20: 314–321.

Pan, F., Lu, X., Wang, Y., Chen, S., Wang, T., Yan, Y., (2014a). Synthesis and crystallization kinetics of ZSM-5 without organic template from coal-series kaolinite. *Microporous Mesoporous Materials*, 184, 134–140.

Pan, F., Lu, X., Wang, Y., Chen, S., Wang, T., Yan, Y., (2014b). Organic template-free synthesis of ZSM-5 zeolite from coal-series kaolinite. *Materials Letters*, 115: 5 – 8.

Panda, A. K., Misha, B. G., Misha, D. K. and Singh, R. K. (2010). Effect of Sulfuric Acid Reaction Sequence from Infrared Absorption Spectra. *Journal of American Ceramic Society*, 57: 57-61.

Percival, H. J., Duncan, J. F. and Foster, P. K. (1974), Interpretation of the Kaolinite–Mullite Reaction Sequence from Infrared Absorption Spectra. *Journal of American Ceramic Society*, 57: 57–61.

Perry, R.H.; Green, D.W (1997). Perry's Chemical Engineers Handbook, McGraw-Hill Book Co., pp 28-36, 38-43.

Pinheiro, P.G., J.D. Fabris, Mussel, W.N., E. Murad, Scovzelli, R.B. and V.K.Garg (2005). Beneficiation of a commercial kaolin from Mar de Espanha, Minas Gerais, Brazil: Chemistry and Mineralogy. *Journal of South American Earth Sciences*, 20, 267-271.

Raseev, S., Thermal & Catalytic Processes in Petroleum Refining, Marcel Dekker Inc.: New York; 2003.

Ríos, C.A., Williams, C.D. and Roberts, C. (2011) Synthesis and Characterization of SOD-CAN- and JBW-Type Structure by Hydrothermal Reaction of Kaolinite at 200 C. Dyna, No. 166, 38-47.

Ríos, C. A., Williams, C. D and Fullen, M. A. (2009), Nucleation and Growth History of Zeolite LTA Synthesized from Kaolinite by Two Different Method, *Applied Clay Science*, 42: pp. 446-454.

Robson, H. (2001), "Verified Synthesis of Zeolitic Materials" 2nd edition. Published on behalf of the Synthesis Commission of the International Zeolite Association, Amsterdam, Netherlands, Elsevier.

Rouquerol, F., Rouquerol, J. and Sing, K. (1999), Adsorption by powders and porous solids: principle, methodology and applications, London Academic press 465.

Ruiz, R., Blanco, C., Gonzalez, F., Benito, I. and Lopez, J.L. (1997) Zeolitization of Bentonite and Its Application to the Removal of Ammonium Ion from Waste Water. *Applied Clay Science*, 12, 73-83.

Salou, M., Kooli, F., Kiyozumi, Y., Mikamizu, F., (2001). Effect of aluminium source and content on the synthesis of zeolite ZSM-5 from kanemite via solid-state transformation. *Journal of Materials Chemistry*, 11, 1476–1481.

Saikia, N. J., Bharali, D. J., Sengupta, P., Bordolo, I. D., Goswamee, R. L., Saikia, P. C. and Borthakur, P. C. (2003), Characterization, beneficiation and utilization of a kaolinite clay from Assam, India. *Applied Clay Science*, 24, 93–103.

Salahudeen, N. (2015), Development of Zeolite Y and ZSM-5 Composite Catalyst from Kankara Kaolin. Unpublished Ph D Thesis, Department of Chemical Engineering, Ahmadu Bello University, Zaria, Nigeria.

Selim, M.M. and Abdel-Maksoud, I.H. (2005) Preparation of Na-A Zeolite from Egyptian Kaolin. Patent No. 23, 353.

Shen, Y., Zhao, P. and Shao, Q. (2014), Porous Silica and Carbon Derived Materials from Rice Husk Pyrolysis Char. *Microporous and Mesoporous Materials*, 188: 46–76.

Sherman, J. D. (1999), Synthetic Zeolites and other Microporous Oxide Moleculae Sieves, *Proceedings of the National Academy of Science*, 96 (7): 3471-3478.

Shoumkov, S., Dimitrov, Z., Brakalov, L. (1987). High-gradient magnetic treatment of kaolin. Interceram 6, 26–28.

Silva, N.A.A., Rodrigues, J.J., Soares, R.R., Napolitano, M.N. and Rodrigues, M.G.F. (2013), Cobalt Supported on ZSM-5 Zeolite Using Kaolin as Silica and Aluminum Sources for Ficher-Tropsch Synthesis. Brazilian Journal of Petroleum and Gas, 083-094, ISSN: 1982-0593.

Sinnott, R. K. (1999), Chemical Engineering Design; Third edition, Vol. 6, Replika press pvt. Ltd., Kundli, India.

Shoumkov, S., Dimitrov, Z., Brakalov, L. (1987). High-gradient magnetic treatment of kaolin. Interceram 6, 26–28.

Silva, N.A.A., Rodrigues, J.J., Soares, R.R., Napolitano, M.N. and Rodrigues, M.G.F. (2013), Cobalt Supported on ZSM-5 Zeolite Using Kaolin as Silica and Aluminum Sources for Ficher-Tropsch Synthesis. Brazilian Journal of Petroleum and Gas, 083-094, ISSN: 1982-0593.

Singh Shraddha R., Chaturvedi A*, Lal Dori, Ranjan A., Lodhi S. K., Singh A., Gola Neeraj (2013), Hydro cracking for Maximizing Middle Distillates, *International Journal of Scientific Research and Reviews*, 2(2), 27-35.

Songfang, Z., Shangchang, Q., Yuying, Z., Lei, C. and Yong, G., (2011), Synthesis and Characterization of Kaolin with Polystyrene via Insitupolymerization and their Application on Polypropylene. *Materials and Design*, 32: 957–963.

Srikanth, V. (2011), Fluid Catalytic Cracking Unit, FCC Operations and Salient Design.

Steudel, A., Batenburg, L. F., Fischer, H. R., Weidler, P. G. and Emmerich, K. (2009), Alteration of Swelling Clay Minerals by Acid Activation. *Applied Clay Science*, 44: 105–115.

Toussaint F., Fripiat J.J. & Gastuche M.C. (1963). Dehydroxylation of Kaolinite. I. Kinetics. *Journal of Physical Chemistry*, 67, 26-30.

Treacy, M. M. J. and Higgins, J. B. (2001), Collection of Simulated XRD Powder Patterns for Zeolites, 5th Revised Edn., Elsevier.

Triantafyllidis, K.S., Nalbandian, L., Trikalitis, P.N., Ladavos, A.K., Mavromoustakos, T., Nicolaides, C.P., (2004). Structural, compositional and acidic characteristics of nanosized amorphous or partially crystalline ZSM-5 zeolite-based materials. *Microporous and Mesoporous Materials*, 75, 89–100.

Vaculikova, L., Plevova, E., Vallova, S. and Koutnik, I. (2011), Characterization and Differentiation of Kaolinites from Selected Czech Using Infrared Spectroscopy and Differential Thermal Amalysis. *Acta Geodynamics Geomaterials*, 8(161): 59-67.

Veglio, F., Passariello, B., Toro, L. and Marabini, A. M. (1996), Development of a bleaching process for a kaolin of industrial interest by oxalic, ascorbic and sulphuric acids: Preliminary study using statistical methods of experimental design. *Industrial Engineering Chemistry Research*, 35, 1680–1687.

Verma, H.R. (2007), Atomic and nuclear analytic method: XRF, Mossbauer, XPS, NAA and ion beam spectroscopic techniques, New York Springer 386.

Wada. T., Kaneda. K., Murate. S., Nomura.M. (1996). Effect of modifier Pd metal on hydrocracking of polyaromatic compounds over Ni-loaded Y-zeolite and its application as hydrodesulfurization catalyst. *Catalysis Today*, 31, pp.113-120.

Wajima, T., Haga, M., Kazuwa, K., Ishimoto, H., Tamada, O., Ito, K., Nishiyama, T. Downs,R. T. and Rakovan, J. F. (2006), Zeolite Synthesis from Paper Sludge Ash at Low Temperature (90°C) with Addition of Diatomite, *Journal of Hazardous Materials*, B132: 244-252.

Walas, S.M. (1990). Chemical Process Equipment: Selection and Design. Reed publishers, Butterworth-Heineman, USA.

Wang, Z.B., Yashima, T., Komatsu, T., Kamo, A., Yoneda, T., (1997), Applied Catalysis A: General, (159) 119.

Weitkamp, J. and Puppe, L. (1999), Catalysis and zeolites: fundamentals and applications. Berlin Springer 564.

Weller, M.T., Inorganic materials chemistry 1994, Oxford university press 92.

Wang, Z.B., Yashima, T., Komatsu, T., Kamo, A., Yoneda, T., (1997), *Applied Catalysis A*: *General*, (159) 119.

Xu, R., Pang, W., Yu, J., Huo, Q., and Chen, J. (2007), Chemistry of Zeolites and Related Porous Materials: Synthesis and Structure, John wiley & sonsa pte Ltd, Singapore.

Yunusa, S. 2015. Synthesis and Characterization of Nano-sized ZSM-5 from Kankara Kaolin, Unpublished PhD Thesis, Ahmadu Bello University, Zaria, Nigeria.

Yusuf, M. (2015), Production of High grade Sodium Silicate and Silica Sol from Kankara kaolin for ZSM-5 Synthesis. Unpublished MSc Thesis, Ahmadu Bello University, Zaria, Nigeria.

Zhang, Y., Liu, Y. and Li, Y. (2008), Synthesis and Characteristics of Y-Zeolite/MCM-48 Biporous Molecular Sieve. *Applied Catalysis A: General*, 345: 73–79.

Raw Material Research and Development Council (2010), Raw Materials and Consumer Industries in Nigeria, www.rmrdc.org.

http://www.premiumtimesng.com/business/196250-nigerian-refineries-now-produce-6-7-illion-litres-of-petrol-daily-nnpc.html. January 5, 2016Premium Times

U.S. Downstream Processing of Fresh Feed Input by Catalytic Cracking Units (Energy Information Administration, U.S. Dept. of Energy

http://chemeducator.org/sbibs/s0004003/spapers/430114wv.htm, 2008, lasted cited 31/0708.
www.nigeria.gov.ng/2012-10-29-11-05-46/
www.chemistryexplained.com/Va-Z/Zeolite.html

APPENDIX A

DEALUMINATION REACTOR CALCULATION

Basis: Dealumination of 2.5 kg metakaolin per batch

Average alumina content from several X-ray fluorescence (XRF) analysis = 40%

The basic dealumination equation is:

$$Al_2Si_2O_{7\,(s)} + 3H_2SO_{4\,(l)} \longrightarrow Al_2(SO_4)_{3(l)}.3H_2O + 2SiO_{2\,(s)} \qquad (A1)$$

Metakaolin Sulphuric acid Alum Silica

2500g metakaolin contains 0.40(2500) g Al_2O_3

= 1000 g Al_2O_3

From stoichiometry

102 g Al_2O_3 requires 294 g H_2SO_4 (100 wt%)

1000 g requires $^{1000 \times 294}/_{102} = 2882.353\ g$

Amount of 98% H_2SO_4 Required

$= {}^{100 \times 288.353\ g}/_{98} = 2941.177\ g$

ρ_{98} @ 30ºC = 1.8261 gcm^{-3}

$$Volume = {}^{mass}/_{density} \qquad (A2)$$

V_{98}= 1610.633 cm^3

2.5 fold stoichiometric quantity was used

= 2.5 × 1610.633 cm^3

V_{98} = 4,026.583 cm^3 (Volume of acid needed per batch of 2500 g metakaolin)

To dilute the acid from 98 wt% to 60 wt% H_2SO_4, the required dealumination condition

Table A.1: Density of sulphuric acid at different concentration

Weight percent (%)	25	60	96	98
Density @ 30°C	1.1718	1.4808	1.8255	1.8261

$$60\rho_{60}V_{60} = 98\rho_{98}V_{98} \qquad (A3)$$

$$V_{60} = {98 \times 1.8261 \times 4026.583}/{60 \times 1.4808}$$

$$= 8110.351 \text{ cm}^3$$

Amount of water to be added to dilute to 60%

$$V_w = {\left((\rho_{60} \times V_{60}) - (\rho_{98} \times V_{98})\right)}/{\rho_w} \qquad (A4)$$

$$= {\left((1.4808 \times 8110.351) - (1.8261 \times 4{,}026.583)\right)}/{1}$$

= 4656.865 cm^3

That is the Volume of water needed for metakaolin slurry preparation

Pre-Crystallization Dilution

Prior to Crystallization, the filtrate from dealumination was diluted with water to simulate ≅ 25 wt% original sulphuric acid. This was done to depress the freezing point of the excess sulfuric acid, to avoid alum crystals formation immediately after the dealumination reaction.

$$25\rho_{25}V_{25} = 60\rho_{60}V_{60} \qquad (A5)$$

$$V_{25} = \frac{60 \times 1.4808 \times 8110.351}{25 \times 1.1718}$$

$$= 24597.661 \text{ cm}^3$$

Water added

$V_w = \rho_{25}V_{25} - \rho_{60}V_{60}$

= 1.1718 x 24597.661 – 1.4808 x 8110.351

V_w= 16813.731 cm^3 (Volume of water needed to quench the reaction)

APPENDIX B

TIME OF DEALUMINATION REACTION CALCULATION

The acid is use in excess quantity which makes the assumption of the acid concentration of the reaction components to be constant with reaction time to be valid. More so, the fraction of volume expansion was evaluated as follow:

Volume of reactants = 9683 cm^3

The estimated reaction temperature = 393 K

The data used to plot the graph in Figure B.1, was sourced from Perry (2008) and used to calculate the volume of water that will expand to vapor phase at the initiation of the reaction before the mixture becomes acidic after which remains constant over time of the reaction.

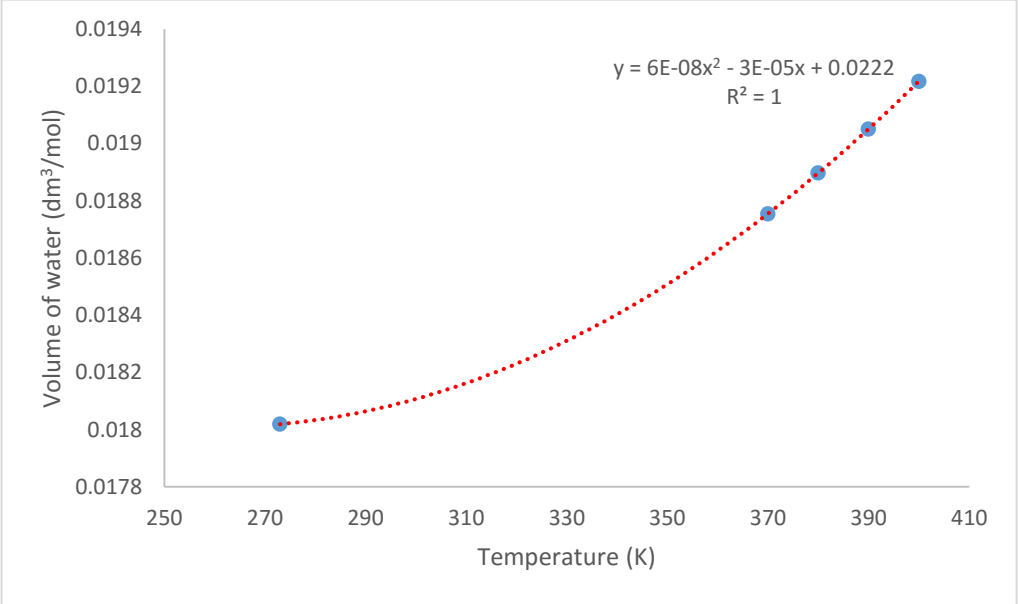


Figure B.1: Graph of water volume expansion with temperature

Volume per mole of water at 300 K	=	18.600 cm^3/mole
Volume per mole of water at 393 K	=	19.677 cm^3/mole
Moles of water	=	258.670 moles

Volume expansion of water in dealuminator = 278.59 cm^3

Percentage of water lost = $\frac{278.59}{4656} \times 100 = 6\%$

0.06 fraction of water will be converted from liquid to vapor at starting point of the reaction.

Since the dealumination reactor uses sulphuric acid for the reaction, and to avoid operating at the boiling point of the sulphuric acid the chat shown in Figure B.2 was used as a guide.

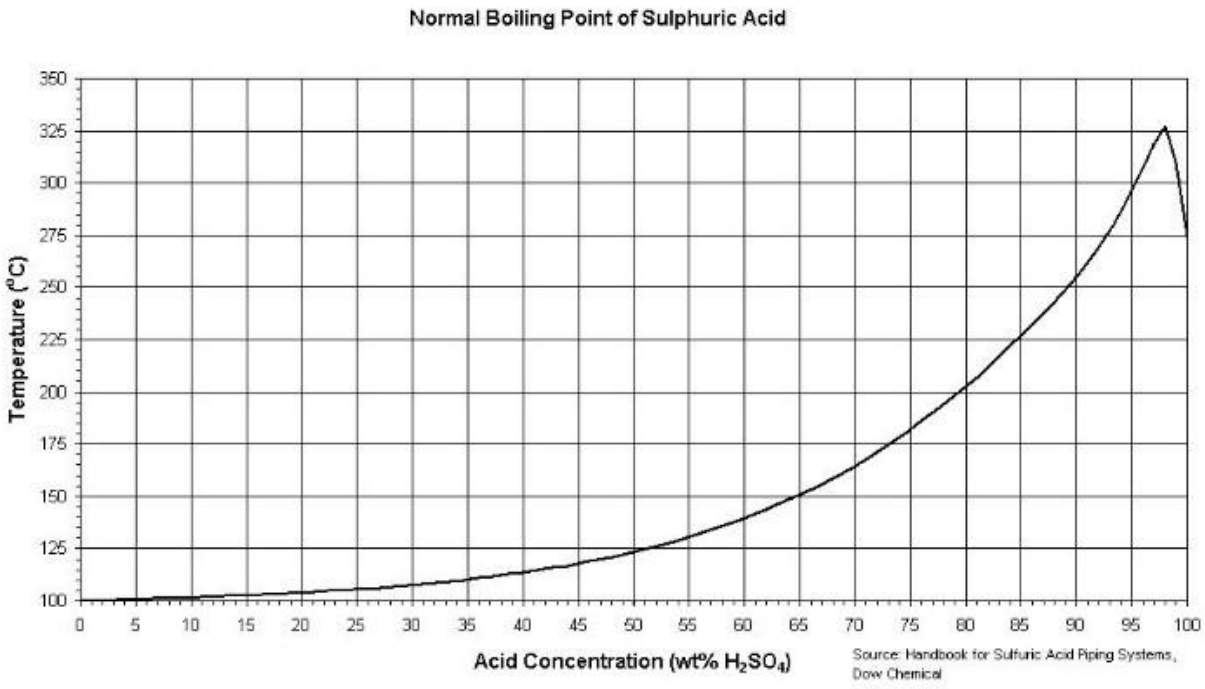


Figure B.2: Sulphuric acid boiling point chat (Source: Perry, 2008)

Consideration of reaction kinetics developed by Aderemi *et al*., 2001 for dealumination reaction

$$-r_{Al} = 131.6e^{\frac{-3837.8}{T}} C_{Ac0} C_{Al} \qquad (B.1)$$

The rate of dealumination was a first order reaction with respect to the leached alumina component, Evaluating the time of reaction for 95% conversion, the batch reactor performance equation was used:

$$t = N_{A0}\int_0^{X_A}\frac{dX_A}{(-r_{Al})V} \qquad (B.2)$$

The reacting specie being solid and liquid was assumed constant, since very small amount of water vaporizes within seconds of the start of the reaction. The boiling temperature of 60wt% acid, evaluated from Figure 3.3, was about 140°C which was close to the reaction temperature.

$$t = \frac{N_{A0}}{V}\int_0^{X_A}\frac{dX_A}{(-r_{Al})} \qquad (B.3)$$

$$t = C_{Al0}\int_0^{X_A}\frac{dX_A}{(-r_{Al})} \qquad (B.4)$$

$-r_A$: Rate of dealumination (g alumina/g metakaolin) $(min)^{-1}$

C_{Al}: Concentration of alumina left in the raffinate (g alumina/g metakaolin)

C_{Ac0}: Acid (mol/dm^3) = 9.066

T: Reaction temperature (K) = 373 K

Assuming conversion of 95%

The pre-exponential factor is 131.6 $dm^3/(mol\ min)$

In terms of conversion the rate of dealumination is expressed as:

$$-r_{Al} = 131.6e^{\frac{-3837.8}{T}}C_{Ac0}C_{Al0}(1 - X_{Al}) \qquad (B.5)$$

$$t = C_{Al0}\int_0^{X_A} \frac{dX_A}{131.6e^{\frac{-3837.8}{T}} C_{Ac0}C_{Al0}(1-X_{Al})} \qquad (B.6)$$

Bring out the constant terms, we have

$$t = \frac{C_{Al0}}{131.6e^{\frac{-3837.8}{T}} C_{Ac0}C_{Al0}}\int_0^{X_A} \frac{dX_A}{(1-X_{Al})} \qquad (B.7)$$

Converting acid concentration from wt% to mol/dm^3, considering 60wt% which is the dealumination condition

$$C_M = \frac{10C_{\%w/w}\rho}{M_M} \qquad (B.8)$$

$$C_M = Concentration\ in\ mol/dm^3$$

$$C_{\%w/w} = Concentration\ in\ wt\%$$

$$\rho = Density\ of\ solution$$

$$C_M = \frac{10 \times 60 \times 1.4808}{98}$$

$$C_M = 9.066\ mol/dm^3$$

C_M is also referred to as C_{Ac0}

Equation (3.11), becomes (T= 393 K and C_{Ac0} = 9.121)

$$t = \frac{1}{0.06862}\int_0^{X_A} \frac{dX_A}{(1-X_{Al})}$$

$$t = 14.573\int_0^{X_A} \frac{dX_A}{(1-X_{Al})}$$

$$t = 14.573\int_0^{0.95} \frac{dX_A}{(1-X_{Al})}$$

$$t = 14.573(-\ln(1-X_A)$$

$$t = 14.573(-\ln(1 - 0.95))$$

$$t = 14.573 \times (-\ln(0.05))$$

$$t = 43.66\ mins$$

The reaction kinetic model was used to generate data of fractional conversion and the corresponding reaction rates. The generated values are presented in Table 4.1 and were used for graphical plots.

Graphical method was also used to estimate the reaction time *via* plots which are shown in Figures B.3 to B.9.

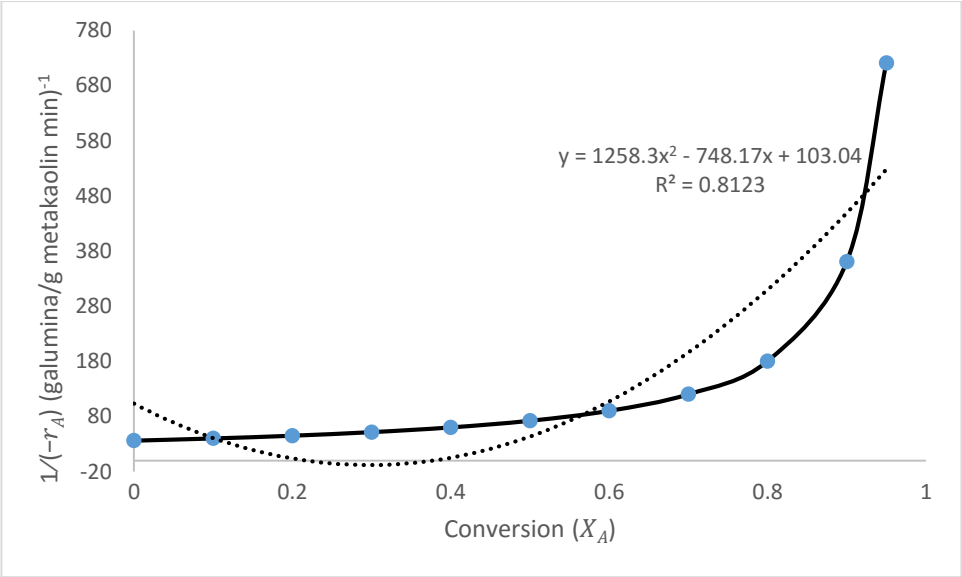


Figure B-3: Quadratic model plot

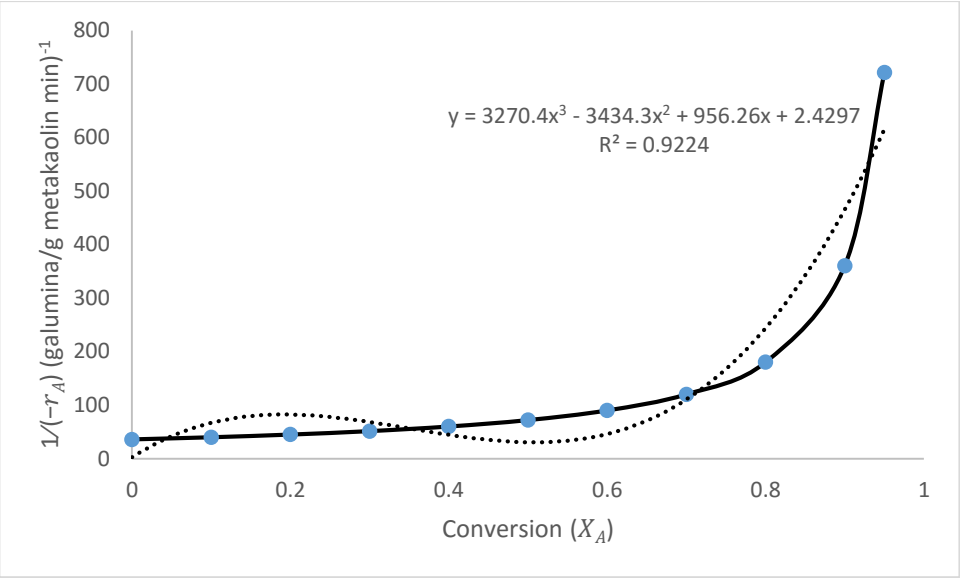


Figure B-4: Polynomial of degree 3 model plot

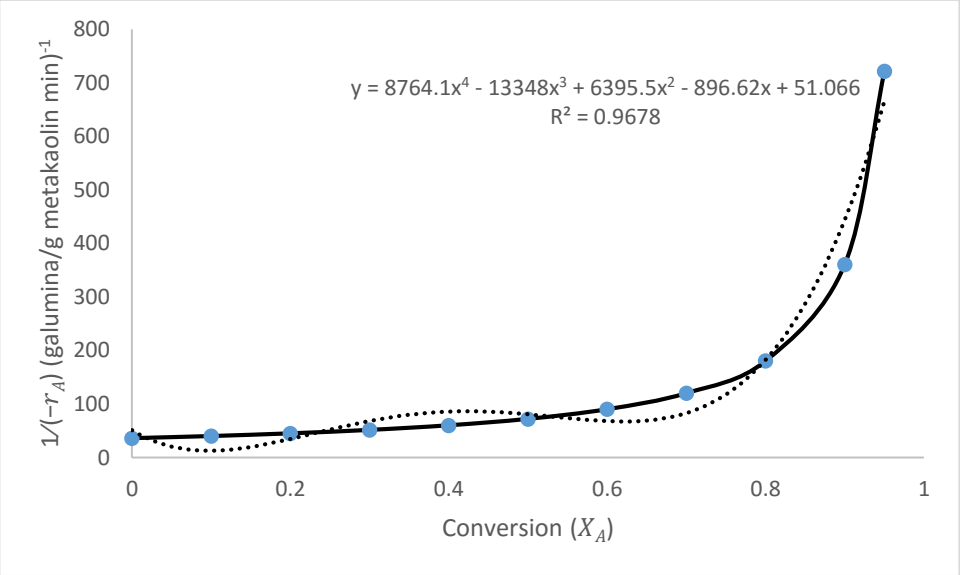


Figure B-5: Polynomial of degree 4 model plot

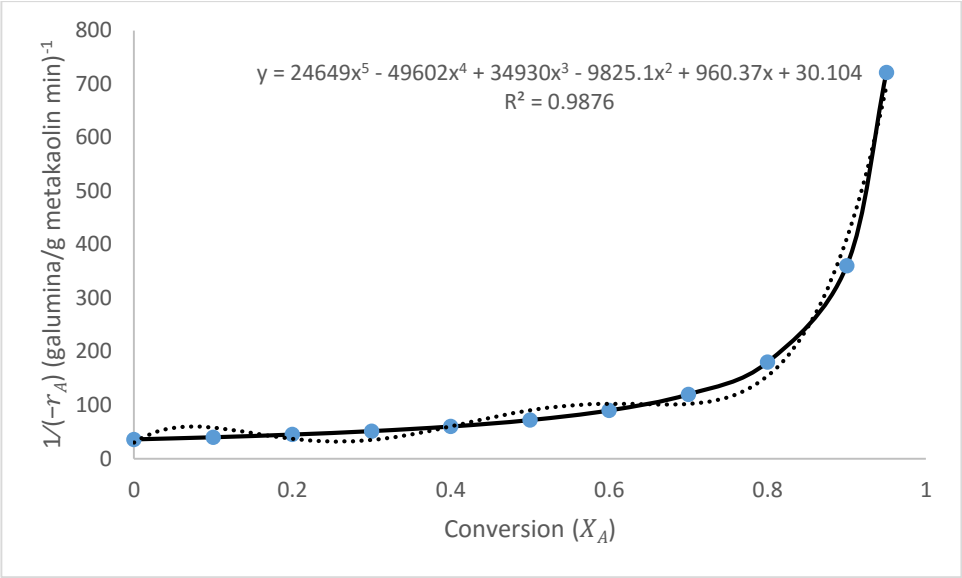


Figure B-6: Polynomial of degree 5 model plot

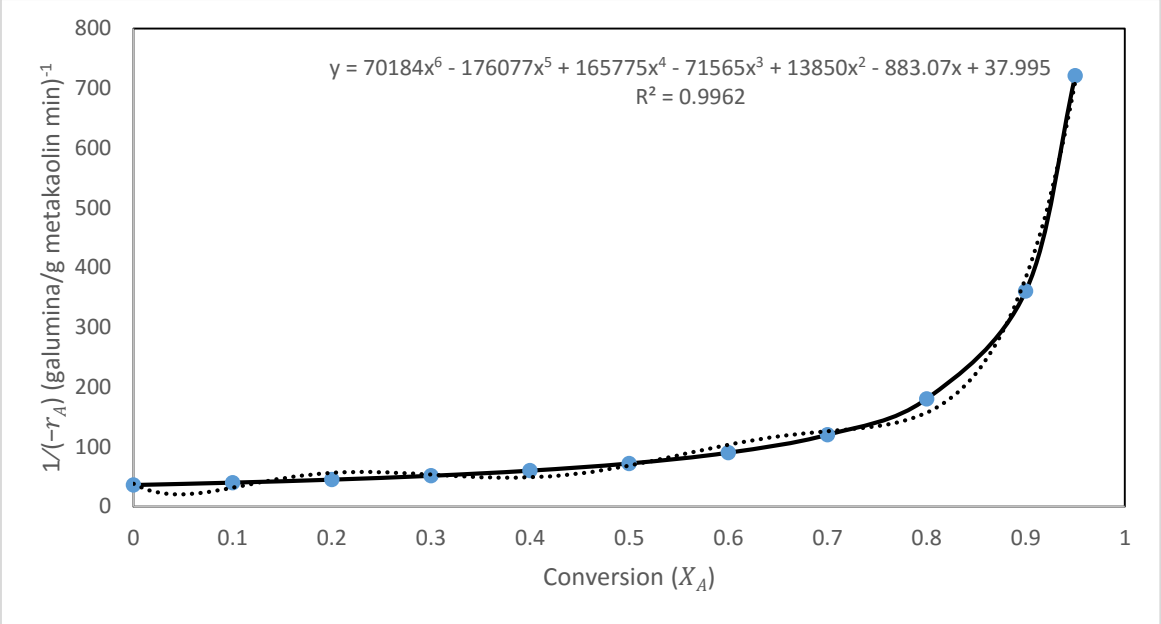


Figure B-7: Polynomial of degree 6 model plot

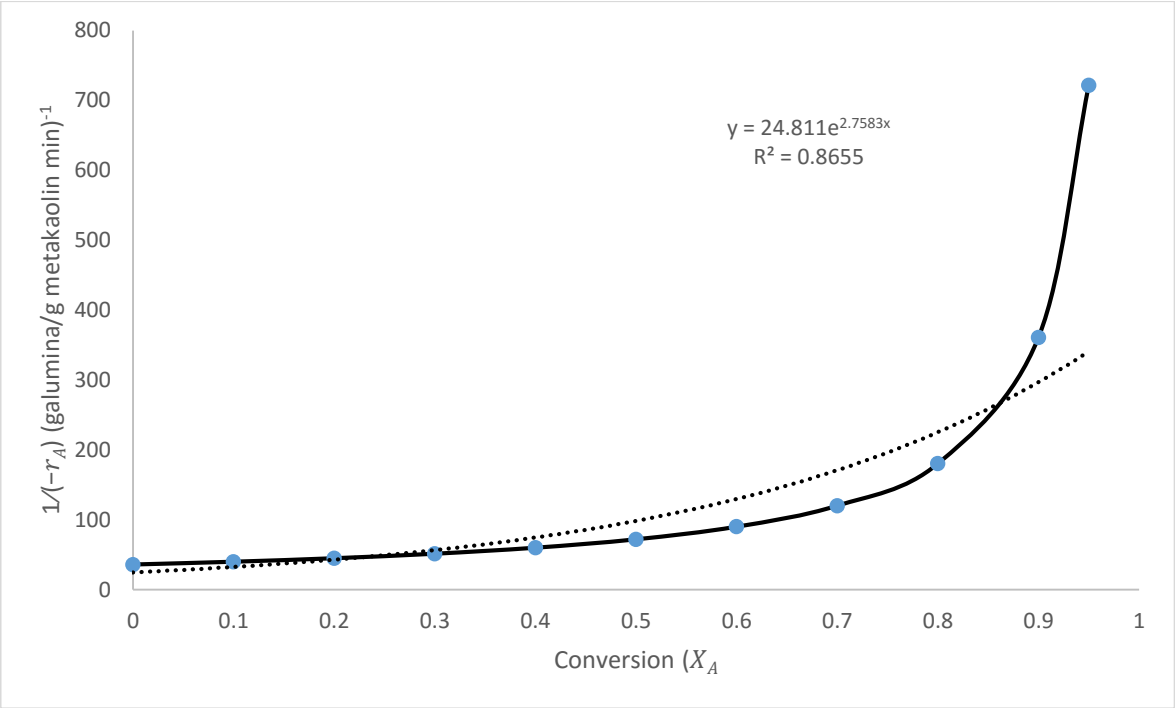


Figure B-8: Exponential model plot

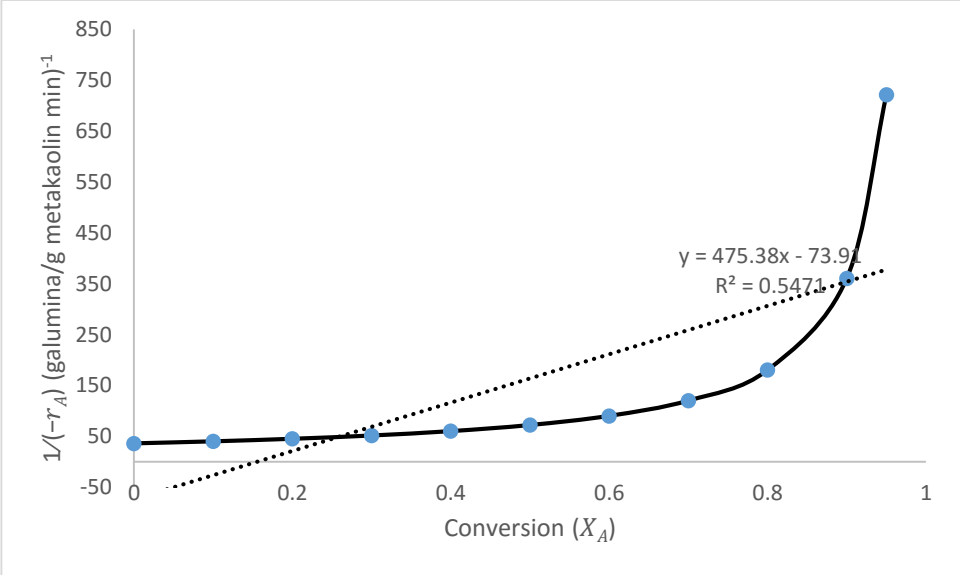


Figure B-9: Linear equation model plot

X_A=0.95 C_{Al0} = 0.39 (g alumina/g metakaolin)

APPENDIX C

MATERIAL BALANCE FOR DEALUMINATION REACTION

Three streams enter the dealuminator were the dealumination reaction takes place. The two resultant products were collected at different point out of the reactor, as steams 4 and 5, as shown in Figure C.1.

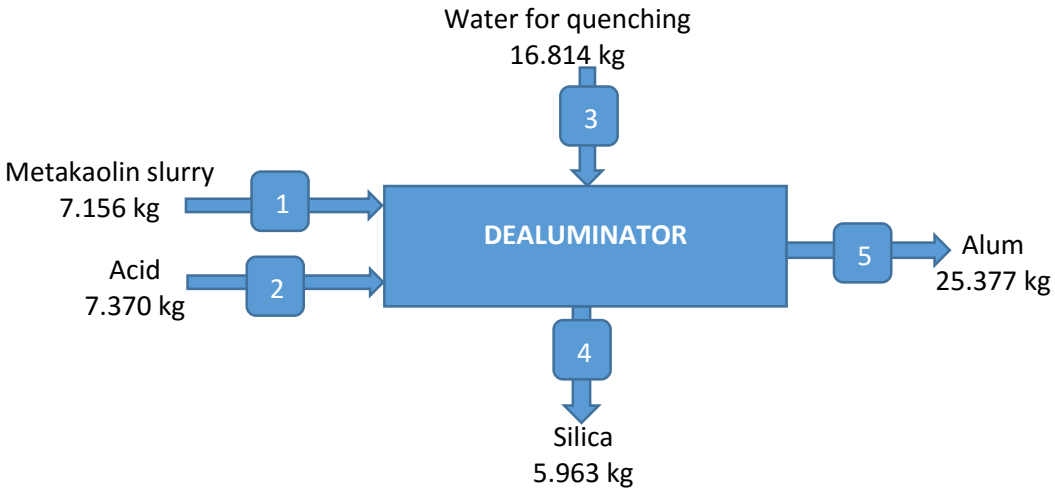


Figure C.1: Material balance around the dealuminator

The detail component balance of the reactants and products in the dealuminator is presented in Table C.1, while Table C.2 shows the computation of the three reactants which were acid, metakaolin and acid.

Table C.1: Material balance in the dealuminator

	Stream 1 Metakaolin slurry (g)	**Stream 2 Acid (g)**	**Stream 3 Quenching water (g)**	**Stream 4 Residue (g)**	**Stream 5 Alum (g)**
Al_2O_3	1000	0	0	20	0
SiO_2	1300	0	0	1287	13
H_2O	4656	147.4	16645.86	4289.852	17159.408
H_2SO_4	0	7150.374	0	357.5187	3932.7057
$Al(SO_4)_3$	0	0	0	0	3840.1496
Impurities	200	72.226	168.14	8.80732	431.55868
Sub-Total	**7156**	**7370**	**16814**	**5963.17802**	**25376.82198**
Total		**31340**		**31340**	

Table C.2 Volume estimation for different reactants

Reactants	Volume (cm^3) (V)	Density (g/cm^3) (ρ)	Mass (g)	Mass fraction $\boldsymbol{X_i}$	$\boldsymbol{\rho_i X_i}$
Water	21470	1.00	21470	0.685	0.685
Acid	4027	1.83	7370	0.235	0.430
Metakaolin	1000	2.50	2500	0.080	0.200
Total			31340	1.000	1.315

Average density $\bar{\rho}_{reactants} = \frac{\sum_{i=1}^{3} \rho_i X_i}{\sum_{i=1}^{3} X_i}$ $(C.1)$

$$= 1.315$$

Volume of dealuminator $V_{d*} = \frac{M_T}{\rho_{reactants}} = \frac{31340}{1.315} = 23832.70\ cm^3$

In order to avoid much pressure, build up in the system, since the dealuminator is not being designed as a pressurized vessel and to also accommodate water vapour that will be generated at the initial stage of the reaction, which will occupy much space (basic properties of gases), a safety factor of 25% was chosen. The actual volume

$$V_d = 1.25 \times 23832.70 \ = 29791 \ cm^3$$

The volume of the dealuminator (V_d) was approximately: 30000 cm^3

Considering cylindrical shape as the dealuminator shape which is common to most reactors, The height ($\boldsymbol{H_d}$) **to** diameter ($\boldsymbol{D_d}$) ratio was taken as 2, which is in agreement with literature (Perry, 2008).

Volume of a cylinder

$$V_c = \frac{\pi D_c^2 H_c}{4} \qquad (C.2)$$

$$V_d = \frac{\pi D_d^2 H_d}{4} \qquad (C.3)$$

$\boldsymbol{H_d}$: 53.46 cm $\boldsymbol{D_d}$: 26.73 cm

APENDIX D

ENERGY CALCULATION OF DEALUMINATOR

D-1 Determination of Insulating Material Thickness

Glass-wool was chosen as the insulating material, its thickness round the reactor to minimize heat loss to the surrounding was evaluated as follow:

Required design model

$$q' = \frac{2\pi L \Delta T_{overall}}{\frac{\ln(\frac{r_2}{r_1})}{k_a} + \frac{\ln(\frac{r_3}{r_2})}{k_b} + \frac{\ln(\frac{r_4}{r_3})}{k_c}} \qquad (D.1)$$

Where q' = energy flow per unit time; k_a= thermal conductivity of material a; L = height of the cylinder. The projected view for the configuration of the dealuminator is shown in Figure D.1.

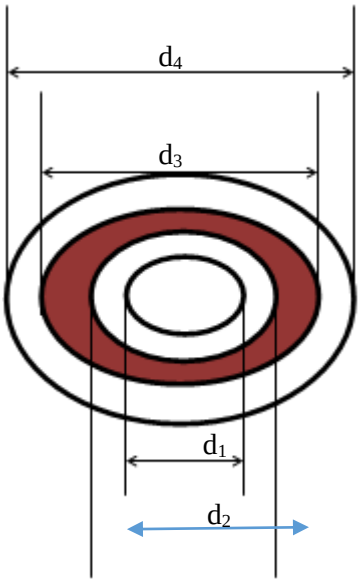


Figure D.1: Project view of dealuminator configuration

Where: d_1 is the inner diameter of the stainless steel

d_2 is the inner diameter of the glass wool

d_3 is the inner diameter of the aluminum casing

d_4 is the outer diameter of the aluminum casing

Table D.1: Thermal conductivity of selected materials of construction

Material	Thermal conductivity, W/mK (ambient Temperature)	Point of use in the reactor
Stainless steel	16.0958	Interior
Glass wool, curled	0.0415	Intermediate
Aluminum	273	External

(Perry, 2008)

Some of the simplified assumption made include:

Ambient temperature was 30°C (303 K)

During dealumination process, due to associated heat of solvation, the average temperature of reacting system was assumed to be 120°C (393 K)

$$q' = \frac{m_{total} Cp_{av} \Delta T}{t} \qquad (D.1)$$

m_{total} : Total mass of the reacting system

Cp_{av}: $Avearage\ specific\ heat\ capacity$

ΔT : $Temparature\ difference$

Ti is the initial temperature of the reacting system during dealumination.

T_f is the final temperature of the reacting system just before quenching.

t is the time for the dealumination reaction, t = 43.33 minutes

$$q' = \frac{14.526 \times 4200 \times 2}{43.66 \times 60}$$

$$q' = 46.58\ W$$

$$q' = \frac{2\pi L \Delta T_{overall}}{\frac{\ln\left(\frac{r_2}{r_1}\right)}{k_s} + \frac{\ln\left(\frac{r_3}{r_2}\right)}{k_w} + \frac{\ln\left(\frac{r_4}{r_3}\right)}{k_a}} \qquad (D.2)$$

Where K_s = 16.0958 W/mK K_w = 0.0415 W/mK K_a = 273 W/mK

$r_1 = 13.5\ cm = 0.135\ m$

$r_2 = 13.7\ cm = 0.137\ m$

$r_3 = (13.7 + d_{gw})cm = (0.137 + d_{gw})\ m$

$d_{gw} = Thickness\ of\ the\ glass\ wool$ (lagging thickness)

$r_4 = (13.9 + d_{gw})cm = (0.139 + d_{gw})\ m$

$$\Delta T \approx 393 - 303 = 90\ K$$

$$L = 53.5\ cm \approx 0.535\ m$$

$$q' = \frac{2\pi(0.535)(90)}{\frac{\ln\left(\frac{0.137}{0.135}\right)}{16.0958} + \frac{\ln\left(\frac{0.137 + t_{gw}}{0.137}\right)}{0.0415} + \frac{\ln\left(\frac{0.139 + t_{gw}}{0.137 + t_{gw}}\right)}{273}}$$

$$46.58 = \frac{302.5746}{0.0000914 + \frac{\ln\left(\frac{0.137 + t_{gw}}{0.137}\right)}{0.0415} + \frac{\ln\left(\frac{0.139 + t_{gw}}{0.137 + t_{gw}}\right)}{273}}$$

$$24.096 \ln\left(\frac{0.137 + t_{gw}}{0.137}\right) + 0.003663 \ln\left(\frac{0.139 + t_{gw}}{0.137 + t_{gw}}\right) = 6.4957$$

$$t_{gw} = 0.042389\, m = 4.24\, cm$$

The casing configuration to cover the insulating material is shown in Figure D.2, which serves as the external part of the dealuminator.

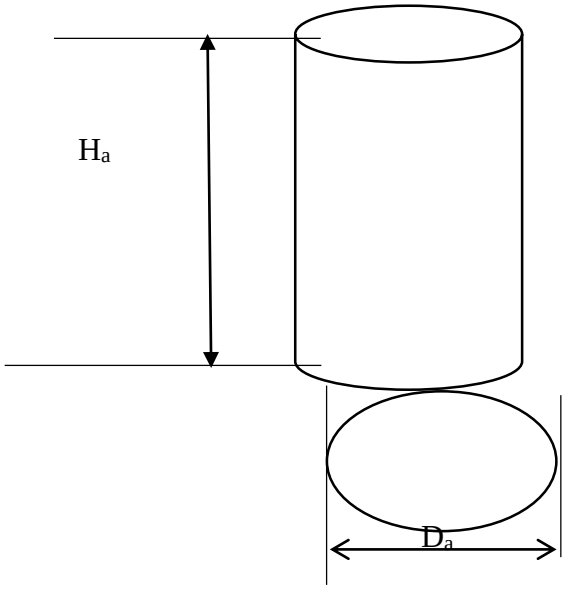


Figure D.2: Reactor casing dimensions

Ha: height of the aluminum casing ≅ 55 cm Do: Diameter of Aluminum casing ≅ 29 cm

APPENDIX E

METAKAOLIN SLURRY MIXING TANK AND ACID HOLDING TANK CALCULATION

E.1 Capacity of the Metakaolin Slurry Tank

The dealumination unit comprised of dealuminator, metakaolin slurry mixing and acid holding tank. This section handles the calculation for the design of the metakaolin slurry tank and acid holding tank. The two feeds into the slurry tank were water and metakaolin as shown in Table E.1.

Table E.1: Parameters for metakaolin slurry components

Reactants	Volume (cm^3) (V)	Density (g/cm^3) $\boldsymbol{\rho_i}$	Mass (kg)	Fractional composition $\boldsymbol{X_i}$	$\boldsymbol{\rho_i X_i}$ g/cm^3
Water	4656	1.00	4.656	0.65	0.650
Metakaolin	1000	2.50	2.500	0.35	0.875
			7.156		1.525

$$\rho_{slurry} = \frac{\sum_{i=1}^{n} \rho_i X_i}{\sum_{i=1}^{n} X_i} = \frac{1.525}{1} = 1.525\ g/cm^3$$

Where ρ_i = density of component i

X_i = mass fraction of component i

$$Volume\ of\ the\ slurry\ mixing\ tank\ (V_{mT}) = \frac{Toatal\ reactans\ mass}{slurry\ density}$$

$$V_{mT} = \frac{7156\ g}{1.525\ {}^{g}/_{cm^3}}$$

$$V_{mT} = 4692.459\ cm^3$$

In sizing the metakaolin slurry tank, volume occupied by the shaft and impeller as well as allowance for vortex formation due to turbulence was accounted for in the safety factor.

Therefore, a safety factor of 25% was chosen.

$$V_{AcmT} = 1.25\, V_{mT}$$

Actual required volume (V_{AcmT}) was

$$V_{AcmT} = 5865.574\ cm^3$$

The slurry tank will also be used as the channel through which the water for quenching will been introduced into the dealumination reactor (dealuminator) at the end of the reaction.

Volume of water for reaction quenching was calculated as: 16814 cm^3.

The total volume required for the metakaolin slurry tank was taken as:

$$V^*_{AcmT} = 20{,}000\ cm^3$$

$$V^*_{AcmT} = 20\ liters$$

Which is above the required volume for water of quenching and is of standard size.

Guide for choosing height to diameter ratio was obtained from literature, H=DT to 2DT, (Perry, 2008) choosing H=1.5DT:

H_{msT}: Metakaolin slurry mixing tank height

D_{msT}: Metakaolin slurry mixing tank diameter

Shape of the tank was chosen to be cylindrical

Volume of a cylinder $V_c = \frac{\pi D_c^2 H_C}{4}$

$$V^*_{AcmT} = \frac{\pi D^2_{msT} H_{msT}}{4} \qquad (E.1)$$

H_{msT}: 38.55 cm **D_{msT}: 25.70 cm**

E.1.1 Power requirement of the motor for metakaolin slurry mixing

The next step is to calculate the power requirement of the motor that will drive the stirrer for good mixing of the metakaolin-water slurry mixture. The following equations and charts are used for this purpose:

$$N_P = f(Re, Fr) \qquad (E.2)$$

Where: $N_P = Power\ number$ $Re = Reynolds\ number$ $Re = Froude\ number$

Equation (E.2) then becomes

$$\frac{P}{\rho N^3 {D_T}^5} = f\left(\frac{\rho N {D_T}^2}{\mu}, \frac{N^2 D_T}{g}\right) \qquad (E.3)$$

Calculating the Impeller diameter, D_I

From literature (Perry, 2008), large diameter impeller ($D_I > D_T/2$) are useful for:

- Avoiding stagnant region in the slurries
- Short mixing times to obtain uniformity throughout a vessel necessary for reaction.
- Promotion of heat transfer, and
- Promoting mass transfer between solid and liquid phases

In this case D_I = 0.6 D_T was chosen, which enables the slurry to be effectively agitated and dead zone avoided in the tank since there are no baffles in the tank. Figure E.1, shows the slurry mixing tank configuration.

$$D_I = 0.6 \times 25.70cm = 15.42\ cm$$

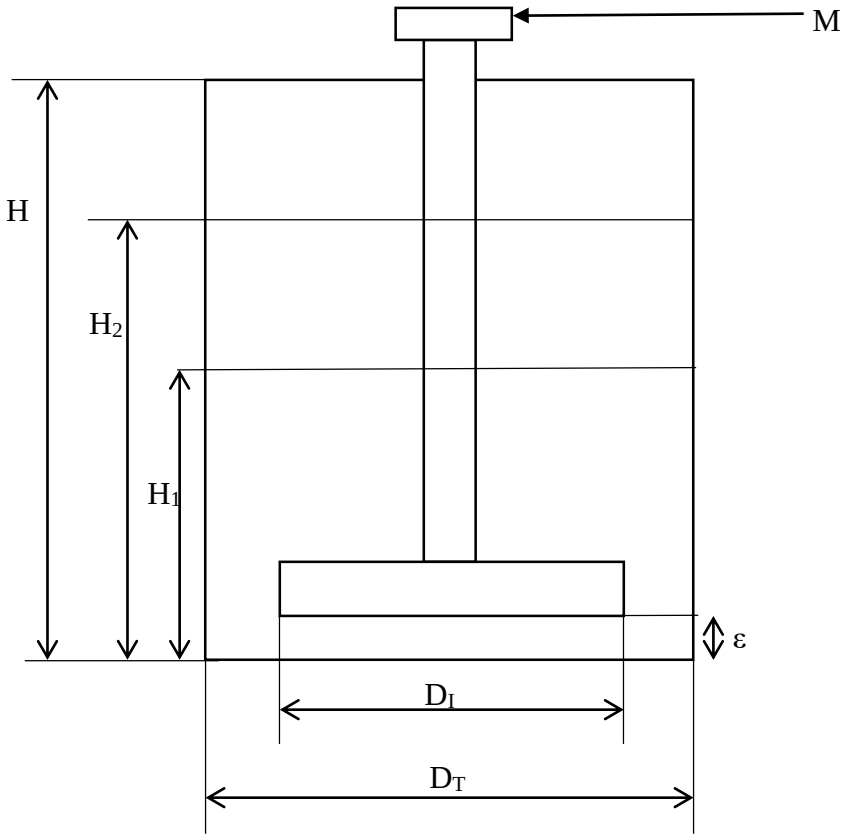


Figure E.1: Mixing configuration

Where D_T = Diameter of mixer = 25.70

D_I = Diameter of impeller =15.42 cm

H_1 = Height of slurry during mixing = 9.05 cm

H_2 = Height of water for quenching = 32.41 cm

H = Height of mixer = 38.55 cm

$\varepsilon = H_1/5 = 1.81$ cm

The low value for ε, the distance between the base of the impeller and the bottom of the slurry mixing tank is necessary to prevent the agglomeration of metakaolin particle in the slurry. By Geldart (1973) classification of solids shown in Figure E.2, the metakaolin particles with average density of 2.5 g/cm^3 and particle size < 20μm belongs to the class C or the cohesive class, therefore suspension of such particle size requires the impellers position to be very close to the bottom of the mixer.

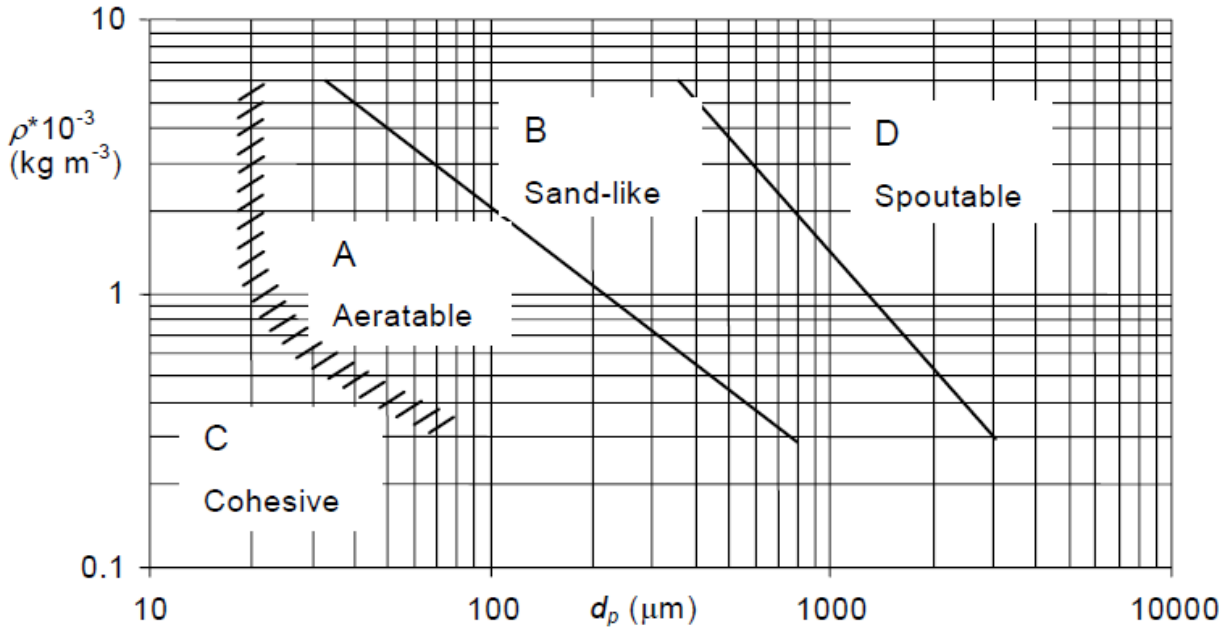


Figure E.2: Diagram of the Geldart classification of particles (Geldart, 1973)

E.1.2 Evaluating the Reynolds number for the metakaolin slurry

$$Re = \frac{\rho N {D_I}^2}{\mu} \qquad (E.4)$$

The density of the slurry had been calculated as = 1.525 g/cm^3

Evaluating the rotational speed, two basic speed ranges are specified and available namely1,150 to 1,750 rev/min with direct drive and 350 to 420 rev/min with gear drive. For suspension of solids (slurry), it is common to use the gear driven units. In this case, N = 390 rev/min (that is N = 6.5 rev/s), was selected as the rotational speed of the impeller.

Viscosity of metakaolin slurry = 17.32cP = 1.732×10^{-2} Pa.s

All units were converted to SI unit for the calculation

$$Re = \frac{1525 \times 6.5 \times 0.1542^2}{1.732 \times 10^{-2}}$$

$$Re = 1.36 \times 10^4$$

The flow pattern in the system during mixing will be turbulence as expected

Impeller type: The type of impeller selected is largely on the basis of the liquid viscosity (Coulson, 1999). For slurry suspension a standard six-blade vertical curved blade turbine impeller (McCabe and Smith 2005), would be selected. It gives good efficiency/unit horsepower for the suspension of cohesive materials, which is applicable in this system.

E.1.3 Power requirement

$$N_p = \frac{P}{\rho N^3 D_I^5} \qquad (E.5)$$

$$\frac{P}{\rho N^3 D_I^5} = f\left(\frac{\rho N D^2}{\mu}, \frac{N^2 D_I}{g}, \frac{D_T}{D}, \ldots\ldots\ldots\right) \qquad (E.6)$$

For un-baffled tanks, at higher Reynolds number, a vortex f and the Froude number has a significant effect on the power number (McCabe and Smith, 2005). The general equation is then modified

$$\frac{N_P}{N_{Fr}^m} = \varphi(N_{Re}, S_1, S_2, \dots\dots\dots S_n) \qquad (E.7)$$

Where:

$$m = \frac{a - log_{10} N_{Re}}{b} \qquad (E.8)$$

And for a six blade turbine: a =1.0 b = 40

$$N_{fr} = \frac{N^2 D_I}{g} \qquad (E.9)$$

Where

$$N_p = \frac{P}{\rho N^3 D_I^5} \; ; Re = \frac{\rho N D^2}{\mu} \; ; N_{fr} = \frac{N^2 D_I}{g}$$

N_{fr} Froude's Number N= rotational speed in r/s = 6.5 rps D_I= Diameter of impeller = 0.1542 m

g= acceleration due to gravity = 9.81m/s^2

$$N_{fr} = \frac{6.5^2 \times 0.1542}{9.81} = 0.664$$

$$m = \frac{1 - log_{10} 13600}{40} = -0.0783$$

Using the power curve in Figure E.3, Curve D corresponds to the power curve for un-baffled six-blade turbine impeller. At Reynolds number of 1.36×10^4, N_p = 1.4

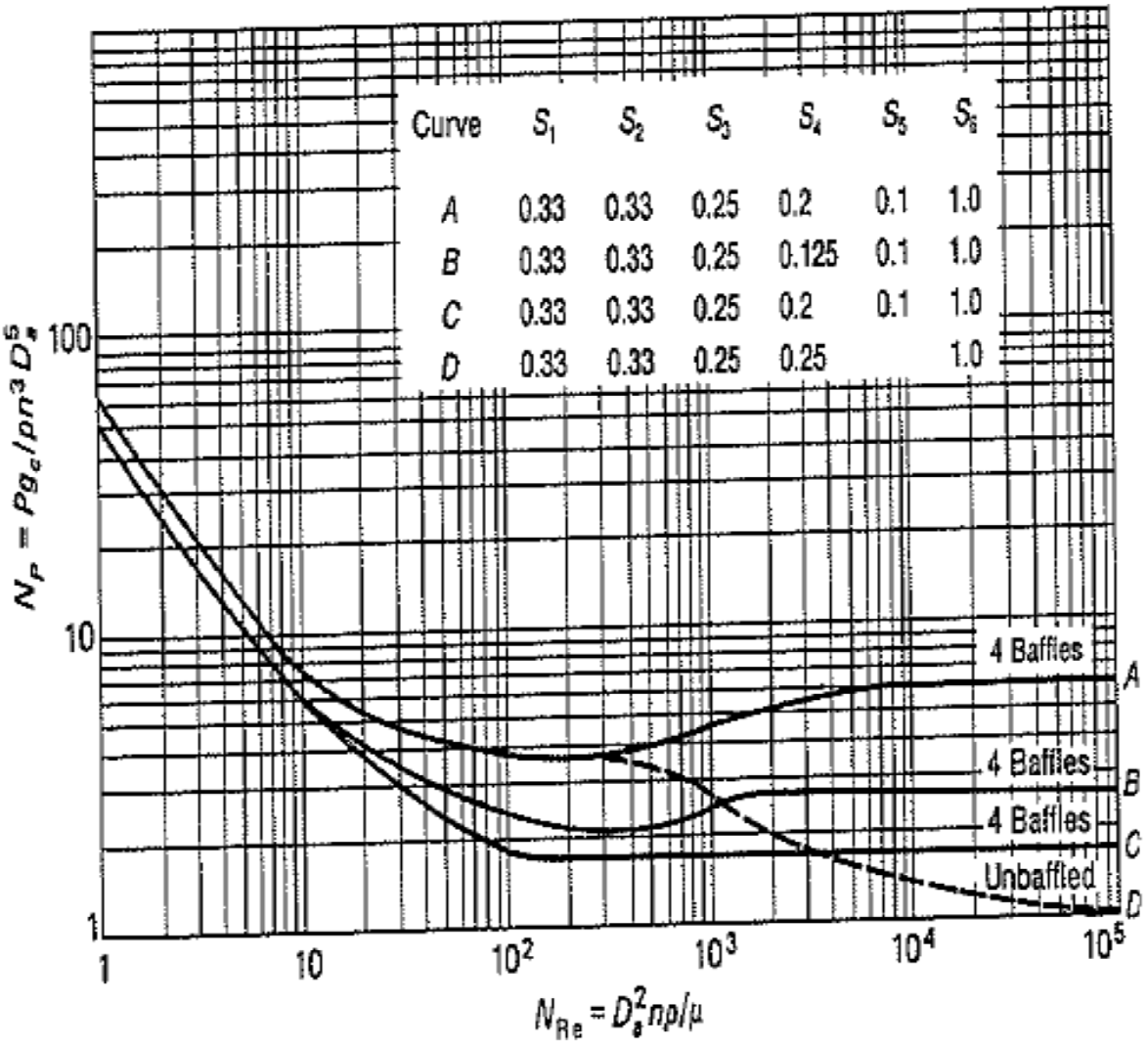


Figure E.3: Power Curve (McCabe and Smith, 2005)

A correction factor is always applied to the value for N_p read from the chat

$$N_p = 0.664^{-0.0783} \times 1.4$$

$$N_p = 1.446$$

$$P = N_p \rho N^3 D_I^5 \qquad (E.10)$$

$$P = 1.446 \times 1525 \times (6.5)^3 \times (0.1542)^5$$

$$P = 52.80\ W$$

The minimum theoretical power requirement is 52.80 W,

However, it is usually not good to operate an un-baffled tank under these conditions of agitation (Re = 1.36×10^4).

From Perry 8th ed., an un-baffled tank can be used to agitate a tank of diameter less than 1.8m

Recall that baffled tanks reduce the formation of vortex and enhances turbulence and hence aids mixing. In our case, we chose un-baffled tank because

i. The diameter of our agitator is 25. 70 cm < 1.8m

ii. Un-baffled tank requires lower power requirement

iii. Simplicity in construction compared to a baffled tank.

To compensate for transmission losses, frictional losses in the gear box and reduced efficiency of the electric motor, a safety factor of 25% was selected.

$$P_{act} = 1.25 \times P_{min}$$

$$P_{act} = 1.25 \times 52.80$$

$$P_{act} = 66\ W$$

E.2. Acid Holding Tank

The tank is where the acid is kept before realising it into the reactor for initiating the reaction when it come in contact with the mixed metakaolin slurry.

Amount of acid needed per batch = 4,027 cm^3

Allowing 20% free board space, the actual volume of acid tank (V_{AT}) required is:

$$V_{AT} = 1.2 \times 4027$$

$$V_{AT} = 4{,}832.40\ cm^3$$

Considering cylindrical shape, with height diameter ration of 2, considering 5,000 cm^3 as the volume of acid tank:

$$V_{AT} = \frac{\pi D_{AT}^2 H_{AT}}{4}$$

$\boldsymbol{H_{AT} = 29.42\ cm}$ $\boldsymbol{D_{AT} = 14.71\ cm}$

APPENDIX F

MATERIAL BALANCE AND SIZING OF ZEOLITE Y REACTOR

E.1 Material Balance

The art of kaolin usage is far older than its science, as such some of the parameter needed for the design of the zeolite reactor from the engineering point of view were not available. Kinetic data for zeolite synthesis using kaolin as source of the recipe could not be found.

Knowledge from the several laboratory syntheses helped in arriving at the sizing of the pilot scale reactor for zeolite Y production. The material in and out of the zeolite Y reactor and details of component balance are shown and presented in. Figure F.1. and Table F.1 respectively.

Basis: 2 kg of Zeolite Y per batch

Reaction temperature	100°C
Reaction time	7 hours
Capacity of heating element	2 kW
Nature of heat supply	Internal and external

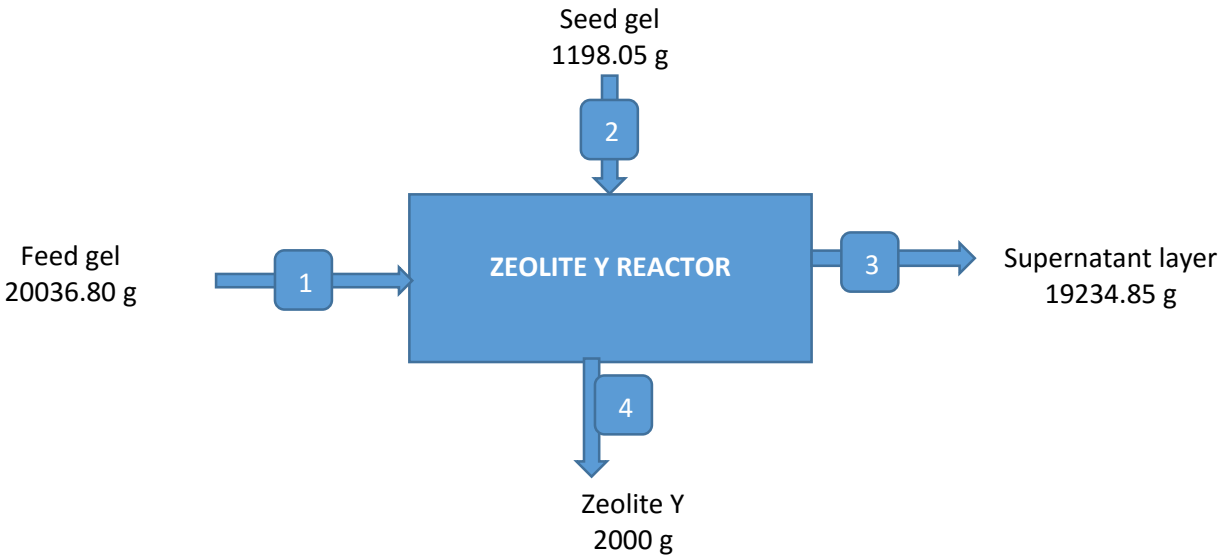


Figure F.1: Diagram of material balance around zeolite Y reactor

Table F.1: Material balance around zeolite Y reactor

	REACTANTS		**PRODUCTS**	
Components	**Stream 1 Seed gel (g)**	**Stream 2 Feed gel (g)**	**Stream 3 Supernatant layer (g)**	**Stream 4 Zeolite Y (g)**
Aluminum hydroxide	49.00	882.00	0.00	0.00
Sodium hydroxide	100.45	9.80	0.00	0.00
Sodium silicate	558.60	9975.00	0.00	0.00
Water	490.00	9170.00	0.00	0.00
Supernatant layer	0.00	0.00	19234.85	0.00
Zeolite Y	0.00	0.00	0.00	2000.00
Sub-Total	**1198.05**	**20036.80**	**19234.85**	**2000.00**
	21234.85		**21234.85**	

Volume computation based on the reactants needed for the targeted amount of Zeolite Y to be produced is shown in Table F.2.

Table F.2: Volume estimation for different reactants

Reactants	Density (g/cm^3) (ρ)	Mass (g)	Mass fraction $\boldsymbol{X_i}$	$\boldsymbol{\rho_i X_i}$
Sodium hydroxide	2.13	110.25	0.005191937	0.011059
Water	1.00	9660.00	0.454912561	0.454913
Aluminum hydroxide	2.42	931.00	0.043843022	0.1061
Sodium silicate	1.55	10533.60	0.49605248	0.768881
Total		21234.85		1.340953

Average density $\bar{\rho}_{reactants} = \frac{\sum_{i=1}^{3} \rho_i X_i}{\sum_{i=1}^{3} X_i}$ $(F.1)$

$$= 1.341$$

Volume of zeolite Y reactor $V_{d*} = \frac{M_T}{\rho_{reactants}} = \frac{21234.85}{1.340953} = 15835.64\ cm^3$

In order to avoid much pressure build up in the system, since the zeolite Y reactor is for low temperature production, as such the rector is not designed as a pressurized vessel. And to also accommodate water vapour that will be generated in the system since the operating temperature is at the boiling temperature of water being one of the reactant, a safety factor of 25% was chosen. The actual volume becomes,

$$V_Y = 1.25 \times 15835.64 \ = 19794.55\ cm^3$$

The volume of the Zeolite Y (V_Y) is approximately: 20000 cm^3

Considering cylindrical shape as the dealuminator shape which is common to most reactors, The height ($\boldsymbol{H_d}$) **to** diameter ($\boldsymbol{D_d}$) ratio was taken as 2, which is in agreement with literature (Perry, 2008).

From the volume of the zeolite Y reactor given as:

$$V_Y = \frac{\pi D_Y^2 H_Y}{4} \qquad (F.2)$$

H_Y: 47.70 cm **D_Y: 23.35 cm**

F.2 Energy Consideration

Total mass of reactant	=	21234.85 g
Initial temperature	=	303 K
Final Temperature	=	373 K
Average heat capacity	=	5 J/kg K
Estimated time to reach final Temperature	=	300 sec.

$$Q_Y = M_{TY} C_{PY} \Delta T_Y \qquad (F.3)$$

$$Power\ rating\ for\ element_Y = \frac{Q_Y}{time\ required}$$

$$= \frac{530871.25}{300}$$

$$= 1769.57\ W$$

APPENDIX G

MATERIAL BALANCE AND SIZING OF ZSM-5 REACTOR

G.1 Material Balance

The material in and out of the ZSM-5 reactor and details of component balance are shown and presented in. Figure G.1. and Table G.1 respectively.

Basis: 4 kg of ZSM-5 per batch

Reaction temperature	95°C
Reaction time	4 days
Capacity of heating element	2 kW
Nature of heat supply	Internal and external

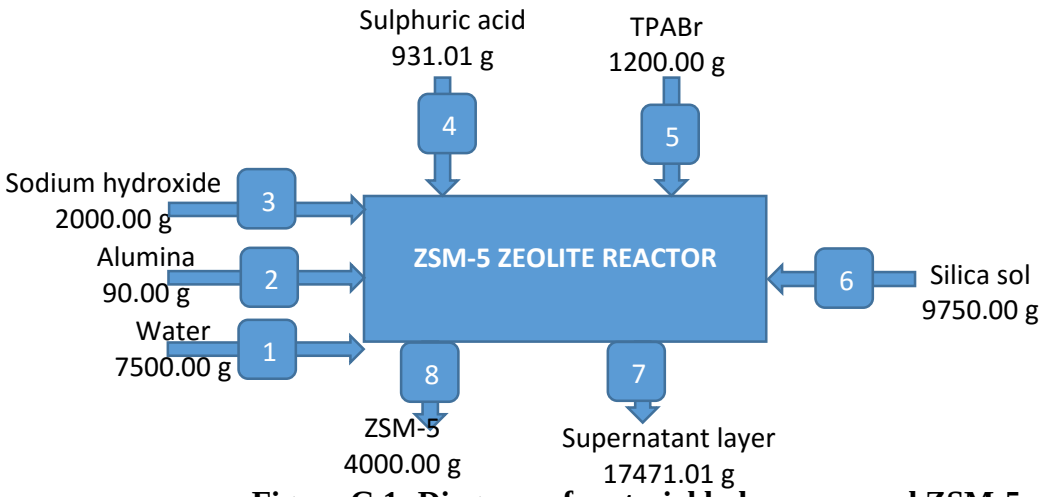


Figure G.1: Diagram of material balance around ZSM-5 reactor

Table G.1: Material balance on ZSM-5 reactor

	REACTANTS						PRODUCTS	
Components	**Stream 1 Water (g)**	**Stream 2 Alumina (g)**	**Stream 3 NaOH (g)**	**Stream 4 H2SO4 (g)**	**Stream 5 TPABr (g)**	**Stream 6 Silica sol (g)**	**Stream 7 Supernatant layer (g)**	**Stream 8 ZSM-5 (g)**
Water	7500	0	0	0	0	0	0	0
Alumina	0	90	0	0	0	0	0	0
NaOH	0	0	2000	0	0	0	0	0
H_2SO_4	0	0	0	931.01	0	0	0	0
TPABr	0	0	0	0	1200	0	0	0
Silica sol	0	0	0	0	0	9750	0	0
Supernatant layer	0	0	0	0	0	0	17471.01	0
ZSM-5	0	0	0	0	0	0	0	4000
Total			**21471.01**				**21471.01**	

Volume computation based on the reactants needed for the targeted amount of Zeolite Y to be produced is shown in Table G.2.

Table G.2: Volume estimation for different reactants

Reactants	Density (g/cm^3) (ρ)	Mass (g)	Mass fraction X_i	$\rho_i X_i$
NaOH	2.13	2000	0.093149	0.198407
H_2O	1	7500	0.349308	0.349308
Al_2O_3	3.9	90	0.004192	0.016348
H_2SO_4	1.8255	931.01	0.043361	0.079156
TPABr	1.7	1200	0.055889	0.095012
Silica sol	1.3	9750	0.454101	0.590331
Total		21471.01		1.328561

From Equation (F.1)

Average density $\bar{\rho}_{reactants} = \frac{\sum_{i=1}^{3} \rho_i X_i}{\sum_{i=1}^{3} X_i}$ $(F.1)$

$= 1.329$ g/cm

Volume of zeolite Y reactor $V_{Z*} = \frac{M_T}{\rho_{reactants}} = \frac{21471.01}{1.328561} = 16161.102\ cm^3$

In order to avoid pressure build up in the system, since the ZSM-5 reactor is for low temperature production, as such the rector is not designed as a pressurized vessel. And to accommodate water vapour that will be generated in the system since the operating temperature is at the boiling temperature of water being one of the reactant, a safety factor of 25% was chosen. The actual volume becomes,

$$V_Z = 1.25 \times 16161 \ = 20201\ cm^3$$

The volume of the ZSM-5 zeolite (V_Z) is approximately: 20000 cm^3 = 20 liters

Considering cylindrical shape as the dealuminator shape which is common to most reactors, The height $(\boldsymbol{H_d})$ **to** diameter $(\boldsymbol{D_d})$ ratio was taken as 2, which is in agreement with literature (Perry, 2008).

From the volume of the ZSM-5 zeolite reactor given as:

$$V_Z = \frac{\pi D_Z^2 H_Z}{4} \qquad (G.1)$$

H_Z: 47.70 cm **D_Z: 23.35 cm**

G.2 Energy Consideration

Total mass of reactant = 21471.01 g = 21.47 kg

Initial temperature	=	303 K
Final Temperature	=	368 K
Average heat capacity	=	5 J/kg K
Estimated time to reach reaction temperature	=	300 sec.

$$Q_Z = M_{TZ} C_{PZ} \Delta T_Z \qquad (G.2)$$

$$Power\ rating\ for\ element_Z = \frac{Q_Z}{time\ required}$$

$$= \frac{536775.125}{300}$$

$$= 1789.25\ W$$

APPENDIX H

Calculation on the production of sodium silicate for zeolite Y production

Basis: 15000 cm^3 of H_2O

Amount of NaOH (30 wt% of basis) = $0.3 \times 15000 = 4500g$ $(4.5\ kg)$

Amount of SiO_2 (34.2 wt% of basis) = $0.342 \times 15000 = 5130g$ $(5.13\ kg)$

$$Amount\ of\ NaOH\ in\ moles = \frac{mass\ of\ NaOH}{Molar\ mass\ of\ NaOH} = \frac{4500\ g}{40\ g/mol} = 112.5\ moles$$

$$Concentration\ of\ NaOH\ in \frac{moles}{dm^3} = \frac{112.5\ moles}{15000\ cm^3} \times \frac{1000\ cm^3}{1\ dm^3} = 7.5\ {}^{moles}/_{dm^3}$$

$$= 7.5\ M$$

$$2NaOH + xSiO_2 + H_2O \longrightarrow Na_2O(SiO_2)_x + 2H_2O \qquad (H.1)$$

Evaluating x:

Component	SiO_2	NaOH
Mass	5130 g	4500 g
Molar Mass	60 g/mol	40 g/mol
Amount in moles	${}^{5130}/_{60} = 85.5\ moles$	${}^{4500}/_{40} =$

$112.5\ moles$

Considering mol ratio of the two reactant from Equation (3.34)

$\frac{SiO_2}{NaOH} = \frac{x}{2} = \frac{85.5}{112.5} = 0.76 \quad x = 2 \times 0.76 = 1.52$

The equation for the sodium silicate production becomes

$$2NaOH + 1.52SiO_2 + H_2O \qquad Na_2O(SiO_2)_{1.52} + 2H_2O \qquad (H.2)$$

APPENDIX I

Calculation on the production of sodium silicate for ZSN-5 zeolite production

Basis: 10000 cm^3 of H_2O

Amount of NaOH (12 wt% of basis) = $0.12 \times 10000 = 1200\ g\ (1.2\ kg)$

Amount of SiO_2 (28.57 wt% of basis) = $0.2857 \times 10000 = 2857\ g\ (5.13\ kg)$

$$Amount\ of\ NaOH\ in\ moles = \frac{mass\ of\ NaOH}{Molar\ mass\ of\ NaOH} = \frac{1200\ g}{40\ g/mol} = 30\ moles$$

$$Concentration\ of\ NaOH\ in \frac{moles}{dm^3} = \frac{30\ moles}{10000\ cm^3} \times \frac{1000\ cm^3}{1\ dm^3} = 3\ {}^{moles}/_{dm^3} = 3\ M$$

$$2NaOH + xSiO_2 + H_2O \longrightarrow Na_2O(SiO_2)_x + 2H_2O \qquad (I.1)$$

Evaluating x:

Component	SiO_2	NaOH
Mass	2857 g	1200 g
Molar Mass	60 g/mol	40 g/mol
Amount in moles	${}^{2857}/_{60} = 47.617\ moles$	${}^{1200}/_{40} = 30\ moles$

Considering mol ratio of the two reactant from Equation (3.34)

$$\frac{SiO_2}{NaOH} = \frac{x}{2} = \frac{47.617}{30} = 1.59$$

$$x = 2 \times 1.59 = 3.2$$

The equation for the sodium silicate production becomes

$$2NaOH + 3.2SiO_2 + H_2O \longrightarrow Na_2O(SiO_2)_{3.2} + 2H_2O \qquad (I.2)$$

APPENDIX J

PRELIMINARY FULL SCALE CALCULATION FOR MAJOR EQUIPMENT

J.1 Zeolite Y Reactor

Basis: 50 tons per year

Attainment = 90%

$$Attainment = \frac{hours\ operated}{8760} \times 100 \qquad (J.1)$$

$$hours\ operated = \frac{8760 \times 90}{100} = 7884\ hours$$

operating hours per batch = 8 hours

$$Number\ of\ batches\ per\ annum = \frac{7884}{8} = 985.5 \approx 986\ batches\ per\ annum$$

$$Output\ per\ batch = \frac{50}{986} = 0.051\ tons\ per\ batch$$

$$Scale - up\ factor = \frac{Production\ rate\ at\ scale\ up}{Production\ rate\ at\ pilot\ scale} \qquad (J.2)$$

$$Scale - up\ factor\ (R) = \frac{50.7\frac{kg}{batch}}{2\frac{kg}{batch}} = 25.35$$

The reactor shape was taken to be cylindrical, and geometrical similarities method scale up was chosen. Height to diameter ration was taken as 2.

$$R = \frac{D_{YF}}{D_{YP}} = \frac{V_{YF}^{(1/3)}}{V_{YP}^{(1/3)}} \qquad (J.3)$$

Where;

D_{YF}: $Diameter\ of\ full\ scale\ zeolite\ Y\ reactor$

D_{Yp}: $Diameter\ of\ pilot\ scale\ zeolite\ Y\ reactor$

V_{YF}: $Volume\ of full\ scale\ zeolite\ Y\ reactor$

V_{Yp}: $Volume\ of\ pilot\ scale\ zeolite\ Y\ reactor$ = 20 liters

From Equation (J.3)

$$V_{YF} = R^3 V_{YP}$$

$$V_{YF} = 25.35^3 \times 20\ liters = 325{,}809.61\ liters = 325.81\ m^3$$

$$D_{YF} = \left(\frac{2V_{YF}}{\pi}\right)^{1/3} = \left(\frac{2 \times 325.81}{\pi}\right)^{1/3} = 5.9\ m$$

$$H_{YF} = 11.8\ m$$

Multiple reactors of same capacity could be built to give room to size of reactor that will be easy to handle.

J.2 ZSM-5 Reactor

Basis: 10 tons per year

Attainment = 90%

$$hours\ operated = \frac{8760 \times 90}{100} = 7884\ hours$$

operating hours per batch = 120 hours

$$Number\ of\ batches\ per\ annum = \frac{7884}{120} = 65.7 \approx 66\ batches\ per\ annum$$

$$Output\ per\ batch = \frac{10}{66} = 0.151\ tons\ per\ batch$$

$$Scale - up\ factor\ (R) = \frac{151\frac{kg}{batch}}{4\frac{kg}{batch}} = 37.75$$

The reactor shape was taken to be cylindrical, and geometrical similarities method scale up was chosen. Height to diameter ration was taken as 2.

$$R = \frac{D_{ZF}}{D_{ZP}} = \frac{V_{ZF}^{(1/3)}}{V_{ZP}^{(1/3)}} \qquad (J.4)$$

Where;

D_{ZF}: $Diameter\ of\ full\ scale\ ZSM-5\ reactor$

D_{Zp}: $Diameter\ of\ pilot\ scale\ ZSM-5\ reactor$

V_{ZF}: $Volume\ of full\ scale ZSM-5\ reactor$

V_{Zp}: $Volume\ of\ pilot\ scale\ ZSM-5\ reactor$ = 20 liters

From Equation (J.4)

$$V_{ZF} = R^3 V_{ZP}$$

$$V_{ZF} = 37.75^3 \times 20\ liters = 1{,}076\ m^3$$

Considering two reactors of equal size

$$V_{YF1} = 538\ m^3$$

$$D_{ZF} = \left(\frac{2V_{YF}}{\pi}\right)^{1/3} = \left(\frac{2 \times 538}{\pi}\right)^{1/3} = 7.0\ m$$

$$H_{YF} = 14\ m$$

Multiple reactors of same capacity could be built to give room to size of reactor that would be easy to handle.

J.3 Dealuminator

Basis: 250 tons per year

Attainment = 90%

$$hours\ operated = \frac{8760 \times 90}{100} = 7884\ hours$$

operating hours per batch = 1 hour

$$Number\ of\ batches\ per\ annum = \frac{7884}{1} = 7884\ batches\ per\ annum$$

$$Output\ per\ batch = \frac{250}{7884} = 0.032\ tons\ per\ batch$$

$$Scale-up\ factor\ (R) = \frac{31.71\ \frac{kg}{batch}}{2.5\ \frac{kg}{batch}} = 12.68$$

The reactor shape was taken to be cylindrical, and geometrical similarities method scale up was chosen. Height to diameter ration was taken as 2.

$$R = \frac{D_{DF}}{D_{DP}} = \frac{V_{DF}^{(1/3)}}{V_{DP}^{(1/3)}} \qquad (J.5)$$

Where;

D_{DF}: $Diameter\ of\ full\ scale\ dealuminator$

D_{Dp}: $Diameter\ of\ pilot\ scale\ dealuminator$

V_{DF}: $Volume\ of full\ scale\ dealuminator$

V_{Dp}: $Volume\ of\ pilot\ scale\ dealuminator$ = 30 liters

From Equation (J.5)

$$V_{DF} = R^3 V_{DP}$$

$$V_{DF} = 12.68^3 \times 0.03\ m^3 = 61.16\ m^3$$

$$D_{DF} = \left(\frac{2V_{YF}}{\pi}\right)^{1/3} = \left(\frac{2 \times 61.16}{\pi}\right)^{1/3} = 3.4\ m$$

$$H_{YF} = 6.8\ m$$

APPENDIX

n-HEXADECANE HYDROCRACKING REACTION ON Pt/H-ZSM-5 RESULTS

Table K1: Products distribution of n-hexadecane hydrocracking on Pt/H-ZSM-5

Reaction Temperature (K)	478	488	498	508	518	528	538
Reaction Temperature (˚C)	205	215	225	235	245	255	265
C1	0	0	0	0	0.024403	0.048214	0.11681
C2	0	0	0	0.023246	0.062304	0.093213	0.253252
C3	3.558126	3.343833	3.382161	3.820795	3.434315	4.005606	7.604908
C3, =	0	0	0	0	0	0	0
n-C4	4.759787	4.724982	5.229153	5.9235	5.803109	6.246585	10.64344
n-C4, =	0	0	0	0	0.001734	0	0
iso-C4	1.208968	1.09038	1.174916	1.224641	0.709011	1.451558	3.297669
iso-C4, =	0	0	0	0	0	0	0
n-C5	5.653883	4.979404	6.18785	7.02874	7.4136	7.691071	11.34969
n-C5, =	0	0	0	0	0	0	0
iso-C5	1.13433	1.253937	1.245068	1.584954	1.733873	2.159337	5.275092
iso-C5, =	0	0	0	0	0	0	0
n-C6	5.525797	4.809789	6.037004	6.612426	7.271678	7.905141	9.287853
n-C6, =	0	0	0	0	0	0	0.008344
iso-C6, multi	0	0	0	0	0.014872	0	0.099632
iso-C6, mono	0.478901	0.775382	1.652042	1.989645	2.388245	3.209756	7.781595
iso-C6, =	0	0	0	0	0.000613	0	0
n-C7	4.595044	4.1071	4.429535	4.42836	5.322247	6.102586	5.28
n-C7, =	0	0	0	0	0.002042	0	0
iso-C7, multi	0	0	0	0	0.039871	0.059142	0.416687
iso-C7, mono	0.374792	1.296341	1.929655	2.117498	2.736077	4.010748	8.23362
iso-C7, =	0	0	0	0	0.007325	0	0.010307
n-C8	4.154754	3.816331	3.731023	3.625317	4.439547	4.920383	2.783804
n-C8, =	0	0	0	0	0	0	0
iso-C8, multi	0	0	0	0	0.06614	0.143999	0.82454
iso-C8, mono	0.375017	1.780955	1.890072	2.116441	2.891774	4.519887	6.44319
iso-C8, =	0	0	0	0	0	0	0
n-C9	4.678087	4.040465	3.941479	3.937025	4.333644	4.04032	1.570552

n-C9, =	0	0	0	0	0	0	0
iso-C9, multi	0	0	0	0	0.116141	0.252641	1.117546
iso-C9, mono	1.232353	2.423068	2.650311	2.984996	3.621519	5.398021	4.063804
iso-C9, =	0	0	0	0	0	0	0
n-C10	4.771226	4.537194	4.164261	3.951817	3.987813	3.0709	0.87362
n-C10, =	0	0	0	0	0	0	0
iso-C10, multi	0	0	0	0.143702	0.307254	0.695565	1.222086
iso-C10, mono	2.450948	3.531621	4.492956	4.90279	5.326009	6.728723	2.597791
iso-C10, =	0	0	0	0	0	0	0
n-C11	4.222206	4.185849	3.632176	3.182587	2.928437	1.85334	0.496196
n-C11, =	0	0	0	0	0	0	0
iso-C11, multi	0	0	0	0.176458	0.539165	1.121132	0.908466
iso-C11, mono	4.408278	5.185365	5.357482	5.606509	5.736863	5.900088	1.649571
iso-C11, =	0	0	0	0	0	0	0
n-C12	4.15683	3.658832	2.992448	2.37109	1.923563	0.995134	0.303313
n-C12, =	0	0	0	0	0	0	0
iso-C12, multi	0	0	0	0.496619	0.594576	1.128847	0.690552
iso-C12, mono	3.915233	4.83402	4.862981	4.717878	4.848312	4.14189	1.196074
iso-C12, =	0	0	0	0	0	0	0
n-C13	2.63578	2.307972	1.433265	1.093618	0.740033	0.314997	0.109448
iso-C13, multi	0	0	0	0.092984	0.378581	0.64478	0.416687
iso-C13, mono	0	2.386722	2.509622	2.395393	2.221237	1.544129	0.449571
n-C14	0	0	0.166055	0.094041	0.079691	0	0
iso-C14, multi	0	0	0	0	0	0	0
iso-C14, mono	0	0	0	0	0	0	0
n-C15	0	0	0	0	0.259827	0	0
iso-C15, multi	0	0	0	0	0	0	0
iso-C15, mono	0	0	0	0	0	0	0
iso-C16, multi	1.06299	0.993458	1.660488	2.62574	2.593568	3.760037	1.056196
iso-C16, mono	34.64667	29.937	25.248	20.73119	15.10099	5.842231	1.568098
n-C16	0	0	0	0	0	0	0